University of Strathclyde

Department of Naval Architecture, Ocean and Marine Engineering

Hydrodynamic Design Aspects of Tension Leg Platforms for Wind Turbines

Elif Oguz

A thesis presented in fulfilment of the requirements for the degree of Doctor of Philosophy

2016

This thesis is the result of the author's original research. It has been composed by the author and has not been previously submitted for examination which has led to the award of a degree.

The copyright belongs to the author under the terms of the United Kingdom Copyright Acts as qualified by University of Strathclyde Regulation 3.50. Due acknowledgement must always be made of the use of any material contained in, or derived from, this thesis.

Signed: Date:

I dedicate my dissertation to my father M. Zeki Oguz and my mother Gonul Oguz. It is their encouragement and support from the very beginning of my life that made it possible for me to reach this stage.

Acknowledgements

First and foremost I would like to express my deepest gratitude to my first supervisor Professor Atilla Incecik for giving me the opportunity to undertake this research as well as for his

encouragement and his significant help whenever it was needed. It has been a great honour for me to work with him and be supervised by him. Due to his immense knowledge and academic support, I had an enthusiastic and unforgettable time during the past three years in Glasgow. In every sense, none of this work would have been possible without him. In addition, I would like to acknowledge the valuable support and help of my second supervisor, Dr Mahdi Khorasanchi.

I would like thank Professor Alexander Day for his continuous help and support to me. Throughout the project, he provided encouragement, sound advice, good teaching, and lots of good ideas. The joy and enthusiasm he has for this research was contagious and motivational for me, even during tough times in the PhD pursuit.

I would also like to sincerely thank to Mr David Clelland for his time, motivation, interest, helpful comments and insightful questions. The numerous discussions are important to this work. Thank you for always believing in me. I will always appreciate all you have done.

I would also like to sincerely thank to Professor M.Sedat Kabdasli for his assistance and guidance in getting my graduate career started on the right foot.

Special thanks go also to the people of Iberdrola Engineering and Construction Group, Juan Amate Lopez, and Gustavo Sánchez for their continuous guidance and their crucial contribution in completion of the project.

Special thanks are also given to José Azcona Armendáriz and Faisal Bouchotrouch from CENER (National Renewable Energy Centre of Spain) for their support.

I would like to specially thank to Charles Keay from Kelvin Hydrodynamic Laboratory for coordinating all procedures in model fabrication, and for his continuous support and understanding whenever it was needed. It was a pleasure to work together with people in our Kelvin Hydrodynamics Laboratory.

Also, I am grateful to Mrs. Thelma Will, our research secretary, for her kind support related with all the administrative details of my PhD and for listening me whenever I needed.

Additionally, Professor Peilin Zhou, I will never forget what you have done for me after my accident in China. I would like to thank all colleagues and students, who helped me during my stay at hospital in China from Harbin Engineering Faculty. Special thanks are also given to Haibin Wang and Haipeng Liu who came to China to pick me up after my accident. I would like to sincerely thank to Professor Atilla Incecik for all his help during this period, I will never forget. I also would like to thank all of my colleagues and friends in Glasgow who visited me

often and helped me during my recovery period after my accident in China. Cagan Diyaroglu, Tahsin Tezdogan, Yigit Kemal Demirel, Konstantinos Dikis, Volkan Arslan, S. Anil Gunbeyaz, Zhiming Yuan, Onder Canbulat, Seda Canbulat. I am very grateful to all other colleagues in the Research Centre of NAOME. They made my life in Glasgow full of unforgettable moments.

I would like to offer special thanks our departmental administrator who has supported me throughout my stay in China even though she is thousands of miles away: Carol Georges. I will always appreciate all you have done.

Special thanks are also given to rest of my friends and colleagues especially Aristeidis Kiourtzis, Georgios Vavourakis, Konstantinos Sfakianakis who I worked at the same box until midnight most of the time.

Special thanks are also given to my friend Ariadni Grammenou for her continuous positive support even though she was in Greece.

I gratefully acknowledge the funding sources that made my PhD work possible. I was funded by Lloyd's Register and University of Strathclyde for the first two years of my PhD. I was also partially supported by Department of Naval Architecture, Ocean and Marine Engineering by a research assistant position. The work was funded under the Innovate UK grant

"TLPWind UK: Driving down the cost of offshore wind in UK waters", project reference 101969.

And finally, I would like to thank my self-sacrificing mother and father for always supporting my decisions and for believing in me.

Contents

List of Figures

List of Tables

Abstract

This thesis describes an experimental and numerical investigation of the dynamic performance of a TLP wind turbine concept in realistic environmental conditions. An extensive test campaign may be costly and time-consuming; nevertheless experiments are widely used for investigating the performance of marine systems and providing a great care is taken can yield reliable results. On the other hand, computational simulations offer a fast, low cost alternative to experiments. Continued technological advances offer ever-increasing computational power, which can be harnessed for fully coupled time-domain aero-hydroservo-elastic simulations to integrate all complex environmental conditions in the same computational environment. Fully coupled analysis methods are rapidly gaining popularity for renewable energy applications. The application of such techniques to determine the performance of FOWTs allow designers to assess hydrodynamic performance at the early design stage enabling any necessary corrective action to be taken before the FOWT is deployed.

The thesis shows that the use of experimental data is an invaluable tool in order to characterise the hydrodynamic performance of FOWTs and can also be used to improve and validate numerical predictions. This research demonstrates that even the most advanced numerical tools can sometimes produce questionable results. In this study it was demonstrated that in some cases the numerical predictions were very close to the results obtained from the experiments but in others the numerical model failed to accurately predict the platform behaviour. Some aspects of the experimental study were also problematic, in particular the amount of time required to set up such a complex experiment and also the problems associated with obtaining the correct mass properties whilst insuring adequate model stiffness in the roll and pitch modes of motion. The Software in the Loop system used to simulate the wind loading has not been validated.

The results from both studies show the benefits of such TLP structures in terms of reduced motions which are vital to obtain a high power output from a wind turbine.

Chapter 1

Introduction

This chapter begins by giving an insight into the topics covered in the thesis then goes on to describe the motivations behind each chapter of the thesis. Individual research aims and objectives are presented and finally the chapter provides an overview of the structure and layout of the thesis.

1.1 Developments in Wind Energy

The world will face a growing shortage in the near future in relation to energy needs. Since traditional energy sources cannot meet the energy demand of the world's increasing population, alternative clean energy sources have become a favourite topic for researchers during the last two decades. Following the Kyoto Protocol in 1997, studies on renewable energy systems have increased significantly and installation of these systems has become widespread. Recently, there has been growing interest in renewable energy sources such as wave energy, tidal energy, solar energy and wind energy which can be counted as the most commonly studied sources of renewable energy.

In order to generate power from wind, wind turbines can be used to convert wind energy to electricity. When compared to other renewable energy sources wind turbines, either onshore or offshore, can yield a large amount of electricity. It was shown by (Sajjadi and Hunt, 2003) that the relatively low surface roughness of the ocean gives rise to higher wind speeds than those found on land. Therefore, offshore wind turbine concepts are the most promising renewable energy systems to generate electricity.

As reported in (Christensen, 2009), wind energy was first used in 1885 to generate electricity by Poul La Cour in Askov, Denmark. In order to provide the electricity demand of Askov High School, he converted an old wooden wind mill into the first wind turbine. Since then, studies on wind turbines and hence the development of wind energy technology to meet the energy demand is increased.

Depending on the water depth, offshore wind turbines can be divided into three main concepts (see Figure 1.1). These are; shallow water foundation, transitional water foundation and deep water wind turbine concepts. The first group consists of three main systems such as monopole structure, gravity base structure and suction bucket structure. These are located in 0m – 30m water depths.

The transitional offshore wind turbines are designed for 30m to 50m depths and are classified as; tripod tower, guyed monopole and enhanced suction bucked or gravity base.

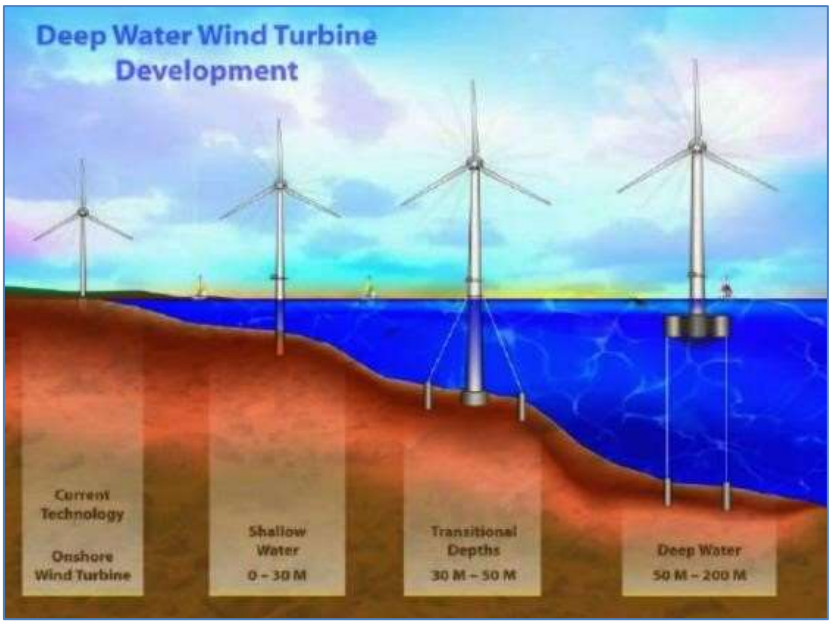

Figure 1.1 Classification of Wind Turbines

Deep water offshore wind turbines are deployed water depths of more than 50m on some form of floating structure or platform. Floating offshore wind turbines (FOWT's) can be categorised in four groups; Spar buoy, Tension Leg Platform, Barge and Semisubmersible.

Due to its significant advantages such as continuity, wind energy has been extensively studied in recent years. A large number of land based installations have been constructed in order to convert wind energy into electricity. These wind farms have some negative environmental effects such as noise, visual impact and some drawbacks for bird life, for these reasons many countries switched their wind energy investments to offshore farms (Esteban et al., 2011, Kaldellis et al., 2012). Compared with land based wind turbines; deep water offshore wind turbines have many benefits such as capturing a more stable wind field with higher average velocities (Pryor and Barthelmie, 2001). Since wind power is proportional to the cube of the wind velocity, a small increase in the wind velocity significantly increases system efficiency

(Kaldellis and Kapsali, 2013). Therefore, floating offshore wind turbines are an attractive option to use the large amount of wind sources in deep water areas.

(Joselin Herbert et al., 2007) presented a list of offshore wind projects built in the last few years in their study. The main projects with respect to installed power were: in the UK, the Lynn and Dowsing (194 MW), in Kentish Flats Project (90MW) and the Burbo Banks project (90MW); in the Netherlands, the Q7 project (120 MW); and in Denmark, the Nysted offshore windfarm (165MW) and the Horns Rev project (160 MW). The cost of the deep water offshore wind projects is higher than shallow water projects. When the water depth is more than 50m, fixed foundations become expensive and are a challenging to design. Consequently many researchers are currently focusing on the application of FOWTs in intermediate and shallow water. In the UK there are a number of sites in the North Sea which are in the range of water depth from 50 to 100m. A summary of all other FOWTs are given in Chapter: 2.

In order to meet the world's energy demands, alternative systems need to be developed. Current developments in offshore wind farms have led to the hope that many countries will satisfy their energy demands using these renewable energy systems. Many governments now support researchers in order to further develop these environmental friendly systems.

In recent years wind energy research has shifted towards floating offshore wind turbines (FOWTs) and a large number of international projects have studied offshore wind and proposed a number of possible alternative designs.

An important development of particular interest is the increase in wind turbine size and capacity. Wind turbine size and other developments are summarised by (Joselin Herbert et al., 2007) (Please see also Chapter:2). The typical wind turbine size was less than 100 kW in the early and mid-1980s. Turbine sizes increased from 100 to 500 kW by the late 1980s and early 1990s and in the mid-1990s, typical turbine size increased from 750 to 1000 kW. This value reached 2.5 MW by the late 1990s. Trends of turbine sizes and capacity are shown in Figure 1.2. Current wind turbines have more than 5MW capacity.

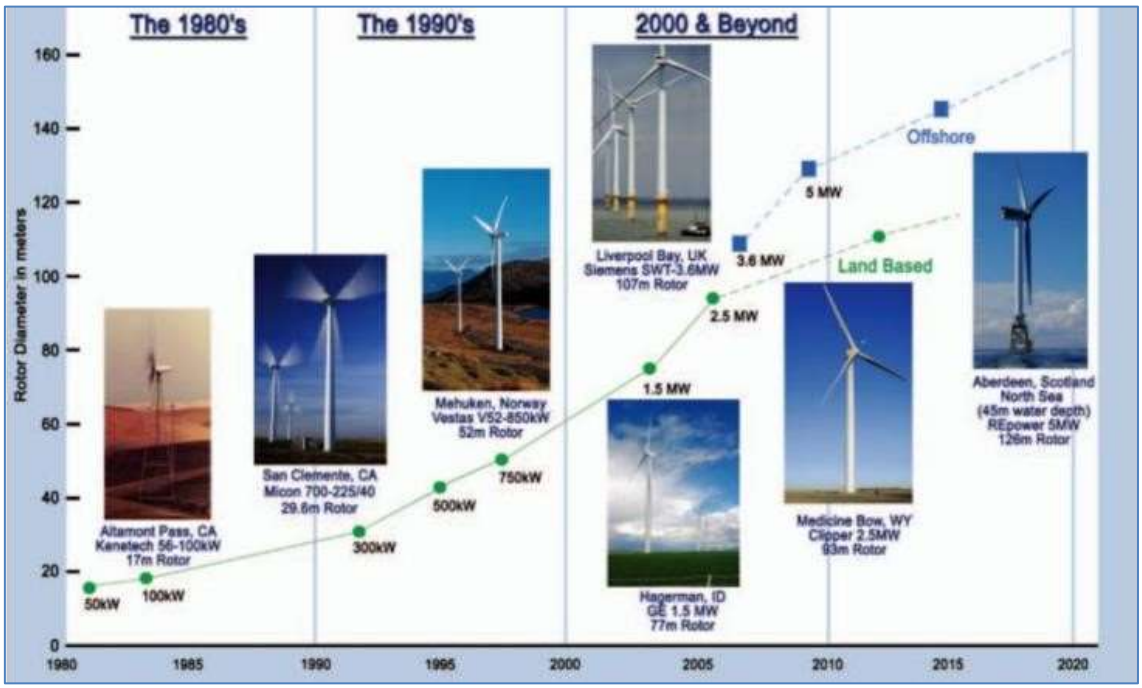

Figure 1.2 Trends of the wind turbine sizes and capacity (US Department of Energy)

In recent years, many studies were carried out to investigate the performance of the floating wind turbines with different turbine capacities. Some of these studies aimed to improve the turbine capacity for the same floater concept and some of them aimed to improve the hydrodynamic performance of the system. Since floating offshore systems have to be designed for each pilot area, the solution is usually unique. For this reason, many optimisation studies were performed to determine the most feasible option for the selected region. The development of FOWT and their performance are discussed in Chapter 2.

Tension Leg Platforms (TLP's) have started to become popular structures both in offshore oil extraction and wind energy sectors. A challenging topic in this field has arisen by the adoption of TLP type wind turbines into water depths of around 70m compared to oil and gas structures with normally operate in greater than 100m water depths. The TLP wind turbine has recently attracted interest due to the negligible heave, pitch and roll motions compared to other floating platforms and the potential to offer significantly reduced structural costs due to the reduced steel weight compared to fixed offshore wind turbines. This thesis will investigate the hydrodynamic performance of TLP employing a 5MW turbine in a water depth of 70m.

1.2 Motivations behind this Work

In order to establish financially viable floating offshore wind turbine designs, the wind energy industry needs to develop cost-effective concepts. Recently a number of different FOWT concepts have been proposed in order to meet this goal. Due to time and cost restraints the first stage design of these concepts requires a numerical approach.

Each FOWT concept needs to be designed for its specific deployment region which usually means each system requires a unique investigation to assess its behaviour. Building and testing the performance of these systems in full scale is not financially viable.

It is critical to be able to predict a FOWT's complex behaviour in the real wind and wave environment which it will experience. This thesis describes a numerical and experimental approach to investigate, in detail, the dynamic performance of a FOWT concept. It presents the results of a detailed correlation study between the two approaches. Similar studies have been published in the literature: but none of these have presented the results of such an extensive study as is reported here. The thesis presents the results of an extensive experiment campaign on a 1:36.67 scale FOWT including free oscillation tests, regular and irregular wave tests. All of the tests were carried out in a simulated wave and wind environment. Numerical predictions were carried out using a fully coupled aero servo hydro elastic code and the predictions are compared with the experimental results.

1.3 Aims and objectives of this research

The main aim of this research is to evaluate the performance of a 5MW FOWT concept deployed in 70m water depth using both numerical and experimental approaches. This thesis aims to fulfil the following tasks.

- *To review the available literature on numerical and experiment methodologies for the prediction of the performance of floating wind turbine systems.*
- *To describe the state of the art numerical tools used in this research and provide results of a program testing study*
- *To describe the experimental set up and test procedure for FOWT concept*
- *To determine the hydrodynamic properties of the FOWT concept and investigate the effect of wind by performing free oscillation tests using numerical and experimental methods*
- *To investigate the platform behaviour in regular waves and simulated wind conditions using a Software In the Loop (SIL) system and compare with numerical predictions.*

- *To characterise the design performance of the FOWT in terms of hydrodynamic responses to realistic environmental loading using numerical and experimental methods.*

1.4 Structure of the Thesis

This thesis begins with an overview of the 'state of the art' in floating offshore wind turbine concepts and presents the main challenges of designing a reliable and cost effective floating concept which has low motion response characteristics in order to provide a stable platform for the wind turbine. The thesis is composed of eight chapters which are summarised below.

CHAPTER 1 (Introduction) presents a general introduction to offshore wind energy, the motivations behind this work and the aims and objectives of the thesis.

CHAPTER 2 (Floating Offshore Wind Turbine Concepts and Methods used to predict their Performance) presents a review of the published literature on the current numerical and experimental techniques developed to predict the behaviour of floating type wind turbines. This chapter first provides a classification of FOWT's, and then describes the developments of the concept. Following this, the numerical and experimental methods used in order to determine the hydrodynamic performance of FOWTs are presented. The advantages of the TLP as a reliable and low cost offshore wind turbine platform are presented.

CHAPTER 3 (Numerical Investigation of the TLP) presents the theoretical background to the numerical programmes used in this thesis along with their assumptions and limitations. The development of a numerical validation model used as a benchmark case study (NREL/MITTLP) is described and the results are presented in this chapter. The modelling of the FOWT used in the study is provided. Finally, a conclusion of the chapter is provided.

CHAPTER 4 (Experimental Setup and Preparation) begins with a description of the Kelvin Hydrodynamics Laboratory where the experimental investigation was carried out and also the scaling criteria for the model used in the experiments. An overview of the experimental procedure for the TLP type wind turbine is presented. Each stage of the calibration methodology is introduced in detail in the subsequent sections. The implementation of Software-in-the-loop (SIL) system is described. This chapter also describes the methodology used in the experimental work. Finally, conclusions relating to the experimental setup are presented.

CHAPTER 5 (Free Oscillation Tests) describes the free oscillation testing procedure performed in the tank to characterise the virtual mass, the natural frequencies and damping of the FOWT.

Free oscillation tests were carried out in four different modes of motion; surge, yaw, heave and pitch. The surge tests were performed for three different wind conditions to determine the impact of wind on the system. Finally, the results are compared to the numerical predictions.

CHAPTER 6 (Regular Wave Tests) describes the regular wave tests carried out to characterise the behaviour of the structure through the motion and tendon tension RAOs. Results of tests performed in head waves with no wind, constant wind load and finally variable wind (SIL) are described. Tests at 45° wave heading are also described in this chapter. Finally, the results of the correlation between experimental and numerical calculations are presented.

CHAPTER 7 (Irregular Wave Tests) describes the key aim of this chapter which is to characterise the motion responses and the tendon loadings of the FOWT under realistic and severe conditions and to compare the experimental results with the numerical predictions. The chapter provides the background theory of the irregular waves and the wind models used in this study. Data processing of experimental results and numerical predictions are provided. Wave analysis, motion analysis, spectral analysis of motions and tendon tensions for storm case are described in detail. Following this, experiment/numerical comparisons for three configuration of the FOWT are given. In addition the experimental results to show the effect of the wind direction on the system are given. Finally, a summary of the chapter is provided.

CHAPTER 8 (Discussion and Conclusions) evaluates the thesis in terms of achieved aims and objectives. This chapter also provides a discussion on the proposed FOWT. Lastly, suggestions for future research are given.

Chapter 2

Floating Offshore Wind Turbine Concepts and Methods used to predict their Performance

This chapter reviews the activities surrounding the development of offshore floating wind turbines (FOWT's). Firstly the motivation behind the development of FOWT's is given in the introduction. Next follows a review of developments in Japan, United States and Europe.

FOWT's are classified into three main concepts and a review of the development of each of these concepts is presented. Following this is a review of the current numerical and experimental techniques used to predict the behaviour of FOWT's. (Jonkman and Musial, 2010)

2.1 Introduction

Wind energy is one of the primary sources of energy amongst renewable sources. Besides solar and marine energy, there is a fair amount of interest in generating energy from wind and therefore a significant amount of research is performed on wind energy converters in developed and developing countries. The total capacity of wind energy converters in the entire world has been reported as 372GW in the end of 2014 by World Wind Energy Association (WWEA) (2015). It is also stated in the same report that UK has got 54% of the offshore market (36% in 2013) and added 813MW capacity of offshore wind turbines. As more than half of all offshore wind turbines are currently installed in British waters, UK makes a significant contribution to the development of the offshore wind sector.

According to the European Wind Energy Association 2015 Statistics on Wind Energy, 13GW of wind power capacity was installed and grid-connected in the EU during 2015 with an increase of 6.3% on 2014 installations. Around 10GW of total capacity were installed onshore and 3GW were installed offshore. It is important to note that 7.8% of annual onshore market reduced in the EU in 2015, while offshore installations more than doubled compared to 2014. Figure 2.1 illustrates that the offshore wind power installations represented 13% of the annual EU wind energy market in 2014 and 24% of the annual EU wind energy market in 2015 (February 2016).

It is also stated in the same report that the total wind power installations are more than any other form of power generation in 2015. Cumulative wind power installations in Europe by the end of 2015 are shown in Figure 2.2 and it illustrates that Germany has the largest installed capacity with 45GW. Spain (23GW), UK (14GW) and France (10GW) followed Germany. Based on 2015 statistics, 16 EU countries have over 1GW wind power capacity installed and nine of these have more than 5GW. It should be noted that Germany has 47% of all new installations in 2015. Poland, France and UK followed with 1.3GW, 1GW and 970MW respectively (February 2016).

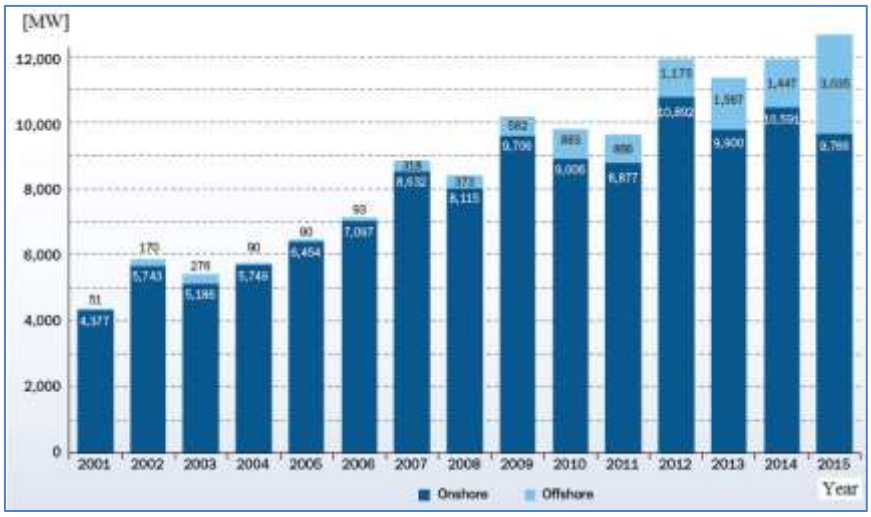

Figure 2.1 Annual Onshore and Offshore Installations (MW) (EWEA, 2015 European Statistics)

Compared to land based installations, offshore wind farms have many benefits such as provision of a more stable source of energy and higher energy extraction due to higher wind velocity in offshore locations. Since wind power is proportional to the cube of the wind velocity, a small increase in the wind velocity significantly increases the power output (Kaldellis and Kapsali, 2013). Land based installations have some negative effects such as visual impacts, noise and impacts on birdlife. In order to avoid the negative effects of the land based wind farms, many developed countries made attempts to deploy offshore wind farms during the last decade (Esteban et al., 2011, Kaldellis et al., 2012). Based on successful applications, there has been growing interest in offshore wind energy. In 2011, 2% of the total wind farms in the world have been reported as offshore installations.

The harnessing of energy from wind has become a very challenging topic for the researchers over the last two decades. Since onshore wind energy systems are not always welcome by public, engineers started to search for alternatives to address this issue and subsequently the design, construction and installation of fixed and floating offshore wind turbines started.

Deployment depths for offshore wind farms and accordingly their distance from the shoreline continue to increase as new and larger structures are designed. The shift towards deeper water leads to such wind farms encountering a much more severe wave environment. With increase in design wave heights, environmental forces acting on the structure also become significant. (Henderson et. al., 2009) reviewed the benefits of applying floating support structures and summarised the technical difficulties of several floating wind turbine systems.

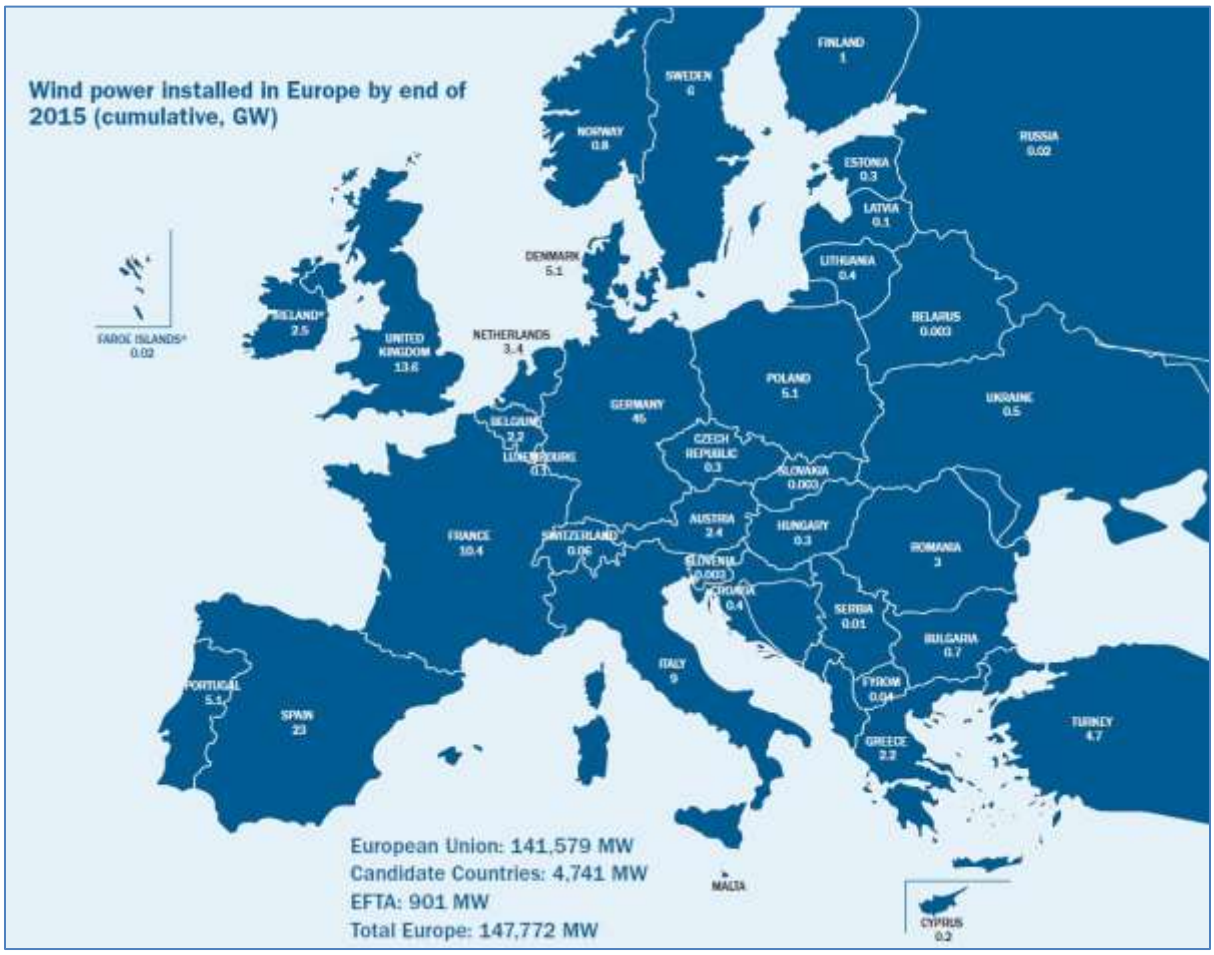

Figure 2.2 Wind Power installed in Europe by end of 2015 (EWEA, 2015 European Statistics)

(Nielsen et al., 2009) performed a detailed study on the ocean, wind and wave utilisation and a brief review of offshore wind energy in Europe was discussed in (Henderson et al., 2003). (Watson et al., 2005) summarised the developments of offshore wind energy in United States in their study. A brief review of the floating wind turbine research can be found in (Wang et al., 2010).

There is still a need for a considerable amount of research concerning offshore wind farms in terms of selection of their optimum configurations for a given location, the development of design and analysis tools, access, inspection and maintenance strategies and environmental impacts.

2.2 Classification of Offshore Floating Wind Turbines

To facilitate the design process of offshore floating wind turbines, a framework was developed by the National Renewable Energy Laboratory (NREL) as described in

(Butterfield et al., 2007) and (Walter Musial and Bonnie Ram, September 2010). Known as the "stability triangle", shown in Figure 2.3, which classifies floating wind turbine platforms considering their methods of achieving static stability into three idealised structures; barge, spar buoy and TLP or semisubmersible, examples of which are shown in Figure 2.4.

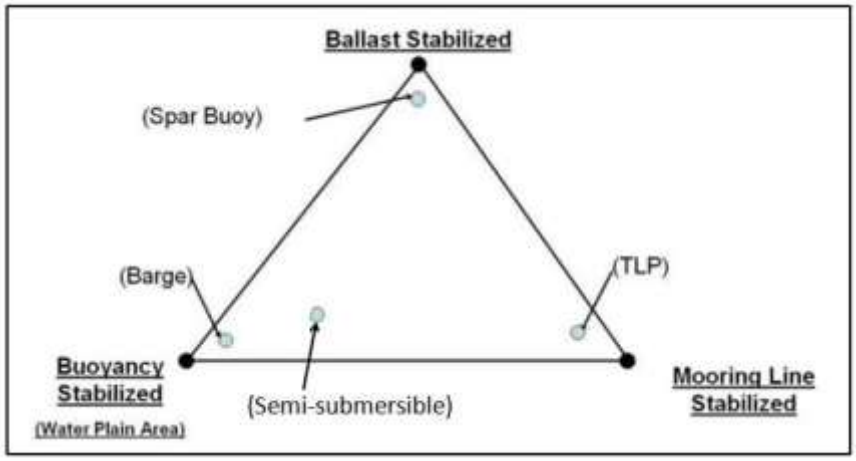

Figure 2.3 Stability triangle for classifying floating substructures according to method of achieving static stability (NREL, 2007 and 2010)

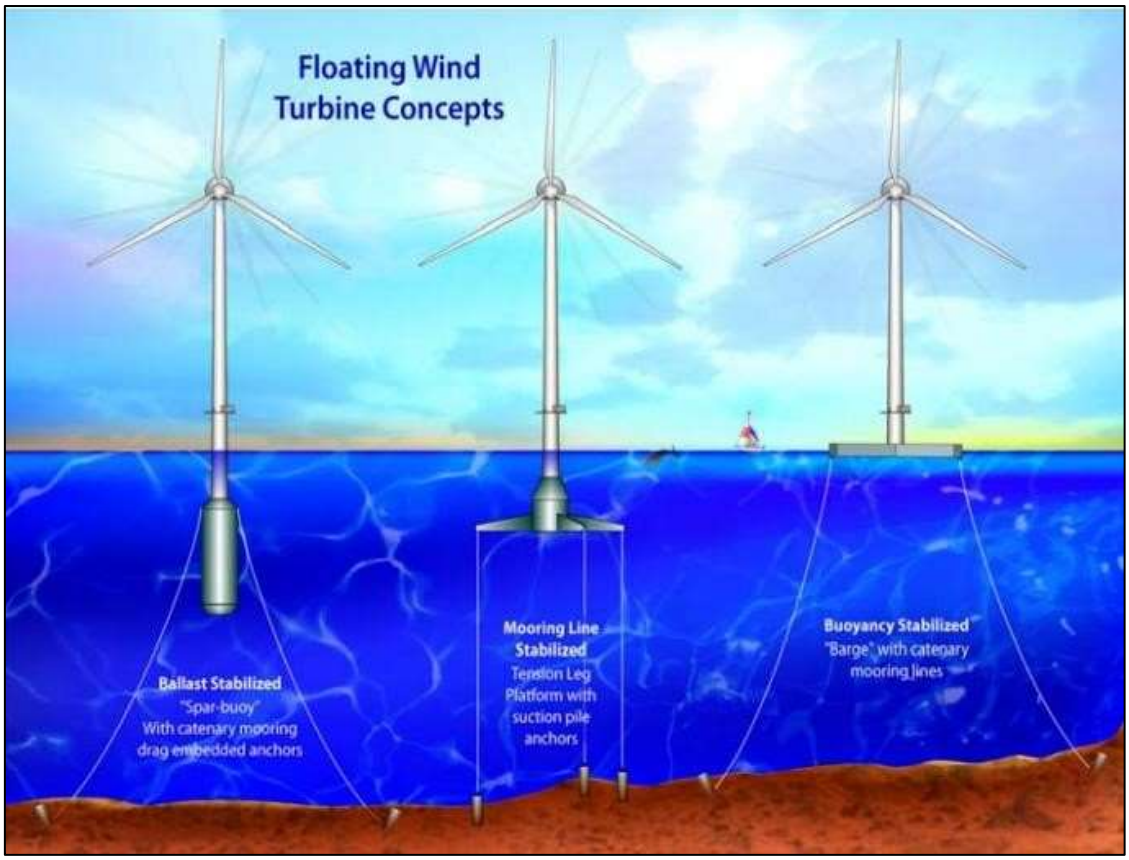

Figure 2.4 Typical Floating Platform Static Stability Concepts (Butterfield et al., October 2007)

Ballast Stabilised: Platforms such as a spar-buoy achieve stability by using ballast weights hung below a central buoyancy tank which creates a righting moment and a high inertial resistance to pitch and roll and they usually have sufficient draft to minimise heave motion (Butterfield et al., October 2007). **Mooring Lines:** Platforms such as Tension Leg Platforms (TLP's) achieve stability through high mooring line tension (Butterfield et al., October 2007). **Buoyancy:** Platforms such as barges achieve stability by using distributed buoyancy, taking advantage of large water plane area for stability. An extensive analysis of the engineering challenges for floating offshore wind turbines was carried out by the NREL and the MIT (Butterfield et al., 2007) in order to identify the multidisciplinary technical problems which require to be addressed before a floating offshore wind turbine can become commercialised. They summarised the benefits and drawbacks of these systems in their study which are summarised in Table 2.1. The table indicates that the TLP provides the highest benefit, high inherent stability and low motions means that the TLP concept is most suitable for the wind turbine design and wind turbine dynamics than the other floating platform concepts although due to the TLP's complex mooring/anchoring arrangements it is also the most expensive solution. The barge type platform is the worst as it is subject to higher wave loading which causes large motions. A barge based solution will require a turbine which can tolerate the larger tower accelerations which will increase turbine cost and lower reliability. The spar buoy concept which is a ballast-dominated system is much heavier that TLP or Barge systems; hence, it can be an expensive solution to deploy. It also has poorer motion damping characteristics than a TLP. Each design challenge and classification of these challenges are explained in detail in (Butterfield et al., 2007). Semi-submersible concept will also be discussed in the following.

Table 2.1 Design Challenge Trade-offs for Stability Criteria (Butterfield et al., 2007)

(+ advantage - minus disadvantage blank neutral.)

	Floating Platform Technical Challenges			
	Platform Stability Classifications			
Platform Design Challenge	**Buoyancy (Barge)**	**Mooring Line (TLP)**	**Ballast (Spar)**	**Semisubmersible**
Design Tools and Methods	-	+	-	+
Buoyancy Tank Cost/Complexity	-	+	-	+
Mooring Line System Cost/ Complexity	-	+	-	

Anchors Cost/Complexity	+	-	+	
Load Out Cost/ Complexity (potential)	+	-		+
Onsite Installation Simplicity (potential)	+	-	+	+
Decommissioning & Maintainability	+	-	+	+
Corrosion Resistance	-	+	+	
Depth Independence	+	-	-	-
Sensitivity to Bottom Condition	+	-	+	
Minimum Footprint	-	+	-	
Wave Sensitivity	-	+	+	+
Impact of Stability Class on Turbine Design				
Turbine Weight	+	-	-	-
Tower Top Motion	-	+	-	
Controls Complexity	-	+	-	
Maximum Healing Angle	-	+	-	

Growing interest in the offshore floating wind turbines has given rise to a large number of concepts and designs. The world's first full-scale floating wind turbine, Hywind, is a spar type design employing a catenary mooring system deployed in the Norwegian sector. Norwegian Renewables Company SWAY® developed is another floating spar type concept with a single taut tether for use in 60-300 m water depths (http://www.sway.no/).

There are also other types of floating platforms that can be used for wind turbines such as semisubmersible types. These are referred to as hybrid concepts since stability is achieved by employing the features from a combination of the three classes outlined in the 'stability triangle'. (Perez, 2014) stated that, this type also can be an alternative "*due to its easier and lower-cost installation as its construction, assembly, outfitting and commissioning can be done quay-side: minimal dynamic coupling between wave-induced and turbine-induced motion and possibility of carrying more on-board systems"*. The WindFloat concept developed by the US based company Principle Power is an example of a semisubmersible platform with catenary mooring lines. The world's second full-scale floating wind turbine, WindFloat, is operating with rated capacity (2MW) roughly 5km offshore of Agucadoura, Portugal. It is a three-legged

floating type foundation which can accommodate a 5MW or larger wind turbine (Roddier et al., 2010). Hywind and WindFloat are operational full scale floating wind turbine prototypes which have provided valuable full scale data which has been used by many researchers in this field. These two concepts have also contributed to the development of standards by classification societies such as DNV (DNV-OS-J103). Japan has a full size prototype floating wind turbine deployed off the coast of Fukushima and Japan also plans to expand this by building two more full scale prototypes (Fukushima-Forward., 2013). WindFloat, Hywind, Ishihara's concept and Hexicon are illustrated in Figure 2.5.

Figure 2.5 Floating wind turbine concepts. From left: WindFloat, Hywind, Ishihara's concept and Hexicon

NREL have designed a 5MW wind turbine (Jonkman et al., 2009) which is used as a reference wind turbine in many studies. It was derived from an onshore wind turbine based on the IEC 61400-3 design standard for Offshore Wind Turbines (IEC, 2009). As a consequence of this the designs of three floating platforms supporting the rotor, nacelle and tower of the NREL 5MW reference system have emerged. These well-known floating wind turbine concepts are shown in Figure 2.6.

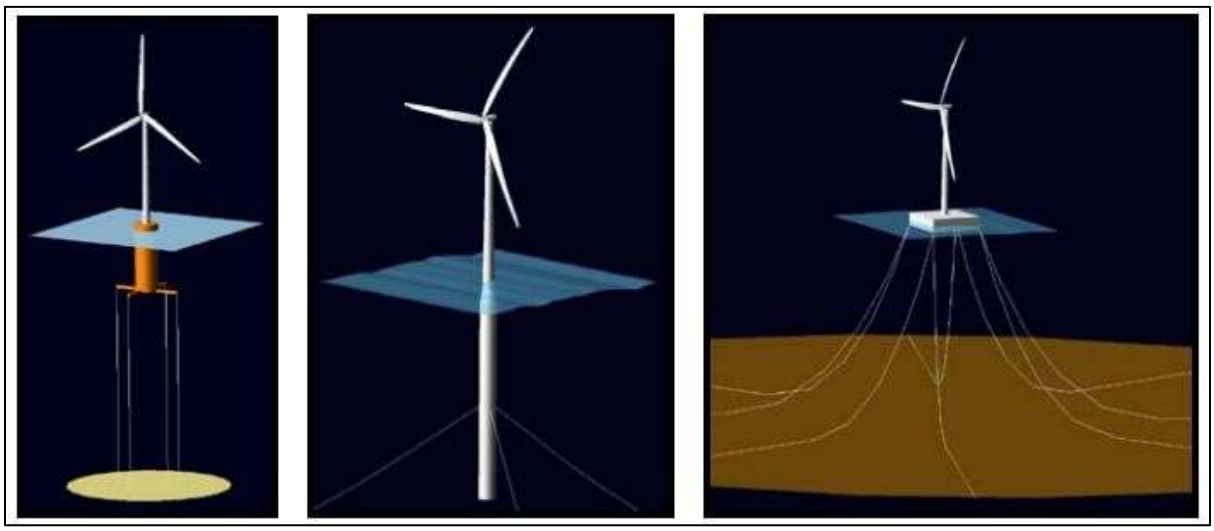

Figure 2.6 NREL 5MW wind turbine on the MIT/NREL TLP, the OC3-Hywind Spar Buoy, and the ITI Energy Barge (Jonkman and Matha, March, 2010)

The MIT/NREL TLP is a modified version of a TLP developed by (Tracy, 2007) from MIT. Tracy carried out a very comprehensive parametric design optimisation process using linear frequency-domain solution techniques for TLPs which can be used with wind turbines. After modifications, the final TLP (the MIT/NREL TLP) consists of a cylindrical platform which is ballasted with concrete and moored by four pairs of vertical tendons in tension. As can be seen from Figure 2.6, each pair of tendons attaches to a spoke that radiates horizontally from the bottom of the platform. The design properties of MIT/NREL TLP are discussed in Chapter 3 and more details can be found in (Matha, 2009).

As a part of the Offshore Code Comparison Collaboration (OC3) Project, OC3-Hywind spar buoy concept was developed (Jonkman and Musial, Technical Report, 2010). The Hywind concept coupled with the NREL 5MW reference turbine was investigated in this project (Jonkman, Technical Report, May 2010).

The ITI Energy barge concept was developed by the Department of Naval Architecture and Marine Engineering at the Universities of Glasgow and Strathclyde through a contract with ITI Energy. The barge is square, ballasted with seawater and employs eight catenary mooring lines. Stability problems required the control system for the NREL 5MW reference turbine to be re-tuned (Jonkman, 2007). Three floating offshore wind turbine concepts described above are compared and summarised in (Jonkman and Matha, March, 2010).

In order to form a reliable and functional base for offshore wind turbines, three main concepts have emerged, namely TLP's, spar buoys and semisubmersibles. TLP's are still in development for intermediate to deep waters and together with the other alternative foundations such as spar buoys and semi-submersibles continue to attract a great deal of interest from the FOWT industry.

TLP's are used in the oil and gas industry due to their excellent motion characteristics. Designed for deep water, their initial construction and deployment costs are high even for this sector. The TLP concept is nevertheless an attractive solution for FOWT's because the total weight of such structures are considerably lighter than those designed for the oil and gas industry. For example the displacement of the MIT/NREL FOWT is 12,500tonnes whereas the displacement of the Ursa Oil and Gas Production TLP is 97,500tonnes. TLP based FOWT designs have a far smaller displacement and water plane area than other concepts. The wave

induced forces on a FOWT TLP structure are relatively small which simplifies the mooring system design due to the lower required initial tensions leading to smaller diameter mooring cables (tendons) and a simpler subsea connection. The most important characteristics of a TLP structure is the significant reduction of vertical and rotational motions, leading to minimal motion excitation to the wind turbine stationed on it.

This section has presented the classification of FOWT s into three main concepts namely Ballast Stabilised, Mooring Line Stabilised and Buoyancy Stabilised. The ballast and mooring stabilised systems have characteristically reduced motions and FOWTs are generally based on these concepts. The buoyancy Stabilised systems in general, have large motions leading to a more complex turbine design. The hybrid concepts such as semisubmersibles employing a range of different mooring systems are also of interest. Since the optimal solution is site-specific for floating offshore wind turbine systems, developments of these different systems will continue in the future.

2.3 Offshore Floating Renewable Energy Developments

This section describes the growing number of floating wind turbine concepts currently being developed all around the world. The differing requirements of floating technology worldwide have led to many different developments which depend on the local wind resources and water depth. The next sections provide an overview of floating wind turbine developments in the areas around the world with a significant amount of activity i.e. Japan, US, and Europe.

2.3.1 Japan

New Energy and Industrial Technology Development Organisation (NEDO) indicated that 80% of Japan's offshore wind resources are in the deep water.

After the Fukushima nuclear accident in March 2011, floating offshore wind turbines gained importance in Japan. In February 2013, the Tokyo Smart Energy Week Exhibition and Conference was held in Japan with the participation of the international floating wind industry to discuss the implementation of new deep water floating wind turbine projects. This event provided insight into Japan's projects such as Fukushima Floating Offshore Wind Farm Demonstration Project. As explained in (Report, May 2013), from that point onwards, Japan became major player in the development of the offshore floating wind turbines. It is indicated in (Report, May 2013) that various floating wind turbine projects in Japan and Europe are in the design and development stage and many of the designs were also investigated through experiments in the ocean basins.

Two advanced spar concepts with different wind turbine capacity, 4 column semisubmersible and a 3 column semi-submersible were tested as a part of the Fukushima Floating Offshore Wind Farm Demonstration Project are described in
(http://www.marubeni.com).

The Wind Lens Project was developed by Kyushu University's Division of Renewable Energy Dynamics. In 2011, The University launched a one year test with a scale model of an 18 meter diameter floating platform mounted with two 3kW turbines 600 m from shore in Hakate Bay in Japan. Solar panels were also attached to this pilot prototype. In the second stage of this project a 80 m diameter TLP type floating wind turbine with 200kw capacity was tested 2km from land. It was reported that the final design also includes wave power besides wind and solar (http://www.riam.kyushu-u.ac.jp).

Another project developed for Japanese waters involved a spar-buoy type floating offshore wind turbine for 80-100m water depth near Kabashima Island in Kyushu. Installation of a 2MW turbine was planned for mid-2013 with the full scale pilot (http://www.kyoto-u.ac.jp).

Japan Marine United's Advanced Spar was developed in collaboration with the University of Tokyo. In order to minimise the impact from sway and heave, "reduced vacillation fins" which are drag surfaces which are added to the substructure were used in the design. It was planned to be used for both the Fukushima project and Mitsubishi's 7MW wind turbine (http://www.jmuc.co.jp).

Mitsui Shipbuilding has been developing several floating wind turbine technologies and is mainly focused on TLPs and semi-submersibles. The company have developed a semisubmersible with a 2MW wind turbine as part of Phase 1 of the Fukushima project (http://www.mes.co.jp). Mitsui Shipbuilding has also developed a TLP with collaboration with Tokyo University, Shimizu Corporation, Maritime Research Institute of Japan and Tokyo Electric Power Company.

A new hybrid concept was introduced in Tokyo Smart Energy Week in February 2013. This concept consists of a floating wind turbine and a wave generator designed to be deployed near remote island communities. It is reported by MODEC (Mitsui Ocean Development & Engineering Company) that "*the floating structure supports the power generation assembly via a set of rubber mounts like a gimbal to isolate the power generation assembly from the wave*

motion and the Savonius turbine acts as a ballast, making the power generation assembly self-righting" (http://www.modec.com).

Mitsubishi has developed a number of projects over the years. As a part of the Fukushima floating offshore wind demonstration project, a semisubmersible utilising the Mitsubishi's 7MW hydraulic turbine was deployed in 2015 (http://www.mhi.co.jp).

The National Maritime Research Institute (NMRI) developed a floating barge concept to mount wind turbines. After performing numerical calculations, NMRI developed another concept, spar-buoy type floater wind turbine. As this concept achieved good performance, currently it is the main focus of development for the NMRI. After performing tank tests for this concept, a patent application for the spar-buoy concept was filed. NMRI is also took in part the Kabashima Island Spar Project (http://www.nmri.go.jp).

In order to develop a design for a floating offshore wind turbine, Shimizu Corporation has been jointly working with University of Tokyo, Tokyo Electric Power Company and Penta Ocean Construction Co. Ltd. Shimizu's International Institute of Technology has carried out a large number of projects on offshore wind, including the impact of wind and waves on structural integrity (http://www.shimz.co.jp).

2.3.2. The United States

According to the National Renewable Energy Laboratory (NREL), US have 61% of its wind resources in more than 100m water depth.

As reported in (Report, May 2013), the U.S. Government aims to achieve 20% of its total energy supply from onshore and offshore wind by 2030. Since the majority (61%) of US wind resources are in deep water, the US Government and industry have focused on a number of concepts to develop offshore floating technologies. The National Renewable Energy Laboratory (NREL) which is a US Government Organisation plays a major role in the advancement of technologies for offshore floating wind turbines from the concept stage to commercial application stage.

The US Department of Energy announced in 2012 funding of $168 million over six years for seven Advanced Technology Demonstration Projects. The main objectives of these projects were to accomplish more cost effective solutions than existing technologies and to develop viable and reliable solutions for the United States. Three of these projects consist of floating type foundations. In the first project Statoil, North America of Stamford, Connecticut proposed

to deploy four spar-buoy type floaters supporting 3MW wind turbines in the Gulf of Maine off Boothbay Harbour at a water depth of 140m. In order to decrease the installation costs, these spar buoy concepts are planned to be assembled in a harbour and towed to the deployment area. In the second project two concrete semi-submersibles with 6MW directdrive turbines are planned to be deployed as a pilot floating offshore wind farm near Monhegan Island by the University of Maine. The third project was undertaken by Seattle, Washington-based Principle Power to install five semi-submersible floating foundations with 6MW direct-drive wind turbines. The deployment area was selected 10 to 15 miles from Coos Bay, Oregon. To reduce the installation costs, Principle Power planned to assemble the semi-submersible structure near the project site in Oregon (Report, May 2013).

Principle Power, based in Seattle, WA, is a well-known technology developer for offshore market. The WindFloat is attached with patented heave plates (water entrapment) at the base of each column which improved the motion performance of the system due to the increased motion damping. The first full scale 2MW WindFloat was deployed off the coast of Portugal in 2011. It is reported that the Principal Power is also developing other projects in Europe and for off the Oregon coast (http://www.principlepowerinc.com).

In May 2011, researchers from the University of Main performed extensive tank tests of different foundation models at the MARIN's Wind and Wave Test Basin in the Netherlands as a part of the DeepCwind Consortium. Following this, a design was selected 1/8 scale for the pilot test in the Gulf of Maine based on the tank tests results. The concept consists of concrete hull and a composite tower with a 20kw turbine. Two full scale 6MW floating turbine concepts are planned to be deployed in 2016 (http://www.deepcwind.org).

Another well-known concept from the US is Pelastar developed by Glosten PelaStar in 2006. It consists of a TLP type floating offshore wind turbine whose assembly can be done at quayside. It provides a deep water capacity with cost-competitive bottom-fixed turbine foundations in water depths of 60m and greater.

The Advanced Floating Turbine (AFT) developed by Nautica Windpower is a hybrid of tension leg platform (TLP) and semisubmersible. After performing extensive operational studies and design optimisations numerically, Nautica Windpower carried out model testing of turbines in simulated wind and wave environments. Tests were also conducted using small scale models of the AFT in a wave tank to investigate the concept. Following this, larger scale models of the AFT complete with rotor system were tested in the relatively calm water of small ponds and

also in the more severe environment of the Great Lakes. The company plans deploy a prototype in open water in 2016 and plans to produce a commercial design by 2018 (http://www.nauticawindpower.com/).

2.3.3 Europe

Europe has significant offshore wind resources in more than 50m water depths which means utilisation of these resources requires floating technologies.

In 2009, the Hywind spar concept which has 2.3MW turbine deployed in off Karmoy, in south-east Norway. It was anchored to the seabed using a three-point mooring spread. Based on Statoil's report, the Hywind spar in Norway has a capacity factor of over 40%. It is recorded in (http://www.statoil.com) that Hywind generated 10.1GWh of electricity in 2011 giving a capacity factor of 50%. Output was decreased in 2012 due to local grid issues. Potential additional test locations were defined as Norway, Scotland, Maine (USA).

SWAY is a Norwegian development which is capable of carrying a 10MW turbine as well as commercially available 5MW turbines. It is stated in (http://www.sway.no/, Report, May 2013) "the SWAY's floater technology allows economical extraction of wind power in regions with good wind resources and access to water depths of 80-400m within 50-60km from the coast". The first tests of a 1/6 scale model in Hjeltefjorden outside Bergen started in June 2011 but the model sank in November 2011 due to severe wave conditions. According to the report published by Maine International Consulting in 2013, water entered the J-Tube for the cable connection which caused the system to tilt. NREL who collected the data during this demonstration period reported that the wave height was in excess of 6.3m when the model was lost. Another 1/6 scale model was deployed in 2012. In order to deploy in the UK and in China, a version of the SWAY concept with a shorter and wider tower was developed to operate in 50-60m water depths. Developers of the SWAY concept include Statoil, Statkraft, Shell Technology Norway (STN), Lyse, The Research Council of Norway and Inocean with NREL being responsible for data analysis and collection.

The development of the Norwegian WindSea concept started in 2005, initial concept work was completed in 2006 and the concept was granted a patent in 2010. WindSea is a semisubmersible platform with 3 columns and three wind turbines. The platform employs a detachable turret which allows the platform to weathervane (www.windsea.no, 2016).

Poseidon wave energy device absorbs wave energy, by reducing the heights of the waves which creates calm water behind the platform which allows for ease of access for maintenance activities. In 2008/2009 initial full scale tests were conducted off Onsevig Harbour, at the north coast of Lolland in Denmark. These tests were designed to investigate platform stability including the impact of the wave absorption floaters on the overall platform stability. After these successful tests DTU/Risoe and DHI gave approval for the installation of the wind turbines on the Poseidon platform. In 2009/2010, power grid systems and the efficiency of the wave energy absorption floaters were investigated as a part of Test Phase 2. Finally, Test Phase 3 started in September 2012 in order to export power to the grid from both the wind turbines and the wave absorption system (http://www.floatingpowerplant.com).

Prototype tests of Blue H which is a TLP type concept started in December 2007 off the coast of Italy. In 2008, Blue H developed a 2MW TLP as a part of Phase II. In 2013/2014, tests employing a commercial 5MW turbine were completed and tests of the innovative "selfinstalling TLP" were carried out successfully. In 2014/2015, the full scale 5MW demonstrator was installed and tested. It was announced that the Blue H TLP will be developed on a commercial basis from 2016 (http://www.bluehgroup.com).

A multi-megawatt floating wind turbine technology development project, Windflo is the first French floating wind turbine concept. The completion of the demonstrator design phase was announced by Nass et Wind in April 2013. According to (http://www.nass-et-wind.com), a full scale prototype was built in 2013 and deployed in 2014 off Le Croisic on the Brittany peninsula in 35m water depth. Initially, the plan was to use a 2-3MW turbine, however, the demonstrator was fitted with a 1MW two-bladed turbine which was deployed near the island of Groix, the system was deployed for 18 months.

Another development from France known as Vertiwind which was tested in 2009 using a 35Kw horizontal axis turbine as part of a 1/10 scale test. A full scale 2MW prototype was deployed in France in 2013. The next phase of the project will be part of the EU co-funded INFLOW (Industrialisation setup of a Floating Offshore Wind Turbine) project which aims to install an improved 2MW turbine (http://www.technip.com).

The IDEOL platform, another French design is a ring-shape surface floater with a shallow draught and compact dimensions developed jointly by Gamesa and Stuttgart University. Tank tests were carried out in a range of wave, wind and current conditions, with waves up to 25m height and wind up to 90km/h, representing the most severe operating conditions. Currently,

the industry partners are aiming to launch a test platform of IDEOL with a 2MW turbine for a minimum of 2 years (http://www.ideol-offshore.com).

A TLP type wind turbine, GICON-SOF, developed by one of Germany's largest privately owned engineering companies is designed to be deployed in water depths from 20m to 700m. The modular nature of the design allows for cost efficient manufacturing. In order to cater for use in different sea bed conditions, various mooring technology options are possible. Initial tests indicated that the system has low accelerations and low displacements (http://www.gicon.de).

Spanish Company Iberdrola has been developing TLP type concepts to be used with 2MW and 5MW turbines. Iberdrola performed extensive tank testing with both designs at Madrid's CEHIPAR centre. Two different floating designs for 2MW and 5MW turbines at 1/32 and 1/40 model scales were used. Two innovative installation systems for these floaters, barge/pontoon and float mechanism were also tested during this work. The excellent performance of the system was confirmed following a wide range of tests including some tests in very severe sea states.

The TLPWIND UK Project (funded by Innovate UK) aimed to improve and further develop Iberdrola E&C's TLP based floating technology for offshore wind turbines. The project was led by Iberdrola E&C, with partners the University of Strathclyde and the Offshore Renewable Energy (ORE) Catapult. This project focused on developing 5MW TLPWIND floating technology for offshore wind turbines tailored for UK waters (specifically for Aberdeen coast). The tests which were carried out in Kelvin Hydrodynamics Laboratory in the Naval Architecture, Marine and Ocean Engineering department at University of Strathclyde form a part of this thesis.

Another offshore wind technology development from Spain HiPR Wind is a large semisubmersible designed for research purposes. This 1.5MW concept was deployed off the coast of Bilbao in 80m water depth (http://www.hyperwind.eu/).

Sea Twirl (a spar type vertical axis wind turbine) prototype was tested off the coast of Sweden in 2011. After this successful deployment the company built and tested a larger prototype at a scale of 1/50. The prototype test results were successful in rough seas with wind up to 25m/s and waves between 2 and 3m. Parallel to these studies, theoretical work and model tests at 1/500 scale were carried out (http://seatwirl.com/).

The Gusto Trifloater semisubmersible developed in the Netherlands since 2002 was designed to operate in greater than 50m water depth in typical North Sea conditions using a six line catenary mooring arrangement. The latest 5MW design was tested in 2011 at the MARIN test facility (http://www.gustomsc.com).

2.3.4 Summary

This section has highlighted the major projects and developments in the area of offshore floating wind turbines. The majority of concepts involve semisubmersible, spar or TLP type structures. Current developments are focused on 5-6MW turbine solutions. The majority of work in this area has traditionally been concentrated in Japan, US and in Europe. With increasing interest in Asia it is expected that the progress of these technologies will continue to accelerate. The increasing number of offshore wind activities moving towards commercialisation highlights the growing global market for these technologies.

2.4 Numerical Studies on Offshore Floating Wind Turbines

In recent years, the development of numerical simulation tools has increased in order to better predict the performance of FOWT's. Simulation tools and the so called design codes have been developed which integrate the aerodynamic models, control system (servo) models, and structural dynamic (elastic) models into a fully coupled (integrated) simulation environment. Developed for land based systems these tools have now been extended for use in the offshore environment where the additional dynamic behaviour must be considered as well as the dynamic coupling between the motions of the platform and the turbine and also the dynamic characterisation of the mooring system (Jonkman, 2007). (Cordle and Jonkman, 2011) performed an extensive review of the available FOWT computer simulation tools as a part of the European UpWind project. This review included FAST (Fatigue, Aerodynamics, Structures, and Turbulence) ((Jonkman, 2007) and (Karimirad, 2013)), HAWC2 (Karimirad, 2013) and (www.hawc2.dk, 2016), FloVAWT (Collu et al., 2014), Simo-Riflex ((Karimirad, 2013) and (Wang et al., 2014)) and CALIHYPSO of EDF R&D (Antonutti et al., 2016).

As was mentioned previously, the first full scale spar-buoy type floating wind turbine was deployed off the south-west coast of Karmoy Island, Norway as a part of Hywind demonstration project. In order to simulate the dynamic response of the Hywind spar concept, a computer tool was developed by (Skaare et al., 2007b). HAWC2, developed by Risø National Laboratory is a state-of-the-art aero-elastic code designed to analyse the response of fixed foundation wind turbines. SIMO/RIFLEX was developed by MARINTEK to simulate the

dynamic response of marine structures. SIMO/RIFLEX and HAWC2 were subsequently integrated and named SIMO/RIFLEX/HAWC2. This code was tested and verified by separate SIMO/RIFLEX and separate HAWC2 simulations. A SIMO/RIFLEX/HAWC2 model of Hywind used in experiments in 2005 was also developed and tested for the same met ocean conditions and with the use of the same, special, dynamic, blade pitch control system that used in the model scale experiments in MARINTEK laboratory.

According to the IEC 61400-3 design standard for offshore wind turbines, in order to develop a cost-effective, high-performance floating offshore wind turbine an integrated load analysis has to be carried out before a turbine is certified. This analysis is not only a requirement under IEC 61400-3, but it is also important at the concept design stage. The integrated load analysis can be carried out using numerical aero-hydro-servo-elastic simulation tools such as FAST, GH Bladed, or FLEX. These numerical tools are based on an integrated modal and multibody structural-dynamics formulation in the time domain. These codes are preferred by researchers since they are able to carry out numerous design-load scenarios in a relatively short computational time. Modelling of fixed-bottom offshore support structures can also be performed using these numerical tools. It should be noted that the hydrodynamic loads are usually simulated in these codes using Morison's equation which is really only valid for small diameter cylinders. Furthermore, as stated in (Matha, 2009), "important effects for offshore floating platforms, like free-surface, memory or a typical added-mass-induced couplings between modes of motion in the radiation problem, are ignored" in addition in these codes "the diffraction problem is simplified using G.I.Taylor's long-wavelength approximation".

There are also more advanced simulation codes such as MSC ADAMS and SIMPACK which provide higher-fidelity multibody-dynamics and can integrate more advanced aerodynamics formulations such as CFD, free vortex wake models and structural models. These codes are expensive in terms of computational time and they are currently not the best option to carry out all extensive load case simulations defined in the IEC 61400-3 design standard.

The linear frequency-domain approach which is based on finding the response amplitude operators (RAOs) for the platform's six rigid body modes has been used by a number of researchers. (Bulder, 2002) carried out a frequency domain analysis for a tri-floater design employing 5MW turbine. The same method was also used by (Lee, 2005) in order to investigate a 1.5MW turbine, and by (Wayman et al., 2006) and by (Wayman, 2006) to analyse a number of TLP and barge concepts. (Vijfhuizen, 2006) designed a wind and wave power barge which

consists of 5MW turbine with an oscillating water column (OWC). (Tracy, 2007) carried out a parametric study for a TLP optimisation and slack and taut catenary spar-buoy concepts using a frequency domain approach described by (Wayman, 2006).

The Linear frequency domain approaches, by their nature, do not account for the nonlinear structural dynamics, aerodynamics, hydrodynamics and transient effects. A number of research groups used time domain simulation methods to overcome the abovementioned limitations. In order to investigate the effects of platform motions on turbine fatigue loads, a so-called state-domain method was applied by (Henderson and Patel, 2003). (Withee, 2004) used a modified version of aero-servo-elastic design code including platform motion and hydrodynamic loading based on Morison's equation.

In this research, all the numerical load analysis was carried out using the sophisticated GLcertified (Manjock, 2005) aero-servo-elastic design code FAST: Fatigue, Aerodynamic,
Structures and Turbulence developed by the NREL's National Wind Technology Center (NWTC). FAST provides a fully coupled integrated simulation environment for modelling floating offshore wind turbine concepts. It uses a combined modal and multibody approach, including structural dynamics and employs an advanced blade element momentum approach (BEM) in order to represent the aerodynamic properties. FAST includes module AeroDyn, and it is also enhanced by the coupled hydrodynamics module HydroDyn. The AeroDyn module calculates the aerodynamics using a state-of-the-art blade element moment approach (BEM) together with empirical corrections to calculate the rotor aerodynamics. The HydroDyn module enables simulations in time domain taking into account the linear hydrostatic restoring, nonlinear viscous drag, and sea current forces. It calculates the added mass and damping values from the linear radiation potential, including the free-surface memory effects, and the incident-wave excitation forces from the linear incident and diffraction potentials, and includes a quasi-static mooring line module.

(Jonkman, 2007) used FAST to analyse the ITI Energy Barge concept, where he defined the dynamic response and extreme loads and instabilities resulting from the dynamic coupling between the turbine and the floating barge system. The effects of the increased pitch motion on the extreme loads and characterisation of the instabilities in yaw are some of the important results from his thesis. Additionally, (Jonkman, Technical Report, May 2010) defined and developed a preliminary FAST model of the well-known OC3 (Offshore Code Comparison

Collaboration) Hywind spar-buoy concept as a part of the Benchmark Exercise of AeroElastic Offshore Wind Turbine Codes project.

(Sclavounos, 2007) performed a fully coupled analysis for a floating wind turbine system supporting a 5MW wind turbine moored to the sea bed using pre-tensioned tendons in a TLP arrangement as well as a standard catenary arrangement. The results indicated that TLPs are superior choices due to their low RMS accelerations and negligible heave and pitch motions.

Many researchers ((Shimada et al., 2007), (Ishihara et al., 2007a) and (Ishihara et al., 2007b)) carried out studies in order to determine the dynamic response of a semi-submersible type floating offshore wind turbines. In particular these researchers investigated resonance conditions during which the subsequent large nacelle accelerations increase the turbine and drive chain loads and hence affect turbine reliability.

The importance of control strategies on fatigue life of floating wind turbines was discussed by (Skaare et al., 2007a). They tested a wide range of environmental conditions and different wind turbine control schemes. Their study indicated the importance of the effect of pitchangle control of blades on the dynamic response of the floating wind turbine for wind speeds above the rated speed. (Suzuki and Sato, 2007) carried out a study to investigate the load on turbine blade induced by motion of floating platform and to define the design requirement for the platform. In their paper, the effect of stabilising the fin attached at the base of the floating foundation in reducing the pitch motion of the spar-buoy type floating offshore wind turbine was investigated.

(Matsukuma and Utsunomiya, 2008) carried out a motion analysis of a spar-buoy type FOWT considering the rotor rotation under steady wind conditions. The Blade Element Momentum (BEM) theory was employed in order to calculate the wind loads acting on the rotor blades. Motions such as yaw, sway and roll included the effects of the gyroscopic moment due to the rotor rotation. (Karimirad and Moan, 2010) performed a structural dynamic response analyses of a spar-buoy type FOWT for extreme sea conditions. They carried out a numerous numerical simulations to determine the structural responses of the parked floating wind turbine under extreme conditions. The dynamic analysis of a spar-buoy type floating offshore wind turbine was investigated by (Bagbanci et al., 2011).

(Henderson and Patel, 1998) presented analytical and numerical design tools in order to assess the performance of semi-submersible floating wind turbines. (Zambrano et al., 2006) developed a numerical model for a deep water offshore design incorporating three wind turbines tested in the

Gulf of Mexico storm conditions. They used a Fourier spectrum based model and WAMIT to model the wave forces on the platform.

A fully coupled dynamic analysis of an FOWT was investigated by (Withee and Sclavounos, 2004). Fully coupled time domain numerical simulations for a 1.5MW wind turbine mounted on a TLP floater were performed to determine the system responses under wind and wave forces. The authors indicated that the damping from the turbine rotor appears to obey a linear law and had a similar magnitude to the hydrodynamic damping.

(Lee, 2004) performed a numerical study to analyse the responses of FOWT's under wind and wave conditions. In order to compare the performance of the two floater concepts, he carried out a frequency domain response analysis for both TLP and spar-type designs in his thesis.

(Bae et al., 2010) carried out a rotor-floater-tether coupled dynamic analysis on a mini TLP type floating offshore wind turbine. The dynamic coupling between platform, mooring-floater and rotating blades was taken into account and analysed.

(Sclavounos et al., 2010) developed two low weight, motion resistant FOWT concepts for deployment in water depths ranging from 30 to 150m and in sea states with significant wave heights up to 14 m. The first concept was a TLP moored to gravity anchors with tensioned vertical tendons while the second concept the Taught Leg Buoy (TLB) is moored to the gravity anchors with taught mooring lines inclined relative to the seafloor. The authors used WAMIT to calculate the linear wave forces and moments acting of the buoy floater and the LINES computer program to model the mooring line static and dynamic loads. They also extended this program in order to take into account the elastic deformations, hybrid mooring lines including segments made out of chain, wire and synthetic materials and intermediate ballast loads. FAST also was used in order to model the wind turbine rigid body dynamics. It is found that the fluctuating wind forces on the wind turbine rotor do not significantly affect the rigid body responses of the TLP and TLB. The linear wave loads and the system responses were resolved for both concepts in the frequency domain. The TLB dynamic tensions in water depths of 30-50m showed comparable performance with the tensions of TLP in water depths more than 50m. The authors concluded that the TLB is suitable for the water depths less than 50m and the TLP is more suitable for deployment in water depths greater than 50m.

(Zhao et al., 2012) developed a new multi-column TLP foundation (WindStar TLP) for the NREL offshore 5MW reference turbine using the same site-specific environmental conditions as the OC3-Hywind (NREL) conditions. FAST was used as a numerical tool to carry out an

aero-hydro-servo-elastic coupled analysis for the proposed design. The results indicated that the elasticity of the turbine system and TLP plays an important role in predicting the natural frequencies of the floating wind turbine. Furthermore it was reported that for all conditions the turbine did not excite any of the resonant modes of the platform. All statistics of key parameters were also compared with MIT/NREL TLP design. The results showed that the WindStar TLP exhibited good motion characteristics under extreme wind and wave conditions with a lighter and smaller design.

There are also studies based solely on the optimisation of floating wind turbine foundations. In a study carried out by (Bachynski and Moan, 2012), five different parametric singlecolumn TLPWTs have been designed and analysed under four different wind-wave conditions by using the Simo, Riflex and Aerodyn numerical tools in a coupled analysis to estimate the platform motions and structural loads on the turbine components and tendons.

Several design codes developed for wind turbines are compared within the framework of *Offshore Code Comparison Collaboration Project* and its successor (known as OC3 & OC4) (Jonkman and Musial, 2010). The codes known as *FAST*, *Bladed*, *ADAMS*, *HAWC2*, *3Dfloat*, *Simo* and *SESAM/DeepC* were compared for OC3 Phase IV, which addressed the spar-buoy concept called" Hywind". Results for free oscillation tests in surge showed good agreement between codes. *FAST* was used by both *NREL* and *POSTECH* (Pohang University of Science and Technology) and the results generally compare well; however POSTECH's results suggested underestimation of hydrodynamic damping. The results showed that the codes which do not include quasi-static model such as *SESAM* and *DeepC* that model the dynamics of the mooring system give higher energy in the spectra of fairlead tension above the peak wave period. Mooring loads were different depending on quasi-static model versus those using a dynamic model. In general, the results show that numerical stabilities can be an issue depending on the version used for simulations. *MSC ADAMS* and *SIMPACK* are found to be expensive in terms of simulation time. Therefore, considering issues of accuracy, availability and simulation time, *FAST* version 7 was selected for the present study and all relevant modules were used to carry out all numerical analysis for this study. More details are given in Chapter 3.

This section has summarised the numerical approaches used and numerical studies performed in the development of FOWT's. The inherent limitations of frequency domain methods and the advantages of time domain approaches are described.

2.5 Experimental Studies on Offshore Floating Wind Turbines

Model scale tests have advantages compared to full scale tests in terms of reduced time, resources and risk. As explained by (S.K.Chakrabarti, 1987), physical modelling methods have been widely used in many marine hydrodynamics applications such as large scale offshore vessels and structures by the oil and gas industry, military, and marine industries. However, there is still a significant need to investigate the methodology for experimental testing of FOWT concepts particularly due to the complex nature of the interaction between the hydrodynamics of the underwater structure coupled with the aerodynamic loads imposed by the turbine blades. In this section, experimental studies carried out by researchers to investigate the dynamic behaviour of FOWT concepts are summarised.

Force Technology has been developing the WindSea concept since 2006 which is designed for Norwegian waters. This system consists of a three column semi-submersible and three wind turbines. The concept employs skirt dampers attached at the lower end of each column in order to reduce the semisubmersible platform motions. They carried out 1:64 model scale experimental study in a wind tunnel and in a wave basin in order to verify the main principles of the concept and validate the numerical calculations used during the design stage. The results showed that the skirts reduced the air gap but did not improve the motion characteristics of the platform except from heave (www.windsea.no, 2016).

An experimental study of the HYWIND 5 MW spar-buoy type FOWT in 1:47 model scale was carried out by Hydro Oil & Energy at MARINTEK's Ocean Basin Laboratory in Trondheim, Norway in 2005. The first numerical analyses of the motion characteristics of the HYWIND design was presented in (Nielsen et al., 2006a) and (Nielsen et al., 2006b) with the experimental comparison. Experiments were performed to investigate the design under a wide range of environmental conditions. In addition to this, wind turbine control schemes were also tested.

(Ishihara et al., 2009) performed an experimental study in order to analyse the effects of heave plates on the dynamic response of an FOWT. Their results showed that the heave plates increased the natural period of heave leading to a reduction in the heave response at rated and extreme sea state conditions.

(Roddier et al., 2010) carried out an experimental study using a 1:67 scale model of their semi-submersible WindFloat concept in order to confirm the accuracy of the numerical model developed for the engineering design. The concept has a three-legged foundation and is designed to carry a 5-8MW wind turbine and the first full scale WindFloat was deployed in

November 2011. The paper describes the numerical hydrodynamic model of the platform and its mooring system, wave tank testing which included a simplified aerodynamic model of the wind turbine and the development of the coupled model using FAST.

To better understand the behaviour of FOWT's and assess their advantages on the system performance, (Goupee et al., 2012) performed experiments on three FOWT concepts in Maritime Research Institute Netherlands (MARIN). Models at 1:50 scale consisting of a TLP, a spar-buoy and a semisubmersible were investigated each carrying the NREL 5MW reference turbine. Tests included free oscillation tests and test in irregular sea states. In order to achieve high-quality dynamic wind environments, a novel wind machine was designed in order to generate low swirl and turbulence intensity in the flow field. The paper summarised the relative performance advantages of the three concepts in terms of global motions, tower dynamics and the mooring system response. They concluded that for a TLP type wind turbine, although the wind loading increases the pitch response of the system, the pitch response is still very small. It was observed that the operating wind turbine damped the second order pitch response of the spar buoy and the semisubmersible. The results in their paper are constrained within the specific load and design cases so the results cannot be generalised.

(Martin et al., 2012) published a paper describing the experimental methodology used to compare three FOWT concepts; TLP, spar buoy and semi-submersible. In order to increase the aerodynamic performance of the rotor roughen the leading edge of the model blade was artificially roughened in order to trip the boundary layer transition. It was reported that this method may cause erratic wind turbine behaviour and as such should only be used for fine tuning rather that a complete solution for modelling wind turbine aerodynamic performance. It can be concluded from this paper, the best way is to redesign the rotor and use the other techniques sparingly to fine tune the model thrust forces.

(Nihei and Fujioka, 2010) presented tank test results for a 1:100 scale TLP type FOWT incorporating three rotating blades. Tests were carried out in both waves and wind. Similar to (Goupee et al., 2012) their results showed that the blade-wind interaction has a beneficial effect of reducing the floater pitch motion and in addition also decreases the mooring line vibrations.

(Nihei et al., 2011) presented an approach for the optimum design of TLP type FOWT. The optimum design of full scale TLP model was described along with the results from the tank tests. The maximum acceptable displacement for a 5MW turbine and the initial tensions were defined at the start of the optimisation process. Two prototypes (Model 350 and Model 550)

were tested. Model 350 has 846 tons displacement, 21.5m draft and 900kg initial tension in full scale. Model 550 has 3500tons displacement, 38m draft and 2260kg initial tension. They recorded the rotational speed of the blades, motions and tensions on tendons. Good tension values were obtained from Model 550 even during emergency stop out conditions. Model 350 showed slack occurring in the tendons and capsizing in some wind velocities. The authors concluded that the poor behaviour was due to gyroscopic coupling between the heel of the model and the wind turbine rotation which produced a precessional motion in yaw.

In order to investigate the hydrodynamic performance of TLP FOWT a test campaign was carried out by CEHINAV-UPM research group for Iberdrola and published by (Rodriguez et al., 2014). This concept consisted of a central cylindrical column with four square section horizontal pontoons at its base and each pontoon connected with two tendons to the sea bed. Regular, operational, survival, failure and transport tests performed were for a simulated 80m water depth. The paper presents the experimental setup, free decay tests, regular wave motion RAOs, irregular wave responses, tendon loads and accelerations. In order to include wind effect into the tests a calibrated turbine was used and controlled with the data measured through real time platform motion tracking. They also compared their results with available in-house numerical simulations and other results found in literature. Their experimental results indicated that the natural periods and damping values are similar to those published in the literature. The surge values were slightly smaller than reference values which was put down to the reduced water depth as the reason. All the RAOs were very small except surge which is typical for TLP's. Due to the coupling of surge and heave motions, the heave motion response contained components at twice the fundamental wave frequency. It is also reported that no slack in the tendons occurred during the testing period.

(Nihei et al., 2014) presented collaborative work on FOWT's carried out by four universities. They aimed to investigate the performance of different FOWT platforms which can support a 5 MW turbine. Osaka Prefecture University adopted a TLP concept, Yokohama National University used semi-submersible concept, Nihon University used a spar concept and Osaka University adopted semi-submersible with a single-point mooring. All tests were conducted using the same met ocean conditions and the main focus was on the motion performance in terms of RAOs. All the concepts showed good motion performance. The TLP exhibited the best performance in term of motion reduction whereas the spar had the largest accelerations in almost all environmental conditions. Observations showed that gyration effects influenced the spar concept more than the others. The results indicated that there was no impact on RAOs due to the

wind except for the single-point moored semi-submersible which exhibited larger coupling effects between the main floater and the mooring system under the wave and wind conditions.

(Murai et al., 2013) performed a 1:100 scale study to investigate the performance of a multicolumn semi-submersible type FOWT. The correlation with numerical and experimental results was presented and the effectiveness of the model was discussed. Their experimental results agreed with numerical results in surge motion.

(Nihei et al., 2013) discussed the design processes and the motion characteristics of a spar type FOWT concept in their paper. They proposed spar type structure designed for 100m water depth or greater coupled with a 5MW turbine. A wide range of wind and wave tests were performed at a 1/100 model scale. They mainly focused on the floater column design. The heel angle of the system due to wind loads was found to be within 3 degrees. In the case of combined wind and wave load cases, they found that the surge, heave, and pitch motions were at the incident wave frequency.

(Kawai et al., 2013) performed a large number of tests using 1:100 model scale of their new design concept of semi-submersible type FOWT anchored by a single-point mooring. Their experimental results indicated that the motion responses of this concept under wind and waves were in acceptable range in general. Except for pitch in low frequencies they found that the difference between the response in waves alone and in combined wave and wind loading was small. In addition to free decay and regular wave tests, they also carried out weathervane tests under wind loads. Test were performed for ±45, ±90, ±135, 180 degrees in total seven offset angles, it was observed that the weathervane completed in about 100s and the combination of the single point mooring and downwind type rotor is effective in terms of weathervaning.

Most of the tank tests of fixed offshore wind turbines aim to determine the hydrodynamic loads on the support structure especially in storm conditions. Since wind and wave/current loads may be considered to act independently in many cases for these structures, it may not be necessary to simulate all loads at the same time; aero-hydrodynamic coupling may not be an issue in extreme conditions since the turbine is generally shut down. Therefore, in these cases it is possible to perform hydro-dynamic tests without the rotor as long as the mass properties are correctly modelled (see (Ridder et al., 2013)).

Model tests without rotor can be useful at the design stage of the concept in order to compare different support structures' responses to the waves or to validate the numerical models. It is

important to note that the final tests in order to determine the global response of the concept should include representative rotor effects due to the importance of strong coupling between the platform and the rotor generated forces and moments.

Rotor thrust, gyroscopic moments and rotor torque are the most important forces generated on the rotor and influencing the global response of the FOWT concept. Since it is difficult to generate both thrust and torque forces simultaneously in a tank environment, in general, experimental studies focus on achieving the correct thrust force.

Simplified rotor modelling may be used to determine the global response of the system. It is noted that this type of simplification does not aim to determine the power captured by the turbine.

There are several methods to simulate the effect of the rotor without using an accurate representation of the rotor aerodynamics. The steady aerodynamic thrust load was simulated using a lightweight line attached at the rotor hub and tensioned using a weight by (Chujo et al., 2011). This method ignores the aerodynamic damping added by the rotor on the system, gyroscopic effects and steady torque. Moreover, total system mass might not be correct. This method can only be used to generate a rough estimation of the maximum mooring offset without generating wind.

In order to generate a representative wind load in a tank environment, a solid or porous disk can be used to generate aerodynamic drag (representing thrust) in a wind field generated using fans. This method ignores some force components such as the aerodynamic torque applied by the rotor on the platform and blade/tower interactions (Cermelli et al., 2009).
Issues may arise due to unsteady flow around the disk when pitching in waves.

Direct simulation of the rotor in fully coupled tests can be executed by building a working model rotor and testing in a wind field generated by a battery of fans. This method used in (Chujo et al., 2011), (Shin et al., 2013), (Goupee et al., 2012). It becomes challenging where tests include the representation of wind gradients and the wind turbulence. It is also challenging to generate wind in a wave tank close to wavy water surface especially during large wave tests. (Ridder et al., 2013) discussed the design of a wind system to be used over a wave tank.

In order to address the challenge in achieving the thrust force correctly at model scale, (Martin et al., 2012) discussed three possible methods. In order to balance the low thrust coefficient the wind speed is increased beyond the Froude-scale value in the first method. When rotor speed

maintain at Froude-scaled values in order to sustain correct gyroscopic moments, the tip-speed ratio is incorrect which results in incorrect torque. Overturning moment due to thrust is much higher than due to torque so this can be justified. The ratio of unsteady velocity due to platform motions to mean velocity will be reduced resulting in incorrect modelling of effects of unsteady inflow on the rotor. The results showed that the aerodynamic damping of the platform is modelled with a reasonable degree of accuracy.

A second method was described to account for the low Reynolds number effect by using roughened materials to create turbulence along the edge of a blade. This method did not improve the turbine performance in comparison with the full-scale concept.

Third method was to redesign the rotor blade sections in order to account for Reynolds number effects, or changing the number of blades used. (Martin et al., 2012) redesigned the blades using low Reynolds number aerofoils. These parts found to be less affected by laminar separation under low Reynolds number conditions, so the results were correct for scaled thrust and aerodynamic damping using Froude scaled wind speed.

As it is reported in (Day et al., 2015) *"Correct modelling of the gyroscopic moments introduced by the rotor can be achieved by Froude scaling of the mass properties and rotor speed".* In order to model the mass properties of the rotor at small scale, lightweight materials are required in manufacture. It is difficult to achieve the proper geometry and very light mass using conventional experimental model making techniques. It might be possible by using novel materials (such as some coating materials) to achieve the target mass without changing the geometry.

A number of studies have been performed using "Software in the loop" simulations which is based on an active control system driving an actuator in real time in order to create the forces in a model test (aiming to simulate forces which cannot be scaled correctly in the laboratory). (Zamora-Rodriguez et al., 2014) carried out tests using this methodology. Unsteady aerodynamic thrust force in a hydrodynamic test is generated by a speed-controlled fan based on the measurement of the instantaneous velocity at the nacelle. (Bayati et al., 2014) used the SIL method to simulate the hydrodynamic motions of a platform in a wind tunnel by using a hexapod.

The software in the loop method can overcome the most problematic scaling issues related to discrepancies between Reynolds and Froude scaling for the aerodynamic and hydrodynamic

forces on a FOWT concept; however other challenges are introduced. The software in the loop system is discussed in more detail in Chapter 4.

(Ridder et al., 2013) carried out a study to investigate the dynamic response of an offshore wind turbine with realistic flexibility to breaking wave impact. In this study tower stiffness was modelled correctly. However modelling tower stiffness and mass correctly is challenging at smaller model scales, and many experimental studies on floating wind turbine concepts reviewed carried out tests without correctly modelling the tower stiffness.

This section has reviewed the experimental studies which have been carried out in order to investigate the hydrodynamic performance of FOWT's. Many studies have been performed with the focus on semisubmersible, spar and TLP concepts. With growing interest in floating offshore wind concepts, tank tests will continue to play an important role in investigating the performance of FOWT's as well as providing valuable data to verify the results of numerical calculations.

Chapter 3
Numerical Investigation of the TLP

3.1 Introduction

One of the main objectives of this study is to correlate the behaviour of the FOWT system as obtained from the experimental measurements against the numerical predictions. The theoretical background of the numerical tools used in this study is represented in this chapter as well as a description of these tools. A numerical validation model for the MIT/NREL TLP study was carried out and the results obtained are presented in this chapter. The numerical predictions are compared with the experimental results in the thesis.

The assumptions and limitations of the numerical prediction tool: FAST used in this study are described.

A summary of the validation process of the MIT/NREL TLP is given. The numerical setup of the mathematical model is explained and following this, some of the results from the program testing study are given. Finally, a conclusion of the chapter is drawn.

3.2 Aero-Servo-Hydro-Elastic Analysis of a FOWT

In order to predict the complex dynamics of a FOWT a coupled aero-servo-hydro-elastic model which integrates wind-inflow, the turbine control system (servo), hydrodynamic and structural-dynamic (elastic) models is required. Furthermore due to the nonlinear behaviour of a FOWT a time domain approach is required. In this section a description of the theoretical basis for the numerical tool FAST used in this study is presented.

3.2.1 Equations of Motion

When developing the equations of motion for the entire FOWT system, the fully dynamic coupling between the motions of the platform and the wind turbine should be taken into account. The general form of the nonlinear time domain equations of motion for the coupled wind turbine and support platform system are given in the following equation which is stated by (Jonkman, 2007).

$$M_{ij}(q,u,t)\ddot{q}_j = f_i(q,\dot{q},u,t) \tag{3.1}$$

M_{ij} is the (i, j) component of the inertia mass matrix which depends nonlinearly on the system DOFs (q), control inputs (u), and time (t). $\ddot{q}_j$ refers to the second time derivative of DOF j, and f_i denotes the component of the forcing function associated with DOF i. f_i, the forcing function, depends on the nonlinearly of the system DOFs (q) and their first time derivatives $(\dot{q})$, control inputs (u) and time (t). The forcing function is defined as positive in the direction of positive motion of DOF (i) (platform direction). The following equation represents the entire system forces.

$$* F_i + F_i = 0 \quad for\ i = 1,2,3, \dots, n \tag{3.2}$$

n refers the number of degrees of freedom (DOF)

$* F_i$ generalised inertia forces F_i

generalised forces

The generalised inertia forces $*F_i$ consist of tower, nacelle, hub, platform and blade forces.

$$*F_i = *F_i^{Hub} + *F_i^{Nacelle} + *F_i^{Tower} + *F_i^{Platform} + *F_i^{Blades} \quad (3.3)$$

In this study, the main attention is given to $*F_i{}^{Platform}$, which is described in the next sections.

Generalised forces F_i include aerodynamic, hydrodynamic, gravity, drive train and elastic forces.

$$F_i = F_i^{Aero} + F_i^{Hydro} + F_i^{Gravity} + F_i^{Elastic} + F_i^{Drivet} + F_i^{Mooring} + F_i^{Aero} \quad (3.4)$$

$F_i{}^{Hydro}$, hydrodynamic loads are presented in the following section.

3.3 Hydrodynamic Loads

As previously mentioned in the critical review chapter, it is important to correctly model the aerodynamic loads for onshore and shallow-water fixed bottom turbines since their behaviour is dominated by interaction with the wind. For FOWTs the hydrodynamic loads have also to be taken into account. In the long term, the wind generates the waves, aerodynamics and hydrodynamics are related in long term statistical correlation of wind speed, wave height and wave period. Therefore, load cases with high wind speeds and increased aerodynamic loads are usually accompanied by increased wave heights resulting in greater hydrodynamic loads on the floating platform.

The integration of the dynamic pressure of the water over the wetted surface of a floating platform generates the hydrodynamic loads. These loads compose of inertia (added mass) and linear drag (radiation), buoyancy (restoring), incident-wave scattering (diffraction), sea current and nonlinear effects.

3.3.1 Linear Hydrodynamics

A 6 DOF rigid body of a FOWT with small rotational and translational motions is shown in Figure 3.1. The model is described with reference to a global coordinate system, assumed to be a right handed Cartesian system with its origin located at the still water level.

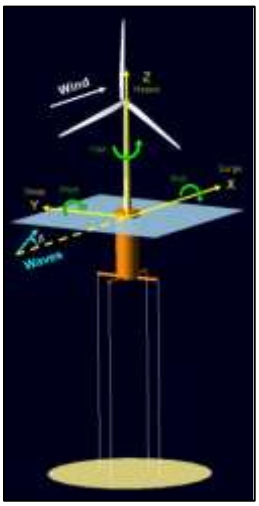

Figure 3.1 Platform modes of motion (Matha, 2009)

Two main assumptions in FAST are made to consider the linear, steady-state hydrodynamic problem:

1) Incident waves propagate with single amplitude, frequency and direction and platform motions respond at the same frequency which allows for the use of regular wave theory (linear Stokes wave theory). Irregular waves are represented as the superposition of a number of such waves.
2) The translational motions of the platform are small compared to its body size. This is the fundamental assumption which allows the hydrodynamic problem to be separated into three parts: diffraction, radiation and hydrostatics (Matha, 2009).

In this study, TLP responded predominantly at the wave frequency but also there is a small response at the surge natural frequency. The linear wave assumption prevents modelling the steep or breaking waves which may result in non-linear wave-induced "slap" and "slam" loading. This linear wave assumption is valid for most waves in operational conditions in deep water and for small-amplitude waves in shallow water. Therefore, high-order wave kinematics theories are required for accurate predictions when waves become extreme or propagate toward shore in shallow water. As discussed in the next section, linear theory also neglects higher order effects such as mean drift forces which can become important for some floating platforms.

In the present case it is shown later that the peak of the surge RAO is large (around five), which could in principle lead to large motions relatively to the diameter in waves close to the surge natural period (23s). However, at this wave period, the diffraction forces are small since the

platform diameter is small relative to the wave length. For lower wave periods where the wave lengths are smaller relative to the platform diameter and the diffraction forces are larger, the platforms motions are much smaller; therefore this assumption can be considered as reasonable.

It should be noted that, apart from these two assumptions, potential flow theory assumes that the flow around the platform is incompressible, inviscid and irrotational, with negligible surface tension effects. The linear hydrodynamic problem is solved by superposition of the independent radiation, diffraction and hydrostatic problems.

3.3.2 Linear Time-Domain Hydrodynamic Model

In the linear time domain hydrodynamic model, the forces acting on the support platform consist of diffraction, radiation and hydrostatic forces (F_i^{Hydro}) as well as the restoring forces from the mooring lines (F_i^{Lines}) and the added inertia of the fully coupled the turbine/platform ($A_{ij}\ddot{q}_j$) (See Jonkman, 2007).

The total external load acting on the support platform, $F_i^{platform}$, can be written as:

$$F_i^{platform} = -A_{ij}\ddot{q}_j + F_i^{Hydro} + F_i^{Lines} \tag{3.5}$$

A_{ij} is the (i, j) component of the added mass matrix.

F_i^{Hydro} is the i[th] component of the applied hydrodynamic load on the support platform F_i^{Lines} is the i[th] component of the load on the support platform from the contribution of all mooring lines

As was previously mentioned, hydrodynamic problem consists of three independent problems: radiation, diffraction and hydrostatic.

$$* F_{iHydro} = F_i^{Waves} + F_{iHydrostatic} - F_i^{Radiation} \tag{3.6}$$

$$* F_i^{Hydro} = F_i^{Waves} + \rho g V_0 \delta_{i3} - C_{ij}^{Hydrostatic} q_j - \int_0^t K_{ij}(t-\tau)\dot{q}_j(\tau)d\tau \tag{3.7}$$

$\boldsymbol{F^{Wave}_i}$ **(Wave excitation load)** denotes the total excitation load on the support platform from incident waves and it is related to the wave elevation. It occurs when a floating structure is restrained from oscillating and incident surface waves are present and scattered by the body.

The wave excitation loads are the result of the undisturbed pressure field (Froude-Krylov) and wave scattering (diffraction loads).

$\boldsymbol{F^{Hydrostatic}_i}$ **Hydrostatic Forces** are the restoring forces of a freely moving body. The hydrostatic force includes buoyancy force and restoring from water plane area and centre of buoyancy.

$$F_i^{Hyrostatic} = \rho g V_0 \delta_{i3} - C_{ij}^{Hydrostatic} q_j \tag{3.8}$$

$\rho g V_0 \delta_{i3}$ refers to the buoyancy force from Archimedes' principle ; it is the force directed vertically upward and equal to the weight of the displaced fluid when the support platform is in its undisplaced position.

ρ is the water density

g is the gravitational acceleration constant

V_0 is the displaced volume of fluid when the support platform is in its undisplaced position

δ_{i3} is the (i,3) component of the Kronecker-Delta function (i.e.identity matrix)

$C_{ij}{}^{Hydrostatics}$ is the (i, j) component of the linear hydrostatic restoring matrix from the effects of water-plane area and COB

q_j is the j^{th} DOF of the platform

$-C_{ij}{}^{Hydrostatic} q_j$ is the change in the hydrostatic force and moment resulting from the effects of the water-plane area and the COB

This equation based on the assumption that the structure is symmetrical around its body-fixed xz-plane and yz-plane.

$F^{Radiation_i}$ **(Radiation Forces)** are steady-state hydrodynamic forces and moments due to forced harmonic rigid body motions with the wave excitation frequency when there are no incident waves.

$$F_i^{Radiation} = \int_0^t K_{ij}(t-\tau)\dot{q}_j(\tau)d_\tau \quad (3.9)$$

The convolution integral represents the load contribution from wave-radiation damping and also additional contribution from added mass which is not included in A_{ij}.

K_{ij} is the wave radiation retardation kernel - the impulse-response function of the radiation problem.

t is simulation time

τ is user variable time

The radiation loads are obtained in the time domain with hydrodynamic added mass and damping matrices.

Morison's representation

As stated in (Bossanyi, December, 2003, Cheng, 2002), Morison's representation is commonly used approach for the analysis of fixed-bottom offshore wind turbines. Based on hydrodynamic strip theory, the structure is divided into a number of elements (strips) where two-dimensional properties (added mass and viscous drag coefficients in the case of Morison's hydrodynamics) are used to determine the three dimensional loading on the structure (Faltinsen, 1990).

(Jonkman, 2007) augmented the linear hydrodynamic-loading equation in HydroDyn by including the nonlinear viscous term from Morison's equation to incorporate the influence of current. HydroDyn is a module in FAST which deals with the hydrodynamics.

3.3.3 Non Linear Effects (Limitations of FAST)

Up to this section, the aero-hydro-servo-elastic simulation model to represent a FOWT includes only first order hydrodynamics, which induce loads and motions that vary with the same frequency as the incident waves. Naturally, linearization of the hydrodynamic problem means that the second or higher order hydrodynamic effects are not included in FAST. As is stated by Jonkman *"Second- or higher-order nonlinear hydrodynamics models more properly account*

for the loading about the actual instantaneous wetted surface of a floating body and may be important when the support platform motions are large relative to their characteristic lengths". These second order effects result in vibrations which cause fatigue damage to the structure by inducing the loads at the sum- and difference- frequencies of the incident wave components. These loads have the frequencies that are equal both the sum and difference of pairs of incident wave frequencies and also these loads are proportional to the square of the wave amplitude. Therefore, as it is stated in (Perez, 2014) "*although the natural frequencies of the structure are designed to be outside the first order wave energy spectrum, the second order loads can excite these frequencies"*. As a result, it should be noted that even though the second order hydrodynamic loads normally are in small magnitude the resonant effect can be significant.

Three second-order hydrodynamic loads neglected in FAST are summarised below:

- **Mean-drift loads**, which result in a mean offset of the body relative to its undisplaced position.
- **Slowly varying loads**, which are the result of the quadratic interactions between separate wave components in an irregular sea condition that have different frequencies. These loads can excite large amplitude resonant motion of the platform at low frequency.
- **Sum frequency loads**, which have a frequency that is higher than the wave frequency and are also generally small in amplitude.

As stated by Jonkman, *"second-order sum frequency excitations are sometimes important when analysing the "ringing" behaviour in support platforms with mooring systems that impose a strong resistance to heave, such as in TLP design".*

Apart from abovementioned three main second-order hydrodynamic loads, there are several non-linear effects which can create these loads or trigger other effects.

- **Interaction between the floaters** in close proximity or large ratio between the wave height and the diameter of the columns which can create unexpected hydrodynamic loads (Faltinsen, 1990).
- **Mathieu effect**, which results in parametric instability concerning a coupling between heave and pitch/roll. This effect is triggered by an oscillating hydrostatic stiffness in the vertical modes (Biran and Pulido, 2014).

- **Envelope effect**, which causes the heave motion to oscillate at two different periods, the heave natural period and the wave period.
- **Vortex-induced loads** derived from vortex shedding may increase the mean drag force and cause the platform to oscillate transversely to the current flow.
- **Viscous damping:** Large wave periods have low frequencies which means that the wave radiation linear damping is small and large amplification of motion occurs close to resonance. Excluding viscous damping can cause overestimated motion amplitudes.

3.4 Simulation Tools used for Model Development

3.4.1 FAST

Fatigue, Aerodynamics, Structures and Turbulence (FAST) is an open-source code developed by researchers from the National Renewable Energy Laboratory (NREL). It was originally developed to investigate fixed wind turbine systems and was extended to include floating concepts. FAST combines dynamic wind fields generated by TurbSIM and hydrodynamic data generated by a large number of hydrodynamic programmes. For this study the hydrodynamic properties of the platform are predicted using WAMIT. TurbSIM is a wind simulation tool which generates the realistic inflow wind velocity fields required by FAST. Hydrodynamic parameters such as hydrostatic restoring coefficients, added mass and damping coefficients and wave excitation forces are calculated by WAMIT. Figure 3.2 gives an overview of the structure of FAST including the various modules which make up the main programme.

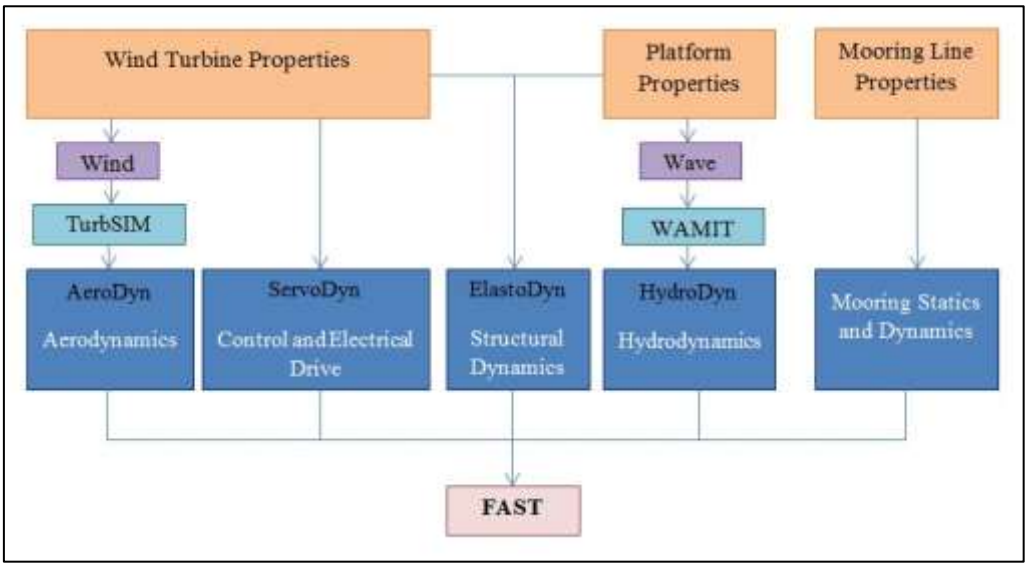

Figure 3.2 FAST Structure

3.4.2 WAMIT

WAMIT is a widely used panel program which solves the boundary-value problem for the interaction of water-waves with prescribed bodies in finite and infinite water depths. WAMIT uses potential flow theory and integrates pressures by the panel method to yield a converged solution of the diffraction and radiation problems on the body surface for a specified solution method (for example considering only diffraction, radiation or both), wave frequency, and wave heading. WAMIT is based on potential flow theory so it neglects flow separation. The hydrodynamic parameters calculated using WAMIT form the main input to module HydroDyn.

3.4.3 HydroDyn

HydroDyn is a time-domain hydrodynamics module which calculates hydrodynamic forces for both fixed-bottom and floating offshore wind turbines. It includes three possible methods to calculate the hydrodynamic loads: a potential flow theory solution, a strip theory solution or a combination of these two. HydroDyn uses linear wave (linear Stokes wave) theory for waves.

Figure 3.3 summarises the HydroDyn calculation process. It combines linear hydrostatic restoring, nonlinear viscous drag, sea currents, platform motions, added-mass and damping in both regular and irregular seas. It does not consider nonlinear steep or breaking waves or second-order effects such as mean drift, slowly varying drift and sum and difference frequency excitation.

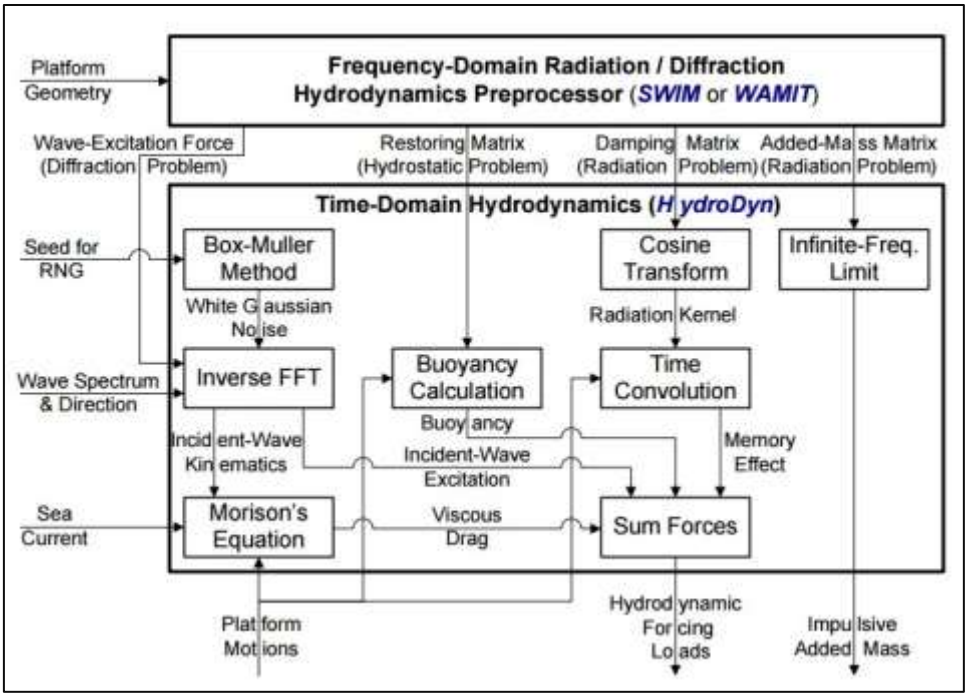

Figure 3.3 Summary of the HydroDyn calculation procedure (Jonkman, 2007)

3.4.4 Mooring System Modelling in FAST

For a TLP, the mooring arrangement is critical to the overall stability of the system. The mooring system consists of a number of cables which are attached to the floating support platform at fairlead connections and the opposite ends are anchored to the sea bed. Restraining forces at the fairleads are provided by tension in the mooring lines. The buoyancy of the support platform, the cable weight in water, and the elasticity in the cable, viscousseparation effects and the geometrical layout of the system effect this tension. Restraining forces at the fairleads change with the changing cable tension because the fairleads move with the support platform in response to the unsteady environmental loading (wind, waves and current). The mooring system has a degree of compliance in order to reduce the peak loads on the mooring cables.

FAST makes the assumption of linear mooring stiffness and also ignores mooring inertia and damping. The total load on the support platform from the contribution of all mooring lines, F_i^{Lines} is represented as: (See Jonkman, 2007)

$$F_i^{Lines} = F_i^{Lines,0} - C_{ij}^{Lines} q_j \qquad (3.10)$$

C_{ij}^{Lines} is the (i, j) component of the linearised restoring matrix from all mooring lines $F_i^{Lines,0}$ is the i[th] component of the total mooring system load acting on the support platform in its un-displaced position

$F_i^{Lines,0}$ represents the result of pre-tension in the mooring lines from positive platform buoyancy in its un-displaced position and also includes the contribution from the weight of the cable in water for taut mooring lines. C_i^{Lines} denotes the combined elastic stiffness of the mooring lines and the effective geometric stiffness brought about by the weight of the cables in water.

The mooring module can model an array of homogenous taut or slack catenary mooring lines and it accounts for the apparent weight in fluid, elastic stretching, and seabed friction of each line, but ignores the individual line bending stiffness. Knowing the fairlead positions for a given platform displacement at any instant in time, this module solves for the tensions by assuming that each cable is in static equilibrium at that instant. By combining the mooring tensions and loading on the platform with hydrodynamic and aerodynamic forces on the turbine FAST solves the dynamic equations of motion to find the accelerations of the major FOWT

components (platform, tower, nacelle and blades). The accelerations are integrated in order to obtain the new platform and fairlead positions for the next time step calculation. This quasi-static method ignores the inertia and hydrodynamic damping of the mooring system.

The mass of the mooring system compared to the mass of the floater is small so inertia effects of tendons are small. Tendon cross section area is small compared to the platform area so tendon drag is small compared to that of the platform, a similar geometry argument can be used to argue that vortex shedding effects of the mooring system will be small compared those of the platform.

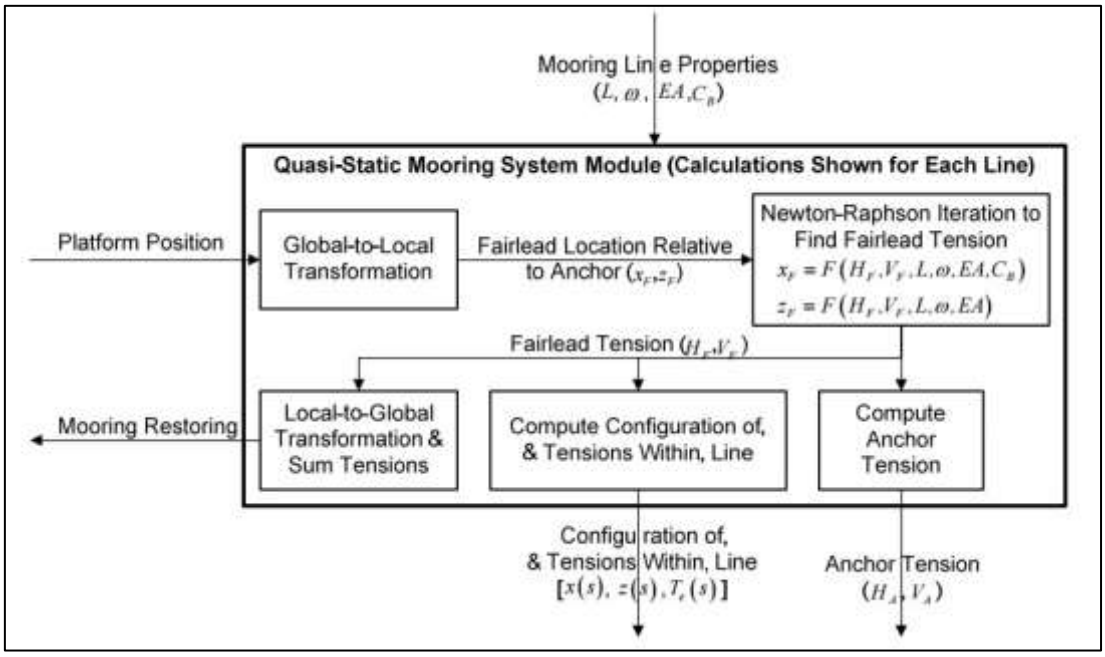

Figure 3.4 Summary of mooring system module using in FAST

Figure 3.4 shows the summary of the calculation processes for the mooring line module. Each mooring line system is analysed separately. The input parameters shown in the figure required for the mooring line calculation are:

L the unstretched length

ω the apparent weight in fluid per unit length

EA the mooring line stiffness

C_B coefficient of seabed static-friction drag

3.4.5 TurbSIM

TurbSIM is a stochastic, full-field, turbulent wind numerical simulation tool which generates the required inflow turbulent wind field on a rectangular grid defined over the rotor plane (Jonkman, Revised August 26, 2009). It generates a time series containing the three wind speed vectors at each point in the grid. Figure 3.5 shows the wind speed vectors at each grid point.

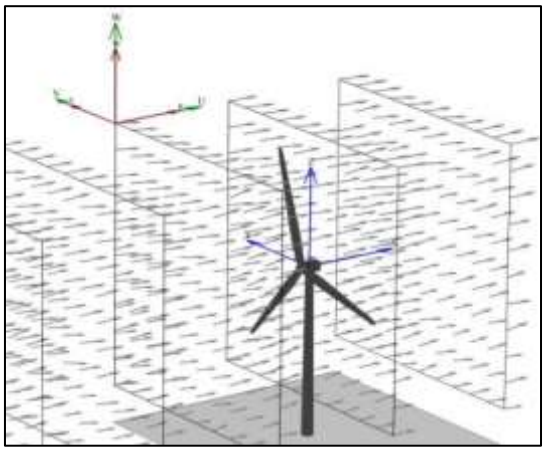

Figure 3.5 Wind speed vectors on each grid

The IEC Kaimal power spectral density function (IECKAI) is selected to describe the turbulence components in the three orthogonal directions typically found in North Sea locations. The spectra for the three wind components, $K = u, v, w$ are given as :

$$S_k(f) = \frac{4\sigma_K^2 L_K/\bar{u}_{hub}}{(1+6fL_K/\bar{u}_{hub})^{5/3}} \tag{3.11}$$

f refers to cyclic frequency

L_K is an integral scale parameter

$\bar{u}_{hub}$ is the mean incident wind speed at the hub height

Integral scale parameters are defined in the IEC 61400-1 as:

$$L_K = \begin{cases} 8.10\Lambda_U\,, K = u \\ 2.70\Lambda_U, K = v \\ 0.66\Lambda_U, K = w \end{cases} \tag{3.12}$$

Λ_U is the turbulence scale parameter

$$\Lambda_U = \begin{cases} 0.7 \min(30m, HubHt), Edition\ 2 \\ 0.7 \min(60m, HubHt), Edition\ 3 \end{cases} \quad (3.13)$$

3.4.6 AeroDyn

AeroDyn is a module of FAST which used associated with an aero elastic code to calculate the aerodynamics of horizontal axis wind turbines. AeroDyn consists of two models in order to calculate the effect of wind turbine wakes, the blade element momentum (BEM) theory and the generalised dynamic wake theory. BEM theory is the commonly used method by many researchers and generalised dynamic wake theory is useful to model skewed and unsteady wake dynamics. BEM theory allows the user to make some corrections such as incorporating the aerodynamic effects of tip losses, hub losses and skewed wakes. The generalised dynamic wake method includes all these effects automatically. These two approaches are used in order to calculate the axial induced velocities from the wake in the rotor plane. AeroDyn is capable of reading a number of different formats of wind input, such as single-point hub-height wind files, multiple-point turbulent winds.

3.5 Validation of MIT/NREL TLP

The MIT/NREL TLP, developed by National Renewable Energy Laboratory (NREL), has been used in a wide range of research studies. There is consequently a large amount of simulation data available for comparison, verification and validation purposes. The MIT/NREL TLP has therefore been selected as a program testing case for this research.

In this section, the hydrodynamic model generated by using WAMITv7 is presented and the validation of this model in both WAMITv7 output and FASTv7 output are given based on (Matha, 2009). This section comprises the model description, model set up, the parametric study for the validation, comparison of WAMITv7. In the last section, some of the validation graphs are given for the developed coupled model using FASTv7.

3.5.1 Model Definition

In order to build up a suitable coupled model for validation purposes, the MIT/NREL TLP floater published in (Martin et al., 2012) and (Matha, 2009) was identified as a program testing case due to its close similarity to the FOWT concept.

The MIT/NREL TLP employs the 'NREL offshore 5 MW baseline wind turbine' which is a utility-scale multi-megawatt turbine designed to be installed in the northern North Sea. The turbine is a conventional three-bladed upwind variable-speed variable blade-pitch-to-

feathercontrolled turbine. The MIT/NREL TLP is used as a floater which was developed specifically to support the rotor, nacelle and tower of the NREL baseline 5 MW systems.

It comprises a cylindrical platform ballasted with concrete and moored by four pairs of vertical tendons in tension. Each pair of tendons attaches to a spoke that radiates horizontally from the bottom of the platform. The concrete ballast is used to ensure that the entire coupled system remains stable in mild met ocean conditions (Jonkman and Matha, March, 2010).
Properties of the MIT TLP#1 are given in Table 3.1.

Table 3.1 Properties of MIT TLP#1 (Tracy, 2007)

Properties	Value
Platform diameter	18 m
Platform draft	47.89 m
Water depth	200 m
Mooring system angle	90˚
Average mooring system tension per line	3931 kN
Ballast at platform bottom:	
Concrete mass	8216000 kg
Concrete height	12.6 m
Total displacement	12187000 kg
Wind Speed (constant, no shear)	11.0 m/s
Sea state significant wave height	10.0 m
Peak spectral wave period	17.6394 sec
Windward static line tension	5290 kN
Leeward static line tension	2570 kN
Steady state surge offset	4394 m
Steady state pitch offset	0.438˚

3.5.2 Model Setup

The first part of the validation was to re-create the hydrodynamic data for the platform. Since WAMIT was used in NREL's study, the results can be compared directly. The hydrodynamic coefficients obtained from WAMIT are used as input to the HydroDyn module in FAST.

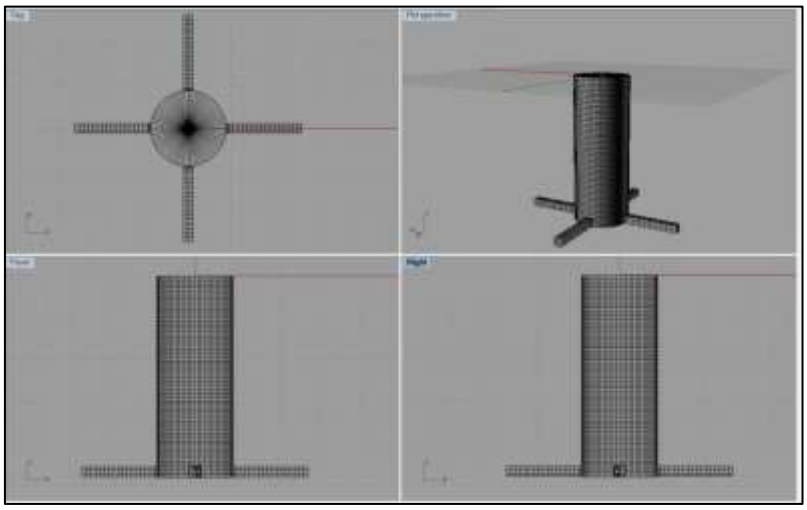

Figure 3.6 Geometric file of benchmark TLP

The mesh was generated using 'Rhinoceros 4.0' software and is shown in Figure 3.6.

The case study was carried out to investigate the sensitivity of the results to:

a) Mesh density
b) The various settings affecting computational approach and time
c) Values of some parameters which were unclear in the NREL report

Standard WAMIT output files were generated for a total of 20 test cases. Each case consisted of 102 wave periods and 37 wave headings. Computational time varied substantially with mesh density as it is expected. It was found that a 72x50 mesh on the surface of the cylinder gave good agreement for all hydrodynamic parameters of interest. Increasing the mesh size to 100x100 dramatically increased computation time with negligible change in results. Results were relatively insensitive to the various computational settings which could be altered (although computation time varied somewhat).

3.5.3 Comparison of WAMIT output files and MIT/NREL TLP HydroDyn Files

The WAMITv7 code generates a number of output files. Three of these files, which describe the added-mass and damping coefficients, wave excitation forces and the hydrostatics, form the inputs to the HydroDyn module in FAST. The hydrodynamic coefficients obtained in the NREL study are compared to those of this study in the following figures. All output values are non-dimensionalised according to (MIT, 1998). Figure 3.7 shows the non-dimensional added mass and damping coefficients and Figure 3.8 shows the magnitude and phase of the wave excitation force. The hydrostatic restoring is shown in Figure 3.9.

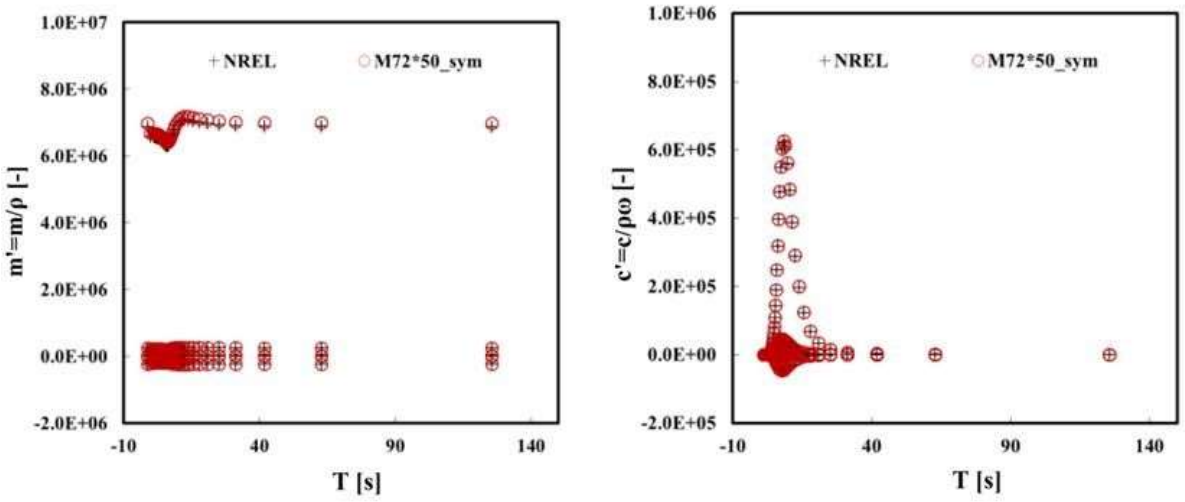

Figure 3.7 Non dimensional added mass and damping coefficients

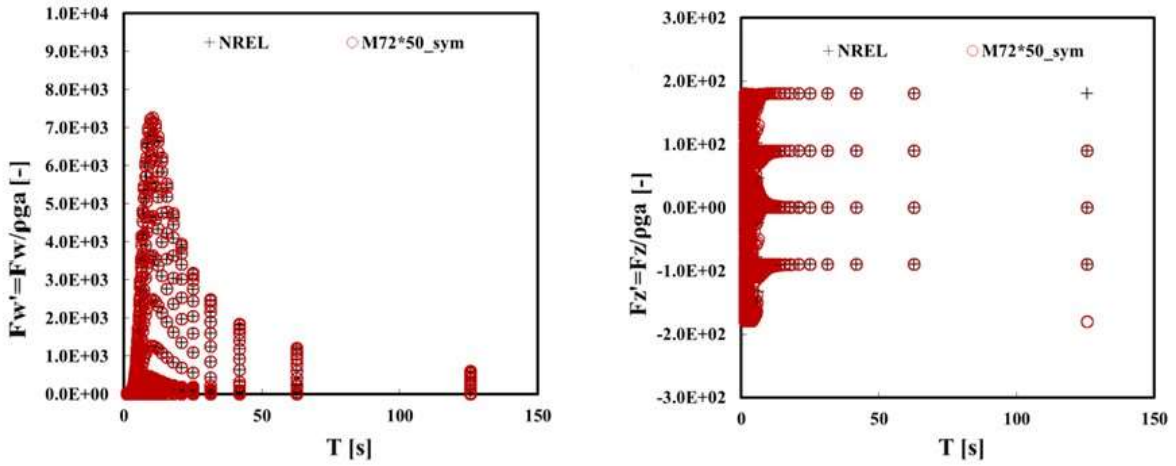

Figure 3.8 Wave excitation forces

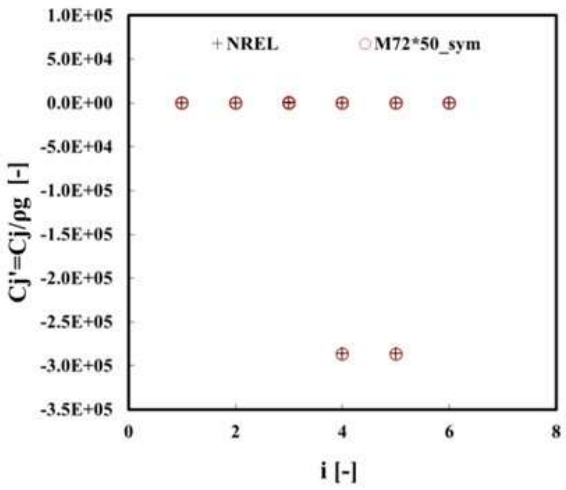

Figure 3.9 Hydrostatic restoring

It is clear from the figures that the results obtained from the hydrodynamic predictions compare favourably with the MIT/NREL TLP results (Matha, 2009).

3.6 Fast comparison with the MIT/NREL TLP test case

After the validation of the hydrodynamic coefficients, the validated numerical results are inputed to the HydroDyn module. A comparison of surge and heave motions for rated wind speed are given in Figure 3.10 and Figure 3.11. It can be seen from these figures that the model results give good agreement with the benchmark study.

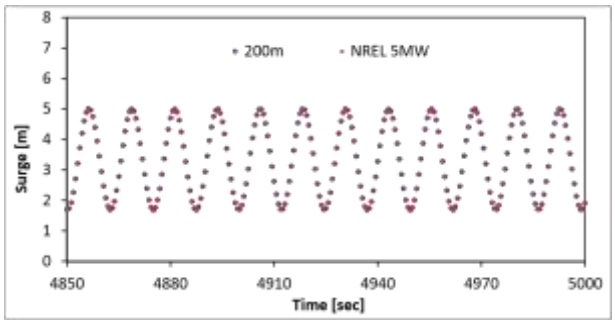

Figure 3.10 Comparison of surge motion for 200m water depth

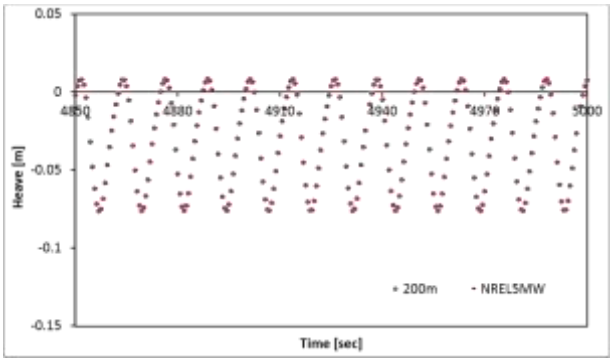

Figure 3.11 Comparison of heave motion for 200m water depth

3.7 Hydrodynamic modelling of proposed FOWT

This section describes the modelling of the proposed FOWT concept. The 72 x 50 element mesh is shown in Figure 3.12. The proposed FOWT system has a varying section in the main column in contrast to MIT/NREL TLP study. Hydrodynamic coefficients were calculated in WAMIT and are inputed to the HydroDyn module as in the program testing case. Figure 3.13 shows the non-dimensional added mass and damping coefficients and Figure 3.14 shows the magnitude and phase of the wave excitation force. The hydrostatic restoring is shown in Figure 3.15. All numerical results and comparisons are presented in the following chapters.

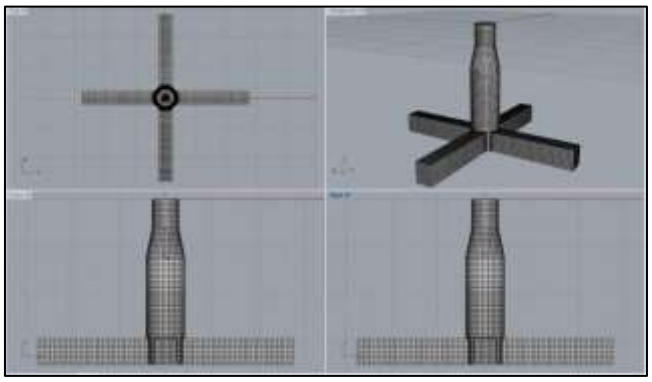

Figure 3.12 Geometric file of proposed FOWT

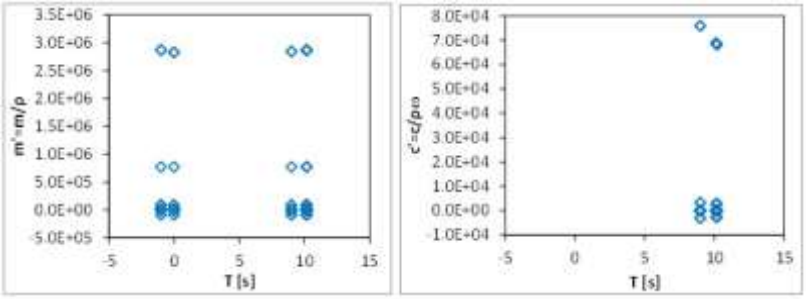

Figure 3.13 Non dimensional added mass and damping coefficients

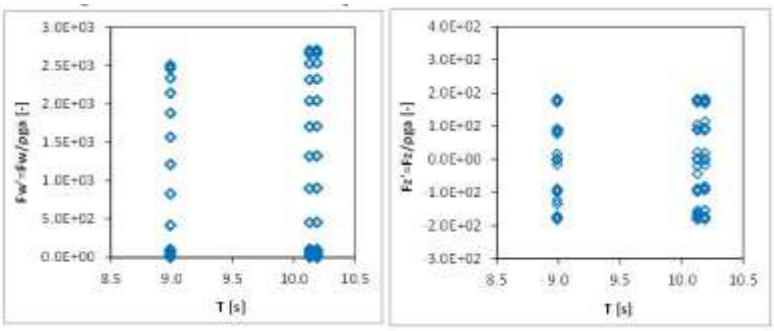

Figure 3.14 Wave excitation forces

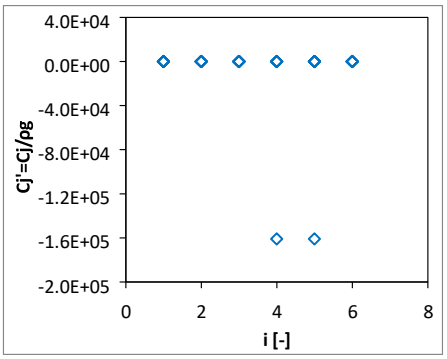

Figure 3.15 Hydrostatic restoring

3.8 TLPWIND modelling in FAST

In order to generate a model of a TLP floating wind turbine concept FAST version 7 (with AeroDyn and HydroDyn) was selected for this study since it was the most thoroughly validated version of FAST when the first numerical calculations of this study were carried out. FAST version 8 was still under validation at that time, and there were thus some concerns in regards to the reliability of the code. Key modelling parameters were set up as described below:

Tendons were modelled using the standard approach adopted in FASTv7 (see section 5.6). Necessary parameters such as unstretched line length in [m] *(LUnstrLen),* anchor point angle in [deg] *(LAngAnch),* anchor point depth in [m] *(LDpthAnch),* tendon diameter in [m] *(LDiam),* axial stiffness (Young's modulus cross sectional area of the line) in [N] *(LEAStff),* anchor point radius in [m] *(LRadAnch)* in water depth, mass per unit length of the element in [kg/m] *(LMassDen)* were set up in the standard platform input file. All degrees of freedom were activated for irregular and regular wave tests in the platform file.

In order to generate turbulent wind for sea states TurbSim was used and *WindFile* name inputted to the AeroDyn standard input file. For free oscillation tests in surge *PtfmSurge* (Initial or fixed horizontal surge translational displacement of platform) was defined as 1.0m in the platform file while for free oscillation in heave *PtfmHeave* (Initial or fixed vertical heave translational displacement of platform) was used as 0.01m. Similarly *PtfmPitch* (Initial or fixed pitch tilt rotational displacement of platform) was defined as 0.1degrees in the platform file to perform free oscillation tests in pitch whilst *PtfmYaw* (Initial or fixed yaw rotational displacement of platform) was used as 0.1degrees for yaw free oscillation test. Apart from all these free oscillation tests, initial translational or rotational displacements were set to zero in the numerical calculations.

The incident wave kinematics model was set using the variable *WaveMod* (Incident wave kinematics model [0: none=still water, 1: plane progressive (regular), 2: JONSWAP/PiersonMoskowitz spectrum (irregular)] according to the test type. *WaveHs* (Significant wave height of incident waves (meters) [used only when *WaveMod*=1 or 2) and *WaveTp* (Peak spectral period of incident waves (sec) [used only when *WaveMod*=1 or 2]) were selected for each test in regular and irregular waves.

Total simulation time was selected based on the test type in the *.fst* file. Free oscillation tests were run for 800sec while irregular and regular tests were run for 9999.999sec (maximum simulation time allowed in FAST).

PitchControl mode was selected to be zero (none) for no wind condition in free oscillation tests and the controller dll "*DISCON_OC3Hywind_win32.dll*" was used when wind was considered. Further details of FAST parameters are given in Chapter 6, 7, 8. Sample input files are presented in Appendix B.

3.9 Conclusions

The theoretical background to the numerical tools used in this study was presented in this chapter along with the assumptions and limitations of the FAST software.

A correlation study was carried out using the MIT/NREL TLP floater carrying the NREL offshore 5 MW baseline wind turbine. The results from the program testing study gave very similar results to those from the NREL study.

The proposed FOWT concept was briefly introduced and the results of the hydrodynamic modelling were presented. This model was subsequently used as part of the comparison with the experimental results described in Chapter 5, Chapter 6 and Chapter 7.

Chapter 4

Experimental Setup and Preparation

4.1 Introduction

This chapter begins with a description of the Kelvin Hydrodynamics Laboratory and also the scaling criteria used in the model experiments. The experimental work was designed to investigate the performance of a TLP type floating wind turbine. An overview of the experimental procedure for a TLP type wind turbine is presented. Each stage of the calibration methodology is introduced in detail in the subsequent sections. This chapter also describes the methodology used in the experimental work for example daily checks conducted during the testing campaign. Finally, conclusions relating to the experimental setup and preparation are presented.

4.1.1 Background to tests

The test program described in this thesis forms part of a collaborative project between the partners Iberdrola Engineering and Construction, the University of Strathclyde, and the ORE Catapult. The Floater test campaign to assess the motion performance of a TLP type wind turbine in 1:36.67 scale was carried out in the Kelvin Hydrodynamic Laboratory of Naval Architecture, Ocean and Marine Engineering Department of University of Strathclyde, Glasgow.

4.1.2 Kelvin Laboratory Facilities

The model tests were carried out in the Kelvin Hydrodynamics Laboratory at the University of Strathclyde. The tank has dimensions of 76 m L x 4.6 m W x 2.5 m D, and is equipped with a four-paddle active-absorbing wavemaker, capable of moving vertically to accommodate water

depths from 1.6m to 2.3m which can generate both regular and irregular waves over 0.6m in height. The wavemaker is shown in Figure 4.1.

Before the start of the testing campaign an extended beach of 12m length was constructed to improve the absorption over the frequency range of interest. This was required due to the specific nature of the experiments which involved long run lengths coupled with a very sensitive measurements of motions and forces. A series of tests were performed using the newly extended beach in order to evaluate its performance. Results showed that reflection coefficients were less than 5% over a frequency range from 0.3-1.2Hz. The model was installed in the centre of the tank both longitudinally and transversely on a mounting frame installed on the base of the tank arranged to allow the model to be rotated through 45 degrees. A detailed drawing of the plan and profile view of the tank showing the experimental setup is given in Figure 4.2.

Figure 4.1Wave maker in KHL

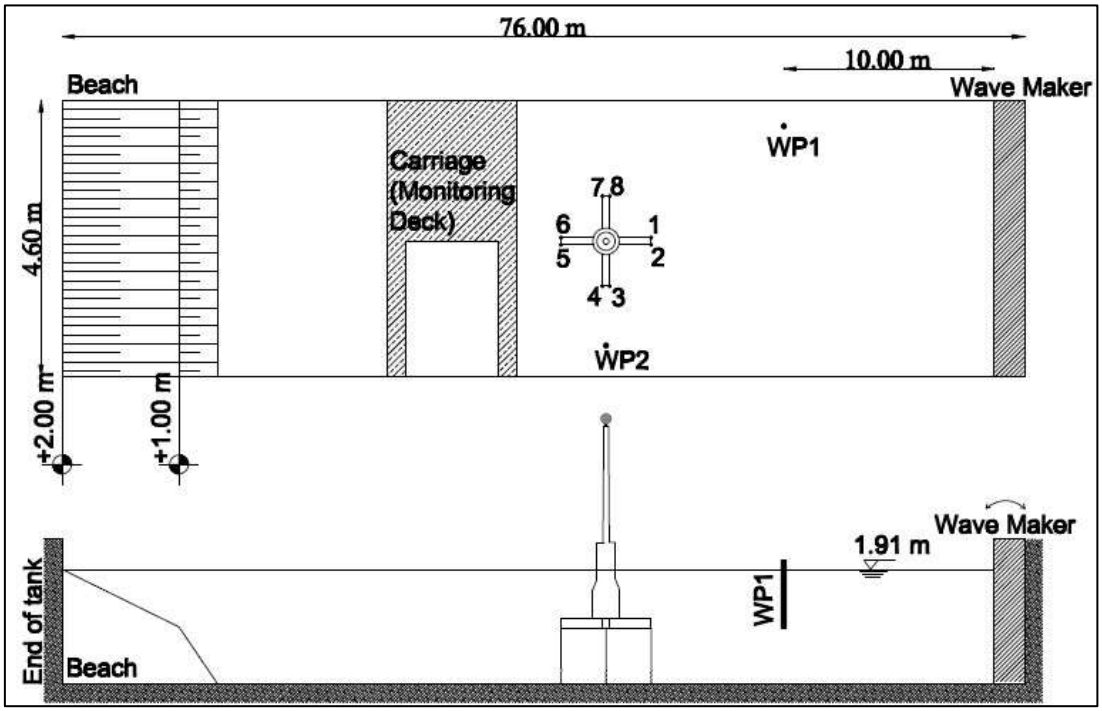

Figure 4.2 Schematic view of the model installed in the tank

Apart from a set of tests conducted to define the effect of varying water depth on the system due to tide, the water depth was kept at a value of 70m in full scale for all tests. Water depth was measured from the top of the attachment frame which was mounted 130mm from the tank bottom. Due to the importance of tendon lengths for TLP system dynamics, tendon lengths were modelled correctly. Therefore, water depth was 74.7m (for full scale water depth) used in the experiments instead of 70m. This leads to minor inconsistency in wave kinematics but the correct dynamic response of the platform. A view of the model in the KHL tank looking towards wave maker is given in Figure 4.3.

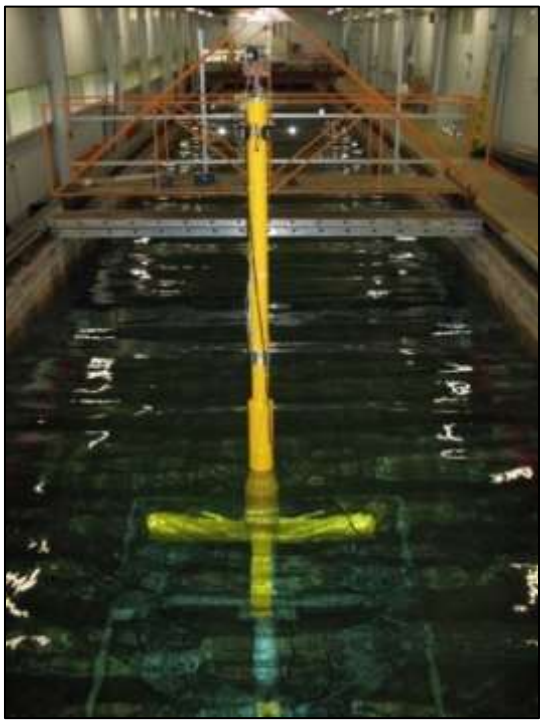

Figure 4.3 View of the model in KHL tank looking towards wave maker

4.2 Scaling

In order to carry out a reliable test, scaling of the model and environmental conditions are very important. Although there is no unique scaling and modelling technique for floating wind turbines, this section will give an explanation on how the final model scale was selected and applied.

4.2.1 Model Scaling Methodology

A suitable scaling methodology must be chosen in order to correctly model the dynamic behaviour of floating wind turbine system. In all experiments of this type there is always the major problem to overcome the inability of simultaneously maintaining Froude and Reynolds numbers for scaled floating wind turbine experiment. In order to represent the relationship of viscous and inertial forces for a fluid flow, Reynolds scaling is commonly used to establish model parameters in wind tunnel experiments (Çengel and Cimbala, 2006). On the other hand, Froude scaling is the most common similitude for wave basin experiments as it properly scales the gravitational and inertial properties of wave forces and the dominant external wave forces for a floating structure (S.K.Chakrabarti, 1987).

Froude scaling was adopted for the experiments due to the advantage of proper scaling of wave forces and inertial effects. There are, however, some parameters which cannot be properly

scaled using the Froude approach in particular Young Modulus (EA) of mooring lines and the effects of viscous forces.

To achieve a Froude scale stiffness the scaling dimensions and scaling material modulus should be known at the same time. In practice, the materials used in the experiments are not same as the full scale structure which means both have different material densities and Young modulus. Due to this reason, material density, stiffness and geometry are usually considered together to obtain the all dimensions, mass properties and stiffness of the model at the same time.

Reynolds number is the ratio of inertia forces to viscous forces which is given as:

$$Re = \frac{\rho V L}{\mu} \quad (4.1)$$

ρ denotes the fluid density, V denotes the mean velocity of the object relative to the fluid, μ is the dynamic viscosity and L is the fluid length of travel of interest. Reynolds number scaling is particularly used where maintaining the viscous and inertial properties of fluid flow is critical such as wind tunnel testing of air foil sections, wind turbines (Çengel and Cimbala, 2006). Since Froude scale model is selected for this study, Reynolds number similitude is not maintained. As the structure is dominated by inertia and gravitational forces instead viscous forces, therefore, viscous effects are ignored for this study.

The scaling relationships used to define the scale of TLP type floating turbine model are presented in the following section.

4.2.2 Scaling Criteria

The Froude scaling relationships for the model are described below.

The Froude number for a free surface wave is:

$$Fr_{wave} = \frac{C}{\sqrt{gL}} \quad (4.2)$$

C is wave celerity, g is the local acceleration due to gravity and L is a characteristic length. Considering a scale factor of λ and geometric similarity, the scaling relationship between model scale and full scale is given as:

$$Fr_p = Fr_m \quad (4.3)$$

where p and m stand for prototype and model, respectively. Based on geometric similarity, linear dimensions of the model are scaled linearly using the scale factor λ.

$$l_p = \lambda l_m \tag{4.4}$$

Considering the geometric similarity and Froude scaling most of the established scaling factors for floating wind turbine model testing parameters can be found in (S.K.Chakrabarti, 1987).

4.2.3 Scaled Model dimensions

The principle dimensions of the tank as well as the capability of the wave maker are the most important issues which determine the scale factor to be used for the experiments. Since Reynolds number scaling is not being used the model size should be as large as possible in order to mitigate viscous effects. In addition secondary factors such as ease of model construction, availability of materials and instrumentation systems will also influence the final scale factor selected to some extent.

In order to have the target values of maximum significant wave height and achieve the target water depth, (measured to the bottom of the tendons) of 1.90m the scale was selected to be around 1:36.5. A final scale of 1:36.67 ($\lambda = 36.67$) was selected, allowing the tower to be constructed from readily available stock aluminium tubes.

This is relatively large scale model compared to those tested using working turbines, for example in the OC3 and OC4 projects, which were tested at 1:50. Dimensions for the full scale TLP and its scale model along with other parameters are given in Table 4.1.

Table 4.1 TLP wind turbine prototype and 1:36.67 model dimensions

Item	Full scale	Units	Scale factor	Model Target
Span	55.00	m	λ	1.500
Pontoon width	4.40	m	λ	0.120
Pontoon height	5.50	m	λ	0.150
Central column diameter	8.20	m	λ	0.224
Central column height	23.17	m	λ	0.632
Transition piece height	6.33	m	λ	0.173
Tower toe diameter	5.59	m	λ	0.152
Tower upper diameter	3.87	m	λ	0.106

Tower height	71.10	m	λ	1.938
Water depth (MSL)	70.00	m	λ	1.910
Draft (MSL)	35.50	m	λ	0.970
Freeboard	16.50	m	λ	0.450
Tendon length	34.50	m	λ	0.940
Tendon diameter	90.00	mm	λ	2.450

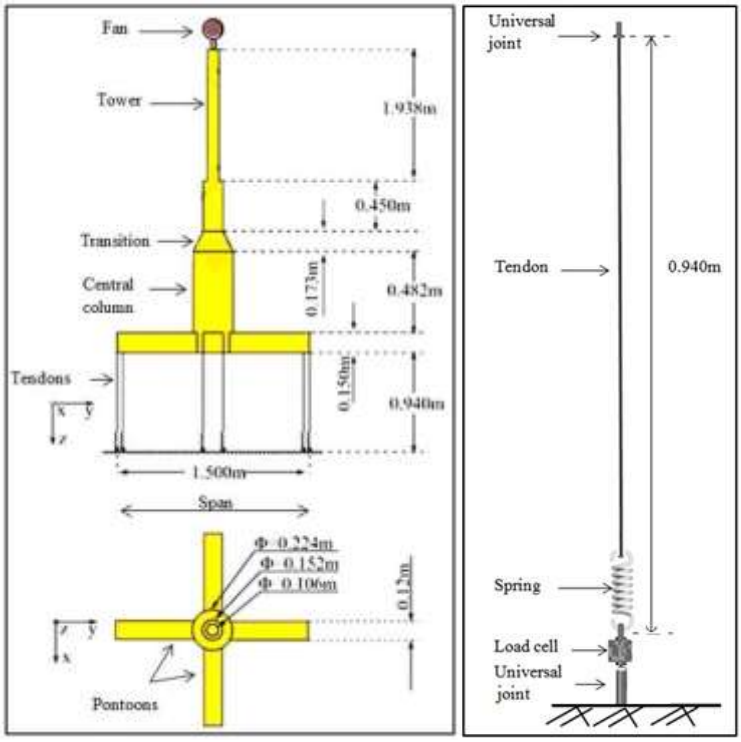

Figure 4.4 TLP wind turbine dimensions in model scale and description

4.3 Model preparation

In this section, the model design, ballasting method and the determination of the model mass properties are described. All target full scale; model scale and the difference of these are given in Table 4.2.

4.3.1 Model Design and Construction

The key challenges for the model were to achieve the mass properties, and in particular, the very large pitch/roll radius of gyration while simultaneously achieving the correct yaw values. The large radius of gyration meant that the majority of the free ballast had to be located in the pontoons with the rest at the tower top. Due to the extent of the testing campaign another important factor was to design a model which could be left in the tank for extended periods without risk of leaking or deforming.

The floater is made up of an aluminium tube, with an accurately-machined plug in the bottom to ensure a watertight seal. The tapered section was CNC machined in divinycell foam in four parts. In order to connect this tube to the tower a further aluminium plug was machined which also made from a stock aluminium tube.

The pontoons were manufactured using a skeleton fabricated from aluminium channel, with welded stiffeners. The pontoon volume was then created through CNC machined divinycell foam. The tendon attachments were machined in aluminium and bolted to the channel sections before being encased in foam. A series of pockets were machined into the lower part of the foam pontoons to accommodate lead ballast. General views of the model during construction are shown in Figure 4.5 and a tendon view during manufacturing is given in Figure 4.6.

a) Pontoons under construction, b) preparation of connectors, c) arranging the mass properties, d) Tower and Fan

Figure 4.5 Floater during construction

The eight tendons were manufactured from 1x19 stainless steel wire attached to custom-made springs in order to scale the stiffness correctly. The spring ends were fixed in clamps so that the tendons could not rotate relative to the springs. Stainless steel universal joints were fixed at top and bottom to minimise rotational friction.

It was difficult to find a correct material for tendon modelling in the laboratory environment considering both mass and stiffness. Correct stiffness was aimed to be achieved using spring plus wire combination. However, there was an error in the selection of wires since they were less stiff than the target value (see section 4.5.6). We could correct pretension for the weight but not for the mass. Tendon diameter was not scaled correctly which means hydrodynamic loading was incorrect. However the hydrodynamic loading on tendons is not expected to be significant.

Due to time and budget restrictions tower stiffness was not modelled during the tests. As a result the accelerations at nacelle did not include the tower dynamics. In the end, the accelerations could not be measured due to vibrations from the fan (see section 4.5.4) while accelerations at CG less affected by this.

Figure 4.6 Tendon during manufacturing

At the top of the tower a platform was manufactured to carry the fan used to simulate turbine thrust. This could be rotated to change the direction of the thrust relative to the floater, and included anti-vibration mount and the load cell used to calibrate the fan. A Collar was also manufactured to carry the wireless transmitter, the Qualisys markers, and some trimming masses used for fine tuning the CG. These are shown in Figure 4.7. A ducted fan unit intended for use on a model aircraft was fitted at the correct vertical location for the drive train. This was capable of developing up to 50N (full scale) of thrust. This was mounted on a load cell and extensively bench-tested to determine the relationship between steady speed and thrust.

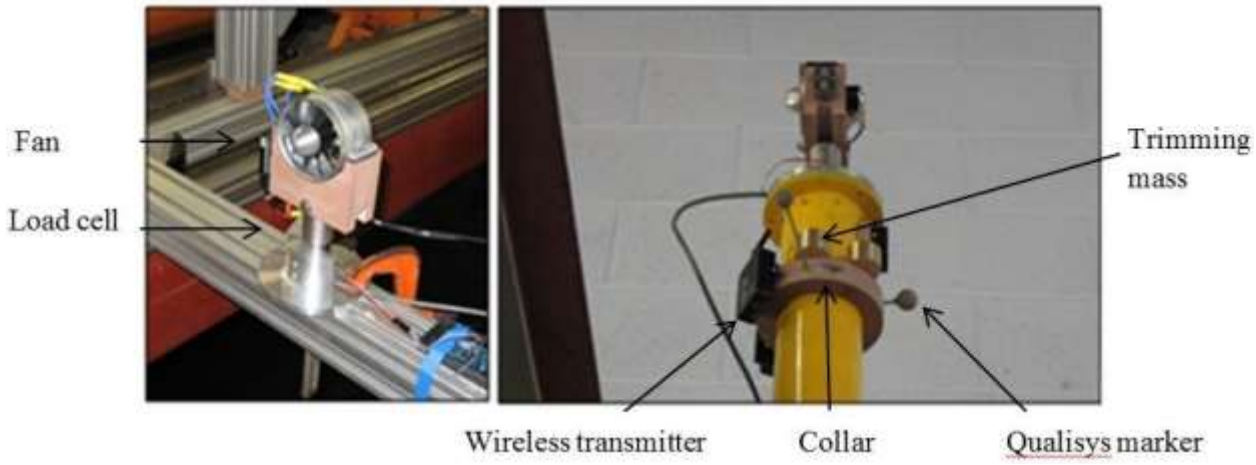

Figure 4.7 Fan and top of tower during construction

4.3.2 Ballasting and Mass Properties

As previously mentioned, the ballasting of the model to achieve the correct mass properties was extremely challenging. The aluminium tube used for the tower was heavier than that used in the design since the chosen tube was not available at the time in the UK. Several other components were slightly heavier than intended, particularly the foam collar on the floater

which was fabricated by a sub-contractor. This reduced the amount of free ballast available. Once the total mass of the model was set to its correctly scaled value, the VCG was adjusted.

For a ship, this would traditionally be implemented using an inclining test in water, but this is impossible for a TLP, as it is unstable without the tendons. For this reason, the VCG was set using a "swing" arrangement which is shown in Figure 4.8. A known mass is moved to a known distance and the angle of the swing is measured. This can then be used to compute the VCG. If the swing is displaced dynamically, the period of oscillation may be measured and used to calculate the radius of gyration in pitch (Kyy) and roll (Kxx). In this case the pitch and roll radii of gyration are equal.

The radius of gyration in roll (Kzz) is found by measuring the period of oscillation in yaw of the model on a platform suspended on two wires – a bifilar suspension. This is shown in Figure 4.8; in this figure the accuracy of the prediction is being tested using two known masses.

Figure 4.8 a) Swing used for VCG and Kyy, b) Bifilar Suspension used for Kzz

Table 4.2 Mass properties of floater

Property	Units	Model	Model Target	Full scale	Full Target	% Error

Mass		Commercial in confidence				0.012
VCG	(m)	0.844	0.835	31.00	30.625	1.2
Kyy	(m)	1.204	1.272	44.20	46.640	-5.3
Kzz	(m)	0.312	0.281	11.50	10.299	11.2

The mass properties achieved are shown above in Table 4.2. The error in the pitch radius of gyration was within 5% of the target value; however the error in yaw radius of gyration was over 11% due to the impact of some components such as the universal joints, and the availability of spaces for the free ballast within the skeleton of the pontoons. To improve these values would require a new model using a different construction technique in order to reduce the weight of the model and give scope for greater variation in the ballast.

4.4 Instrumentation

In this section, the instrumentation systems and Software-in-the-loop (SIL) used during the floater tests are described.

4.4.1 Instrumentation System

In order to select the most suitable instrumentation system for this experimental study, data input range and accuracy were considered as well as the physical size and weight of the sensors. All components chosen for this study were compact, lightweight and provided high resolution and high data rates. In order to reduce the effect of cabling between the model and the land tri – axial accelerations at the nacelle and the model of CoG and the fan thrust where transmitted using a high bandwidth wireless telemetry system.

The fan is used to generate the simulated thrust as discussed in the next section. The beam load cell is used to measure the thrust generated by the fan. The Qualisys system measures the 6-DOF displacements and rotations of the floater. The floater is moored using the tendons, connected to springs, chosen so that the overall stiffness of the tendon / spring combination is correct. Finally, the loads measured using underwater load cells.

The digital Qualisys motion data is converted to 6-DOF analogue output and then passed to the data acquisition system. In all 24 channels of data were logged. Data was sampled at 640Hz using a 16-bit CED 1401 data acquisition system. The schematic layout of instrumentation is given in Figure 4.9, the channel allocation for the data acquisition system is shown in Table 4.3 and the instrumentation summary is shown in Table 4.4.

Table 4.3 Channel allocation for the data acquisition system

Channel Number	Allocation	Units
1	Tendon Load Cell 1	N
2	Tendon Load Cell 2	N
3	Tendon Load Cell 3	N
4	Tendon Load Cell 4	N
5	Tendon Load Cell 5	N
6	Tendon Load Cell 6	N
7	Tendon Load Cell 7	N
8	Tendon Load Cell 8	N
9	Fan Thrust	N
10	Tower Accelerometer Z	m/s^2
11	Tower Accelerometer Y	m/s^2
12	Tower Accelerometer X	m/s^2
13	CoG Accelerometer Y	m/s^2
14	CoG Accelerometer X	m/s^2
15	CoG Accelerometer Z	m/s^2
16	Tower Strain Gauge X	Nm
17	Tower Strain Gauge Y	Nm
18	Surge	mm
19	Sway	mm
20	Heave	mm
21	Yaw	deg
22	Pitch	deg
23	Roll	deg
24	Far wave probe	mm
25	Inline wave probe	mm

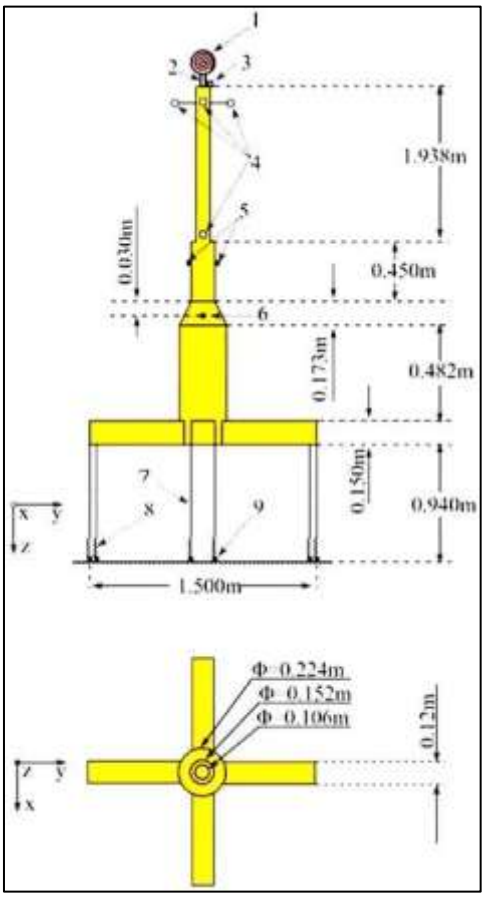

Figure 4.9 Schematic Layout of Instrumentation with dimensions in model scale

Table 4.4 Instrumentation Summary

Item	Contents
1	Fan
2	Beam Load Cell (measure thrust)
3	Tower accelerometer
4	Qualisys motion capture reflection markers
5	Strain gauges
6	CoG accelerometer at VCG (inside)
7	Tendon wires (8 in total)
8	Springs (8 in total)
9	Underwater load cell (8 in total)

4.4.2 Software-in-the-loop (SIL)

For floating offshore wind turbines (FOWTs) there is generally significant coupling between the forces generated by the rotor and the response of the system as a whole. This coupling will affect many aspects of the platform dynamics; in particular the turbine aerodynamics will contribute to the motion damping of the system in modes which affect instantaneous inflow to the turbine. This can affect key parameters such as the accelerations at the nacelle. The mean aerodynamic thrust loads will generate a mean mooring offset which will affect the peak and

long-term mooring loads and may in some cases have a significant impact on some modes of motion while the mean torque on the rotor will generate heeling moments on the floater. In addition to the aerodynamic loads, the turbine generates gyroscopic moments on the floater, which may excite undesirable motions – for example a turbine pitching in colinear wind and waves will generate yawing moments. There may also be some coupling between the blade pitch control system and the platform motions which may result in instabilities of the system.

One possible method of modelling a floating wind turbine in the laboratory environment is to employ a working rotor in a wind field generated by a series of fans. The size of modern wind turbines designed for offshore deployment changes between 1/50 – 1/100 scale ratios.
An alternative possibility is to utilise the idea of "software-in-the-loop" (SIL) in which an active control system drives an actuator in real time to generate some of the system behaviour in a model test. This type of approach requires that the actuated forces acting on the model can be predicted in real time with an acceptable degree of accuracy, and is typically deployed when the forces cannot be generated with sufficient realism by a scale model operating in the same physical manner as the full-scale prototype via aerodynamics, hydrodynamics, structural response, control systems or combination of these.

Several factors may limit the actuating the forces through direct physical simulation. These may be the lack of ability to simulate part of the physical environment (e.g. lack of wind generation in a test tank), issues of the size of the facility (e.g. simulation of spread moorings), or issues of the similarity between model and full-scale prototype as discussed above. Since the Kelvin Laboratory does not have the capability to generate wind directly, software in the loop approach was used to control a fan to simulate the aerodynamic thrust load on the TLP.

The key benefits of SIL approach are summarised below:

- The tests could take place without the need for deployment of a wind generation system – test in wider range of tanks
- There is no need to construct a scale-model (or disorted-scale-model) rotor and drive (It is challenging as explained in Chapter 2.)
- The scale of the tests is dictated only by the hydrodynamics of the floater, which in this case allows a test at relatively large scale (e.g. the model scale was twice that used in (Shin et al., 2013))
- The tests procedure can replicate the forces generated by turbulent or steady wind in a variety of directions relative to the wave heading

- The impact of the turbine control system and blade elasticity on the thrust load may be modelled in the tests
- Correct simulation of the aerodynamic drag load on the tower and parked turbine in extreme conditions is possible
- Some special cases, such as emergency stop tests can be simulated with correct fullscale behaviour

The SIL system deployed in these tests only attemps to simulate the aerodynamic thrust forces. Gyroscopic moments and aerodynamic torque are neglected. Gyroscopic forces could be simulated using a rotating mass (Cermelli et al., 2009), but this was not adopted in the current study due to lack of time. Torque force is less important for TLP, as reported in (Martin et al., 2012) due to the high stiffness in heel. In principle the direction of the thrust vector is arguably incorrect when the platform pitches; however for a TLP, the pitch is extremely small, so it is reasonable to neglect this effect. Technical challenges which must be overcome include generating adequate forces in the direction of interest, and obtaining sufficiently rapid response of the actively-controlled system.

The SIL control system was developed by CENER (Centro Nacional De Energias Renovables). Figure 4.10 shows how the SIL method works. Waves generated by wavemaker excite the 6 DOF motions of the model which are measured in real time using the QUALYSIS motion tracking system and sent to the SIL control computer. The SIL computer runs a modified version of the FAST aero-hydro-servo-elastic code in which the standard hydrodynamic calculations to find instantaneous values for platform position, attitude and velocities are replaced by the values obtained from the tank measurements. The control actions determine the type of the wind file e.g. turbulent, constant or gusting as well as the operational modes of the turbine e.g. power production, idling etc. Then, aerodynamic forces are calculated using desired turbulent wind files previously generated by Turbsim for each sea states. Then the code calculates the aerodynamic thrust expected with the instantaneous platform location and dynamics in the wind field (either steady or turbulent) and outputs the thrust demand to the fan controller. This in turn controls the fan to rotate at the speed associated with the target value of thrust. The system could also be used without SIL where the fan is run at a constant speed in order to generate a constant mean thrust. The calibration of fan used for this study is given in Section 4.5.5.

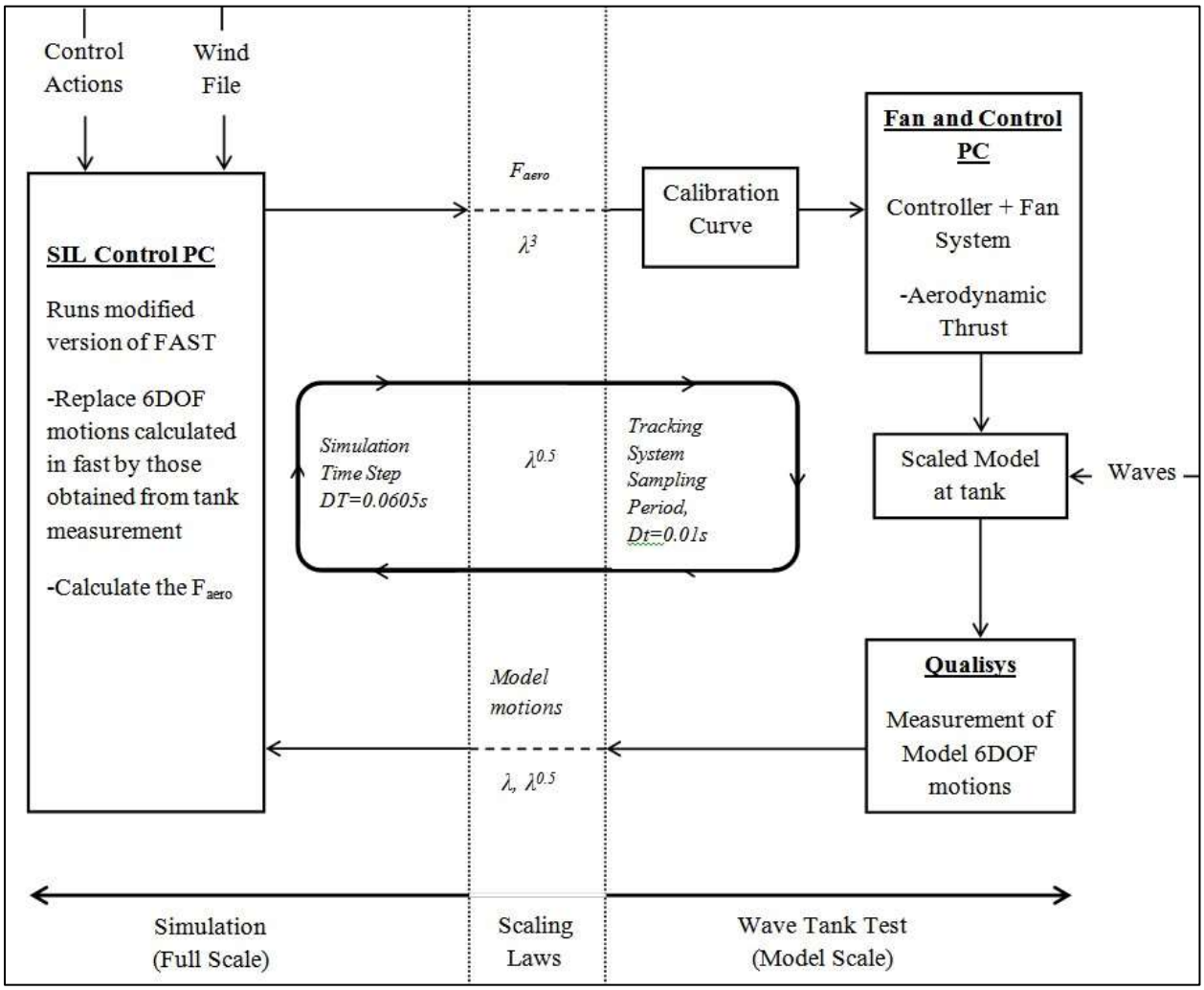

Figure 4.10 Software-in-the-loop (SIL) Method Diagram

There were a number of practical challenges associated with the implementation of the SIL system. Extreme care is required to transform between the different co-ordinate systems adopted by Qualisys and FAST. Furthermore it was found that in spite of the use antivibration mountings, the fan excited the tower-top accelerometer so that the measurements from this accelerometer could not be used in some cases. However since the TLP exhibits almost no pitch and roll, it was found from tests without the fan that accelerations at the platform CG and the tower top were almost identical but it should be noted that the tower stiffness was not modelled.

A specific disadvantage of the software in the loop system as implemented here was related to the vibration due to the fan, since it was discovered that the measurements obtained from tower top accelerometers were strongly affected by the fan, and these results proved to be highly questionable. Calculation of acceleration by differentiation of the positions data from the

Qualisys system was also investigated as an alternative but it was found that results were found too noisy to be meaningful. Future studies should focus some effort to explore the solution for this problem in future.

In general, Software in the loop system is challenging to validate and further systematic study of software in the loop system should be done in future.

4.5 Instrument Calibration

4.5.1 Introduction

The instrument package described in section 4.4 was calibrated over an extended period in order to ensure reliable measurements. This section describes the procedure adopted and presents the results of the calibration process.

4.5.2 Beam Load cell calibration

The beam load cell was used to measure the thrust produced by the fan. Due to its mounting position the load cell is affected by the dynamic (inertial) and static response (trim) of the platform as well as by mechanical and electrical interference from the fan. For these reasons the load cell output was found to be unreliable during tests and the results were therefore not used in this study; however the results were invaluable for calibration of the fan load. During the tests, the output of the load cell was transferred to the load cell amplifier via a wireless link with a built in amplifier and from there to the data acquisition system. In order to check the performance systematically, the load cell was first calibrated using a wired connection to a conventional load cell amplifier. This allowed the performance of the load cell to be quantified. The load cell was calibrated in the standard fashion using calibrated masses hung directly onto the load cell. The specifications of the equipment used are shown in Table 4.5 and Table 4.6.

Table 4.5 Specification of the wired amplifier

Amplifier	
Manufacture	OGAWA SEIKI
Model	DSA-100-6
Serial No	40028
Excitation	9V
Gain	1v/kg

Table 4.6 Specification of the reference mass

Reference Mass	
Manufacture	Kern & Sohn
Material	Brass
Type	OIML M1
Uncertainty	50mg per kg

The calibration result with the wired connection and the residuals of the resulting linear regression are shown in Figure 4.11. Here SN stands for serial number and SEE stands for standard error estimator. Residual of a value is the difference between the measured value and the estimated or fitted value of the quantity of interest.

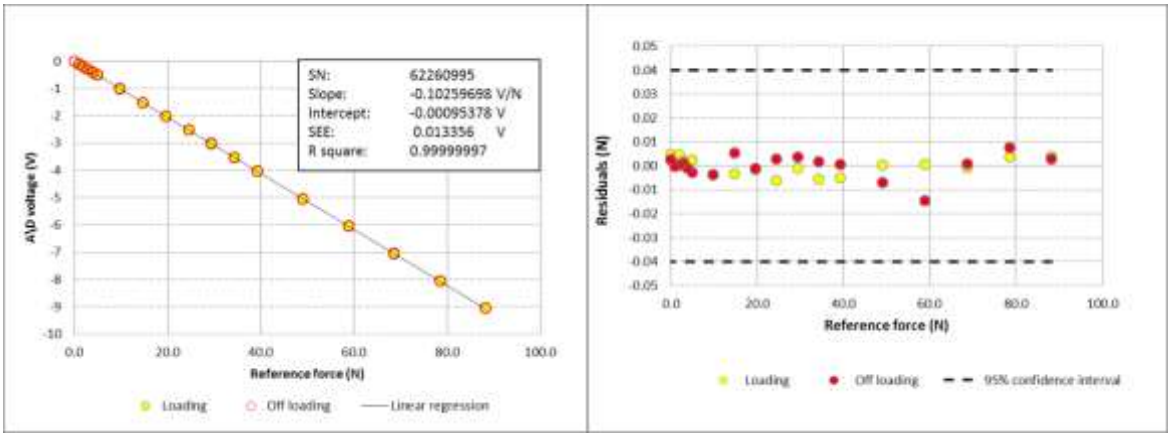

Figure 4.11 Calibration of the beam load cell with wireless amplifier

The wireless transmitter (with built-in amplifier) is illustrated in Figure 4.12. The calibration process was then repeated in order to compare the performance in terms of linearity with the high-quality conventional amplifier. Specifications of the amplifier and reference mass can be found in Table 4.7. The calibration result and residuals of linear regression are shown in Figure 4.13.

Figure 4.12 Wireless transmitter

Table 4.7 Specification of the wireless amplifier

Amplifier	
Manufacture	LORD MicroStrain
Model	V-Link-LXRS
Serial No	1000-46123
Excitation	3V
Gain	2.5mV/V

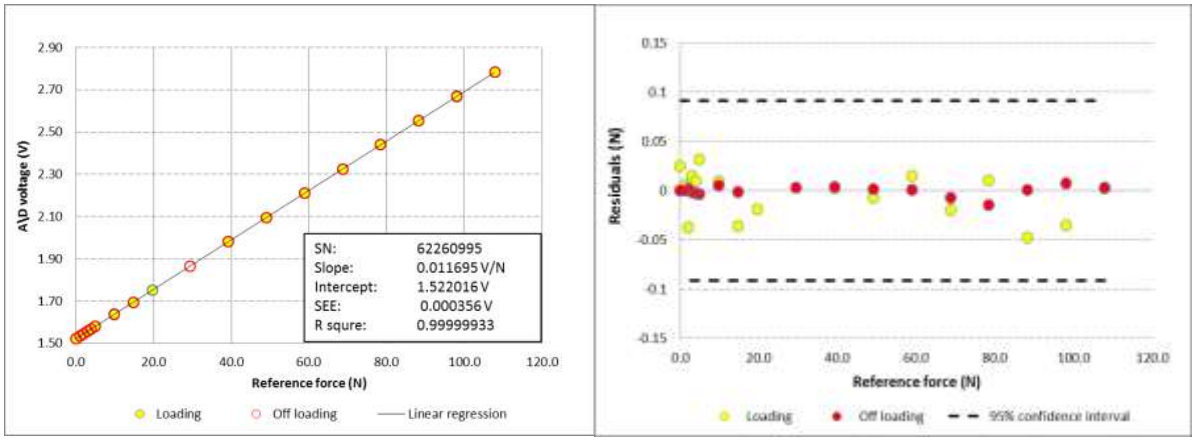

Figure 4.13 Calibration of the beam load cell with wireless amplifier

It can be seen that the linearity of the wireless amplifier is very good, although slightly less good than with the conventional load cell amplifier. Residuals are slightly larger, but the 95% confidence limit is less than 0.1 N. Table 4.8 shows the low, medium and high load check of the beam load cell after calibration.

Table 4.8 Low, medium, high load check of the beam load cell after calibration

Force (N)	**Measured Force (N)**	**Residuals (N)**

0.980525442	1.0350709	-0.054545458
24.51313605	24.485869	0.027267049
53.92889931	53.970305	-0.041405693
107.8577986	107.93809	-0.080291385

4.5.3 Underwater Load Cell Calibration

In this section, calibrations of the underwater load cells used to measure the tendon tensions are presented. The load cells were calibrated in conventional fashion in series as illustrated in Figure 4.14. A typical plot of calibration and linear regression residuals are plotted for one of the nine underwater load cells (eight tendons plus one spare) in Figure 4.15. Low, medium and high load reading checks for all load cells is summarised in Table 4.9. It can be clearly seen that the linearity of the load cells is extremely good.

Figure 4.14 Calibration of underwater load cells

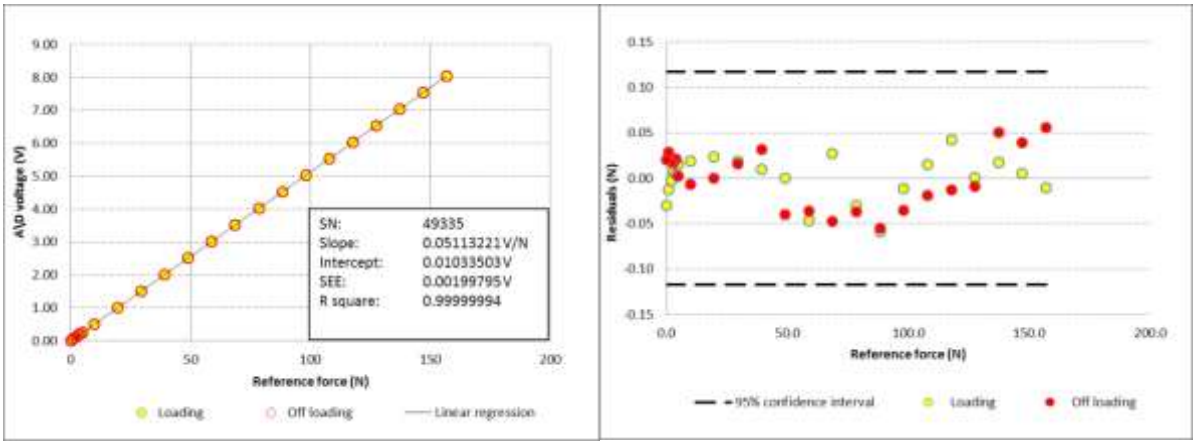

Figure 4.15 Typical Calibration of underwater load cells

The calibration of the underwater load cell was performed in air. As an additional check of the validity of the calibration with the load cell under water, one load cell (serial number 49340) was selected to test in air and underwater with the use of a pulley system as shown in Figure 4.16.

Figure 4.16 Validation of underwater load cell performance in water

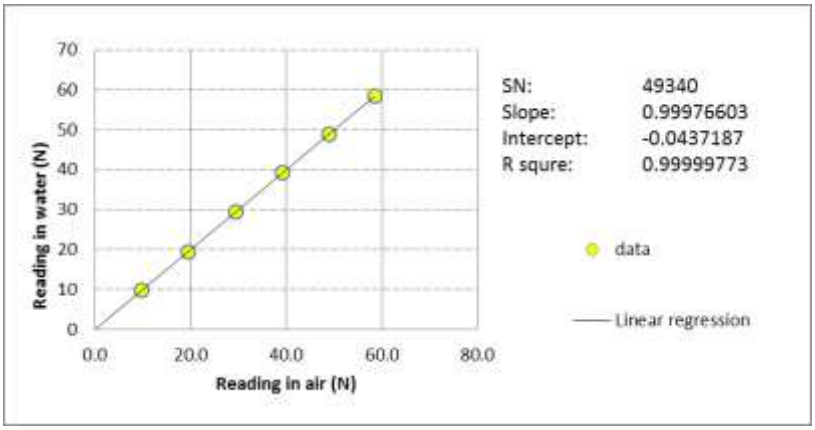

Figure 4.17 Reading of underwater load cell in air against reading underwater

Results are shown in Figure 4.17; if the comparison were perfect, the slope would be 1.0. Some slight error is expected due to friction in the pulley; however the result is extremely satisfactory.

Table 4.9 Low, medium, high load check of underwater load cells

Reading (N)

Reference load (N)	SN:49335	SN:49336	SN:49337	SN:49338	SN:49339	SN:49340	SN:49341	SN:49342	SN:49343
0.980665	0.986844	0.984032	0.981437	0.963137	0.991785	0.937234	0.951379	0.854771	0.944967
78.45320	78.370863	78.463474	78.353643	78.355294	78.419964	78.348111	78.335367	78.231427	78.386338
156.9064	156.899060	156.959660	156.894970	156.914410	156.877850	156.845760	156.829760	156.701310	156.862050

Residuals (N)

Reference load (N)	SN:49335	SN:49336	SN:49337	SN:49338	SN:49339	SN:49340	SN:49341	SN:49342	SN:49343
0.980665	0.006179	0.003367	0.000772	0.011120	-0.043431	-0.029286	-0.125894	-0.035698	
78.45320	-0.082337	0.010274	-0.099557	-0.017528	-0.033236	-0.105089	-0.117833	-0.221773	-0.066862
156.9064	-0.007340	0.053260	-0.011430	-0.097906	-0.028550	-0.060640	-0.076640	-0.205090	-0.044350
				0.008010					

4.5.4 Accelerometer Calibration

In these experiments, two three-axis accelerometers were used. A wireless accelerometer with built-in transmitter deployed at the top of tower. As it was not clear that the wireless transmitter built-in to the wireless device would work inside the tower, a wired accelerometer was selected for CG. However the output from the wired device was transmitted through a wireless link mounted on the tower top to the data acquisition system. The accelerometers were calibrated by accurately tilting at known angles so that the component of gravity could be accurately calculated. Typical calibration results for the tower-top wireless accelerometer are shown in Figure 4.18.

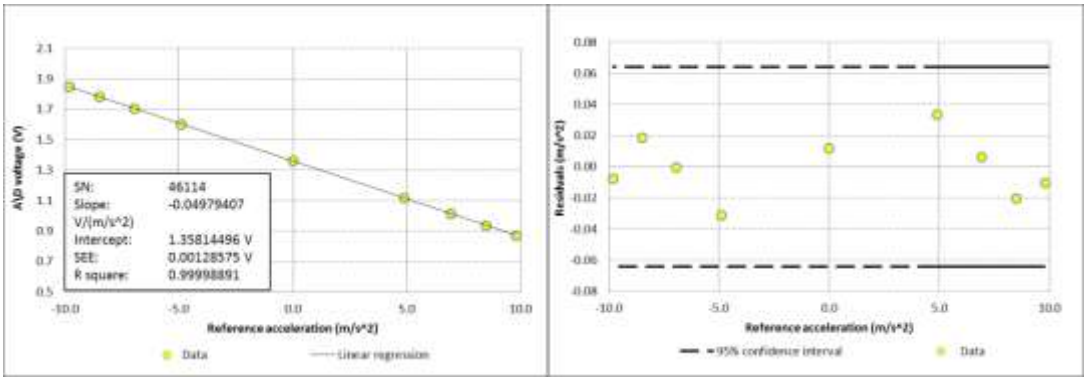

Figure 4.18 Typical Calibration of Tower-top wireless accelerometer

It can be seen that the 95% confidence interval is around 0.06m/s^2. The wired CG accelerometer is shown in Figure 4.19. Typical calibration results are shown in Figure 4.20.

Figure 4.19 Three-axis wired accelerometer

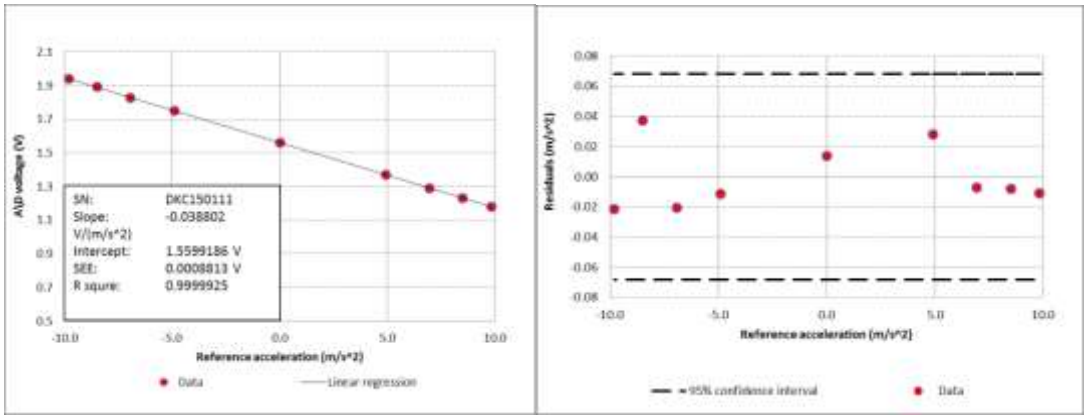

Figure 4.20 Typical Calibration of wired accelerometer at the CG

4.5.5 Fan Calibration

In order to ensure the durability of the fans, the fans used to generate the simulated turbine thrust force were tested extensively prior to calibration. Three fans were purchased in case of failures during the tests.

In the first tests, the fans were ran for 40 minutes at 90 percent of the maximum output to test the feasibility and reliability of running them for the 30 minutes duration of an irregular wave test. This proved satisfactory. All tests were carried out with one fan. Overheating was observed once during the test program, but the fan shut down and tested, and found to be undamaged.

Following this, a static calibration of the fan thrust was carried out using the load cell calibrated previously (see section 4.5.2). The set-up is shown in Figure 4.21.

Figure 4.21 Bench Testing of Fan

Fan control is achieved using a LabVIEW program provided by CENER via an Arduino microcontroller. Six sets of tests were carried out, and a sixth-order polynomial was fitted to the mean results as shown in Figure 4.22:

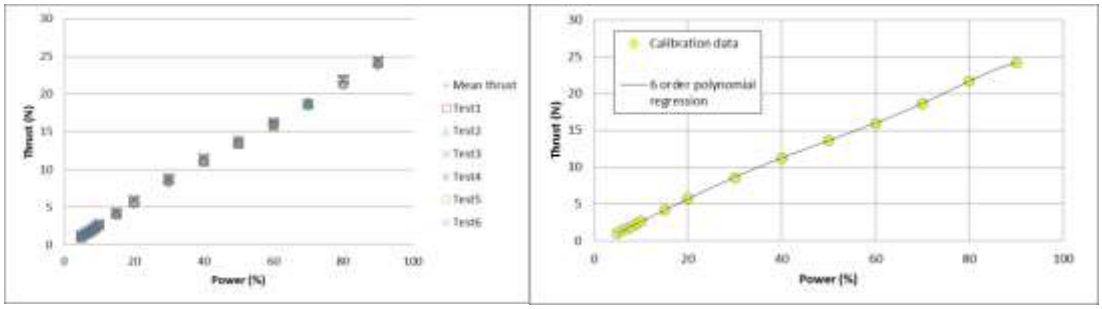

Figure 4.22 Calibration of Fan

After calibration, the results were validated by comparing target thrust with measured values. Results are shown in Figure 4.23. Residuals are typically less than 0.4N.

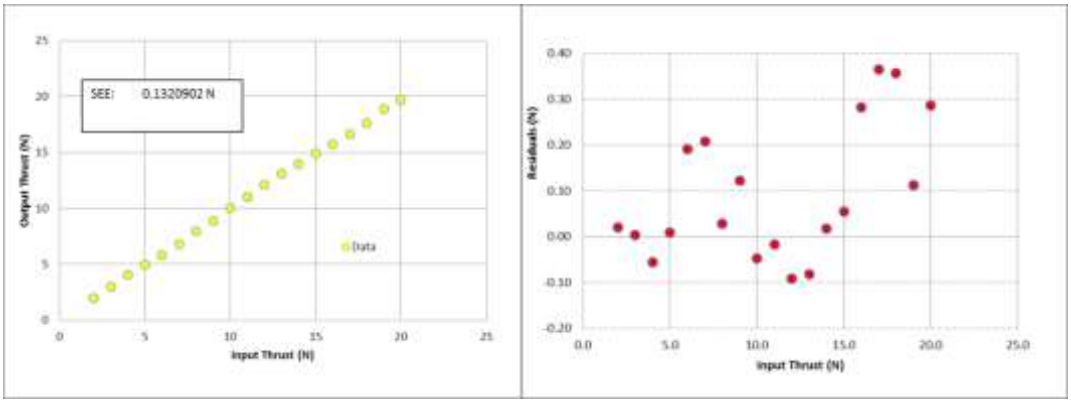

Figure 4.23 Validation of Steady-speed calibration of Fan

All of these tests were carried out with the fan running at steady speed. In practice, the fan must generate a realistic time-varying thrust to account for platform motions and turbulent wind. A time history of thrust (including turbulence) typical for this study was supplied by CENER and a bench test was run in order to examine how accurately the thrust could be generated.

The dynamic calibration of the fan is carried out at a sampling rate of 20Hz due to the limitations of the Arduino controller. For synchronisation purpose, data acquisition is done by Arduino and LabVIEW. Due to the high frequency mechanical noise caused

by the fan, a 50Hz hardware low-pass filter was employed to minimise the noise effect on load readings.

Figure 4.24 presents the complete time history of a dynamic test of the fan system and Figure 4.25 provides a “snapshot” of 20 seconds. It can be seen from the Figure 4.26 that the residual errors over the test record are typically less than 1.0N.

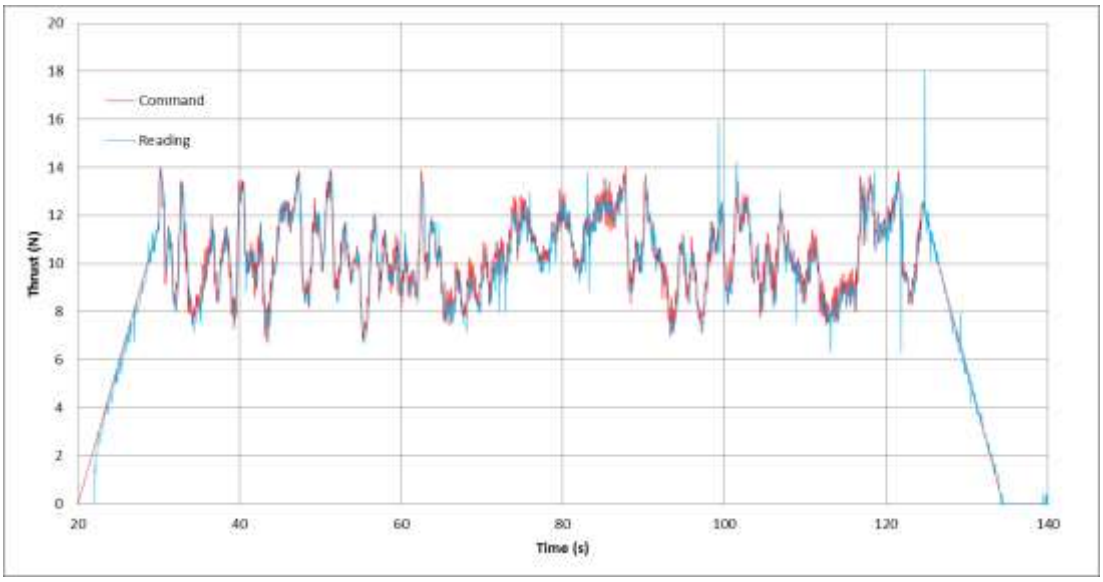

Figure 4.24 Time history of Dynamic Testing of Fan

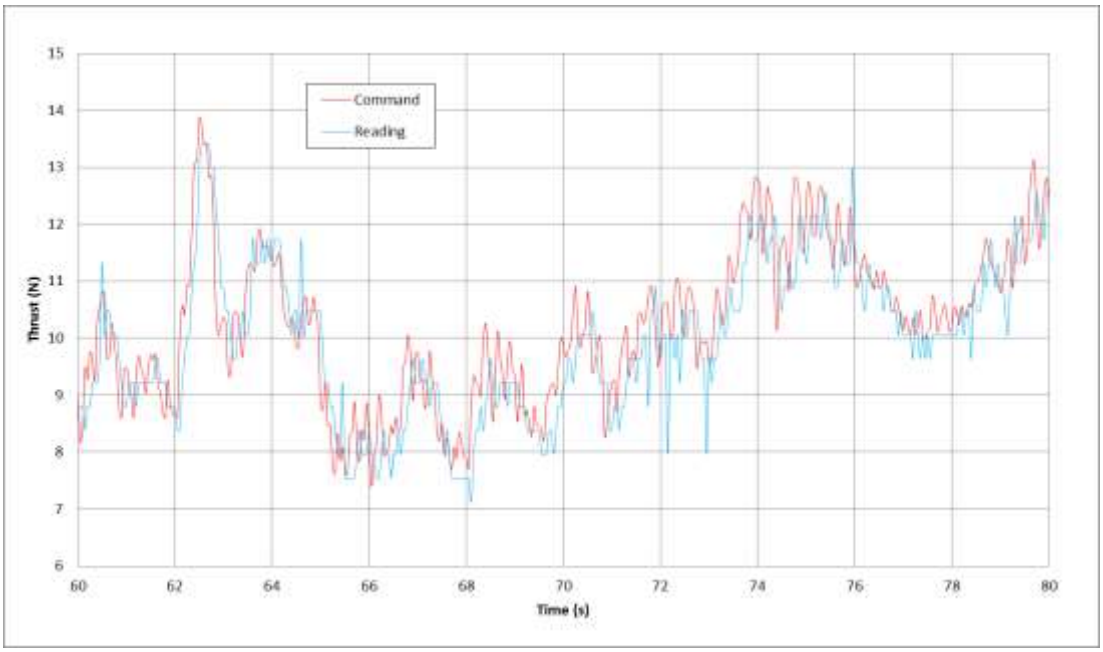

Figure 4.25 Snapshot of Dynamic Testing of Fan

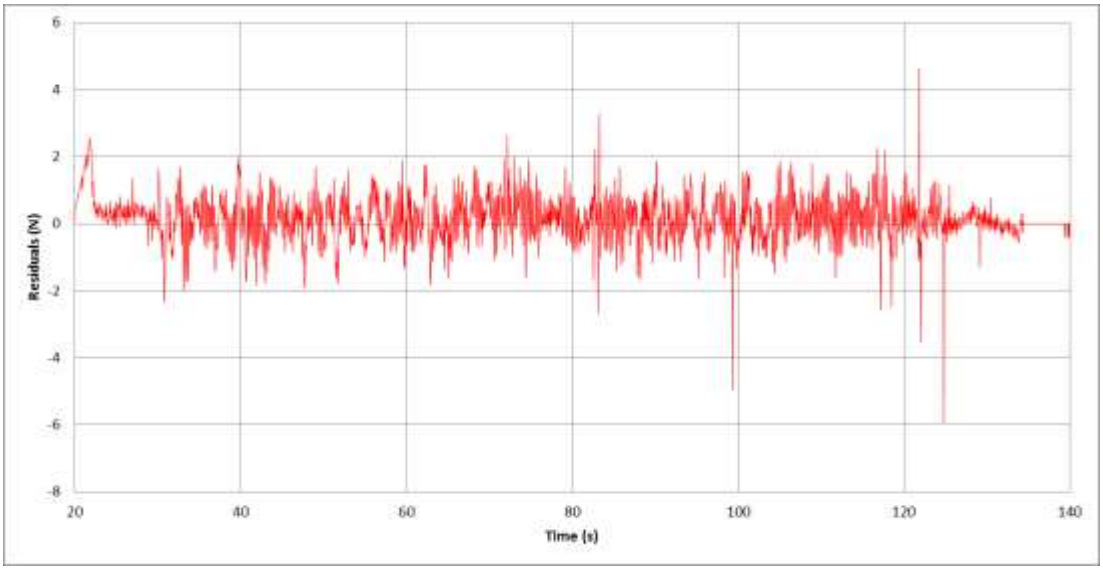

Figure 4.26 Residuals of Dynamic calibration of Fan

Although two more fans have been calibrated in case of fan failure during the test, the results are not included in this thesis.

4.5.6 Tendons

In order to ensure that the tendons had the correct properties special attention was given to correctly scale the stiffness of the tendons used for the tests. As it is not practical to use a wire to achieve the model scale stiffness values, the tendon was represented by a spring connected to a very stiff wire. Effectively the scaled tendon consists of two springs connected in series as shown in Figure 4.27.

Figure 4.27 Schematic view of scaled tendon

In order to measure the length of the tendons correctly, a test rig was used. The measurements are taken from one universal joint to other one. The length of the tendon wires (0.940m in model scale) were checked for 8 tendons. The rig used to measure the tendon lengths is given in Figure 4.28. The variation in tendon lengths was less than 1mm.

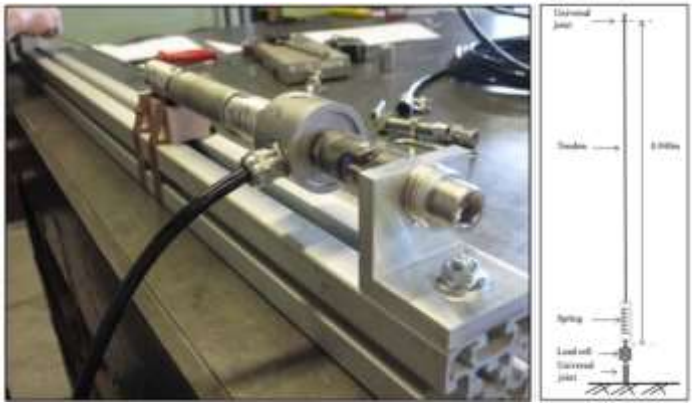

Figure 4.28 Rig to measure tendon length

4.5.6.1 Spring Calibration

In order to calibrate the springs, each spring is hung vertically. After setting the zero when there is no weight on the scale, the spring extension due to the weight pan (reference weight=0.42kg) was recorded. Then each spring was individually loaded and unloaded using calibrated masses in a range of 1-10kg. The process was repeated 5 times for each spring in order to determine the accuracy and repeatability of the calibration process. Finally, spring stiffness was calculated using the extension values. The force-extension graph for spring 2 is shown in Figure 4.29 and forcestiffness graph is shown in Figure 4.30.

It can be seen from Figure 4.30 that stiffness values obtained for loading below 20N showed a nonlinear characteristic and hence these values were not included in the final calculation of the spring stiffness. This is most probably due to the friction between the un-extended coils of the spring and hysteresis effects. It might be worthwhile to explore the use of different spring designs in order to determine the reason of this behaviour clearly in future.

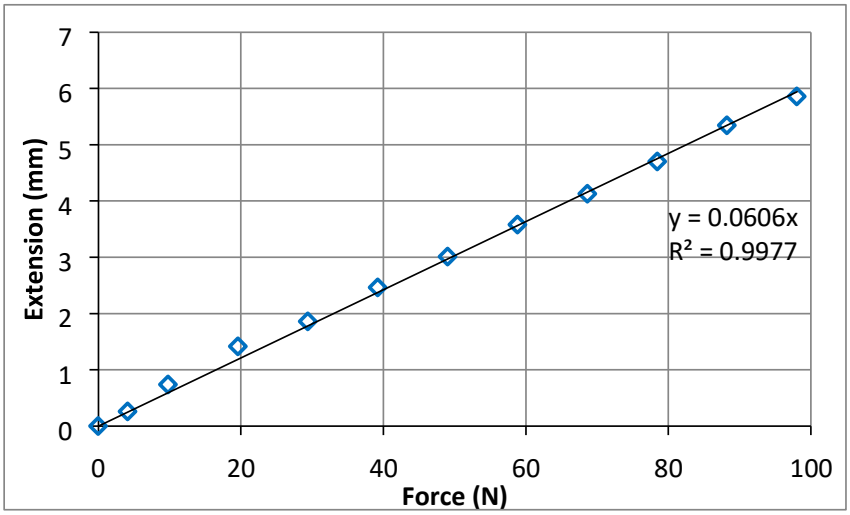

Figure 4.29 Measured extension values for spring 2

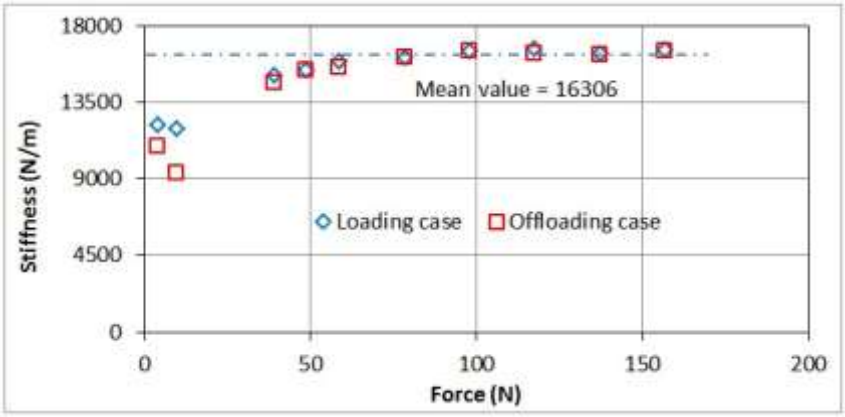

Figure 4.30 Measured stiffness values for spring 2

It can be seen from Figure 4.30 the mean spring stiffness was 16.3 kN/m for tendon 2.

4.5.6.1 Tendon wire Calibration

Before the calibration of the tendon wires they were each pre-loaded with a 40kg mass for a period of 24 hours in order to stabilise the properties of the wire particularly ensuring that the individual wire strands were properly aligned.

a) General arrangement b) Lower connection

Figure 4.31 General arrangement of tendon calibration

The general arrangement of tendon calibration is given in Figure 4.31 and Figure 4.32 respectively. The upper part of the tendon wire is connected to a stiff frame then suspended with a weight pan is connected at the lower part. Known masses were progressively added to (loading) then removed from (offloading) the weight pan and the resulting extension values were measured using a dial gauge as shown in Figure 4.33.

Figure 4.32 Top arrangement

Figure 4.33 Extension Measurements

The force-extension graph for tendon wire 2 is shown in Figure 4.34 and forcestiffness is shown in Figure 4.35. It can be seen from Figure 4.35 that the mean spring stiffness was 139.6 kN/m for tendon 2.

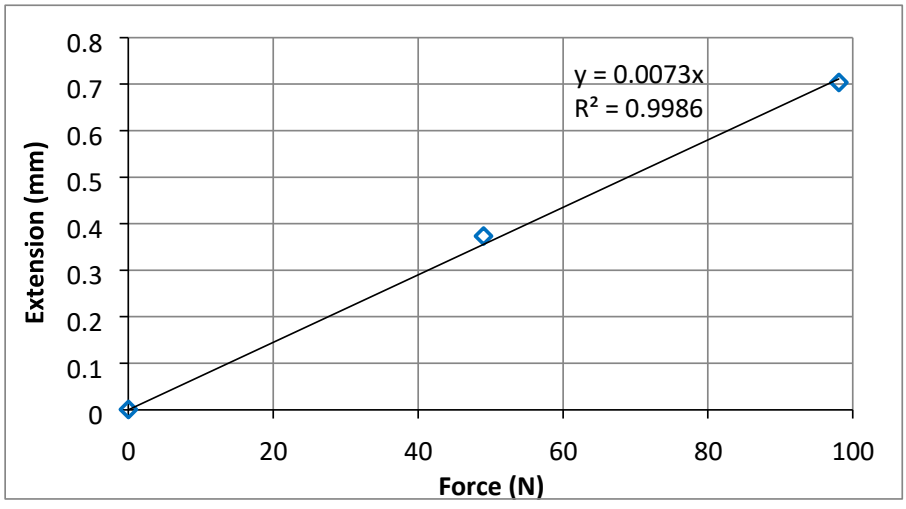

Figure 4.34 Measured extension values for tendon wire 2

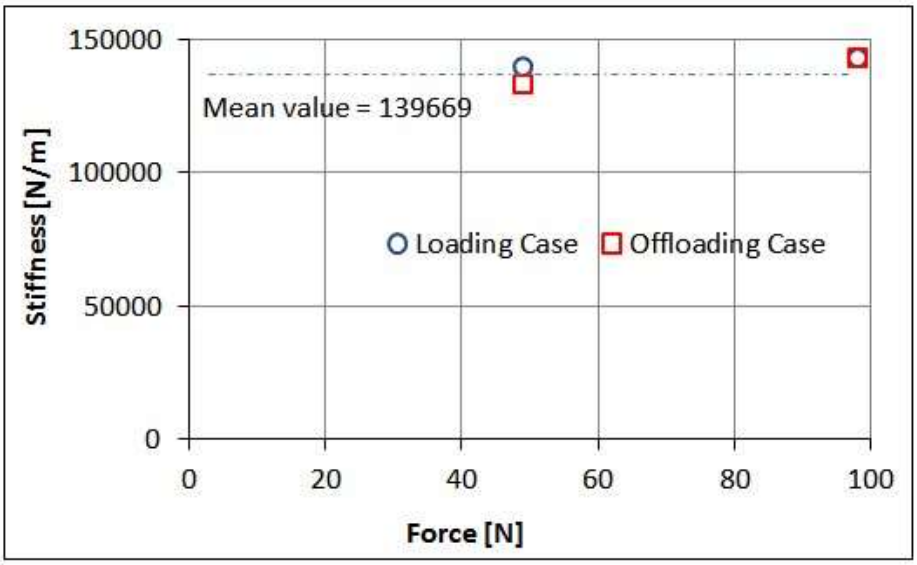

Figure 4.35 Measured stiffness values for tendon wire 2

4.5.6.3 Tendon stiffness

Tendon stiffness consists of tendon wire stiffness and spring stiffness in this experiment. As it is previously mentioned, tendon wire stiffness was measured as 139.6 kN/m and the spring stiffness was calculated as 16.3 kN/m giving a combined stiffness value for the whole tendon of 14.6 kN/m in model scale. Target tendon stiffness in model scale is 16.5 kN/m. This error was due to overestimating the wire stiffness which was practically available. The resulting reduction in the tendon stiffness compared to the target value may cause the motions of the model (particularly in heave) to be slightly larger than expected.

4.5.7 Qualisys

As explained earlier, the six-degree-of-freedom floating body motions were measured using a Qualisys optical tracking camera system. The nature of Qualysis calibration is rather different from the calibration of simple analogue devices, and the results are more difficult to interpret. The standard procedure is to set up the cameras around the measurement volume, and to pass a calibration "wand" through the volume. The wand utilises markers which accurately spaced, and the system computes the time history of the separation of the markers over the duration of the calibration, and computes the mean error.

Six cameras were used in the present study. Three of them were mounted across the tank on an overhead beam, and three of them were mounted along one wall of the tank as shown in Figure 4.36. A set of reflective Qualisys markers were located on the floater near the top with an additional marker near the tower base; the large separation between these markers allows accurate resolution of pitch and roll angles.

The system was calibrated several times over the duration of the tests. The mean residual of the error, which gives an indication of the 95% uncertainty, was typically of the order of 0.3mm.

Figure 4.36 Qualisys camera set-up

4.5.8 Wave probes

As outlined earlier on, the water surface profile was measured via 2 wire resistance type wave probes. A reference probe is permanently located around 10.0m from the paddles. During wave calibration (without the model in place) a second probe is located at the position of the centre of the installation frame. During the tests this probe is moved to one side of the model to record wave phase. This can be seen right-hand image of Figure 4.36.

Prior to installation, the probes are calibrated by moving up and down on a calibration frame with holes precisely machined at 2mm intervals. The wave probes were calculated over a range of +/-60mm, with the main focus on waves of +/-20mm.

A typical calibration curve is given below in Figure 4.37.

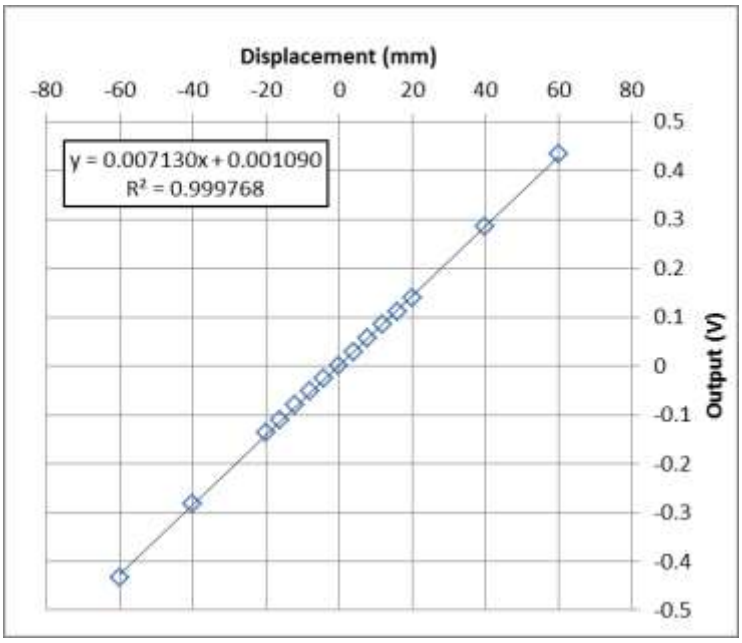

Figure 4.37 Typical wave probe calibration

The standard error estimators calculated from calibrations were typically less than 0.5mm, and hence the 95% uncertainty values for the wave probe calibrations were less than 1mm.

4.6 Wave Calibration

Prior to running the floater tests the sea states were calibrated in order to generate the correct statistical properties. A wave probe was sited at the centre of the model location (in the absence of the model), and the sea states were generated and measured. The significant wave height was then calculated from the time history of the measured data at the model location. If the significant wave height was more than 2% different from the target value, a gain factor was applied to the input data and the process was repeated until the measured value was within the 2% target figure. This usually required two or three iterations.

A spectral analysis was then performed using the data at the model location in order to check the spectral shape in comparison with the target spectrum. This was compared with data from the tank probe located 10m from the wavemaker, and subsequently during the model tests with the data gathered from the inline probe located longitudinally in-line with the model but offset to one side. A typical comparison for storm case (D2027) is given below. Figure 4.38 shows the calculated wave spectra from the wave calibration, and the corresponding values from the in line probe and the tank probe, along with the best-fit Rayleigh distributions.

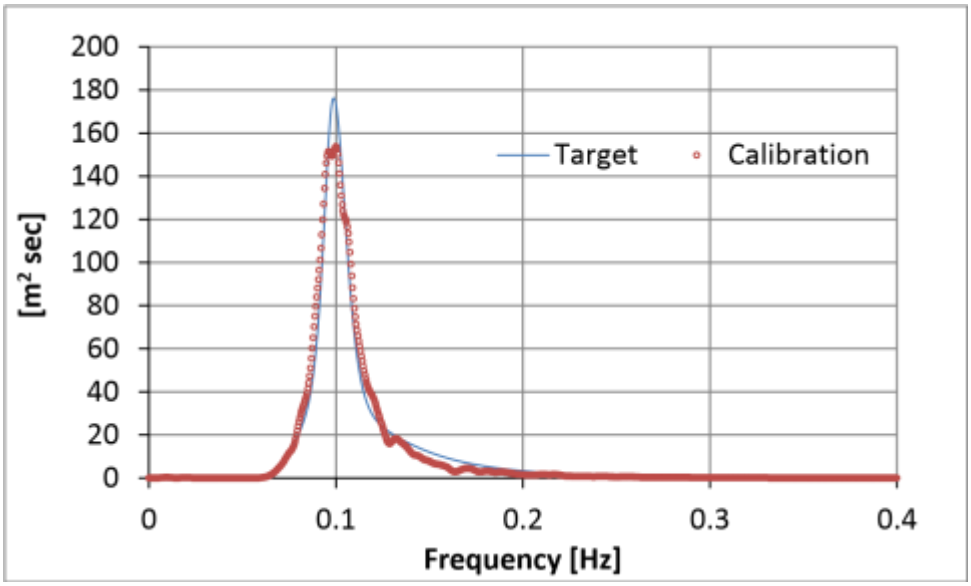

Figure 4.38 Storm condition (H_s=8.46m) Calibration and Target spectra Figure 4.39 shows the pdfs of wave height during wave calibration.

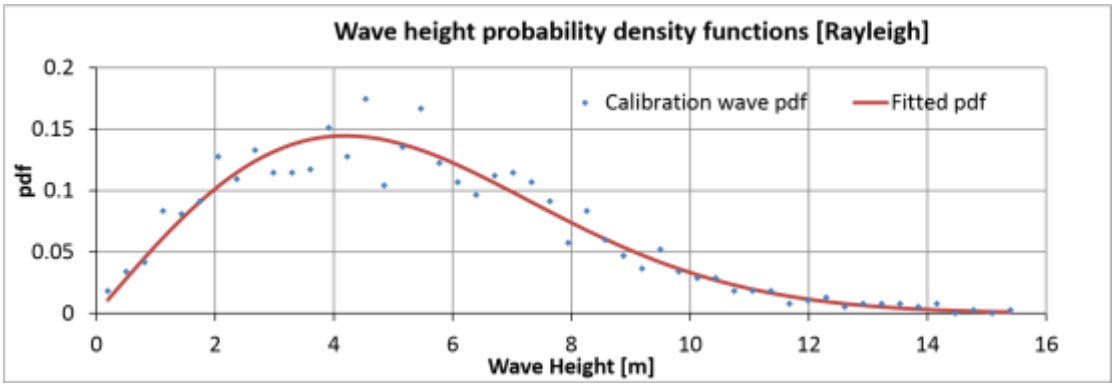

Figure 4.39 Storm condition (H_s=8.46m) Probability Density Functions

When the energy is concentrated over a narrow range of frequencies, the spectrum is called a narrow-band spectrum. The wave elevation follows a Gaussian distribution as it consists of the sum of a large number of monochromatic waves of different wave height and phase. The wave amplitudes have been theoretically shown by (Longuet-Higgins, 1952) to follow the Rayleigh distribution. Figure 4.39 shows the probability density function of the wave heights obtained during the calibration of sea state D2027 compared with a fitted Rayleigh distribution. It can be seen that there is a close correlation between the measured wave height pdf and the Rayleigh pdf. Calibration values of storm case (test D2027) with the target values are given in Table 4.10.

Table 4.10 Wave analysis for Test D2027

D2027 Wave Analysis	Calibration	Target
H(1/3) (m)	8.42	8.46
H_s(elevation) (m)	8.342	8.46
H_s(spectrum) (m)	8.444	8.46
T_p(sec)	10.004	10.13

$H_{(1/3)}$ is calculated by determining the zero crossing points of the wave record and then finding the wave height between successive zero crossing points. The wave heights obtained are ordered and then the mean of the highest 1/3 of the ordered wave heights is determined.

$H_s(\text{elevation})$ is calculated by obtaining the standard deviation of the wave elevation record and multiplying this value by four which gives an estimate of the significant wave height.

$H_s(\text{spectrum})$ is calculated by obtaining the wave spectrum from the wave elevation time history and numerically integrating to find the variance. The significant wave height is found by taking the square root of the variance to give the standard deviation which once again is multiplied by four to give an estimate of the significant wave height.

T_p is calculated by obtaining the spectrum and then finding the frequency, f_p, where the spectrum has a maximum value. The peak period, T_p, is obtained by taking the inverse of the peak frequency.

4.7 Model Installation

The following is a summary of the model installation, calibrations and daily checks.

4.7.1 Installation Frame

An installation frame was designed which could be installed in the tank without divers and without draining the tank on a regular basis. The frame was designed to allow accurate rotation of the structure to allow investigation of different wave headings. This frame consisted of two main parts; the first (static) part was lowered into the tank and held in place with a set of "dogs" or clamps which had been installed in the tank whilst the beach was upgraded. This was carefully aligned with the tank empty and could be repeatably replaced via a set of permanent guides. The base plate and the complete frame are shown in situ in Figure 4.40.

Figure 4.40 a) Installation Frame Base Plate, b) Completed Installation Frame

The second part, formed in the shape of a cross, could be lowered onto the first part and rotated accurately between 0º degrees and 45º degrees via a set of end stops, and then clamped. The tendons were attached to this part of the frame.

4.7.2 Tendon Pre-tension Setup and Validation

The tendon tension has been adjusted so that the SWL (still water level) is at the predefined draft in the given water depth, using accurately measured tendon lengths

which were previously checked for stiffness as described in section 4.5.6. The absolute values (real zeros) of measured static tendon tensions have some degree of uncertainty due to the tendon design however dynamic values were obtained accurately. The measured zero set values were expected to drift over the duration of the tests due to temperature effects, however a procedure was put in place to ensure no drift in the gain was present (see section 4.8.4). The mooring line arrangement is shown in Figure 4.41.

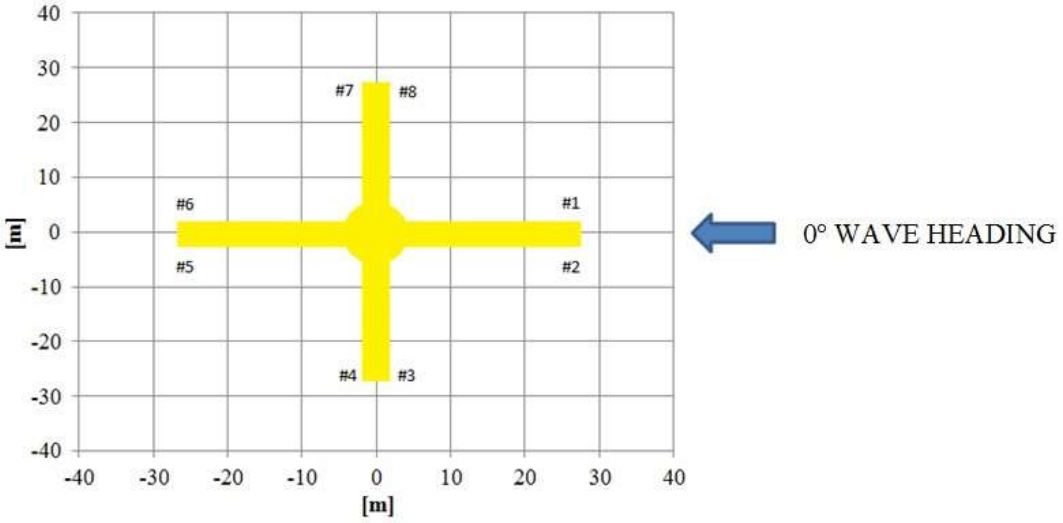

Figure 4.41 Top view of mooring line arrangement

In order to equalise the tensions, a procedure was developed for systematically adjusting tendon tension. The target was to equalise so that all tensions are within 5% of the mean value. The load cells were installed on the support frame and the frame installed in the tank. Following this, the load cells were zeroed in situ at the bottom of the tank, to allow correction for hydrostatic pressure, but with no tendon attached. The frame was then removed and the tendons and model attached, and the frame reinstalled. The tendon tensions were then adjusted using a special spanner via an adjustment bolt located at the top of the tendon, as shown is Figure 4.42 (prior to final painting of model).

Figure 4.42 Tendon tension adjustment bolt on pontoon

Tendons were tensioned in opposing pairs: first 1&2 then 5&6, then 3&4, then 7&8. The process was repeated until the total tension and the variation in tensions was as good as could be achieved, and the model sat on its draft marks in the correct water depth in an upright condition. The results achieved for tendon tension are given in Table 4.11. The corrections to the tendon pre-tensions are calculated by subtracting the measured tendon weight (in water) from the target tendon weight in water, and correcting for the hydrostatic pressure on the load cell.

Table 4.11 Relative value of pretention per tendon

Tendon No	Measured pretention / corrected pretention [-]
1	1.01
2	1.00
3	1.03
4	1.01
5	1.03
6	1.05
7	1.02
8	1.03
Mean	1.0225

As was pointed out in the section 4.5.6., the tendon characteristics had been carefully checked prior to model installation, both with and without the top universal joints (UJs).

4.8 Daily Checks

Due to the complex nature of the instrumentation package deployed a set of tests were carried out daily in order to ensure that the instruments were performing appropriately. These are described as follows.

4.8.1 Water Depth

Given the importance of the tendon pre-tension in these tests it was extremely important to monitor the water level in the tank to ensure that levels remained constant. Small amounts of water are lost over a long period due to evaporation. Water level was checked daily using a fixed ultrasonic wave probe with 95% uncertainty of around 0.6mm and topped up where necessary. This probe was also used to set the water level for the variable water depth tests. The fixed ultrasonic wave probe is shown in Figure 4.43.

Figure 4.43 A fixed ultrasonic wave probe and wave maker

4.8.2 Wave Probes

The wave probes were checked daily to ensure that the gain had not changed. Rather than a full calibration such as that shown in Figure 4.37 (with 15 points), the probes were moved by a known distance up and down on the calibration frame and the measured value checked against the known value. No meaningful changes in gain were observed (i.e. results outside the 95% uncertainty).

4.8.3 Natural frequency check

With a TLP it is difficult to identify a minor leak since the draft does not change. In order to address this, a free oscillation test in surge was carried out every morning. The period of this oscillation is dependent upon the mass, and is highly repeatable (see

Table 5.4 in section 5.4.2); hence a change in period would indicate a change in mass and hence a leak. No changes were in model natural frequencies were observed throughout the duration of the model test campaign. When the model was removed from the tank and the end of the testing period it was completely dry inside.

4.8.4 Tendon Load Cells

The mean value of the amplified output from a strain-gauge type load cell cannot be relied upon to a high level of accuracy over an extended period, as the value is sensitive to changes in temperature of the device (which in the case of an underwater load cell depends on water temperature) and the amplifier (which depends upon air temperature). In the case of the TLP, the calm-water steady-state pre-tension values were measured at the time the floater was installed. The tendon lengths were not adjusted after initial installation. Due to the possibility of slow drift of the mean value, there is no reliable and easy means of checking this pre-tension over an extended period.

For this study, the values measured on installation were taken as the benchmark values for the remainder of the test program. So long as the water level remains constant (as shown by the fixed level measurement described above) and the mass of the floater remain constant (as shown by the free oscillation test described above), the pre-tension must also remain constant.

The gain of the load cells was checked on a daily basis by adding a known mass to the top of the tower and comparing with the measured change in mean pre-tension over all tendons.

4.8.5 Fan

The fan was checked on a daily basis by running at a constant target thrust value, checking the measured thrust, and measuring the floater offset using the Qualisys system to ensure that fan performance did not vary over time.

4.6 Overview of Test Matrix

A large number of tests were performed at the Kelvin Hydrodynamic Laboratory to characterise the behaviour of TLP type offshore wind turbine in a wide range of environmental conditions. The test consisted of free oscillation tests in calm water, regular

wave tests and irregular wave tests at different wind and wave directions. The test was also carried out with combinations of no wind, steady wind and turbulent wind. A summary of the test matrix is given in Table 4.12.

Table 4.12 Summary of System Identification Tests

Test Type	Measurements	Descriptions (in Full Scale)
Free Oscillation Tests	System natural periods and total damping	Surge, Heave, Yaw, Pitch
Free Oscillation + Wind	Damping contribution from wind	Surge
Regular Wave Tests	Linear Response Characteristics (RAOs)	Period Range : 6s-30s Wave Height : 2m (0^o - 45^o Heading)
Regular Wave Tests + Wind	Linear Response Characteristics include wind	Period Range : 6s-30s Wave Height : 2m (0^o Heading)
Irregular Wave Tests + Wind	System behaviour under sea states	8 Sea states (7 combinations of wave and wind direction) Running time : 3 hours

4.7 Conclusions

The experimental methodology to determine the hydrodynamic performance of a TLP type wind turbine was presented in this chapter. Model design and construction, ballasting, instrumentation, instrument calibration, wave calibration, tendon setup and calibration were presented. An overview of the test matrix was described. The reliability of experiments depends on the proper experimental setup as well as daily checks of important system parameters. This chapter provided an essential introduction to the testing campaign. The results showed the fidelity of the model and the instruments used for this study.

The most challenging parts of the test campaign such as setting up the correct mass properties were described in the related sections; some other issues that could be improved for future experimental studies such as modelling of tendons, modelling tower stiffness, measurements of accelerometers in the presence of vibration from the fan have also been discussed.

The following chapters will describe different types of tests carried out in order to investigate the hydrodynamic performance of the TLP type floating wind turbine together with some correlation with numerical calculations using the FAST code.

Chapter 5

Free Oscillation Tests

5.1 Introduction

The natural frequencies are important parameters that affect the dynamic behaviour of the offshore floating wind turbine, so free oscillation tests enable us to determine the natural frequencies which are the function of the mass, added mass, hydrostatic stiffness and damping of the system.

Six sets of free oscillation tests were carried out to characterise the damping coefficients and natural periods (hence added mass) of the system in four different modes of motion as described in Table 5.1. Each test was repeated at least ten times. The surge tests were carried out for three conditions to understand the importance of the representation of wind on the system added mass and damping: no wind, constant predefined thrust (PT), and software in the loop (SIL) controlled thrust, with wind speeds corresponding to the rated wind speed for the turbine. Three level of wind idealisation were used in this study.

1. Pure hydrodynamics (no wind condition)
2. Idealised wind condition – consists of hydrodynamics and constant aerodynamic thrust (predefined thrust condition)
3. Fully realistic condition (Software in the loop - with correct velocity, turbulence, controller etc.)

A possible 4th level could usefully be studied in future using software in the loop without turbulence.

Table 5.1 Free Oscillation Tests

Test ID	Contents
D1001	Surge (no wind)
D1002	Surge (PT w_s=11.4m/s)
D1003	Surge (SIL w_s=11.4m/s)
D1004	Yaw (no wind)
D1005	Heave (no wind)
D1006	Pitch (no wind)

The tests were carried out by displacing the structure in each mode of motion and carefully releasing it. In the case of heave and pitch it proved extremely difficult to achieve reliable results due to the high stiffness of the system, the difficulty of imposing sufficient motion without exciting other modes, and the rapid decay. Consistent results were achieved in surge and yaw. Due to commercial confidentiality only relative values for added mass and damping are presented.

5.2 Methodology

When an underdamped six DOF system is triggered by an initial displacement and/or initial velocity the motion theoretically will continue indefinitely. Offshore floating wind turbine systems, in reality, will always have some damping which means that these systems will dissipate energy and eventually return to an equilibrium position.

The damping ratio shows how quickly oscillations in the system decay after disturbances in any of the six DOF. The ratio of damping constant c to the critical damping constant c_c defined as damping ratio.

$$= \frac{c}{c_c} \tag{5.1}$$

Where $c_c = 2m\omega_n$, m is the system mass and ω_n is called the undamped natural frequency. The data analysis process carried out for the free oscillation tests is as follows: The data was first windowed to remove the initial transients as it is important to set the range of cycles taken into account to do the fit for each test. It was often found that the first half-cycle or so showed evidence of the starting condition. So, the first cycle was always omitted. Where the records were short, the whole of the remaining records were then utilised. However for the long surge records, the records were cut to constant duration (30 seconds) to ensure consistency between records, and to ensure that variations were not introduced by variations in record length.

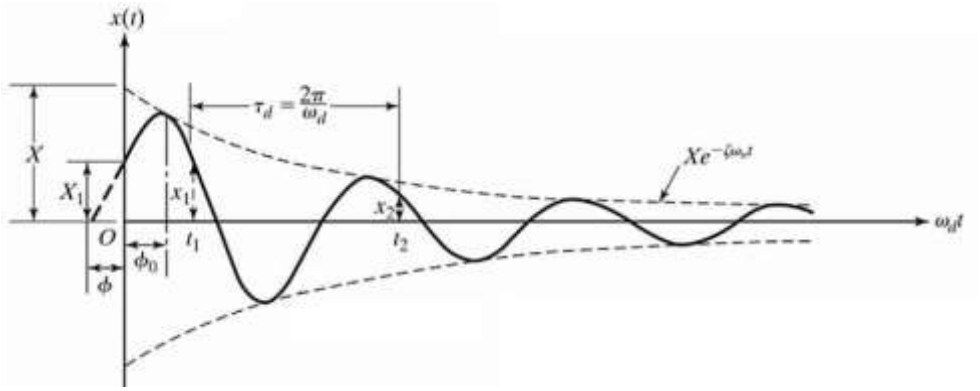

Figure 5.1 Underdamped Oscillation (Rao, 2004)

(Rao, 2004) described the underdamped oscillation case in his study which is shown in Figure 5.1. The experimental data was analysed by fitting an analytical solution for a linear spring-mass-damper system to the time history. This is based on the solution of the linear equation:

$$m\ddot{x} + c\dot{x} + kx = 0 \tag{5.2}$$

The solution takes the form:

$$x(t) = \bar{x} + \hat{x}e^{(-\zeta\omega_n t)}\cos(\sqrt{1-\zeta^2}\omega_n t - \phi_0) \tag{5.3}$$

Here $x(t)$ is the time history of the motion, $\bar{x}$ is the mean value, $\hat{x}$ is the initial amplitude, is the damping ratio, ω_n is the undamped natural frequency, and ϕ_0 is the phase angle. It can be seen from the Figure 5.1 the system oscillates, but the amplitude slowly decreases over time with a period of the damped vibration T_d and at a damped natural frequency ω_d. The relationship between the undamped and damped natural frequency is given by the well-known relationship below.

$$\omega_d = \sqrt{1-\zeta^2}\omega_n \tag{5.4}$$

The fitting process is performed using a non-linear least squares fit (a form of least squares analysis used to fit a set of m observations with a model that is non-linear in n unknown parameters). The non-linear least squares fit aims to fit an approximate model by a linear one and to refine the parameters by successive iterations. Preliminary guesses are made for the five constants in the equation. The simulated time history is then generated, and the RMS error between the simulated time history

and the measured data is calculated. Finally this value is minimised using a Generalised Reduced Gradient (GRG) solver. The Generalised reduced gradient method (GRG) is a precise and accurate method for solving nonlinear programming problems (Lee et al., 2004). Once and ω_d are known, these may be used to characterise the dynamics. If the restoring of the system is known then ω_d may be used to find the virtual mass m and the damping c using:

$$\omega_d = \sqrt{k/m} \tag{5.5}$$

and

$$c = 2\, m\omega_d \tag{5.6}$$

Samples for each of the sets of tests are given in the following section.

The method used in the experiments was to displace the structure in the degree of freedom (DOF) of interest then releasing it, ideally without displacing in the other DOFs. The motions were measured using the Qualisys system. A test in surge is shown in Figure 5.2.

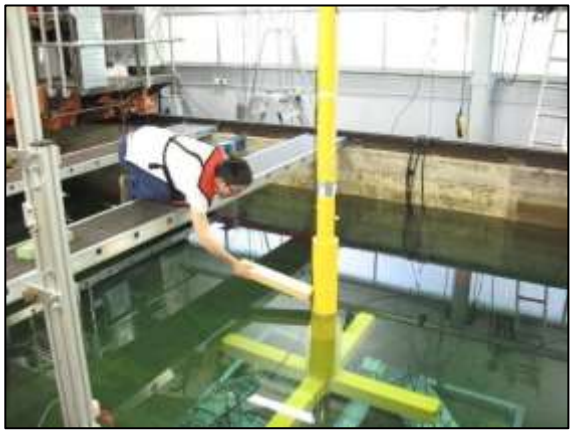

Figure 5.2 Free Oscillation Test in Surge

As was mentioned before, each test was repeated at least ten times. The results of the free oscillation tests in surge in the no wind condition are given in Figure 5.3 .

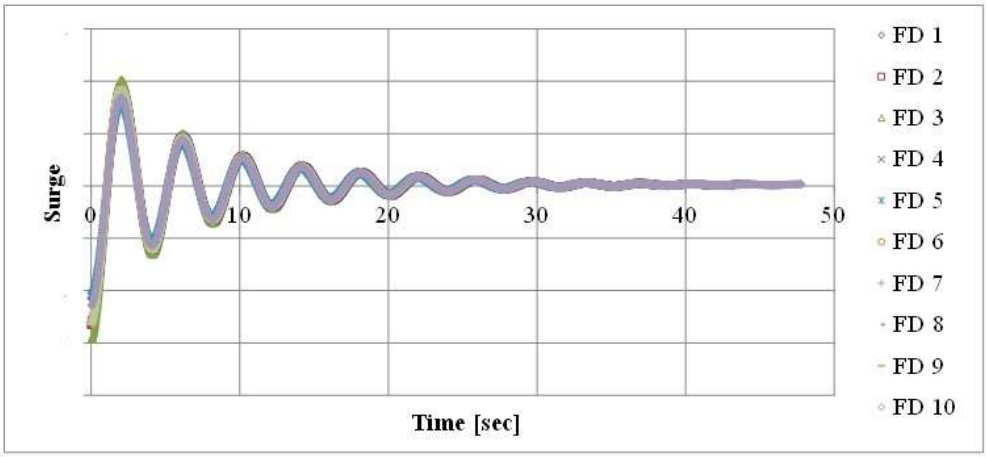

Figure 5.3 Repetitions of Free Oscillation Test in Surge (no wind)

5.3 Sample Fits

5.3.1 Free Oscillation Tests in Surge (No wind)

Figure 5.4 shows that a good fit is achieved for surge in no wind. There is some evidence of non-linear damping, as the fit under predicts the record at the start and over predicts at the end. There is also some evidence of other non-linearity as the period appears to reduce as the motion becomes small. This could indicate slight non-linearity in restoring.

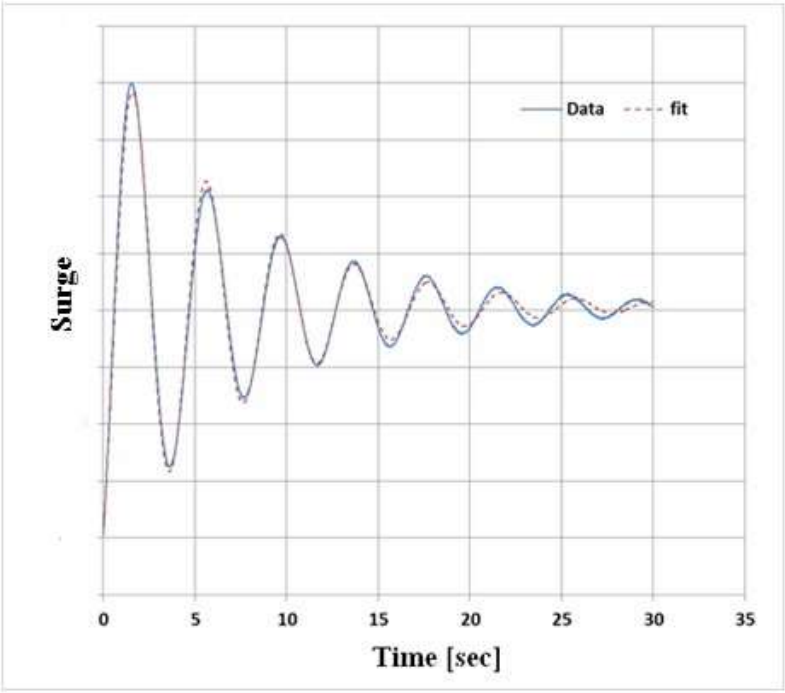

Figure 5.4 Typical fit for surge (No wind)

5.3.2 Free Oscillation Tests in Surge (Predefined Thrust)

A similar quality of fit is obtained in the case of surge with predefined thrust (PT) as shown in Figure 5.5.

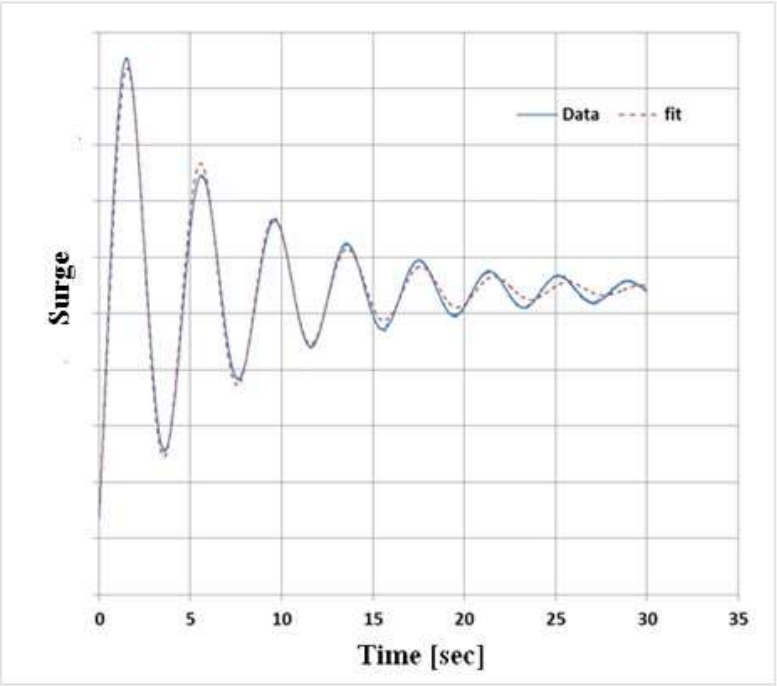

Figure 5.5 Typical fit for surge (predefined thrust)

5.3.3 Free Oscillation Tests in Surge (Software-in-the-loop)

The fit for the SIL case is slightly different as can be seen in Figure 5.6.

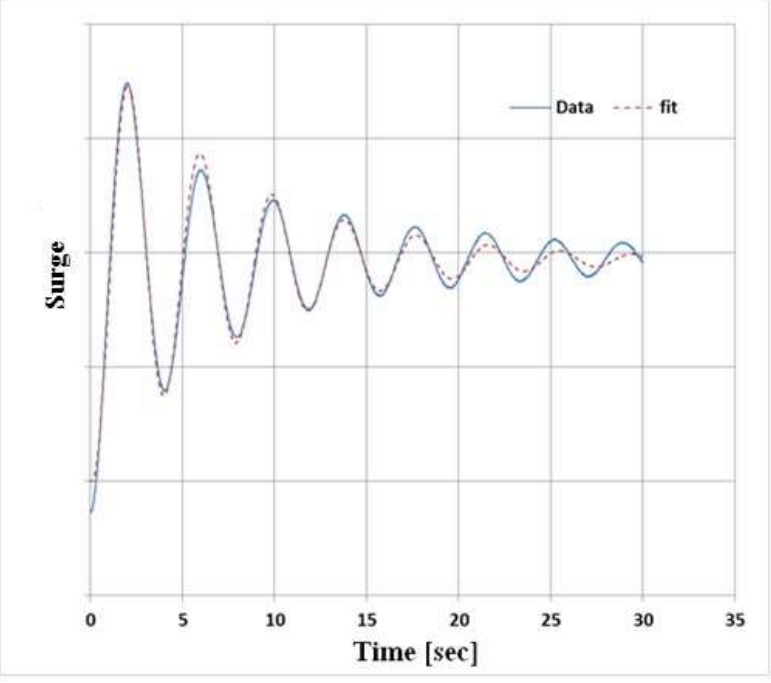

Figure 5.6 Typical fit for surge (SIL)

In this case there is more pronounced differences between the fit and the measured data as time went on. Closer examination of some of the data showed that the surge motion continued long after it might have expected to diminish. This can be seen in Figure 5.7.

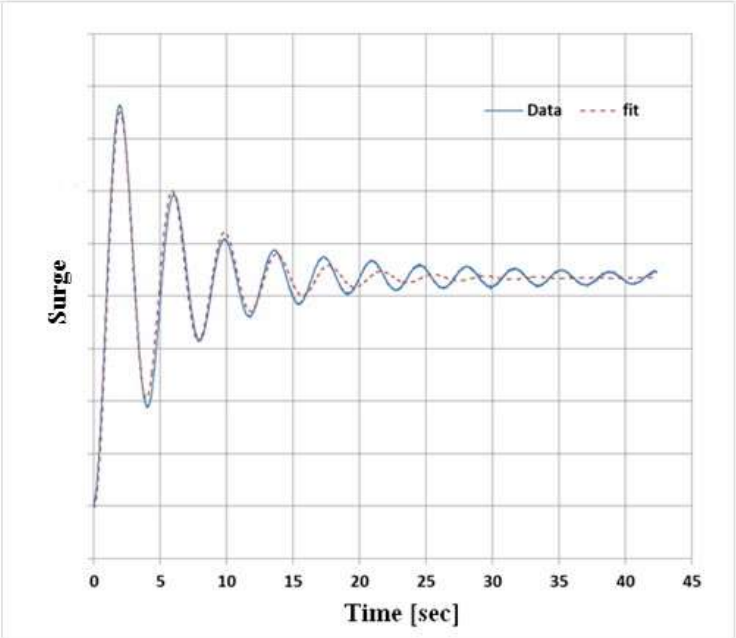

Figure 5.7 Typical fit for surge (SIL) - extended data set

Here it seems that the motion reaches something close to a steady periodic state as time goes on. This may be a suggestion of instability in the controller model simulated in the SIL system.

5.3.4 The wind impact on Surge Free Oscillation Tests

The linear model yielded a good fit for surge in no wind, as shown in Figure 5.4. The quality of fit was similar for the constant predefined thrust; however with SIL active, the damping exhibited a more strong non-linear response.

Sample results for the surge are shown in Figure 5.8. This shows the offset generated by the mean wind. It can be seen that the wind has almost no impact on the natural period, with the mean period for the SIL case found to be around 1% lower than with no wind.

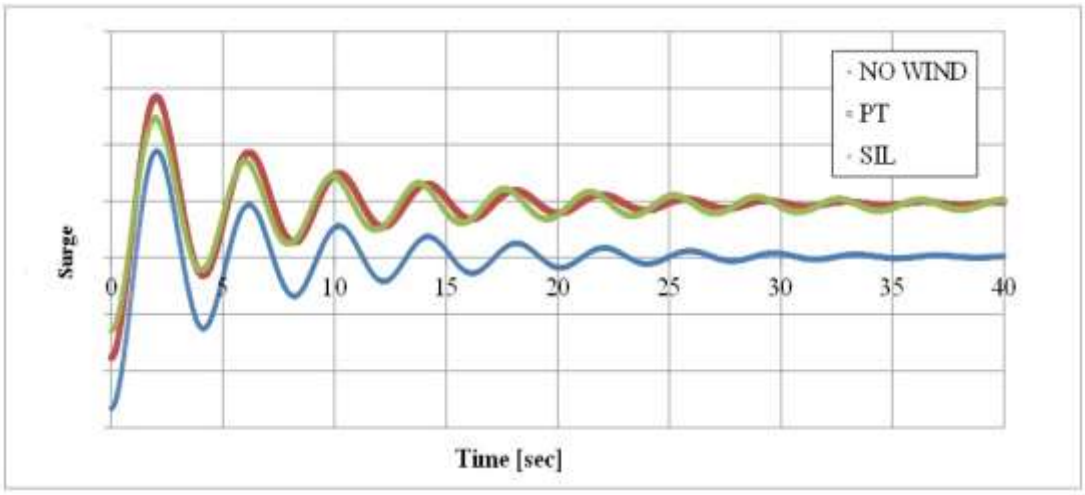

Figure 5.8 Effect of wind on Surge Free Oscillation Tests

5.3.5 Free Oscillation Tests in Yaw (No wind)

In the case of yaw, it was much more difficult to impose pure yaw without also imposing surge or sway. Nonetheless in the end acceptable results were obtained. An example is shown in Figure 5.9.

The measured data is quite noisy, which reflects the small motions, but it can be seen that the fit is good. There is no real need to filter the data in this case, since the fitting process is in itself effectively a filter.

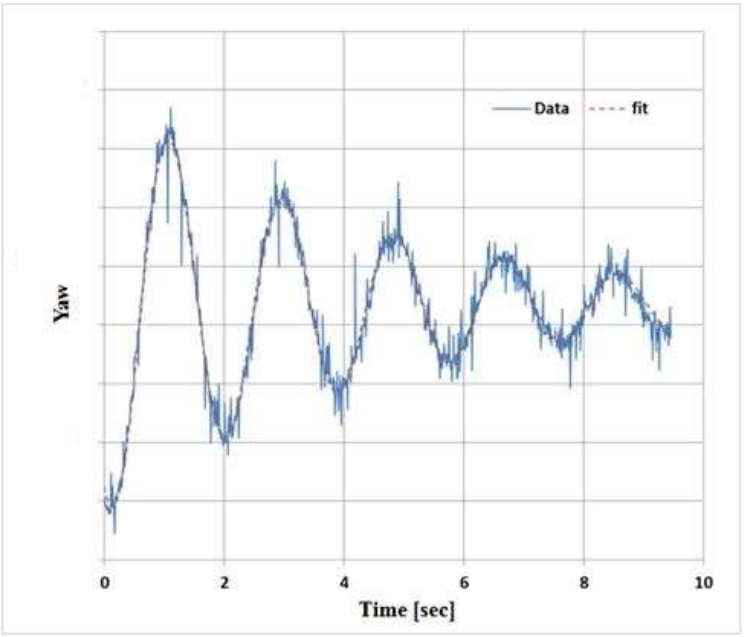

Figure 5.9 Typical fit for yaw

5.3.6 Free Oscillation Tests in Heave and Pitch (No wind)

Both the heave and pitch natural frequency tests proved extremely difficult, and the results are of questionable accuracy. The records are short, and there was substantial coupling between different modes of motion, requiring records to be windowed significantly. An example of a heave record is shown in Figure 5.10. It should be noted that the entire record is only 0.6 seconds long. In spite of this the results shown later suggest that the period is reasonably consistent between tests, but the damping values are highly scattered. One example fit for pitch motion natural frequency tests is given in Figure 5.11.

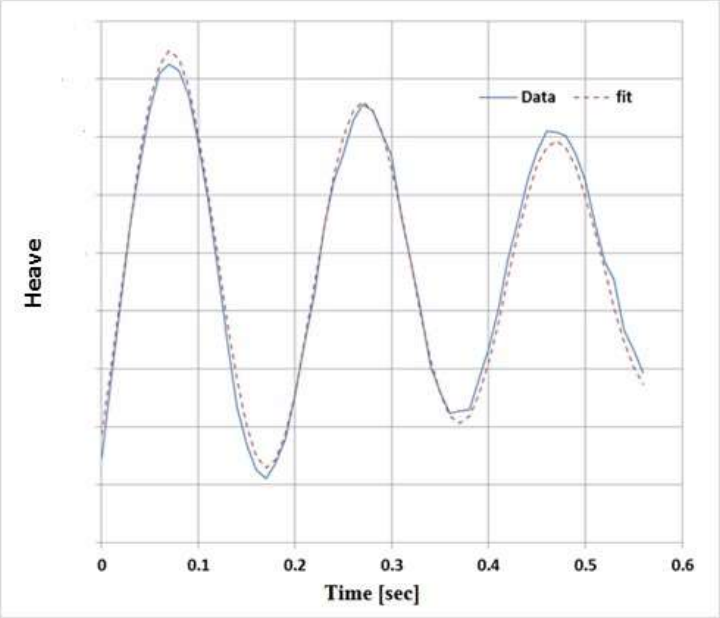

Figure 5.10 Typical fit for heave

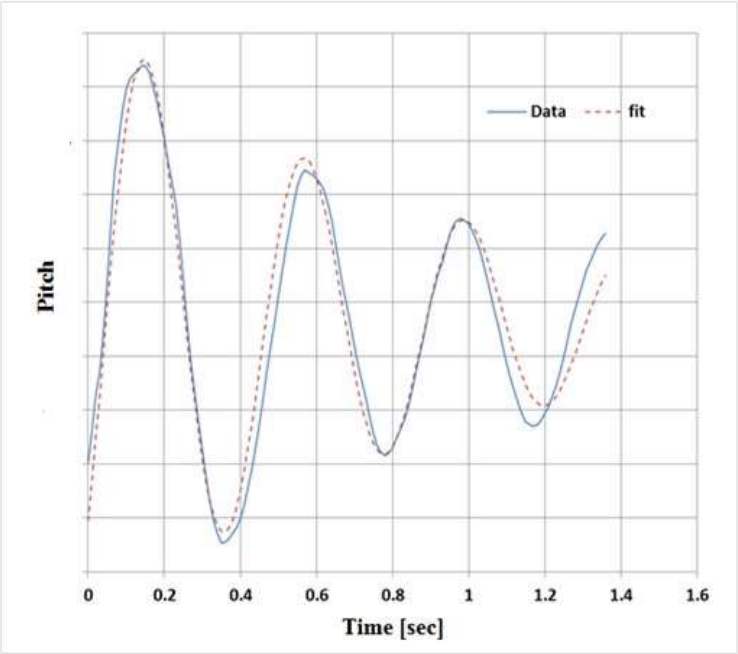

Figure 5.11 Typical fit for pitch

5.4 Results

From the free oscillation tests, natural frequencies and damping ratios are calculated for four different modes of motion following the methodology outlined in section 5.2.

5.4.1 Runs performed

The results are presented in the tables in this section. Blank spaces show the tests where the quality of the data was questionable. Table 5.2 shows the number of cycles examined for each sets of test. It can be seen from Table 5.2 that the run numbers are selected differently depending on the data quality. As the data in surge natural frequency tests are good, selected cycles are consistent and in average 7.5 cycles are considered for surge calculations. This also demonstrates how well the repeatability of surge tests. On the other hand, considered number of cycles reduces for yaw, heave and pitch. This illustrates the challenge getting consistent data from these tests. As discussed previously the surge tests were limited to 30 seconds for consistency, while other tests were over a much shorter time period.

Table 5.2 Number of Cycles

Run number	1	2	3	4						
Surge (no wind)	7.5	7.4	7.5	7.4						
Surge (PT w_s=11.4m/s)	7.5	7.5	7.5	7.4	7.5	7.5	7.5	7.5	7.5	
Surge (SIL w_s=11.4m/s)	7.7	7.7	7.6	7.5		7.4	7.7	7.7	7.6	7.4
					5	6	7	8	9	10
					7.5	7.5	7.5	7.4	7.4	7.5
					7.3					
Yaw (no wind)	5.1	3.5	3.9	3.5	3.9					
Heave (no wind)			2.3	2.9		2.4	3.1			2.9
Pitch (no wind)	3.6	2.7	8.4	4.9	8.4		3.3		4.2	2.7

Table 5.3 shows the relative RMS fit error (RMS fit error divided by the range of the signal) over the duration of the fit. It should be remembered that this includes the effect of noise in the measured data.

Table 5.3 Relative RMS fit error

	1	2	3	4	5	6	7	8	9	10	
Mean error fit	0.017	0.020	0.022	0.020	0.016	0.020	0.019	0.020	0.020	0.018	Mean
Surge (no wind)											0.02
Surge (PT ws=11.4m/s)	0.020	0.022	0.021	0.023	0.020	0.022	0.024	0.024	0.020	0.001	0.02
Surge (SIL ws=11.4m/s)	0.019	0.031	0.026	0.018	0.012	0.014	0.032	0.037	0.040	0.016	0.02
Yaw (no wind)	0.039	0.037	0.052	0.037	0.045	0.069	0.066	0.077	0.051	0.057	0.05
Heave (no wind)			0.162	0.290		0.074	0.043			0.035	0.12
Pitch (no wind)	0.147	0.130	0.043	0.008	0.017		0.087		0.118	0.108	0.07

The measured error in surge is generally good considering that the oscillations typically started with relatively small amplitude. It can be seen from the Table 5.3 that for the three surge test cases the relative error remains constant at a value around 0.02 and repeatability is good. Yaw and pitch relative errors of 0.05 and 0.07 are 2-3 times greater than in surge with less repeatability; heave natural frequency measurements were the most difficult to perform with a relative error of 0.12 and were the least repeatable free oscillation tests.

5.4.2 Natural Periods

Table 5.4 shows the natural periods obtained through the fitting process in model scale. These are generally extremely consistent for surge and yaw, but rather less so for heave and pitch.

Table 5.4 Natural Periods (sec)

	1	2	3	4	5	6	7	8	9	10	
Run Number	4.015	4.028	4.027	4.029	4.015	4.026	4.027	4.03	4.032	4.024	**mean**
Surge (no wind)											4.03
Surge (PT w_s=11.4m/s)	4.002	4.025	4.024	4.03	4.018	4.014	4.025	4.025	4.017		4.02
Surge (SIL w_s=11.4m/s)	3.899	3.899	3.934	3.976	4.098	4.063	3.905	3.885	3.972	4.082	3.97
		1.867	1.918	1.881	1.913	1.926	1.933	1.954	1.89	1.919	
Yaw (no wind)	1.871										1.91
Heave (no wind)			0.242	0.279		0.234	0.206			0.199	0.23
Pitch (no wind)	0.463	0.48	0.382	0.377	0.379		0.419		0.421	0.46	0.42

The statistics of the periods in model scale are shown in Table 5.5. This shows the mean and standard deviation, and the standard deviation expressed as a percentage of the mean value.

Table 5.5 Natural Period statistics in Model Scale

Parameter	Count	Mean	STD	STD (%)
Surge (no wind)	10	4.025	0.006	0.1
Surge (PT w_s=11.4m/s)	9	4.020	0.009	0.2
Surge (SIL w_s=11.4m/s)	10	3.971	0.082	2.1
Yaw (no wind)	10	1.907	0.029	1.5
Heave (no wind)	5	0.232	0.032	13.8
Pitch (no wind)	8	0.423	0.041	9.8

It can be seen that the repeatability of the period is extremely good for surge in no wind and with predefined thrust. The values for surge with SIL and yaw are slightly less good, and the values for heave and pitch are rather scattered. These are scaled to full scale in Table 5.6.

Table 5.6 Natural Period statistics in Full Scale

Parameter	Count	Mean	STD	STD (%)
Surge (no wind)	10	24.376	0.035	0.1
Surge (PT w_s=11.4m/s)	9	24.344	0.052	0.2
Surge (SIL w_s=11.4m/s)	10	24.049	0.497	2.1
Yaw (no wind)	10	11.549	0.174	1.5
Heave (no wind)	5	1.404	0.193	13.8

Pitch (no wind)	8	2.560	0.251	9.8

As is described in Section 7.3 the first order wave excitation range changes between 0.07Hz (14.3sec) to 0.25Hz (4sec). It is observed that apart from yaw all natural periods are outside this range. Considering the platform symmetry and the pontoon position (far from the free surface) wave induced motions will be small.

The natural periods of proposed FOWT are similar to those published for 80m water depth by (Rodriguez et al., 2014). Natural periods represented in Table 5.7.

Table 5.7 Natural Periods of TLPWT for 80m water depth (Rodriguez et al., 2014)

Motion	T [s]
Surge - Sway	25.21
Heave	1.09
Roll - Pitch	3.88
Yaw	11.42

5.4.3 Relative Damping Ratios

Mean relative (to surge no wind case) damping ratios and the corresponding statistics are given in Table 5.8.

Table 5.8 Relative Damping Ratio Statistics

Parameter	Count	Mean	STD
Surge (no wind)	10	1.000	0.003
Surge (PT w_s=11.4m/s)	9	1.033	0.003
Surge (SIL w_s=11.4m/s)	10	0.822	0.026
Yaw (no wind)	10	1.066	0.020
Heave (no wind)	6	0.844	0.043
Pitch (no wind)	8	0.800	0.049

Table 5.8 shows that the damping is substantially less repeatable that the period, typically an order of magnitude less so. The values for surge in no wind and with predefined thrust are still quite good with standard deviation less than 5% of the mean. The value for the predefined thrust is slightly higher than the value for no wind, which might be expected. The scatter of the results for surge with SIL is high, which reflects some of the unexpected behaviour which may be associated with controller instability. The standard deviation for yaw is also high, but the results are still arguably

meaningful, whilst the values for heave and pitch are so high as to be essentially unreliable.

5.5 Derived Quantities

5.5.1 Added Mass in Surge

The TLP can be considered as an inverted pendulum and the restoring or stiffness can be calculated from the knowledge of its geometry and mass properties (see Figure 5.12). Here F is the net buoyancy force (i.e. the buoyancy minus weight) while L is the length of the tendons between the points of rotation at each end, and n is the number of tendons.

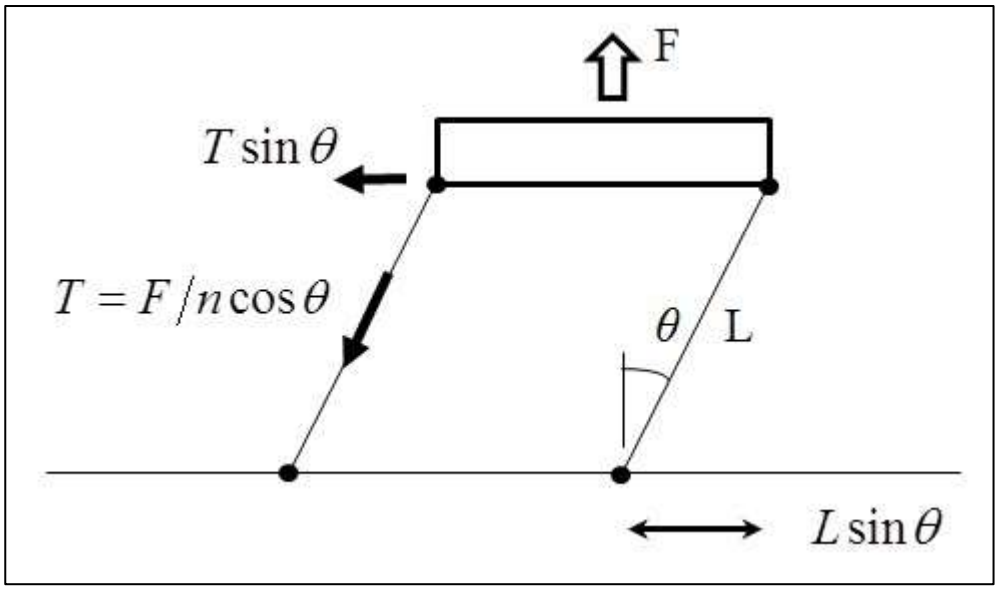

Figure 5.12 Surge model of TLP

For small displacement, the restoring force may be considered to be a linear function of the displacement (strictly for small angles of the tendon). In this case, $sin \approx$ and $cos \approx 1$ hence the restoring per tendon is F/n, and the total restoring is thus F . Similarly, the deflection is L and hence the stiffness is $k = F/L$.

Since

$$\omega_d = \sqrt{k/m_v} \tag{5.7}$$

Hence the virtual mass (added mass + mass) is found from

$$m_v = \frac{k}{\omega_d{}^2} = k.\left(\frac{T}{2\pi}\right)^2 \quad (5.8)$$

The virtual mass coefficient is defined as:

$$C_m = m_v/\rho\nabla \quad (5.9)$$

The virtual mass calculated in this manner is assumed to be independent of frequency. For a surface piercing body such as a TLP for the oscillations in surge there will be some frequency dependent component to the added mass related to wave scattering.

However this is assumed to be negligible in the current case since the surface piercing part of the floater is extremely small. Videos of the free oscillation test in surge show no visible wave scattering.

Furthermore, any small component of wave scattering is captured at the natural frequency of the system which is the point at which the largest oscillations might be expected to occur. Hence the results obtained from the free oscillation test will be correct in this case.

5.5.2 Virtual Mass Moment of Inertia in Yaw

For the tests in yaw, a similar analysis yields the yaw stiffness as

$$k = Fd^2/4L \quad (5.10)$$

Where *d* is the diagonal separation of opposing pairs of tendons, F is the net buoyancy force and L is the tendon length.

The virtual mass moment of inertia calculated in this manner is once again assumed to be independent of frequency. For a surface piercing body such as the TLP floater oscillating in yaw the surface piercing central column of the floater will not generate any significant wave scattering. Since the pontoons are deeply submerged, it is reasonable to assume that wave scattering from yaw motion is negligible.

5.5.3 Results

The absolute values of the total mass and the virtual mass coefficient are not presented here due to commercial confidentiality. Relative (to surge no wind case) added mass values are given in Table 5.9.

Table 5.9 Relative added mass values

Test Type	Relative Added Mass
Surge (no wind)	1.000
Surge (PT)	0.997
Surge (SIL)	0.973

5.6 Free Oscillation Tests using Numerical Tools (FASTv7)

In order to compare the natural period and damping values obtained from the experiments with the numerical results, free oscillation tests were also carried out using FAST code. The free oscillation tests in surge, heave and pitch with no wind were performed numerically and in addition constant wind and turbulent wind cases were carried out for surge. All numerical results and comparison to experimental results are given in this section.

To carry out free oscillation tests in FAST, the initial displacements were set up as non-zero. For example, to do free oscillation tests in surge direction initial surge (or fixed horizontal surge translational displacement of platform) was set as 1.0m in the platform file. In a similar manner, initial heave (or fixed vertical heave translational displacement of platform) was taken as 0.01m and initial pitch (or fixed pitch tilt rotational displacement of platform) was used as 0.1 degrees. The FAST variable *GenDof* (Generator DOF [flag]) was taken false for no wind case while *GenDof* was true for wind cases. *BlPitch* (1to3 - Blade 1,2,3 final pitch for pitch maneuvers [degrees]) was taken as 90 for no wind case whilst 0 for the rest. *PitchControl* was selected 0 for no wind case; *"DISCON_OC3Hywind_win32.dll"* was used for wind cases. *RotSpeed* (Initial or fixed rotor speed [rpm]) was taken as 0rpm for no wind condition and 12.1rpm was used for wind condition. *WaveMod* (Incident wave kinematics model) was taken as 0 which represents none=still water. Full details of the input file for the free oscillation tests and the wave tests can be seen in Appendix B.

It is important to note that the conditions for the comparison between the numerical and experimental results are not exactly the same. Real damping is non-linear but FAST has only linear damping. The tower is treated as flexible with correct stiffness in FAST while it is not correctly scaled in the experiments. It is hard to comment on

what effect that has. Due to modelling challenges in tendons, tendon rigidity in the experiments is not the same as FAST. Some of these discrepancies could have been addressed by modifying the source code in FAST to allow matching the experimental set up but this was out of the scope of this study.

Since Fast version 7 does not have the OrcaFlexInterface module, tendons were modelled using the standard approach and input files. In order to have improved predictions of tendon tensions, tendons could be modelled using the OrcaFlexInterface module which is available in FAST v8, in which all hydrodynamic and mooring loads can be computed using OrcaFlex.

The fit to the linear free decay model for surge with no wind is shown in Figure 5.13; it can be seen from this figure that the fit is very good and hence that FAST predicts linear damping behaviour as expected.

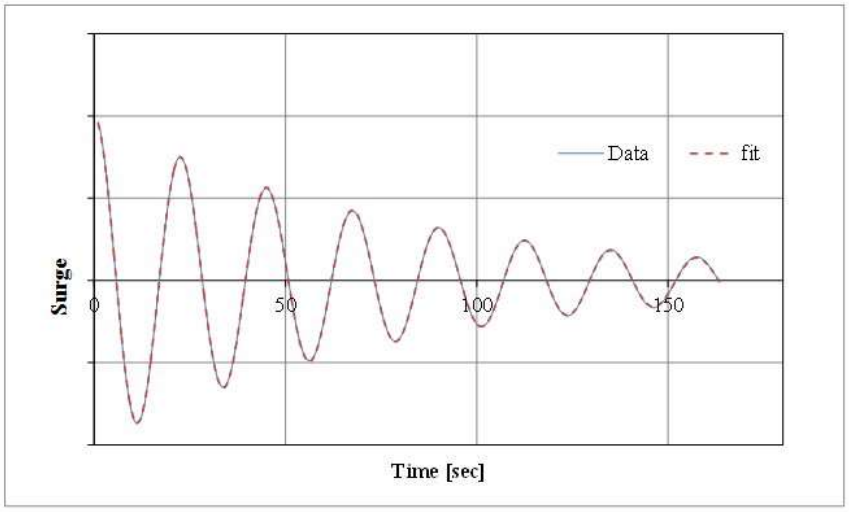

Figure 5.13 Free Oscillation Test in Surge no wind (FAST)

5.7 Comparison of numerical and experimental FOT

The comparison of natural period and damping values for surge no wind condition is given in Table 5.10.

Table 5.10 Comparison of natural period and damping values for surge no wind

Surge (no wind)	Experiment	Numerical	Error (%)
Mean natural period [sec]	24.376	22.475	7.7

The fit for surge with constant wind is shown in Figure 5.14. The comparison of natural period and damping values for surge constant wind condition is given in Table 5.11. Natural period is a function of stiffness and mass. Since tendon length was properly modelled using Froude scale in the experiments, error in period should be dominated by mass. The achieved solid mass in the experiments and the mass value used in the numerical model are correct therefore the error seems to be associated with the numerical prediction of added mass. Experimental results for added mass could be obtained in principle with forced oscillation test, but carrying out forced oscillation test is very difficult for this kind of structure. It is therefore suggested that the difference in surge natural period between the experimental and numerical values may result from modelling errors in WAMIT, since the structure geometry with sharp corners in the pontoons may cause flow separation which will not be correctly modelled in a potential flow code.

As it can be seen from the Table 5.10 damping values obtained from experimental results are 50% higher than results obtained from FAST in the case of no wind condition. Neglecting the viscous damping of the platform and damping in tendons is the probable cause of this difference. It is also important to mention that possible friction in universal joints used in the experiments might be another factor. Therefore, this difference may not depend entirely on one methodology; it may be a combination of numerical and experimental errors.

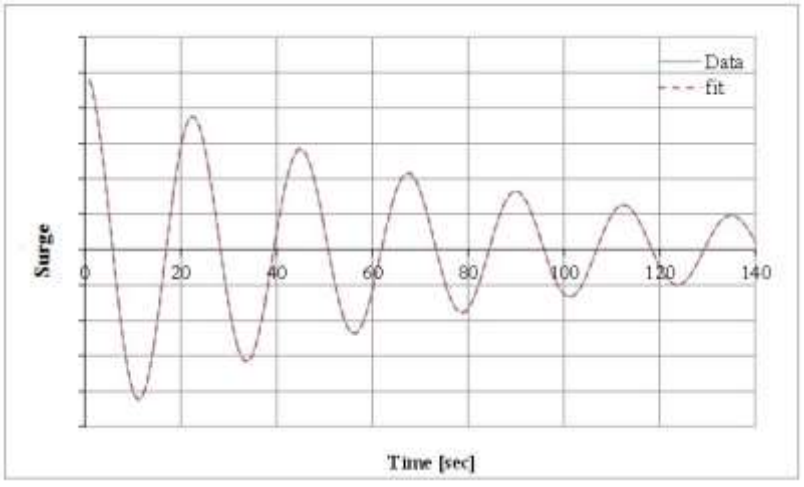

Figure 5.14 Free Oscillation Test in Surge (Constant wind)

As can be seen from Table 5.11 natural period was calculated as 22.468s in the case of surge with constant wind. The natural periods and damping values for no wind and constant wind cases are very similar. The constant wind model in FAST uses the mean wind speed at the wind turbine hub, which results in variable thrust due to impact of platform motions; in contrast the predefined thrust in the experiments uses mean thrust force at wind turbine hub. Although they are not exactly the same, the comparison of these tests is provided here.

Table 5.11 Comparison of natural period and damping values for surge with constant wind (FAST)

Surge (PT)	Experiment	Numerical	Error (%)
Mean natural period [sec]	24.344	22.468	7.7
Mean Damping Ratio			52

The fit for surge with turbulent wind is given in Figure 5.15. The natural period was calculated as 22.355s in the case of surge with turbulent wind (we can say that equals to SIL condition in the experiment).

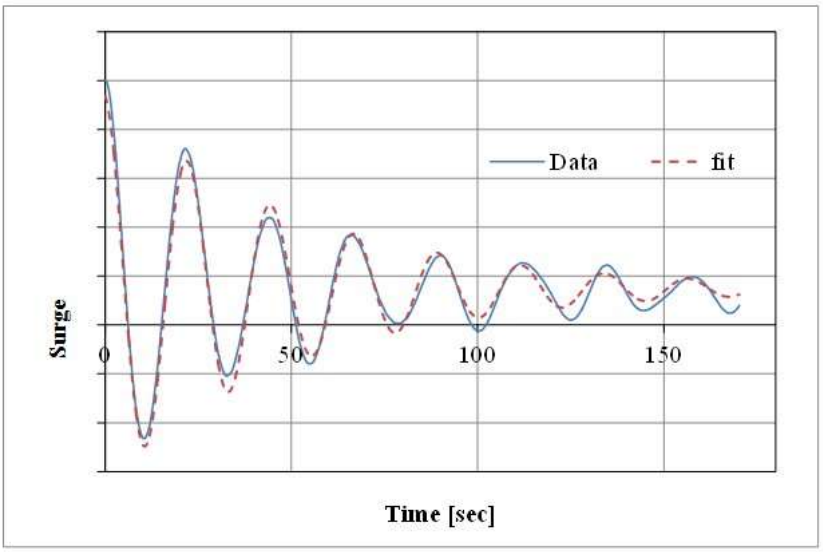

Figure 5.15 Free Oscillation Test in Surge with turbulent wind (FAST)

The comparison of natural period and damping values for surge with turbulent wind is given in Table 5.12.

Table 5.12 Comparison of natural period and damping values for surge with turbulent wind (FAST)

Surge (SIL)	Experiment	Numerical	Error (%)
Mean natural period [sec]	24.649	22.355	9.31
Mean Damping Ratio			9.18

Virtual mass values obtained in section 5.5.3 are compared with the numerical virtual mass values in Table 5.13. Virtual mass results in surge show good agreement with the numerical values for all of the wind cases. The numerical predictions underestimate the virtual mass by around 15%.

Table 5.13 Comparison of numerical and experimental Virtual Mass Values

Calculated value	% Added Mass Error
Surge (no wind)	14.9
Surge (PT)	14.8
Surge (SIL)	13.5

The fit for heave without wind condition is shown in Figure 5.16.

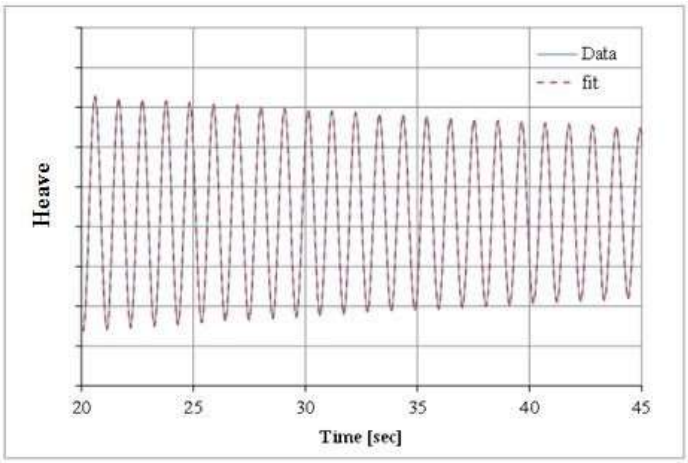

Figure 5.16 Free Oscillation Test in Heave (FAST)

Comparison of natural period and damping values for heave motion is given in Table 5.14. A number of runs were performed using both the target and the measured values of tendon stiffness. Results from FAST were seen to be insensitive to the stiffness variation and several stiffness values gave the same results. All subsequent numerical calculations were carried out using the target stiffness values.

Table 5.14 Comparison of natural period and damping values for heave

Heave (no wind)	Experiment	Numerical	Error (%)
Mean natural period [sec]	1.40	1.057	24.5
Mean Damping Ratio			97.40

As mentioned in section 5.4.1, the free oscillation experiments in heave were difficult to perform and the values obtain had considerable variation leading to the mean value for heave damping ratio having a high degree of uncertainty. Moreover the FAST code has a number of theoretical assumptions (viscosity for example) that will generally lead to the underestimation of damping values. These factors explain to some extent the difference between the numerical and experimental values obtained for the heave damping.

The last run performed for pitch motion with no wind and the fit for this simulation case is given in Figure 5.17. As can be seen from this figure that the damping value calculated from FAST simulation is very small compared to the mean value obtained from the experiments.

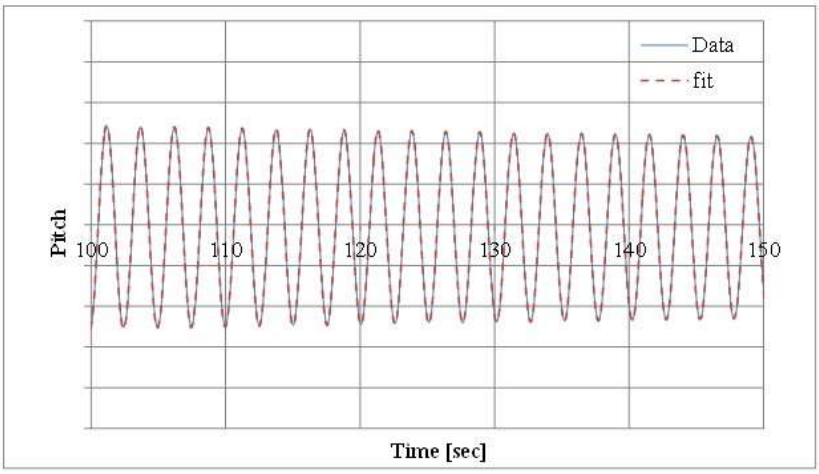

Figure 5.17 Free Oscillation Test in Pitch (FAST)

The comparison of natural period and damping values for pitch motion is given in Table 5.15. As was mentioned previously, performing the free oscillation tests in pitch was also very difficult like free oscillation tests in heave. The results from the pitch free oscillation tests displayed a large variation. The comparison of the values obtained

from the experimental measurements and numerical predictions are given in Table 5.15 which illustrates the challenge in obtaining an accurate value for pitch damping.

Table 5.15 Comparison of natural period and damping values for pitch

Pitch (no wind)	Experiment	Numerical	Error (%)
Mean natural period [sec]	2.560	2.522	1.48
Mean Damping Ratio			98

5.8 Conclusions

The analysis of the free oscillation tests showed that the repeatability of the natural period measurements is extremely good for surge in no wind and predefined thrust. The natural periods in surge with SIL and in yaw are not as consistent as in the no wind condition. The heave and pitch natural period values are widely scattered due to the difficulties of performing these tests. As expected the virtual mass values closely follow the trends observed in the natural frequency results.

The damping values showed that the damping ratio is less repeatable than the natural period of the system. Results for surge no wind and with predefined thrust have standard deviation less than 5% of the mean which means that the damping ratio values are still good for these tests. It should be noted that the value for predefined thrust is slightly higher than for no wind condition, which might be expected. High scattered results are observed for surge with SIL, which can be associated with controller stability that caused this unexpected behaviour. Although the standard deviation of yaw tests is high, the results are in an acceptable range. It is hard to conclude the same for the heave and pitch results as they seem unreliable.

The natural period results from the numerical study show good correlation with measurements in surge with 7-9% error. There are some modelling differences between the experiments and numerical calculations (e.g. Pontoons were modelled using a potential flow approach) which may cause some differences in the results. In a similar manner, due to some assumptions (i.e. neglecting viscous damping) in FAST and modelling in practice (i.e. possible friction in UJs) error in damping values were high in some cases. Simultaneously generating an accurate representation of the

prototype geometry and creating the numerical model is not a simple endeavour. The comparisons of pitch and heave oscillation tests proved more problematic as discussed in section 5.6.

In principle the numerical model could have been modified using the source code in FAST to match the experimental set up more closely, but this was out of the scope of the study. Since Fast version 7 does not have OrcaFlexInterface module, tendons modelled using the standard approach in FASTv7. In order to have improved predictions on tendon tensions, tendons could be modelled using OrcaFlexInterface module which is available used in FAST v8 in which all hydrodynamic and mooring loads can be computed using OrcaFlex.

Chapter 6

Regular Wave Tests

6.1 Introduction

The Regular wave tests were carried out to characterise the behaviour of the structure through the motion and tendon tension RAOs. Four sets of regular wave tests were performed and are described below. Three sets in head seas were carried out following the pattern of the tests with no wind, constant predefined thrust (PT), and software-in-the-loop (SIL) controlled thrust respectively. In order to investigate the effect of wave heading on motion RAOs, the fourth set of tests were carried out for the case of quartering sea state with no wind. Tests were performed in regular waves with a target amplitude of 1.0m at full scale. Tests with wind used a full-scale wind speed of 11.4m/s, the rated speed of the NREL 5MW turbine. Wave frequencies varied from 0.25-1.0 Hz at model scale, corresponding to full scale periods in the range 6-30s.

Results are scaled to full scale using Froude scaling as previously mentioned in Chapter 3.

This chapter is organised as follows. Test matrix is given in section 6.2. Section 6.3 explains the analysis convention in detail applied to data. Next, in Section 6.4, motion response data for head waves with three different wind models and for quartering waves are given, with details provided in the contained sub-sections. Then, tendon tension RAOs are presented in order to show the effect of these parameters on the system. In Section 6.6, a subset of the motion RAOs and tension transfer functions obtained from the experimental results are compared to those from the numerical results for 0° head seas and no wind cases. Finally, in Section 6.7, a conclusion of the chapter is drawn.

6.2 Test matrix

Four sets of tests were performed in regular waves as described in Table 6.1 and Table 6.2. The first three configurations were carried out to define the wind impact on the FOWT system. The fourth configuration was performed in quartering seas to determine the effect of wave heading on the system.

Table 6.1 Overview of regular wave test matrix

Configuration	Wave/Wind heading(deg)	Wind condition
1	0/0	No wind
2	0/0	Software in the loop
3	0/0	Predefined Thrust
4	45/0	No wind

Table 6.2 Regular waves test matrix

Configuration	**Test ID**	**Wave Height [m]**	**Wave Period [s]**	**Wind speed [m/s]**
1	D008	2	4	0
	D023	2	6	0
	D024	2	8	0
	D018	2	10	0
	D025	2	12	0
	D013	2	14	0
	D014	2	16	0
	D015	2	18	0
	D016	2	20	0
	D017	2	22	0

	D019	2	24	0
	D020	2	26	0
	D021	2	28	0
	D022	2	30	0
2	D1038	2	4	11.40
	D1042	2	6	11.40
	D1043	2	8	11.40
	D1044	2	10	11.40
	D1040	2	12	11.40
	D1045	2	14	11.40
	D1046	2	16	11.40
	D1055	2	18	11.40
	D1056	2	20	11.40
	D1050	2	22	11.40
	D1039	2	24	11.40
	D1057	2	26	11.40
	D1058	2	28	11.40
	D1041	2	30	11.40
3	D1027	2	4	11.40
	D1028	2	6	11.40
	D1029	2	8	11.40
	D1030	2	10	11.40
	D1031	2	12	11.40
	D1032	2	14	11.40
	D1033	2	16	11.40
	D1034	2	18	11.40
	D1035	2	20	11.40
	D1036	2	22	11.40
	D1037	2	24	11.40
	D1051	2	26	11.40
	D1052	2	28	11.40
	D1053	2	30	11.40
4	D5039	2	4	0
	D5040	2	6	0
	D5041	2	8	0
	D5042	2	10	0
	D5043	2	12	0
	D5044	2	14	0
	D5045	2	16	0
	D5046	2	18	0
	D5047	2	20	0
	D5048	2	22	0
	D5049	2	24	0
	D5050	2	26	0
	D5051	2	28	0

	D5052	2	30	0

6.3 Analysis Conventions

The analysis convention to determine the RAOs of the FOWT is briefly presented in this section. The translational motions are presented at the origin of the body fixed co-ordinate system. The wave elevation from the model tests is fitted in the form:

$$(t) = \hat{} \sin(\omega t) \tag{6.1}$$

The value of the wave amplitude$\hat{}$ can be obtained using non-linear least-squares fit. A typical set of data for motions is shown in Figure 6.1 and the fit is illustrated in the figure. In this figure, the signals are in the following order from top: Wave / Pitch / Yaw / Z / Y / X, where X is the longitudinal displacement (surge), Y is the transverse displacement (sway), and Z is vertical displacement (heave). In each case the green trace is the recorded data and the red trace is the least squares sinusoidal fit. The wave elevation from the model tests fitted extremely well to the sinusoidal form, as expected. In some cases the response data presented could also be based on the amplitudes of sinusoidal functions fitted to the experiment data using a similar nonlinear least-square fitting procedure, and with frequency essentially identical to the waves; this can be seen for the longitudinal motion in Figure 6.1. Hence a function can be fitted of the form:

$$X(t) = X \sin(\omega t - _X) \tag{6.2}$$

In the case of some signals the fit is extremely good. Where the function has dimensions of the length the transfer function is non-dimensional, and can thus be regarded as a Response Amplitude Operator (RAO).

Figure 6.1 Typical recorded wave and motion data (head waves no wind) From top: Wave/Pitch/Yaw/Z/Y/X

However, in some cases the response is far from sinusoidal, even though the period of the response is equal to the wave period. In Figure 6.1, for example, it can be seen that the (very small) yaw response resembles a saw-tooth wave. In some other cases the response is at some harmonic of the wave period. For example the vertical motion in Figure 6.1 exhibits a frequency double that of the planar motions, and furthermore the response is clearly non-sinusoidal, with amplitude of successive minima alternating in amplitude. Hence responses were typically characterised in terms of the range of response rather than the amplitude of a fitted sinusoid.

In order that a consistent approach is adopted for all signals, the RAOs (transfer functions) are all presented here in terms of the range of the filtered response as:

$$TF_X(f) = (X_{max} - X_{min})/\hat{} \qquad (6.3)$$

6.4 RAOs for Six Degree of Freedom Motions

In this section, RAOs for six degree of freedom motions are presented in the first four sections. Following this, the impact of wind model on surge motion is given in section 6.4.5. Finally, the impact of heading angle on longitudinal motion is shown in the end of this section.

6.4.1 Head waves - No wind

Regular wave tests in head waves and no wind condition are given in this section. The translational motion responses for the case of head waves and no wind are presented in Figure 6.2, Figure 6.3 and Figure 6.4 below. It should be noted that widely varying magnitude of the responses: the sway and heave motions are an order of magnitude smaller than the surge motions.

The sway motions arise from some small asymmetry in the orientation of the floater leading to some cross-coupling with surge and roll. The Heave responses occur at twice the frequency of the planar motions, as shown previously in Figure 6.1.

The free oscillation test showed an undamped natural period of 24.4s in surge as previously shown in Chapter 5, and it can be seen that the peak of the RAOs occurs at the frequency closest to this value. Maximum RAO in surge was found to be just over 5 in a period range of 20-25s which is quite close to previously published results reported in (Rodriguez et al., 2014). In Figure 6.3 (sway), there is the suggestion of a slight "hump" near 16s but this does not correspond to any of the natural periods observed in the free oscillation tests. The test tank transverse sloshing frequency was calculated and found to be 15.76 seconds which can describe the slight hump at period 16s in sway RAO.

Sloshing frequency was calculated using the formula is given below (Housner, 1963).

$$f_c = \frac{1}{2\pi}\sqrt{\frac{3.16\, g \tanh(3.16\frac{h}{L})}{L}} \tag{6.4}$$

$f_c = sloshing\ frequency\ (Hz)\ h$

$= height\ of\ water\ in\ tank\ (m)$

$L = lenght\ of\ rectangular\ tank\ along\ direction\ of\ excitation\ (m)\ g$

$= acceleration\ due\ to\ gravity\ (^{m}/_{s2})$

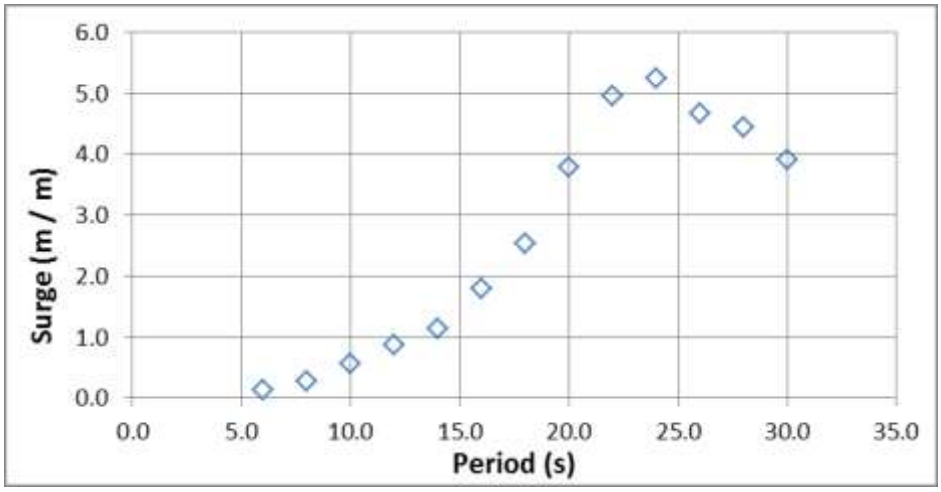

Figure 6.2 RAOs of surge motion in the case of head waves, no wind

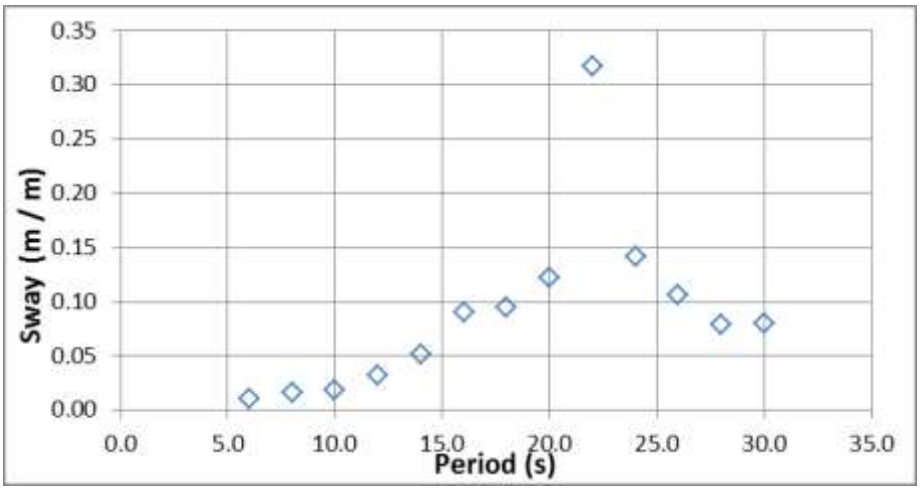

Figure 6.3 RAOs of sway motion in the case of head waves, no wind

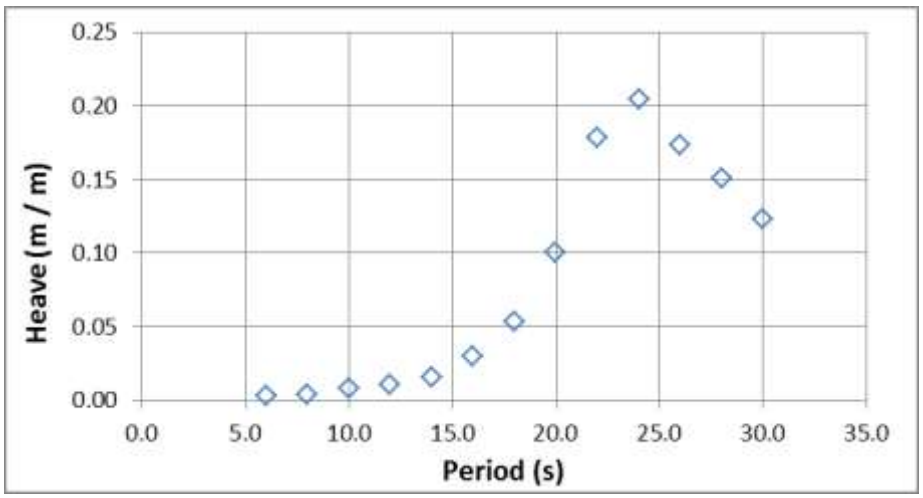

Figure 6.4 RAOs of heave motion in the case of head waves, no wind

The heave motions are coupled to the surge motions through the kinematics of the tendons, and hence it is expected that the frequency of peak heave motions corresponds to the peak of the surge motions. The Heave responses occur at twice the frequency of the planar motions, as shown previously in Figure 6.1. The highest vertical displacement occurs with the tendons upright, and the platform is displaced downwards as it surges both forward and backwards relative to the wave direction. The magnitude of the cycles alternate due to a slight mean offset of the platform in surge. However the peak sway motion occurs at a very slightly lower period.

The corresponding rotational motions are presented as transfer functions in deg/m at full scale in Figure 6.6, Figure 6.7 and Figure 6.8. It can be clearly seen that all the rotational motions are very small as would be expected in this condition. The yaw motions are non-sinusoidal. The natural period in yaw was previously shown to be around 11.5 seconds from the free oscillation tests, and a local peak near this period can clearly be seen in the yaw RAOs.

It is interesting to note that the pitch transfer function exhibits two peaks: one which is coupled to the peak in surge at around 24s, and a secondary peak at 18s. The peak is reflected in the other angular motions, but the physical source of this is not obvious, as it is well away from any of the natural periods.

In order to check the repeatability of the regular waves, tests were repeated 5 times corresponding to the surge natural period (T=24sec). It was observed that the difference between the results is less than 1% which means wave maker is capable of producing the same wave height at the peak period. The repeatability of the regular waves at for a wave period equal to the surge natural period is given in Figure 6.5.

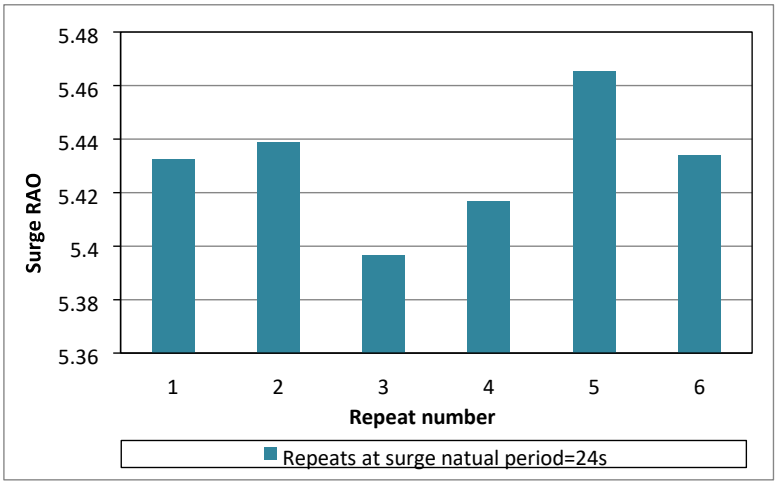

Figure 6.5 Repeatability of wave maker at surge natural period

As outlined in Chapter 4, the wave probe calibration results showed that the standard error calculated from probe calibration were typically less than 0.5mm, and hence the 95% uncertainty values for the wave probe calibrations were less than 1mm.

It also should be noted that an extended beach of 12m length was constructed to improve the absorption over the frequency range of interest before the start of the experimental campaign. Reflection coefficients less than 5% were observed over a frequency range from 0.3-1.2Hz. Therefore, the unexpected measurements does not stem from wave reflection.

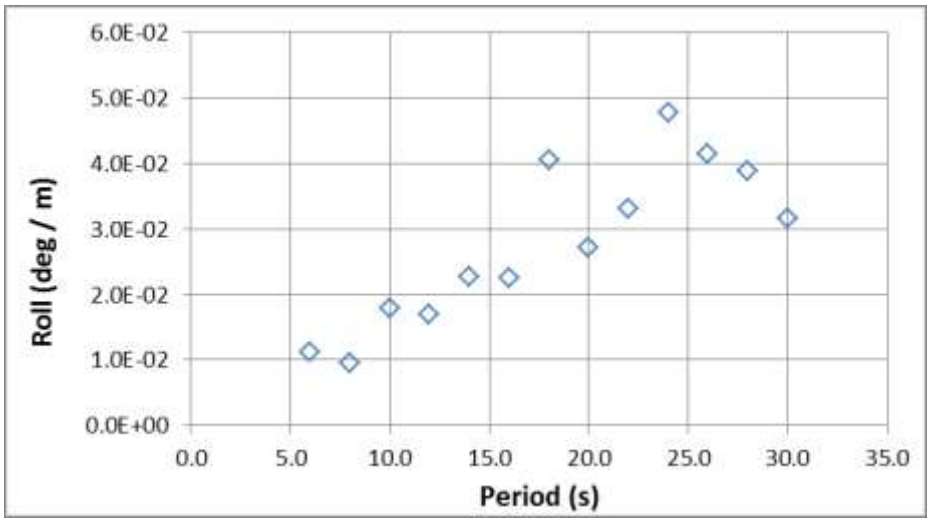

Figure 6.6 Transfer functions of roll motion in the case of head waves, no wind

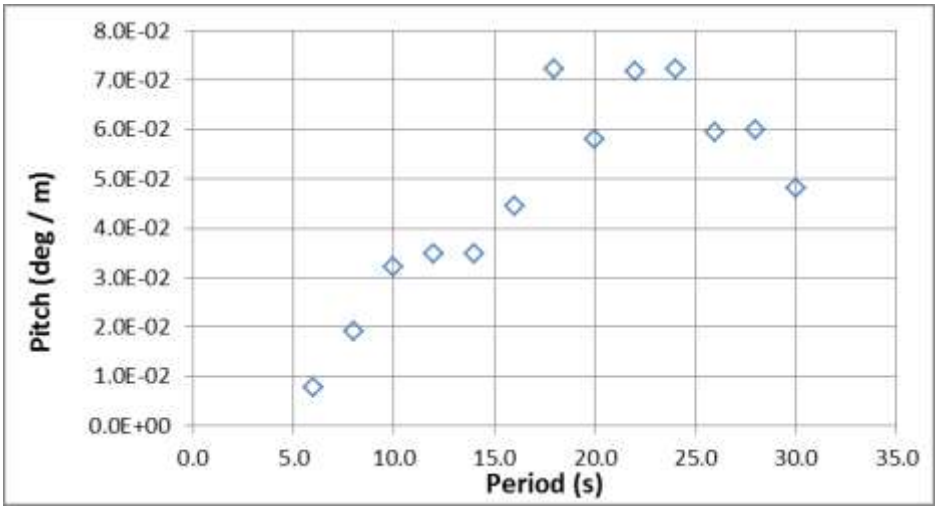

Figure 6.7 Transfer functions of pitch motion in the case of head waves, no wind

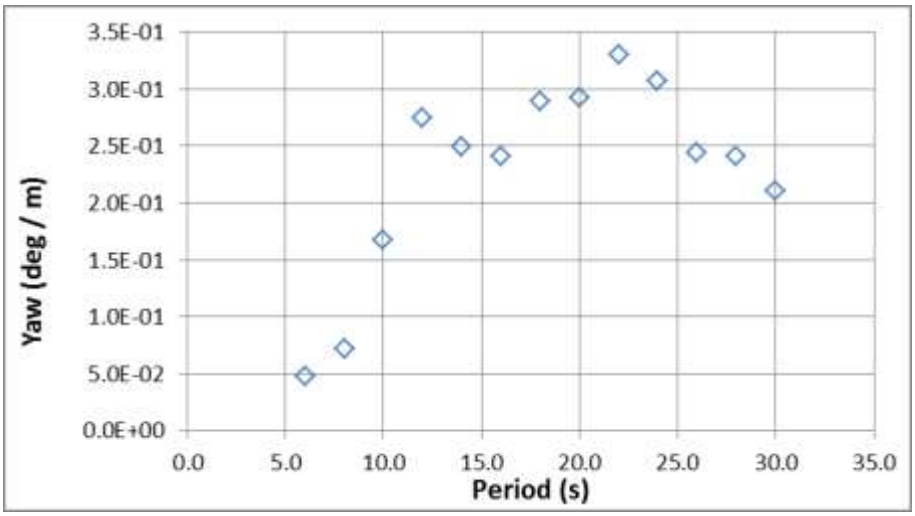

Figure 6.8 Transfer functions of yaw motion in the case of head waves, no wind

6.4.2 Head waves – Predefined Thrust (PT)

The translational motion responses for the case of head waves and predefined thrust are presented in Figure 6.9 below. The key difference in this case is that there is a substantial longitudinal offset of the floater caused by the wind load. However this has little impact on the magnitude of the dynamic longitudinal responses.

Figure 6.9 shows the Wave / Yaw / Z / Y / X. The heave responses, once again, occur at twice the frequency of the planar motions. The heave responses are even more strongly non-sinusoidal and larger than those shown in Figure 6.1 for the no wind case, as the oscillations are now around the mean offset generated by the predefined thrust.

It can be seen that the yaw signals, although small (the total range in this plot is 0.5 deg) are strongly non-sinusoidal. The yaw motions show a secondary peak at the yaw natural period.

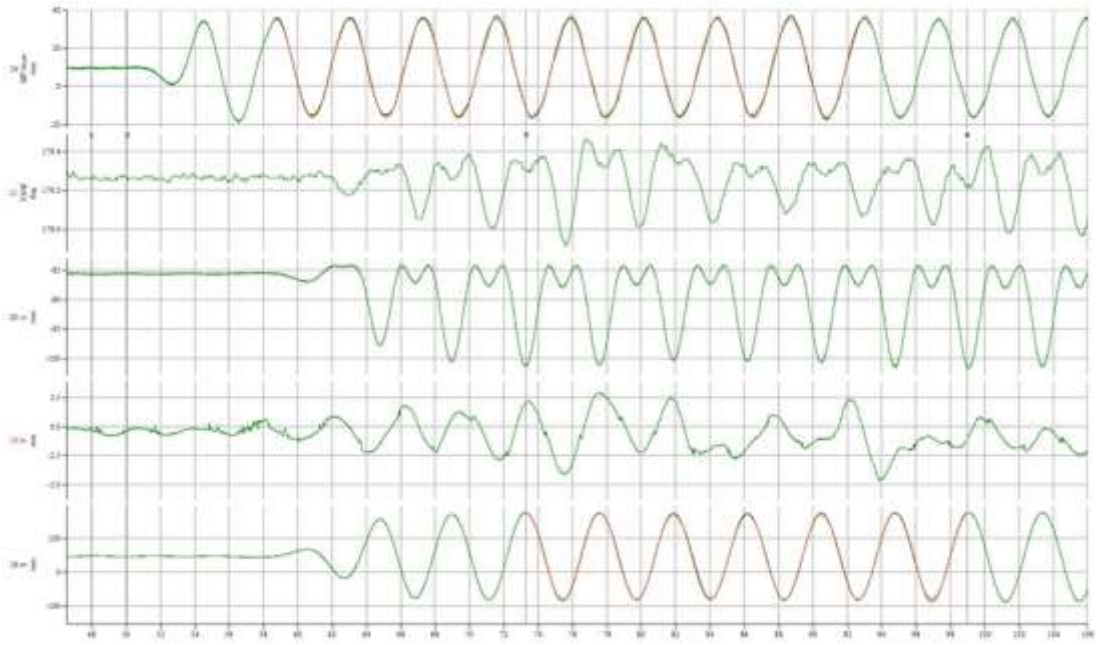

Figure 6.9 Typical recorded wave and motion data (head waves + PT) From top: Wave /Yaw/Z/Y/X

It can also be seen that the sway motions in this case are quite unlike those in Figure 6.1, and are strongly non-sinusoidal, and arguably non-periodic. Thus these results should be treated with some caution. It should be noted that the sway responses are small – the entire range in the screen shot shown is around 7mm at model scale, or about 0.25m at full scale.

All RAOs for rotational and translational motions of the floater for the case of head waves with Predefined Thrust are presented in Figure 6.10 to Figure 6.15, respectively.

In the case of predefined thrust, the surge natural period from the free oscillation tests was found as 24.3s and it can be seen from the Figure 6.10 that the peak of the RAOs for surge motion occurs at the period which is close to this value.

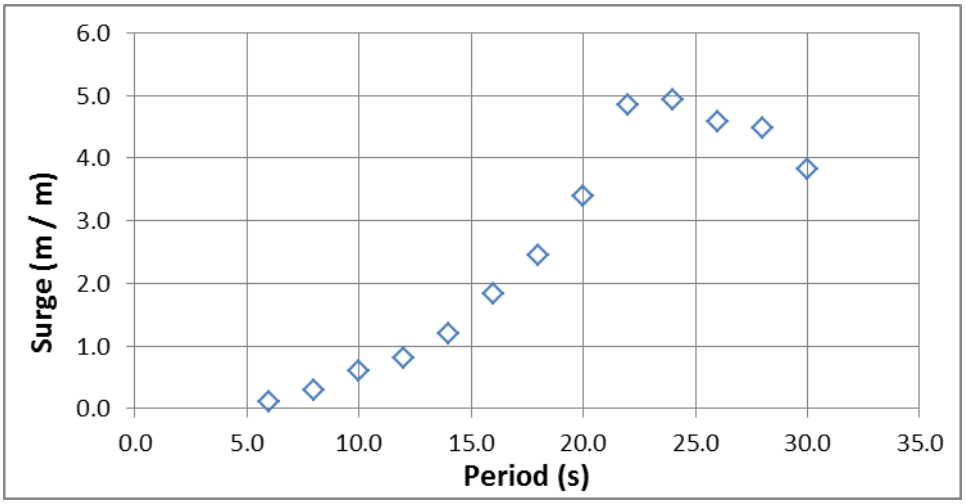

Figure 6.10 RAOs of surge motion in the case of head waves, Predefined Thrust

The peak of the sway RAOs occur at the period which is close to surge natural period obtained from the free oscillation tests as discussed previously. It can be seen from Figure 6.11 that there is also slight drop at the period of 11.5s which occurs near to the yaw natural period. There are two slight drops around 18s and 26s which do not match with any natural periods.

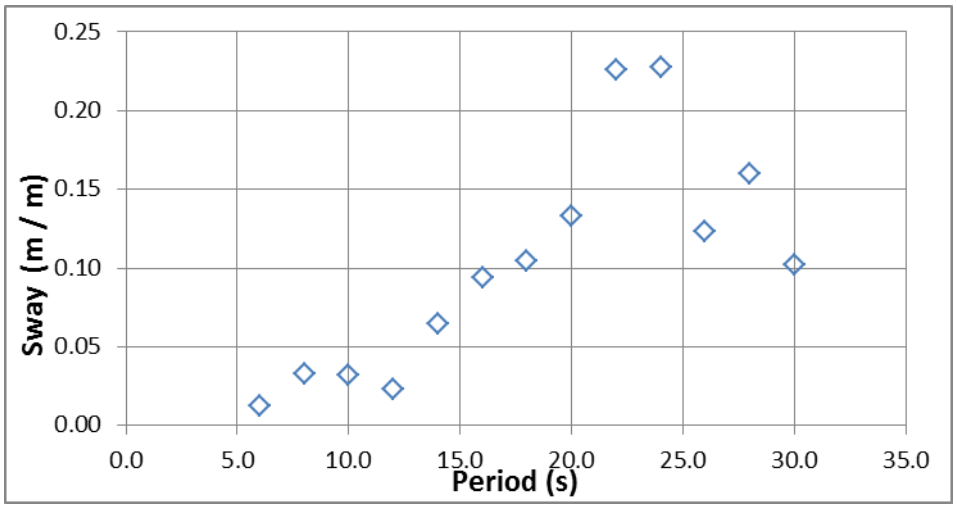

Figure 6.11 RAOs of sway motion in the case of head waves, Predefined Thrust

As can be seen from the Figure 6.12 the peak period of the heave motions in the case of head waves and constant thrust occurs at the natural period of the surge motions since the heave motions are coupled to the surge motions via the tendon kinematics.

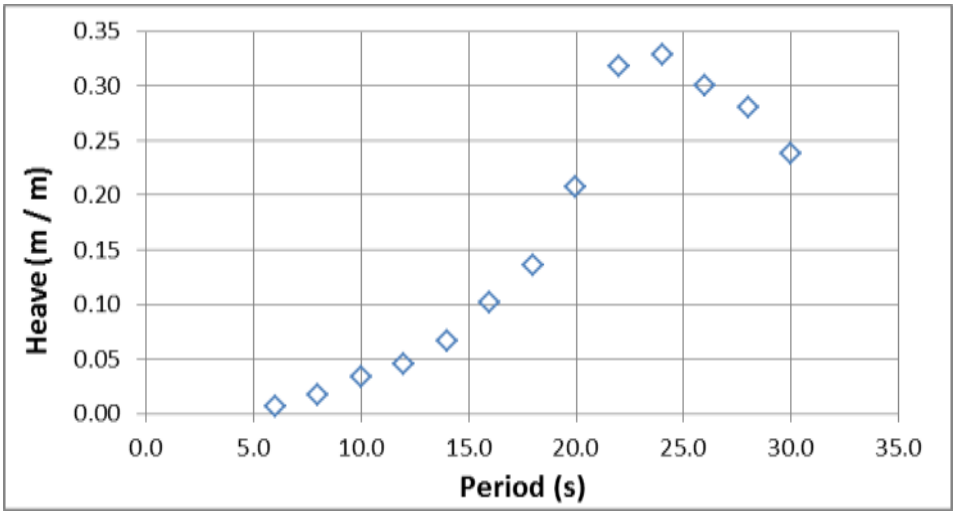

Figure 6.12 RAOs of heave motion in the case of head waves, Predefined Thrust

Figure 6.13 shows the roll transfer function; there is one obvious peak which occurs close to the surge natural period. The magnitude of the roll RAOs are very small at all frequencies.

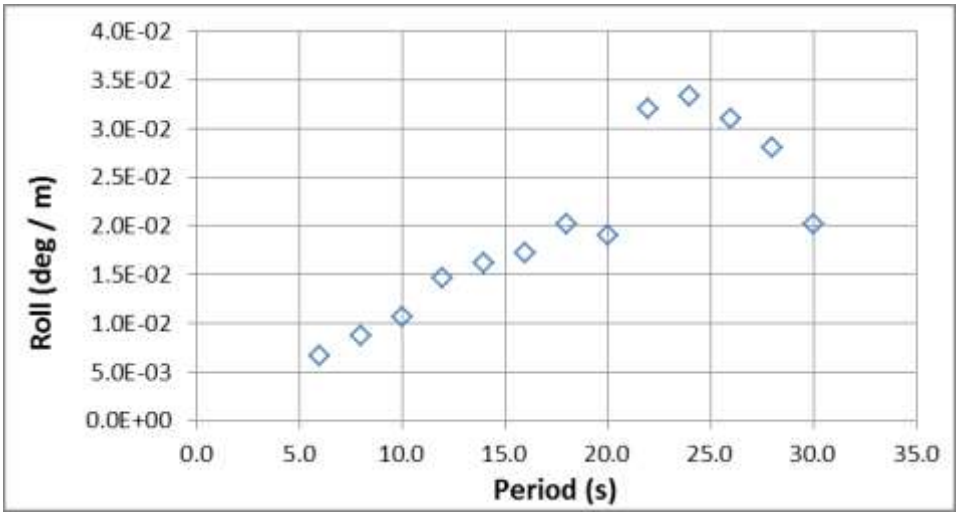

Figure 6.13 Transfer function of roll motion in the case of head waves, Predefined Thrust

It can be seen from Figure 6.14 that there is a large peak in the pitch transfer function occurring at the natural period of the surge motions. There is a smaller drop at around 11.5s which coincides with the yaw natural period.

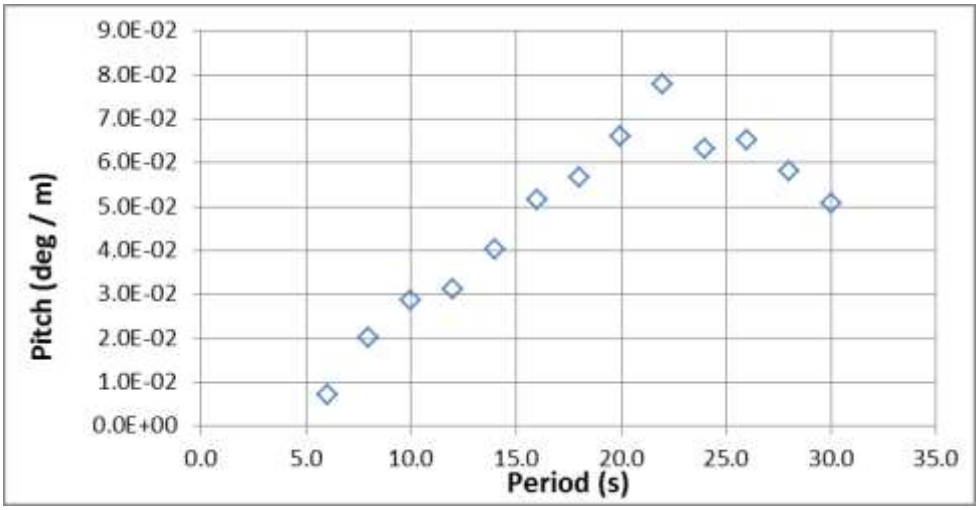

Figure 6.14 Transfer functions of pitch motion in the case of head waves, Predefined Thrust

It can be seen from Figure 6.15 that there are two large peaks in the yaw transfer function occurring at the natural period of surge and yaw at 24 and 11.5 seconds respectively. There is a smaller drop at around 20s which does not coincide with any natural periods.

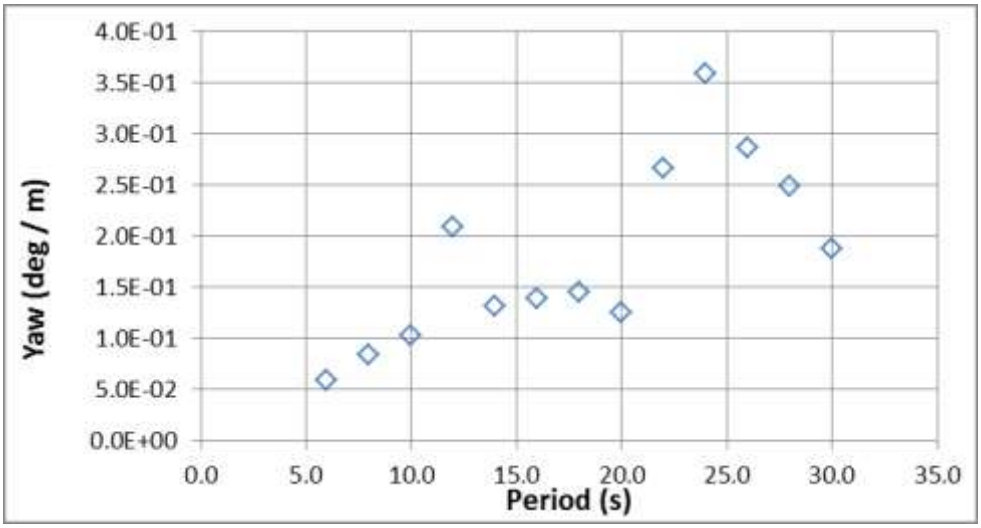

Figure 6.15 Transfer functions of yaw motion in the case of head waves, Predefined Thrust

6.4.3 Head waves – Software-in-the-loop (SIL)

As the wind is deployed the mean offset of the platform increases, and the damping changes somewhat; these effects naturally have some impact on the motions. In particular, the heave motions change. The difference in magnitude between alternate cycles increases, as shown in Figure 6.16; as the mean offset increases, the platform

displacement is greater in the downwind direction than in the upwind direction, and hence the asymmetry between the cycles is magnified. As the wind speed increases, the mean offset increases, and it could be expected that once the mean offset is greater than the surge amplitudes, the platform would respond in heave at the wave frequency rather than at twice the wave frequency.

The patterns for Software-in-the-loop (SIL) case broadly follow those for the PT case. A typical screen shot of the motion signals is shown in Figure 6.16.

Figure 6.16 Typical recorded wave and motion data (head waves + SIL) From top:Wave/Pitch/Yaw/Z/Y/X

Once more the non-sinusoidal nature of the yaw, sway, and vertical motion signals can be seen. In this case, the sway motions appear to exhibit a “beating” type responses; the motions in this case are larger than those shown in Figure 6.9, but the total range is still only around 12mm at model scale, or about 0.44m at full scale.

The following figures present the RAOs of the FOWT with the SIL system in operation. In general, the results are very similar to those obtained for the constant wind case. The peak of the sway RAOs is greater, pitch and yaw results also exhibit more variation for the SIL case.

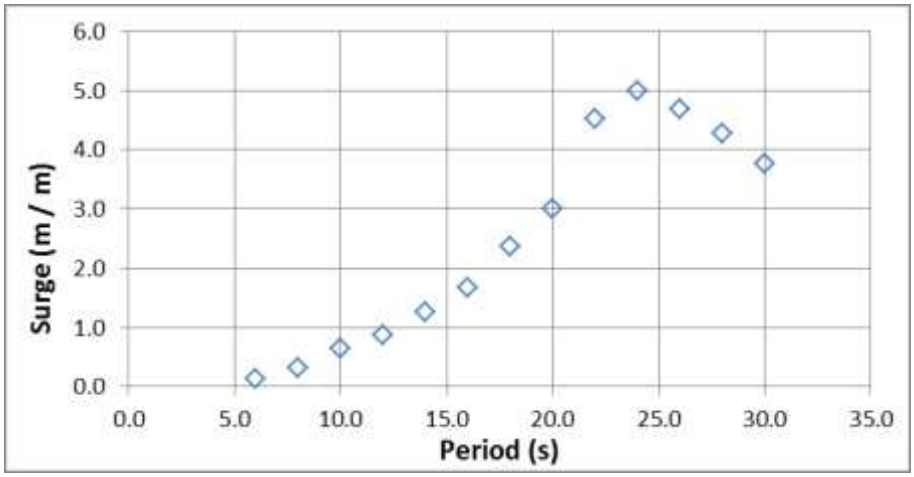

Figure 6.17 RAOs of surge motion in the case of head waves, SIL

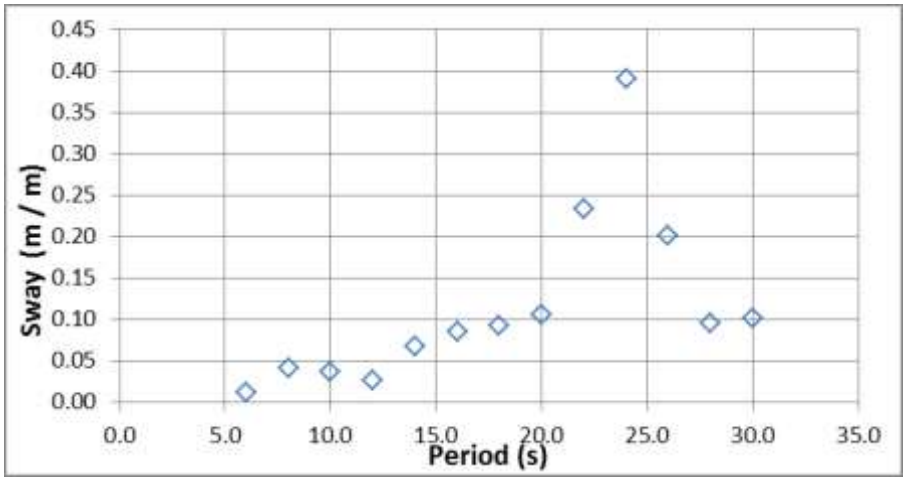

Figure 6.18 RAOs of sway motion in the case of head waves, SIL

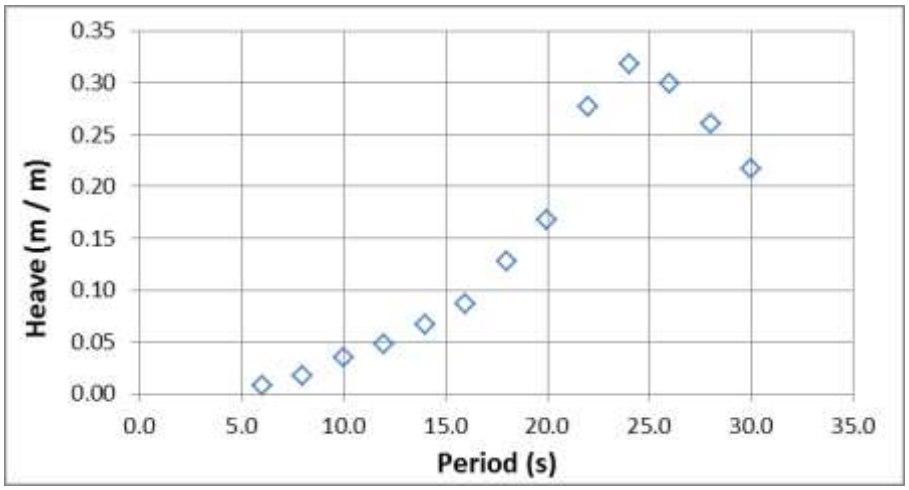

Figure 6.19 RAOs for heave motion in the case of head waves, SIL

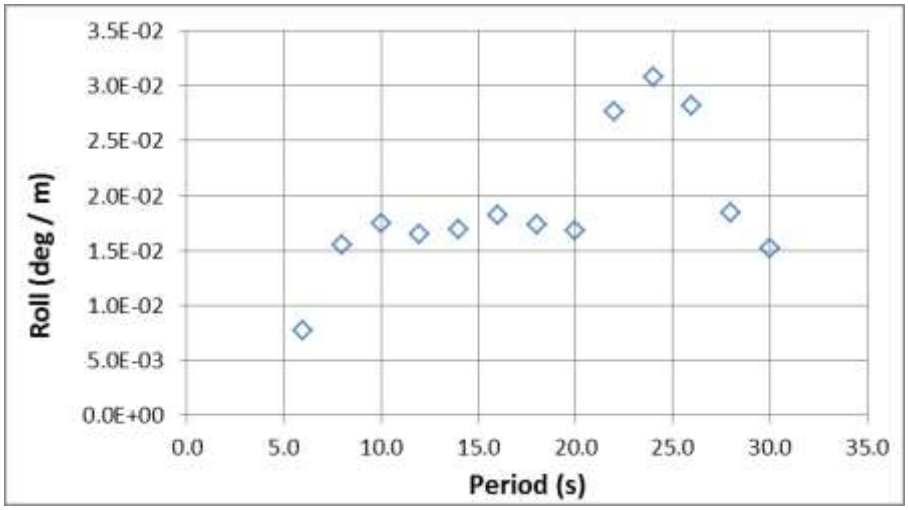

Figure 6.20 Transfer functions of roll motion in the case of head waves, SIL

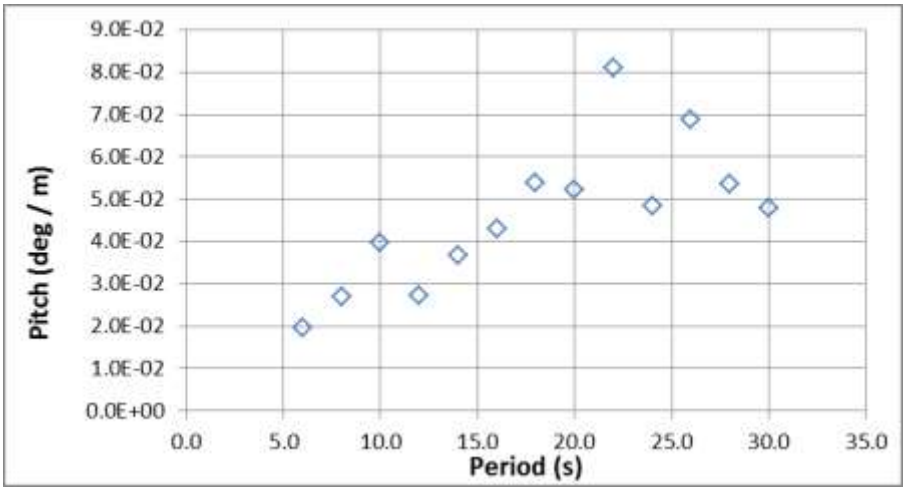

Figure 6.21 Transfer functions of pitch motion in the case of head waves, SIL

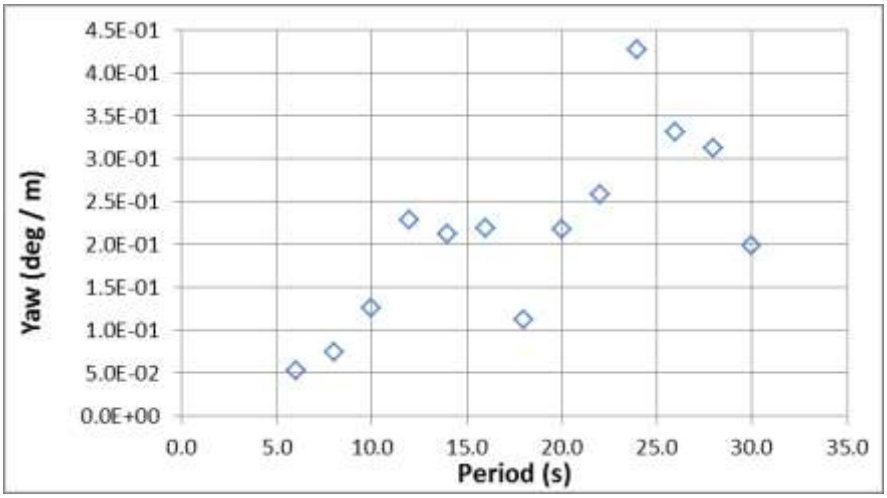

Figure 6.22 Transfer functions of yaw motion in the case of head waves, SIL

6.4.4 Quartering Seas – No wind

The final set of tests in regular waves was carried out with the model rotated through 45 degrees, and with no wind. It should be noted that the motions measured were in the global X and Y directions as required by the software in the loop system, rather than in a body-fixed system.

The following figures present the RAOs of the FOWT for quartering seas with no wind. In general, the results are very similar to those obtained for the 0° wave condition. It can however be observed from the figures that the yaw, roll and pitch motions are higher at the shortest wave periods.

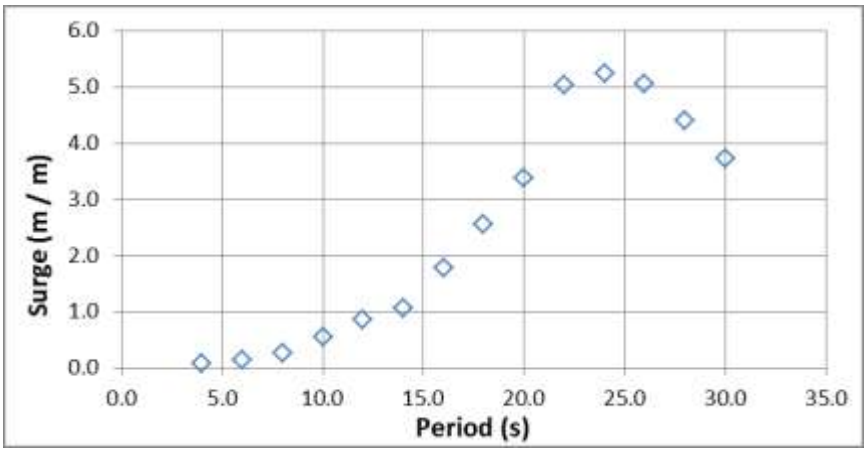

Figure 6.23 RAOs of surge motion in the case of quartering waves, no wind

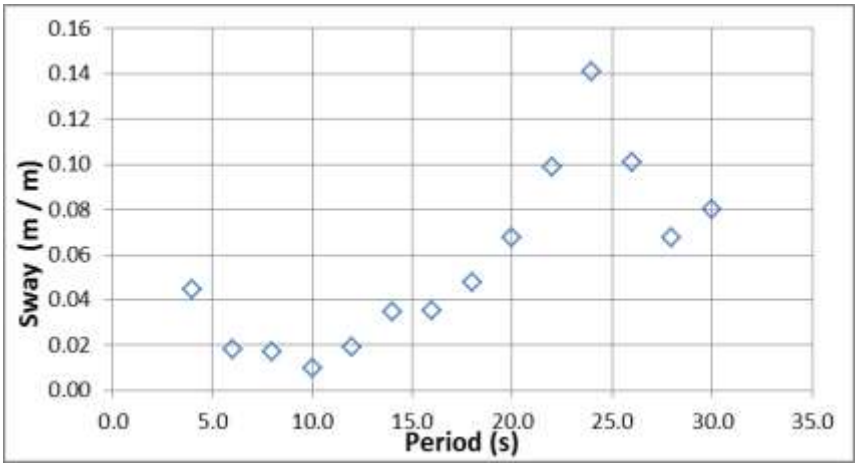

Figure 6.24 RAOs of sway motion in the case of quartering waves, no wind

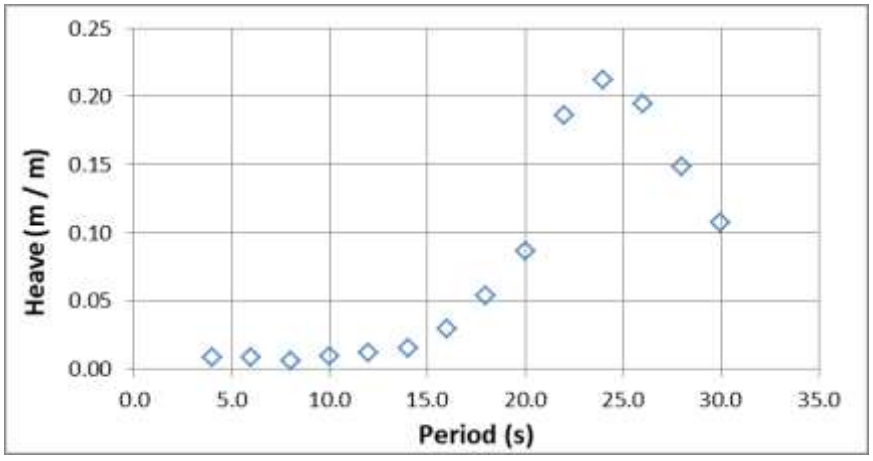

Figure 6.25 RAOs of heave motion in the case of quartering waves, no wind

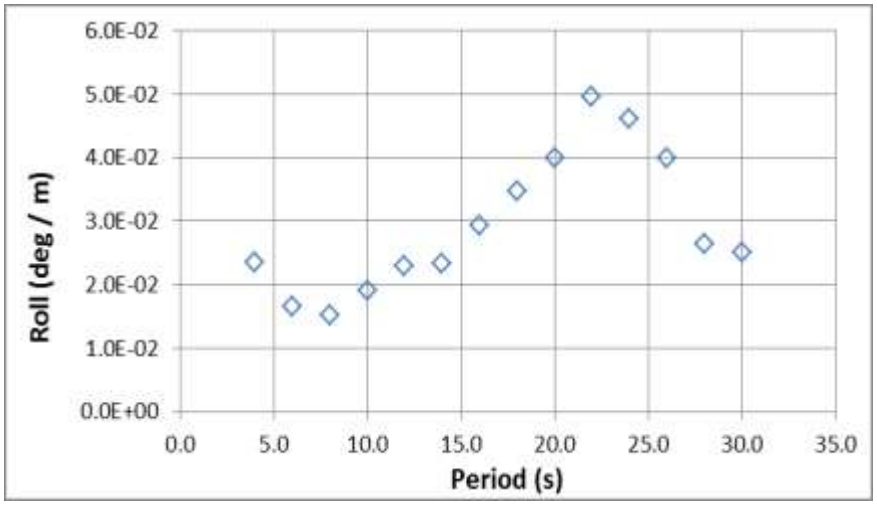

Figure 6.26 Transfer functions of roll motion in the case of quartering waves, no wind

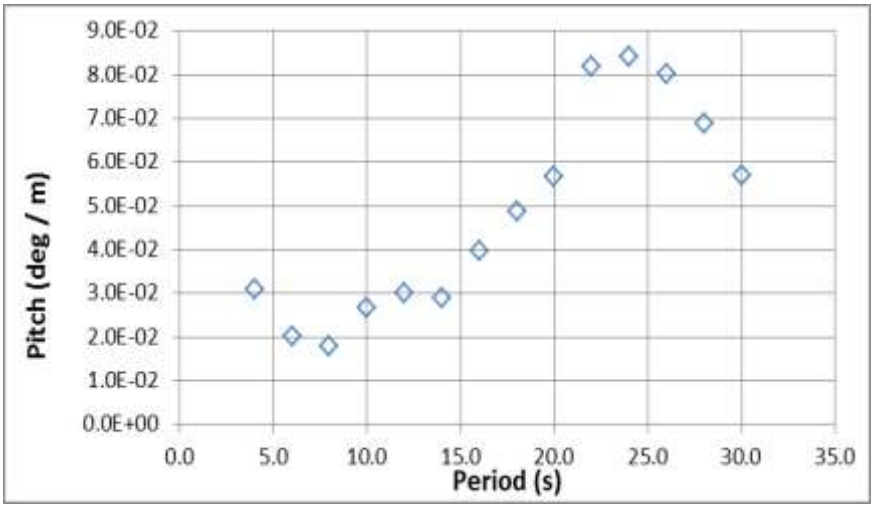

Figure 6.27 Transfer functions of pitch motion in the case of quartering waves, no wind

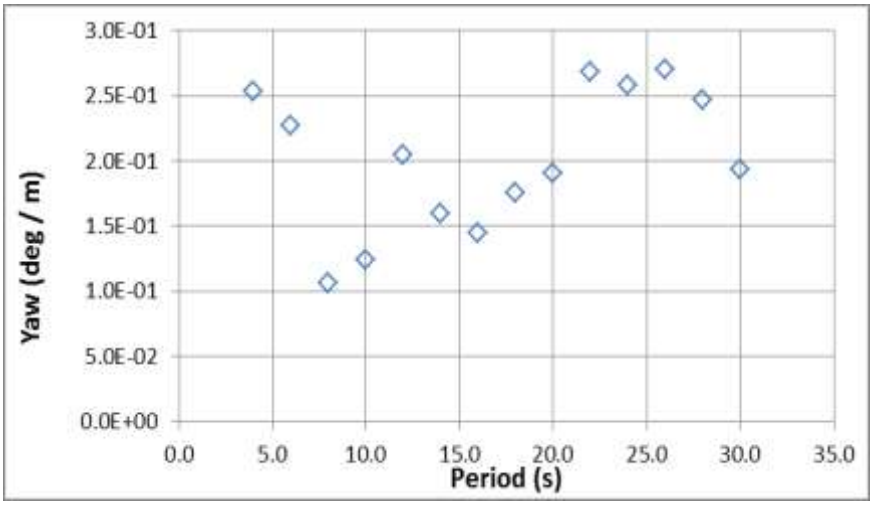

Figure 6.28 Transfer functions of yaw motion in the case of quartering waves, no wind

6.4.5 Impact of Wind Model on Surge RAO

The largest response naturally is in the surge direction, and hence it is interesting to examine what impact the choice of wind model has upon the surge RAOs. The comparison of three cases is shown in Figure 6.29.

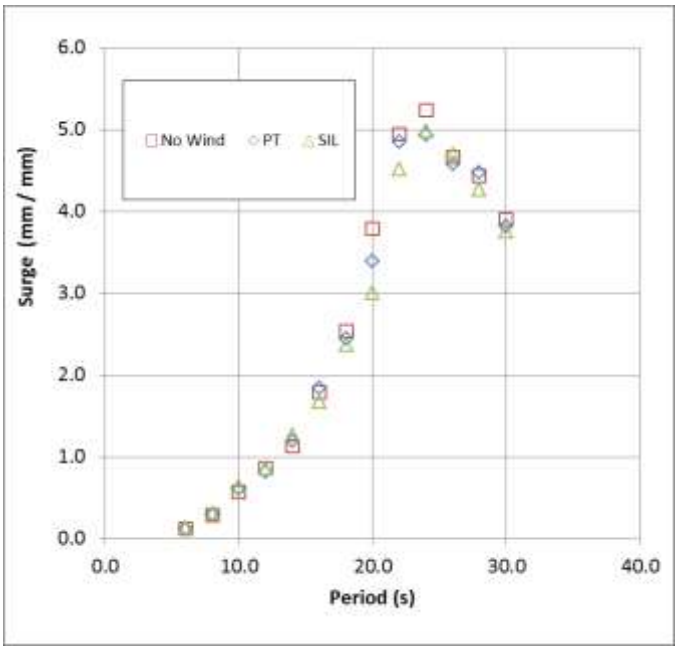

Figure 6.29 Surge RAOs for three different wind models

It can be seen that the largest response is for the case with no wind, as might reasonably be expected, since it is known that the aerodynamic forces contribute to the damping of the motions. The smallest response is for the SIL case. However the difference is relatively small at most frequencies, with the SIL leading to a reduction of about 6% of the surge RAOs at the peak, and around 11% at 20s period.

6.4.6 Impact of Heading Angle on Longitudinal Motion

Similarly it is interesting to compare the surge motions in the case of quartering seas with those for head seas. This is shown in Figure 6.30. It can be seen that the platform motions are relatively insensitive to the wave heading. It is also reported previously that the wave heading does not have a significant impact on the surge motion in (Rodriguez et al., 2014).

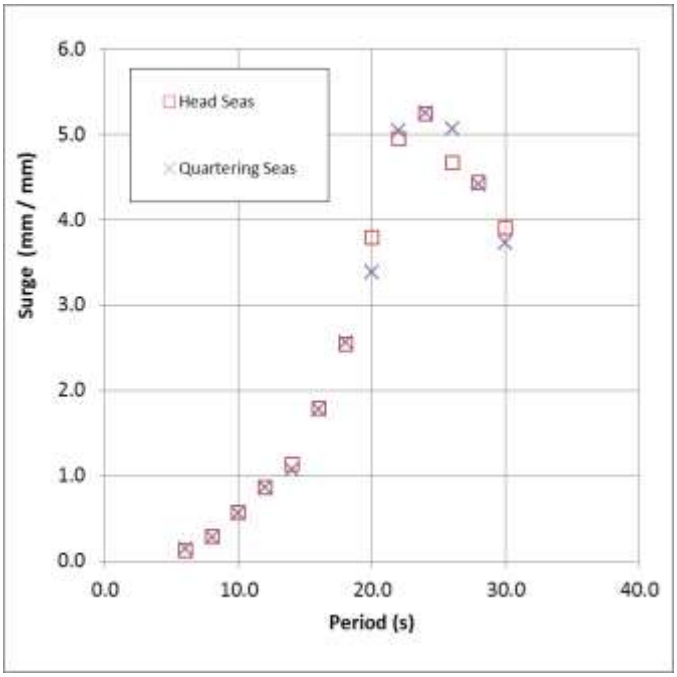

Figure 6.30 Longitudinal motion RAOs for two different wave headings

6.5 Dynamic Tendon Tensions

In this section, dynamic tendon tension plots are given. Tendons are numbered 1&2 on the up-wave side, 3&4 on the starboard side, 5&6 on the down-wave side then clockwise seen above round to 7&8 on the port side as shown in Figure 6.31.

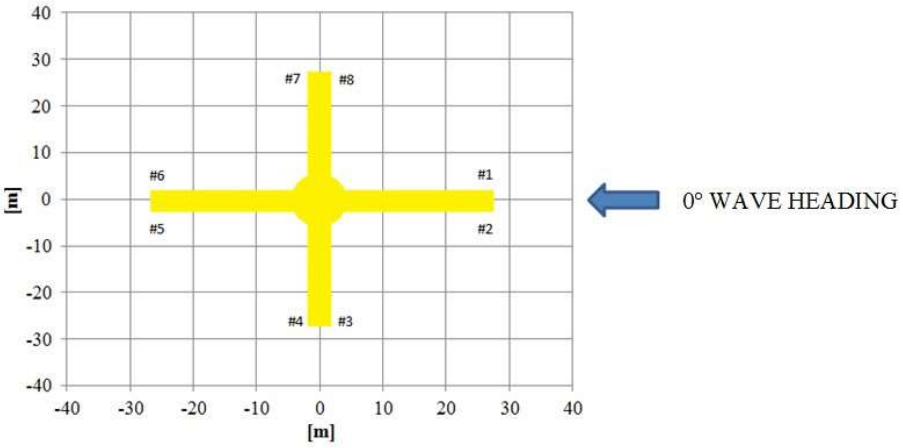

Figure 6.31 Tendon numbering

The dynamic tendon tension force transfer functions for head waves and no wind condition are given in Figure 6.32. Slight discrepancies can be seen between the tendons in each pair presumably due to small asymmetries in the model installation, leading to some small yaw angle even in head waves. Given the stiffness of the tendons, relatively small variations in position can lead to relatively large variations in the tension forces.

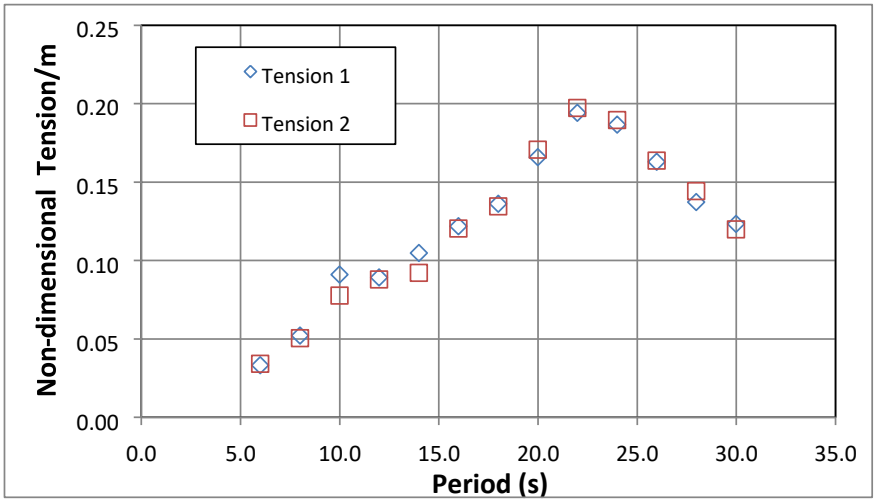

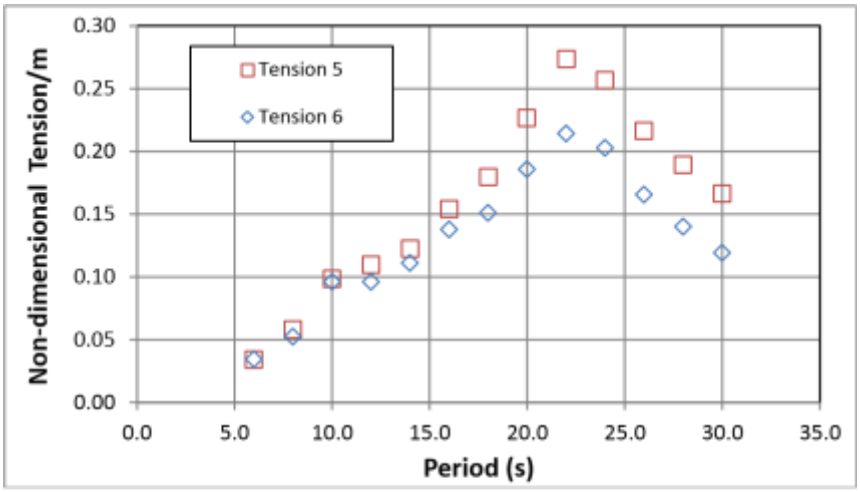

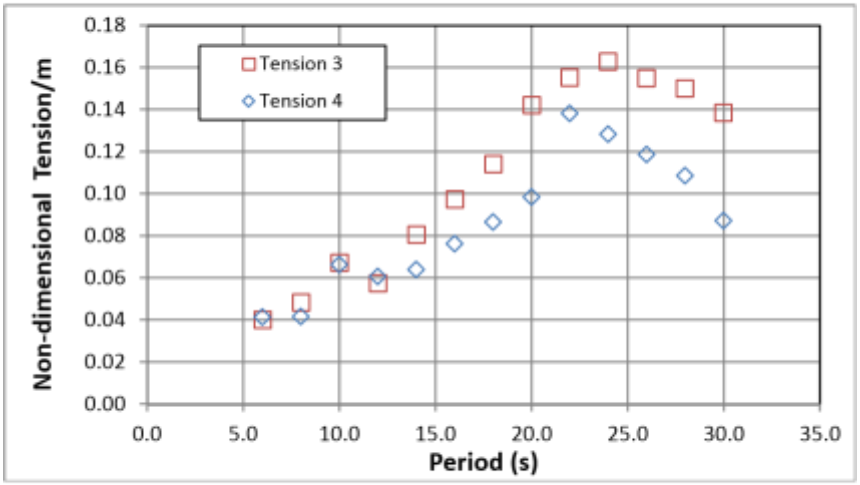

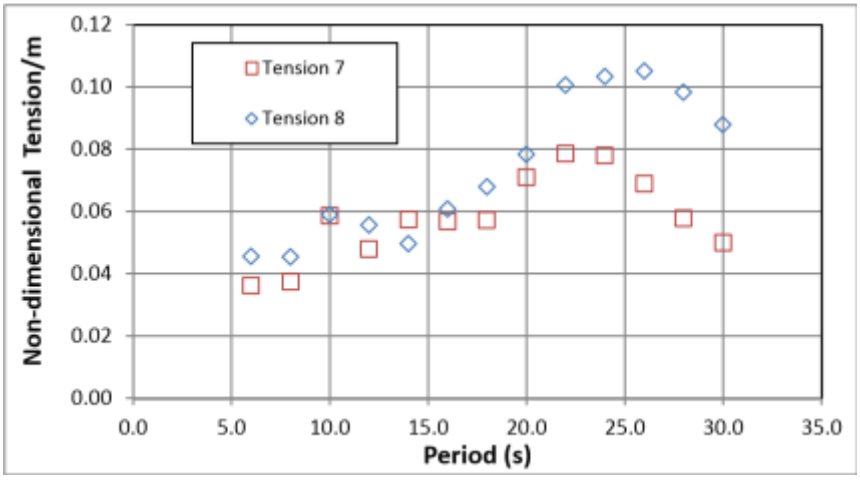

Figure 6.32 Tendon tensions : Head waves, no wind

The greatest dynamic tension forces observed at the down-wave side (5&6), followed by the up-side (1&2). The side tendons experience the smallest dynamic forces. In the side tendons,

it can be seen that the up wave tendons (3&8) experience greater dynamic forces than the down wave tendons (4&7). The peak of the tension forces occurs at the period close to the maximum surge motion. A small local maximum in the tension forces at the sides appears near the yaw natural frequency of 11s.

Figure 6.33 shows the dynamic tendon tension force transfer functions for the PT case. The results show a very similar trend with those measured in no wind, although the differences between the forces occurring upwave and downwave tendons are slightly reduced.

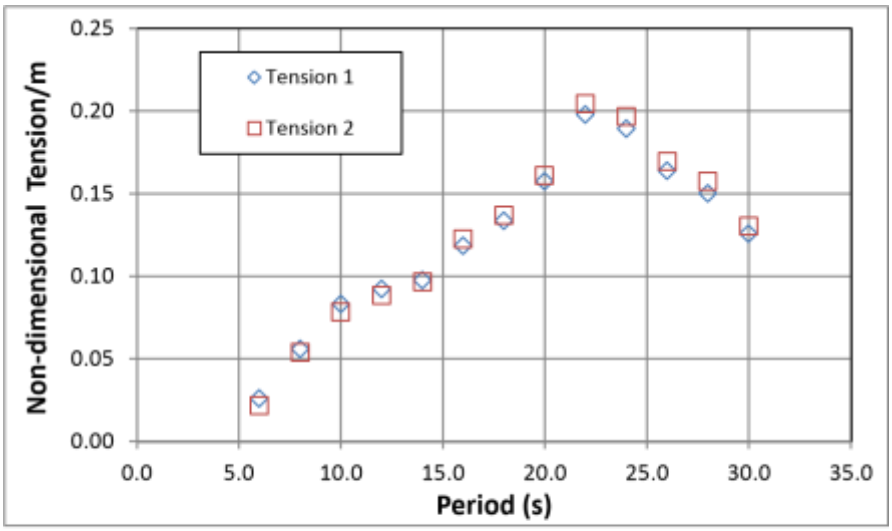

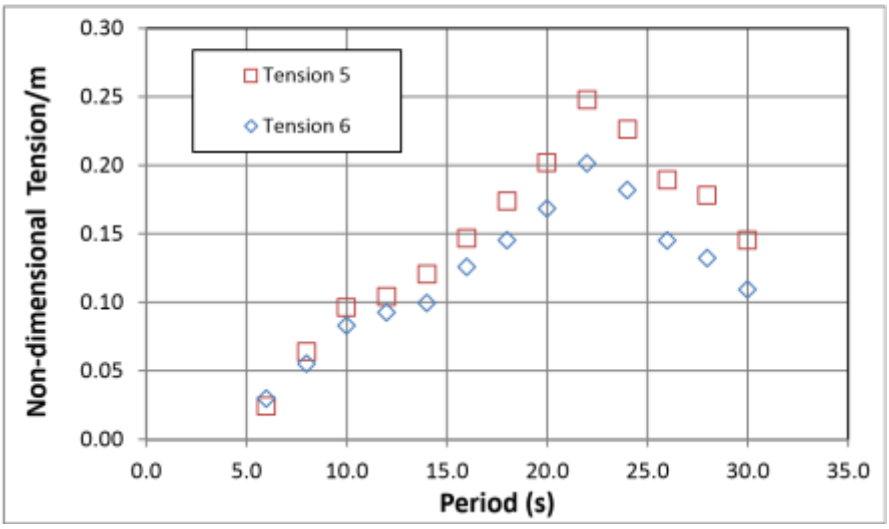

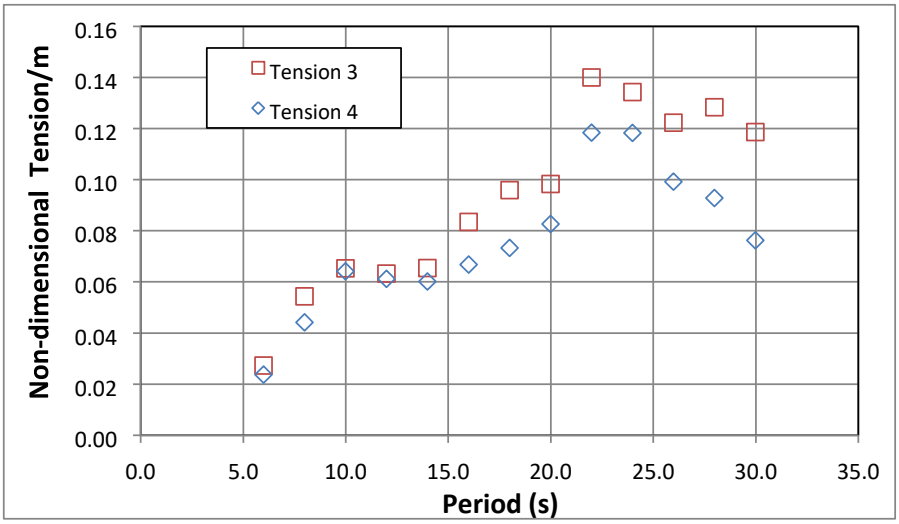

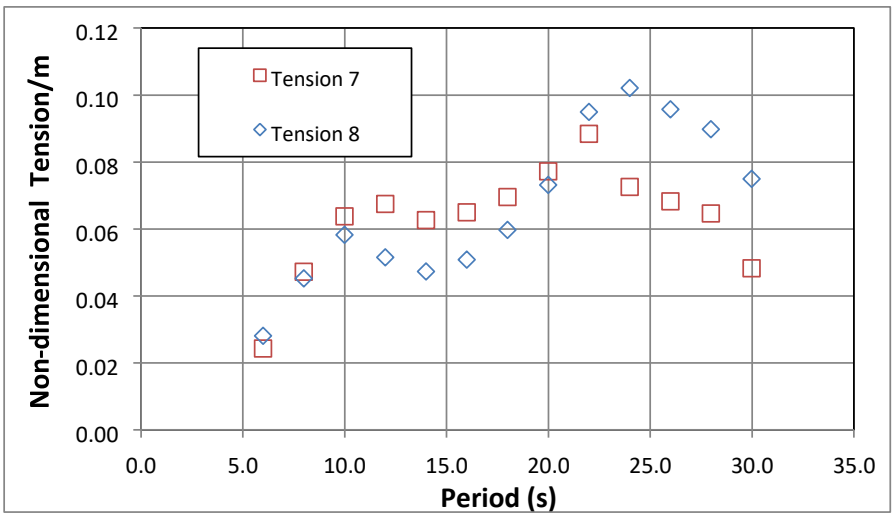

Figure 6.33 Tendon tensions: Head waves, Predefined Thrust (PT)

The corresponding plots for the SIL case are shown in Figure 6.34. The dynamic tension forces are slightly higher than those for the PT case, and a curious double peak is exhibited in tendon 1,2,5 and 6. The reasons for this are not obvious.

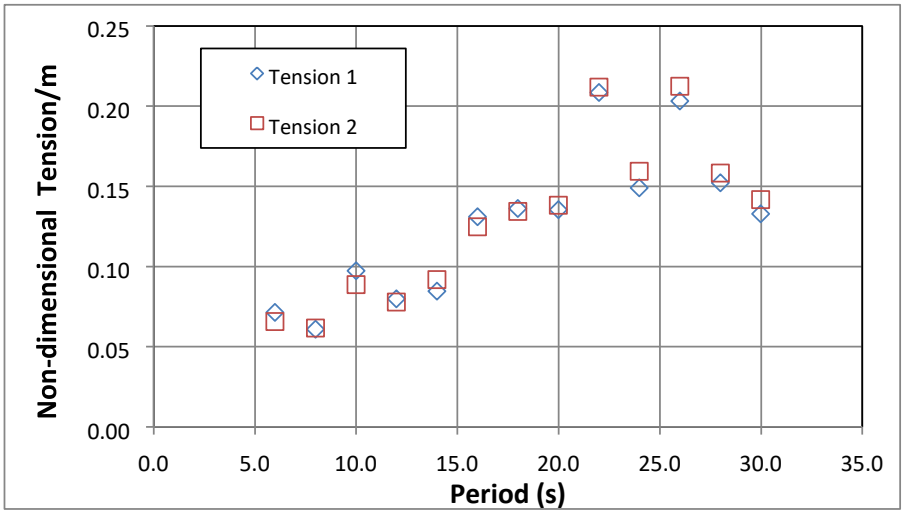
Non-dimensional Tension/m
0.25
0.20
0.15
0.10
0.05
0.00
Tension 1
Tension 2
0.0
5.0
10.0
15.0
20.0
25.0
30.0
35.0
Period (s)

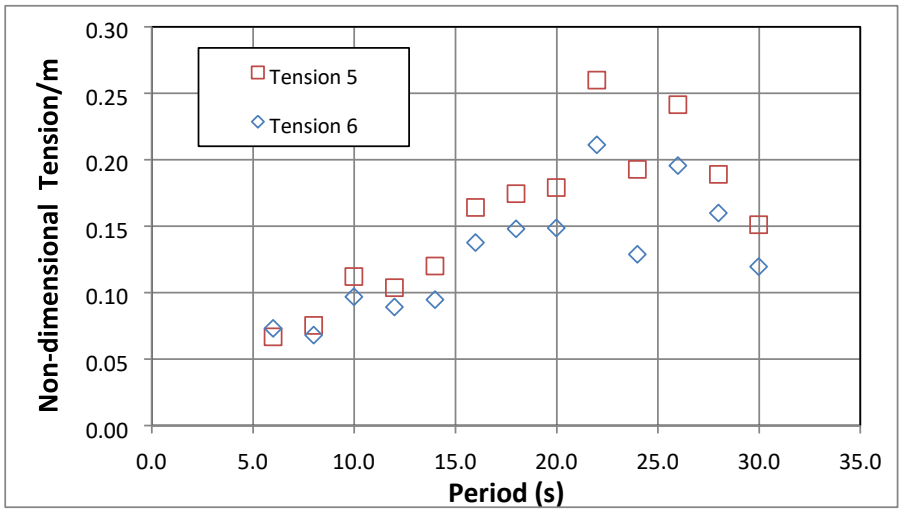
Non-dimensional Tension/m
0.30
0.25
0.20
0.15
0.10
0.05
0.00
Tension 5
Tension 6
0.0
5.0
10.0
15.0
20.0
25.0
30.0
35.0
Period (s)

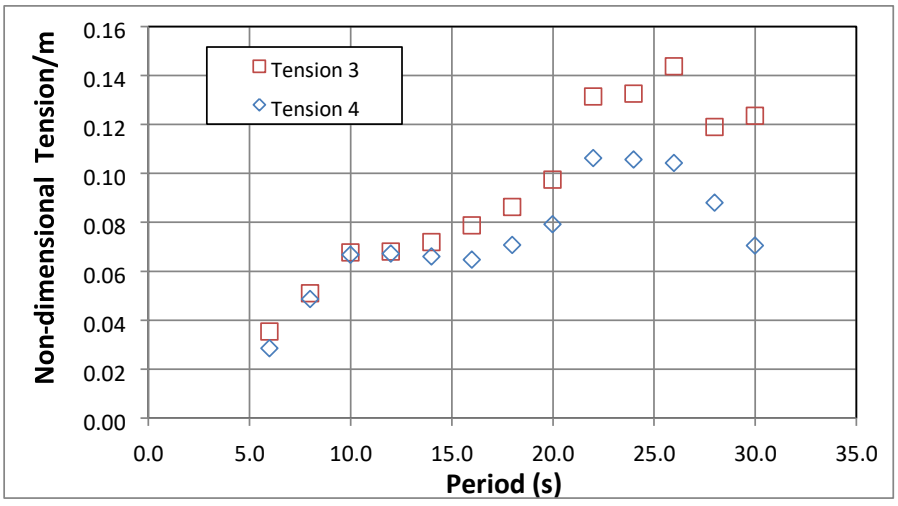
Non-dimensional Tension/m
0.16
0.14
0.12
0.10
0.08
0.06
0.04
0.02
0.00
Tension 3
Tension 4
0.0
5.0
10.0
15.0
20.0
25.0
30.0
35.0
Period (s)

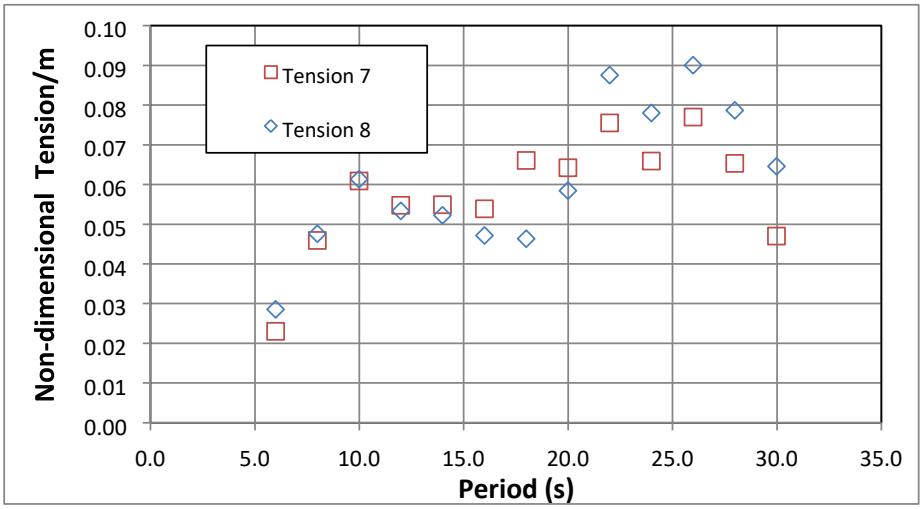

Figure 6.34 Tendon tensions: Head wave, SIL

Finally, the following figures describe the dynamic tension transfer functions for the quartering seas tests. Tendon 1 has significantly lower values across the frequency range in the quartering seas case in comparison to the head sea condition. Tendons 2 and 6 give very similar results as observed in the head seas condition whereas the other tendon tension force values are higher for the quartering seas condition.

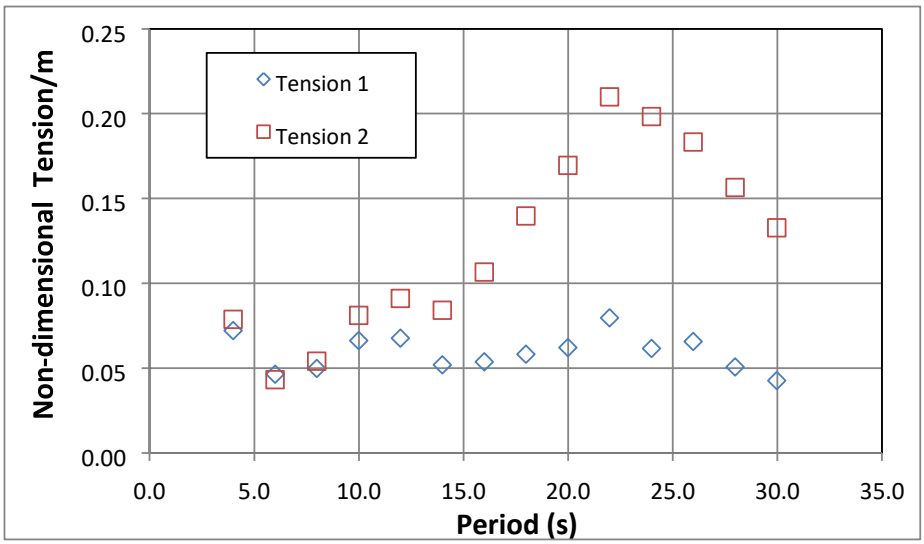

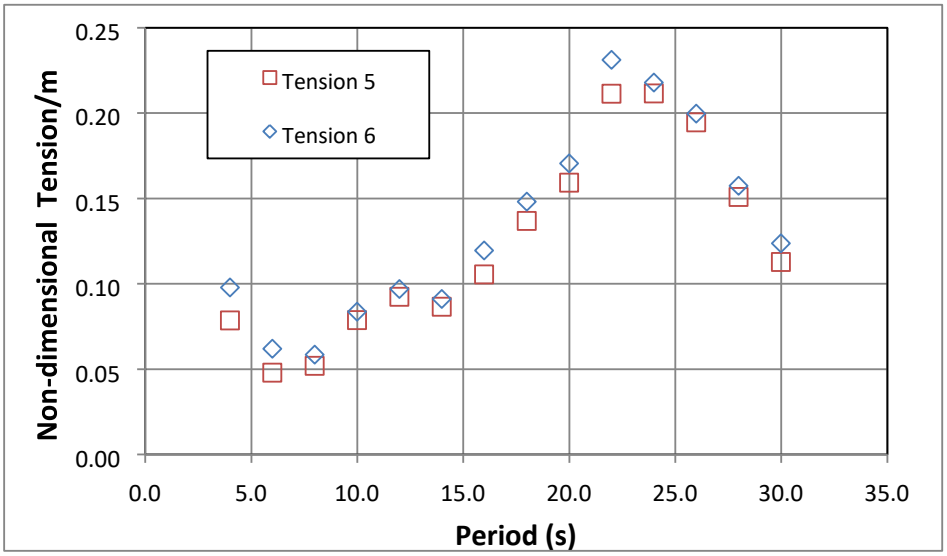
Tension 5
Tension 6
Non-dimensional Tension/m
Period (s)
0.25
0.20
0.15
0.10
0.05
0.00
0.0
5.0
10.0
15.0
20.0
25.0
30.0
35.0

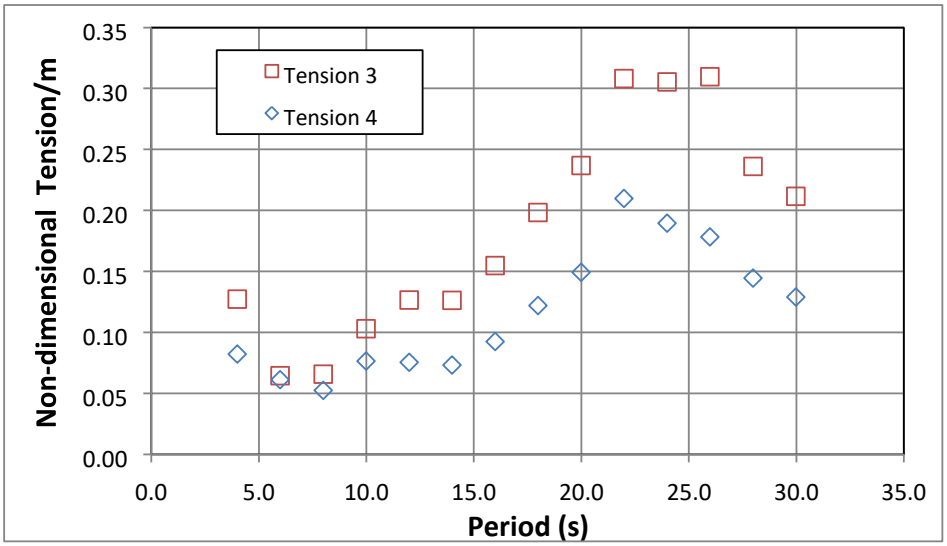
Tension 3
Tension 4
Non-dimensional Tension/m
Period (s)
0.35
0.30
0.25
0.20
0.15
0.10
0.05
0.00
0.0
5.0
10.0
15.0
20.0
25.0
30.0
35.0

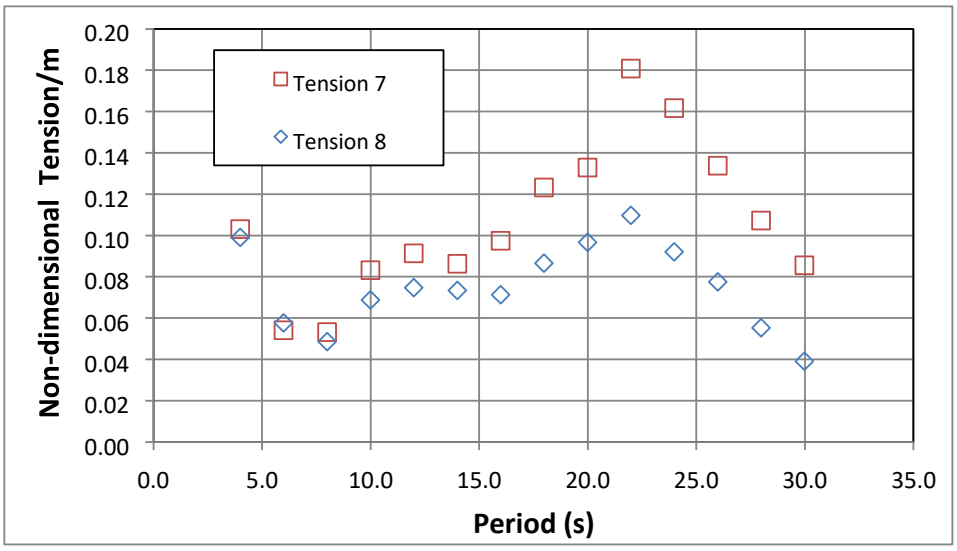
Tension 7
Tension 8
Non-dimensional Tension/m
Period (s)
0.20
0.18
0.16
0.14
0.12
0.10
0.08
0.06
0.04
0.02
0.00
0.0
5.0
10.0
15.0
20.0
25.0
30.0
35.0

Figure 6.35 Tendon tensions : Quartering Waves No Wind

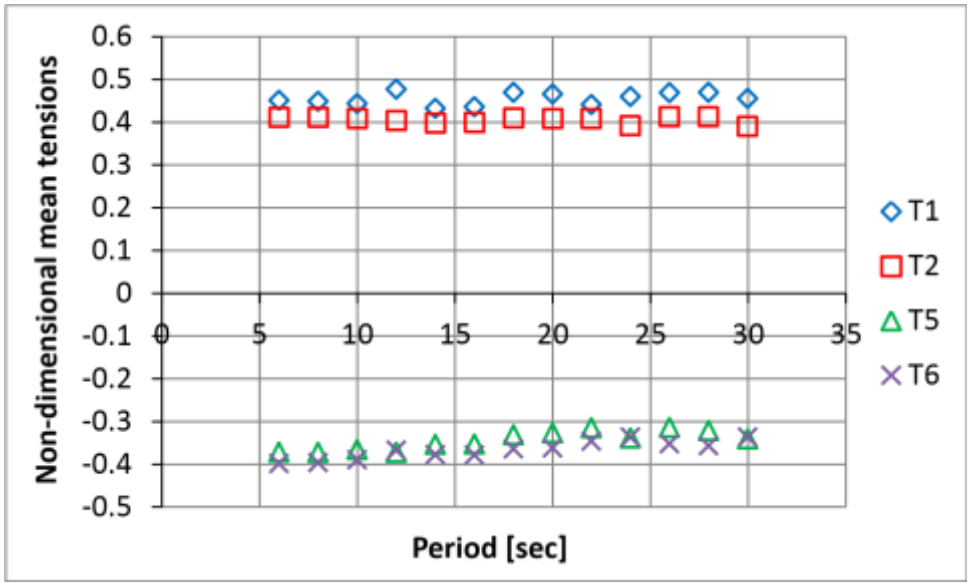

Figure 6.36 Mean tension values for front and back tendons

It can be seen from Figure 6.36 that mean front tendon tensions in regular wave tests with wind (in this case for the software in the loop condition) are higher than the back tendon tensions; the trend is this similar to the irregular wave tests in the case of 0°/0° configuration.

6.6 Comparison of experimental results with numerical predictions

In order to compare the motion RAOs and tension force transfer functions obtained from the experimental results with the numerical results, tests in regular waves with no wind condition were also carried out using FAST code.

Some of the parameters were set up before running the simulations. *WaveMod* (Incident wave kinematics model) was taken as 1 which represents plane progressive (regular) waves. Numerical tests were run with both flexible and rigid towers; better agreement was obtained with the rigid tower, and these results are presented here. A typical input file is shown in Appendix B.

In this section the motion RAO's and tension force transfer functions obtained from the experimental results are compared to those from the numerical results for 0° head seas with no wind cases.

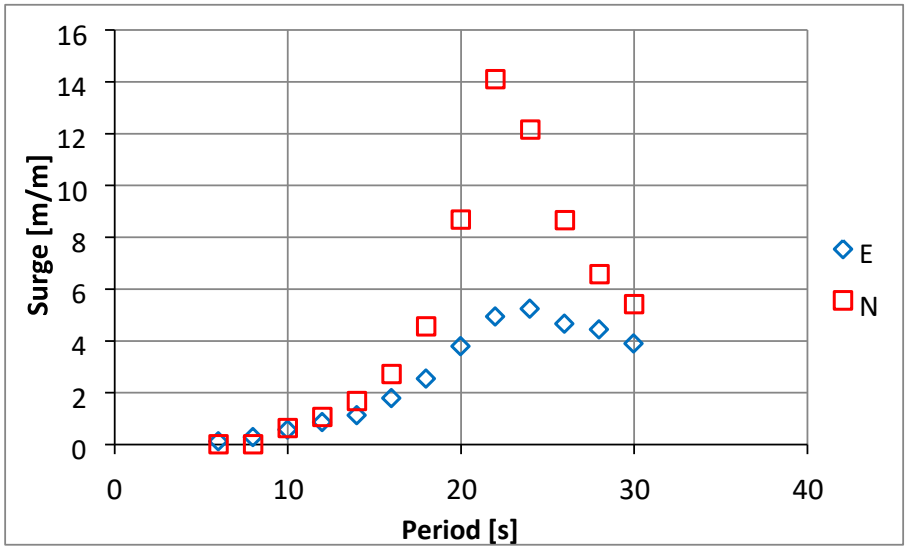

Figure 6.37 Comparison of surge motion

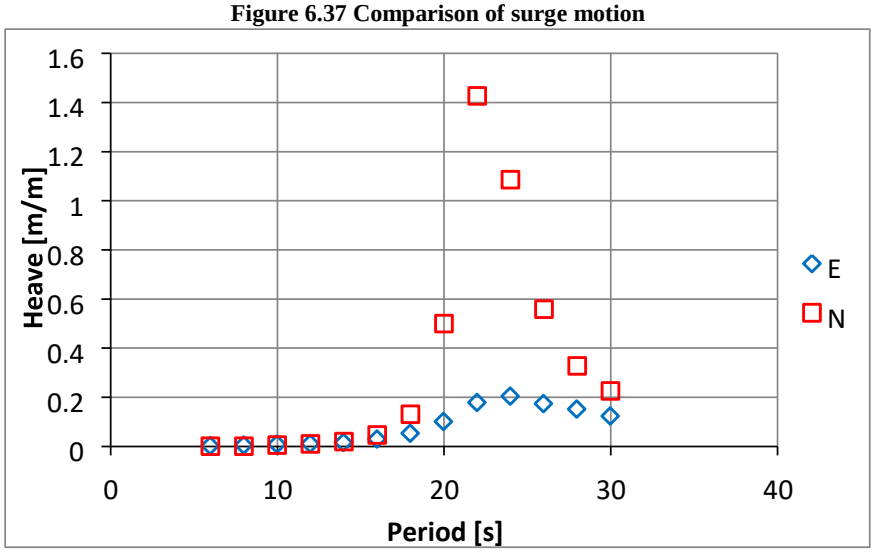

Figure 6.38 Comparison of heave motion

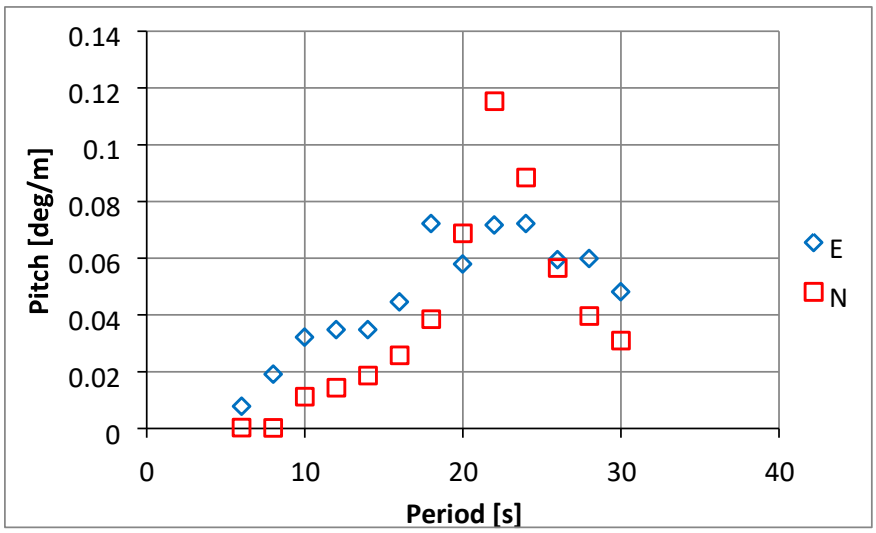

Figure 6.39 Comparison of pitch motion

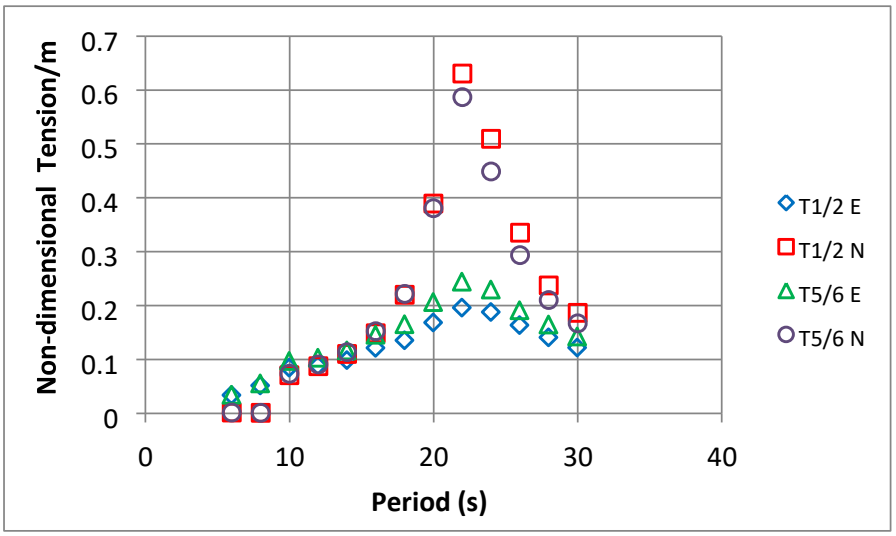

Figure 6.40 Average front-back tendon tension transfer functions

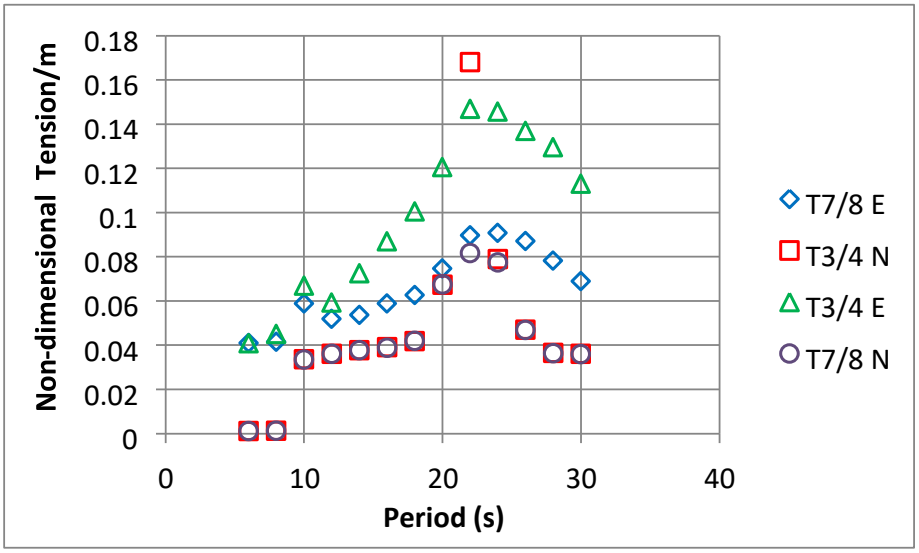

Figure 6.41 Average side tendon tension transfer functions

All of the motion and tension forces responses show good agreement for wave periods between 5 to 20 seconds and from around 28 seconds. The pitch motions give the closest agreement between the measurements and numerical predictions over the whole range of wave periods. For the remaining responses the numerical predictions overestimate the experimental values particularly in the region of the surge natural period (22-25 seconds) when damping dominates. As it is reported in

(Wayman et al., 2006) the RAO in surge of the MIT/NREL TLP (benchmark study) shows a large spike at around its natural frequency similar to the results presented here. In order to investigate the viscous damping effect on this spike, (Wayman et al., 2006) added 2 different viscous damping ratios (γ). The results showed that as viscous damping increases, the peak responses decreases. This describes the overestimated RAO values at around surge and heave natural periods. (Due to FAST viscous simplifications, RAOs at the peak period are higher than those obtained from the experiments.) Future work may look at adding an additional viscous damping term in FAST.

6.7 Conclusions

In this chapter, tests in regular waves were described. These tests were important to understand the general behaviour of the proposed FOWT system.

The surge responses of the FOWT dominate all of the motion responses. All of the other motion responses are very small compared to the surge responses. The results indicated that the surge responses for the case with no wind are larger than those obtained with either of the wind simulated cases. The effect of wave heading has only a small effect on the motion responses.

The largest dynamic tension forces were observed for the down wave tendons (5 and 6) with the side tendons showing the smallest variation. Maximum tension forces coincided with the maximum surge motion at a period of around 24s. Some small effects at the 11.5s yaw natural period were also observed. The effect of the wind model did not significantly affect the dynamic tension forces. Unlike the motion response results the wave heading had a significant effect on the tension forces.

A subset of the motion RAO's and tension forces transfer functions obtained from the experimental results are compared to those from the numerical results for 0° head seas with no wind cases. In general good correlation was evident over the 5-20 sec wave period range whilst the responses were over predicted in the region of the surge natural period. Peak of RAOs is dominated by damping. Free oscillation tests show FAST underestimates damping by 50% (see section 5.6). The discrepancies at the peaks of the RAOs are consistent with this.

Chapter 7

Irregular Wave Tests

7.1 Introduction

A substantial part of the experimental and numerical study was carried out in simulated realistic environmental conditions. The FOWT was subjected to eight sea states and seven wind combinations with different wave/wind heading configurations. The response of the structure to these inputs was obtained from the experiments and for each case was also computed numerically. The FOWT was also subjected to above rated severe wind conditions.

A key goal of this study is to characterise the motion responses and the tendon loadings of the FOWT under realistic and severe conditions and to compare the experimental results with the numerical predictions.

Background theory of irregular waves is given in section 7.2. Section 7.3 explains the sea state selection in detail. In Section 7.4, wind models used in the research are described. Then, tests matrix of irregular waves is presented. In Section 7.6, the test procedure is described. Data processing of experimental results are described in detail in Section 7.7. Wave analysis, motion analysis, spectral analysis of motions and tendon tensions for storm case are described in detail in section 7.8. Data processing for numerical predictions is given in section 7.9. Following this, experiment/numerical comparisons for three configuration of the FOWT are given. The remaining experimental results are given showing the wind direction effect on the system. Finally, a conclusion of this chapter is drawn.

7.2 Wave model

Wind driven waves are irregular in nature but they can be represented as the superposition of many regular harmonic wave components, each with its own amplitude, length, period and direction of propagation (M.St.Denis and W.J.Pierson, 1953).

Wave conditions can be represented in two ways in the case of structural design purposes. The first case is the deterministic design method which is used for quasistatic response of structures where the wave excitation is characterised by wave length, wave period, wave height and wave crest as described in (S.K.Chakrabarti, 1987). The second one involves stochastic modelling of the sea surface which is a required for structures with a complex or non-linear dynamic response. In this method, the sea state is characterised by irregular waves which have an energy distribution with frequency as defined by a particular wave spectrum.

The most common irregular wave model, the linear long-crested wave model is given as:

$$\eta_1(t) = \sum_{k=1}^{N} A_k \cos(\omega_k t + \varepsilon_k) \qquad (7.1)$$

$_1(t)$ describes the wave elevation variation with time.

$_k$ are a set of independent random phases uniformly distributed between 0 and 2π radians.

A_k are the Rayleigh distributed amplitudes of the individual wave components given by :

$$A_k = \sqrt{2S(\omega_k)\Delta\omega_k} \qquad (7.2)$$

$S(\omega_k)$ denotes the value of the wave spectrum at frequency ω_k

$\Delta\omega_k = \omega_k - \omega_{k-1}$ is the difference between successive frequencies.

In order to accurately represent the wave elevation a large number of frequencies, hence a small $\Delta\omega_k$ is often used. For the experimental program over 2000 components were used to represent each wave elevation.

7.2.1 Wave Spectrum

A wave spectrum is often parameterised by a significant wave height (H_s), a peak enhancement factor, usually referred to as (γ) and a corresponding peak frequency (ω_p) which is the frequency where the spectrum has a maximum value. It is usually assumed to be a stationary random process. Depending on the location the period of

stationarity can range from 30 minutes to 10 hours. In this study three hours was selected as being representative of the North Sea area where the proposed FOWT will be deployed. However this did not prove possible for the SIL cases due to software limitations on the size of the files storing the time histories of the turbulent wind. These experimental runs were limited to 166 minutes at full scale.

A particular wave spectrum depends on the geographical area, local bathymetry and the severity of the sea state. A wave spectrum represents the power spectral density function of the vertical sea surface displacement as a function of wave frequency.

There are number of spectral formulations in the literature. Pierson-Moskowitz (PM) spectrum is one of the simplest descriptions for the energy distribution which developed in 1964 based on the measurements in the North Atlantic. The PM spectrum represents a fully developed sea i.e. the wind blows steadily for a long time over a large area such that the waves reach a point of equilibrium with the wind.

The JONSWAP spectrum is one of the most frequently used spectrums. It was based on empirical observations and was developed by the Joint North Sea Wave Project in 1973 and described by Hasselmann et al. (1973). The JONSWAP spectrum is a fetch-limited version of the PM spectrum, where the wave spectrum is never fully developed and may continue to develop due to non-linear wave-wave interactions for a long time. So, waves continue to grow with distance or time in the JONSWAP spectrum. The peakedness which is related to the bandwidth of the spectrum is defined by gamma (γ) parameter.

The JONSWAP spectrum is described by:

$$S_J(\omega) = A_\gamma S_{PM}(\omega)\gamma^{\exp\left(-0.5\left(\frac{\omega-\omega_p}{\sigma\omega_p}\right)^2\right)} \quad (7.3)$$

ω represents the frequency of the wave component, ω_p represents the peak frequency, $A_\gamma = 1 - 0.287\ln(\gamma)$ is a normalising factor and σ denotes the spectral width parameter which has a value of either 0.07 or 0.09 depending on the frequency.

The value of the peak enhancement factor γ depends on the particular sea state and is found from:

$$\gamma = 5 \text{ for } \frac{T_p}{\sqrt{H_s}} \leq 3.6 \tag{7.4}$$

$$\gamma = \exp(5.75 - 1.15\frac{T_p}{\sqrt{H_s}}) \text{ for } 3.6 < \frac{T_p}{\sqrt{H_s}} < 5 \tag{7.5}$$

$$\gamma = 1 \text{ for } \frac{T_p}{\sqrt{H_s}} \geq 5 \tag{7.6}$$

7.3 Sea state selection

In order to characterise the behaviour of the FOWT during its entire deployment period, the probability of occurrence of the sea states in the deployment area is necessary. The environmental conditions for the tests were selected based on an analysis of the proposed site (Iberdrola Engineering & Construction, 2014) where the wave conditions were characterised by a JONSWAP spectrum. Parameters of significant wave height and peak period and peak enhancement factor for each sea state are given in Table 7.1.

Table 7.1 JONSWAP Parameters

Sea State	Hs (m)	Tp (s)	$T_p/\sqrt{H_s}$	Gamma
N1	4.55	9.00	4.2	2.45
N2	1.50	6.61	5.4	1.00
N3	8.46	10.13	3.5	5.00
N4	0.75	5.44	6.3	1.00
N5	1.25	6.36	5.7	1.00
N6	1.75	6.86	5.2	1.00
N7	7.80	4.7	1.41	2.75
N8	6.00	10.28	4.2	2.53

The wave spectra are shown in Figure 7.1 and Figure 7.2. Figure 7.1 shows the spectra for the larger wave heights $H_s \geq 4.55m$. Figure 7.2 shows the spectra for the smaller wave heights $H_s \leq 2.75m$.

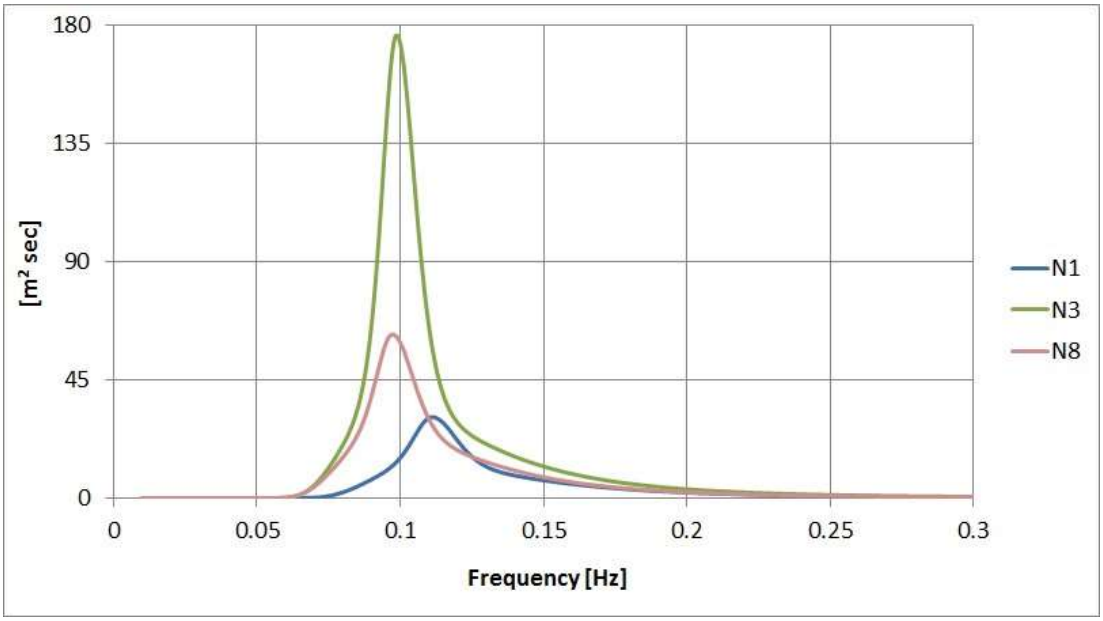

Figure 7.1 Theoretical JONSWAP spectra for larger wave heights

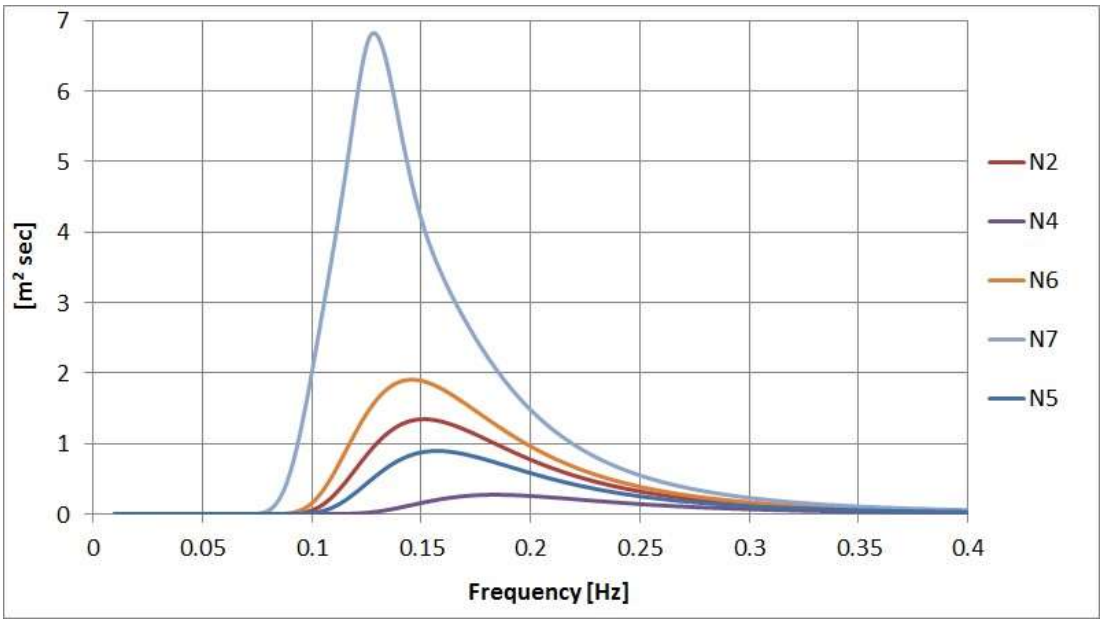

Figure 7.2 Theoretical JONSWAP spectra for smaller wave heights

Figure 7.1 and Figure 7.2 show that apart from wave spectrum N8 as the value of H_s increases the frequency where the energy reaches a maximum value reduces. The greatest energy density occurs for wave spectrum N3 which represents the storm case. Considering all of the wave spectra the range of frequencies where there is significant wave excitation is from 0.07 Hz (14.3sec) to 0.25Hz (4sec). This range of frequencies is outside any of the natural frequencies of the FOWT. The closest natural frequencies are yaw 0.087Hz (11.5sec) and

pitch at 0.39Hz (2.56sec) all other natural frequencies are some distance from the wave excitation frequency. Due to the location of the FOWT natural frequencies it is expected that the wave induced motions will be small. This was confirmed in the regular wave tests presented in Chapter 6. Figure 7.3 indicates the location of all the natural frequencies above the natural frequencies in relation to the range of the wave excitation frequencies.

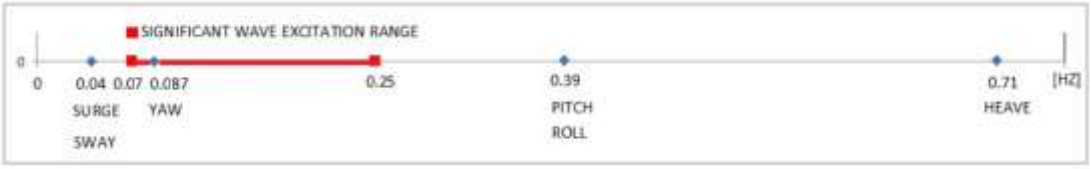

Figure 7.3 Location of natural frequencies

7.4 Wind models

Two wind models were considered for the numerical study: Turbulent wind, using the same data generated in TurbSim for the SIL system used in the experiments and also constant wind data using values (e.g. hub height) corresponding to the turbulent cases.

Table 7.2 shows the environmental conditions for the proposed FOWT. The table shows the relationship between sea state and the mean wind speed at the hub height of the NREL 5MW turbine. The turbine has a cut-in speed of 3m/s, a rated speed of 11.4m/s and cut-out speed 25m/s. One severe condition which has 38.76m/s wind speed was also tested corresponding to 100 year event in the North Sea. Turbulence intensity selected from 13.37% to 29.69% percent according to wind speed. The constant wind cases used the mean wind speed values in Table 7.2.

Table 7.2 Environmental Conditions

Sea State	H_s (m)	T_p (s)	Gamma	Mean Wind Speed(m/s)	Turbulence intensity (%)
N1	55	9.00	2.45	11.40	20.45
N2	1.50	6.61	1.00	11.40	20.45
N3	8.46	10.13	5.00	38.76*	13.37
N4	0.75	5.44	1.00	6.05	29.69
N5	1.25	6.36	1.00	9.18	22.98
N6	1.75	6.86	1.00	12.80	19.31

N7	2.75	7.80	1.41	16.80	17.09
N8	6.00	10.28	2.52	25.00	14.76

* above rated wind condition

As described in Chapter 3 the IEC Kaimal power spectral density function was selected to generate the three orthogonal turbulence components typical of those found in deployment area (North Sea). The spectra for the three wind components are found from:

$$S_k(f) = \frac{4\sigma_K^2 L_K/\overline{u}_{hub}}{(1+6fL_K/\overline{u}_{hub})^{5/3}} \tag{7.7}$$

Where $k= u, v, w$ (the three orthogonal wind components)

The most conservative turbulence model was selected corresponding to turbulence category "A" according to IEC 61400-3 (IEC, 2009). Figure 7.4 shows the time history of the *u* component of the wind speed (normal to the turbine) for the storm condition. Figure 7.5 shows the spectrum obtained from this time history and the theoretical Kaimal spectrum obtained from Equation (7.7).

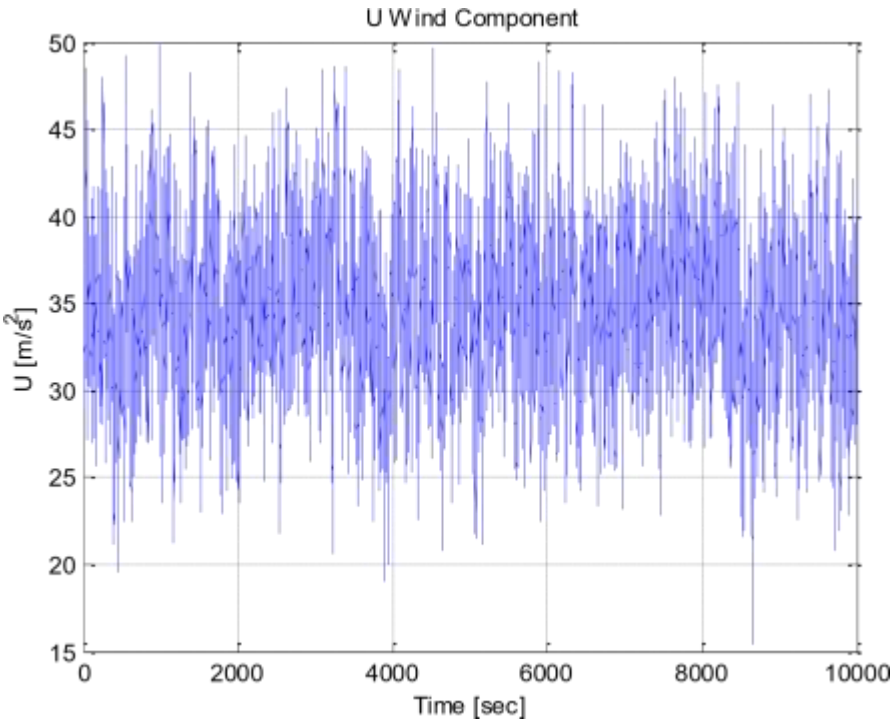

Figure 7.4 Storm condition - u component time history

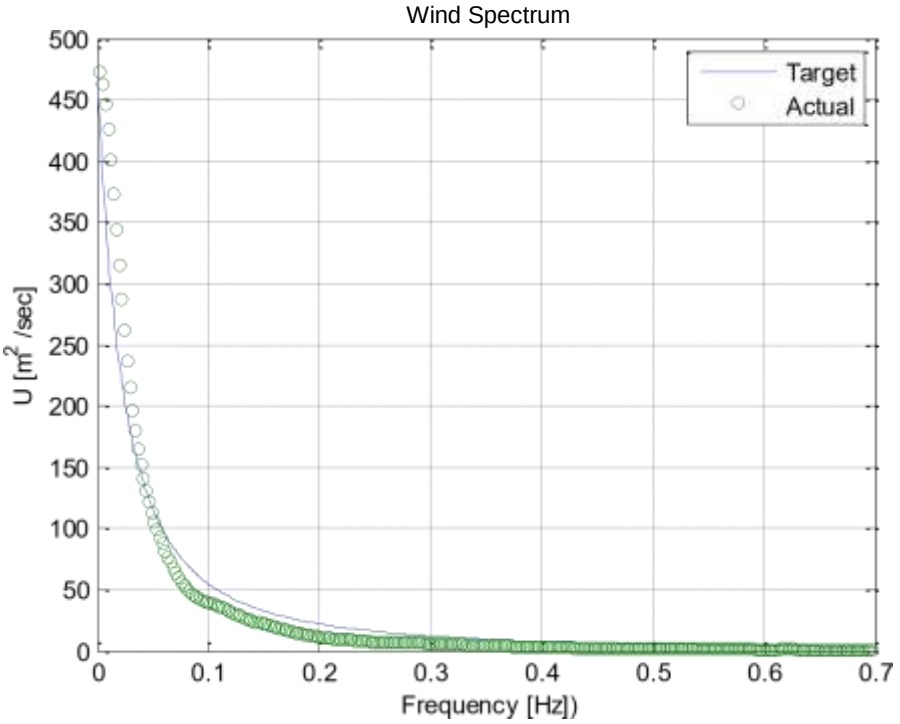

Figure 7.5 Storm condition - u component spectrum and theoretical Kaimal spectrum

7.5 Test Matrix

A comprehensive set of tests were performed at the Kelvin Hydrodynamic Laboratory in order to characterise the behaviour of the FOWT in a range of wave and wind conditions including extreme conditions. Numerical tests, which mirrored the experiments, were also conducted using FAST in order to allow for correlation between the experimental and numerical results. Froude scaling, previously described in Section 4.2, was used to select the conditions for the experiments and also used to convert the experiment results to full scale. All of the results from the experiments and the numerical study are presented at full scale. Seven configurations were used in the experimental study which are summarised in Table 7.3. Configurations 1, 3 and 4 were used in the comparison study between the numerical prediction and the experiment results.

Table 7.3 Overview of test matrix in irregular waves

Configuration	Wave/Wind heading(deg)	Experiment	Numerical	
		Turbulent	Turbulent	Constant
1	0/0	+	+	+
2	0/45	+		

3	0/225	+	+	+
4	45/0	+	+	+
5	45/45	+		
6	45/-45	+		
7	45/225	+		

Details of all of tests carried out in irregular waves are given in Table 7.4.

Table 7.4 Test matrix in irregular waves

Configuration	Test ID	Wave/Wind heading	Sea State	H_s [m]	T_p[s]	Wind Speed [m/s]
	D2004	0/0	N5	1.25	6.36	9.18
	D2002	0/0	N2	1.50	6.61	11.40
	D2005	0/0	N6	1.75	6.86	12.80
	D2006	0/0	N7	2.75	7.80	16.80
	D2027	0/0	N3	8.46	10.13	38.76
2	D2011	0/45	N4	0.75	5.44	6.05
	D2012	0/45	N5	1.25	6.36	9.18
	D2010	0/45	N2	1.50	6.61	11.40
	D2013	0/45	N6	1.75	6.86	12.80
	D2014	0/45	N7	2.75	7.80	16.80
3	D2021	0/225	N4	0.75	5.44	6.05
	D2022	0/225	N5	1.25	6.36	9.18
	D2018	0/225	N2	1.50	6.61	11.40
	D2023	0/225	N6	1.75	6.86	12.80
	D2016	0/225	N1	4.55	9.00	11.40
	D2024	0/225	N8	6.00	10.28	25.00
	D2020	0/225	N3	8.46	10.13	38.76
4	D4015	45/0	N4	0.75	5.44	6.05
	D4016	45/0	N5	1.25	6.36	9.18
	D4012	45/0	N2	1.50	6.61	11.40
	D4017	45/0	N6	1.75	6.86	12.80
	D4018	45/0	N7	2.75	7.80	16.80
	D4010	45/0	N1	4.55	9.00	11.40

	D4014	45/0	N3	8.46	10.13	38.76
5	D4019	45/45	N4	0.75	5.44	6.05
	D4020	45/45	N5	1.25	6.36	9.18
	D4021	45/45	N6	1.75	6.86	12.80
6	D4005	45/-45	N5	1.25	6.36	9.18
	D4002	45/-45	N2	1.50	6.61	11.40
	D4006	45/-45	N6	1.75	6.86	12.80
	D4007	45/-45	N7	2.75	7.80	16.80
	D4008	45/-45	N8	6.00	10.28	25.00
	D4004	45/-45	N3	8.46	10.13	38.76
7	D4024	45/225	N4	0.75	5.44	6.05
	D4025	45/225	N5	1.25	6.36	9.18
	D4026	45/225	N6	1.75	6.86	12.80
	D4027	45/225	N8	6.00	10.28	25.00
	D4028	45/225	N8	6.00	10.28	11.40
	D4023	45/225	N3	8.46	10.13	38.76

7.6 Test procedure

A series of irregular wave tests in simulated turbulent wind conditions were conducted in order to characterise the platform response in a realistic environment.

All sea states and wind conditions were generated for a period of just less than three hours at full scale. Variation in wave direction was achieved by rotating the model complete with moorings in the test tank as described in section 4.7.1 and variations in wind direction were supplied by rotating the fan on top of the tower.

Data acquisition arrangements as well as the daily checks on the equipment and measurement systems were the same as described in Chapter 4. In total, 53 irregular cases were tested.

Figure 7.6 shows the model in the tank at wave heading and wind direction of 0°/0° during one of the extreme environment tests.

Figure 7.6 Example of irregular test

7.7 Data Processing of Experimental Results

In this section data processing applied to the recorded experimental data is presented. The data processing scheme used for numerical analysis is presented in section 7.9. Data processing for these tests proved extremely challenging. The high sample rate (640Hz), coupled with the large number of channels (24) and the long runs (30 minutes) meant that files were extremely large, and difficult to process. Each file of raw data contained over 25 million data points.

7.7.1 Filtering and Sub-sampling

There were several distinct sources of noise on the data the most troublesome being caused by the fan which generated high-frequency mechanical vibrations and EM noise in the range of 100-200 Hz.

7.7.2 Data Processing

The raw data from the tank is sampled at 640Hz per channel in order to prevent potential aliasing due to the high frequency noise generated by the fan.

The data from the tank is processed in three stages by two custom written MATLAB programs.

7.7.3 Stage 1 Pre-processing & Re-sampling

For all of the runs the 640 Hz raw data is filtered (8 pole anti-alias) then each channel is sub-sampled to give a new sampling frequency of 20Hz per channel. The

antialiasing filter ensures that high frequency noise greater than the Nyquist frequency of 10Hz is removed from the data set before the sub-sampling procedure is carried out. This subsampled data is used for subsequent processing by stage 2.

7.7.4 Stage 2 Filtering

The 20Hz wave, motion and tendon data are processed by a fourth order low pass filter with a cut-off frequency of 5Hz (0.84Hz full scale). This filter removes noise at frequencies greater than the highest wave excitation frequency and highest natural frequency of the system which is the heave natural frequency of 4.31Hz determined from the free oscillation tests (Section 5.4.2).

A great deal of attention was required in order to remove the noise components without causing degradation of the signals. All of the filters employed have a linear phase characteristic with minimum pass-band ripple.

7.7.5 Stage 2 Data selection & Offset values

1. The mean value of the offset values for all channels (measured before the wave maker has started) are measured and recorded.
2. The start and end points of the measurement region are selected manually by inspection of the inline wave and thrust signals to ensure that the waves are established at the model and that the Software in the loop system is operating for over the entire measurement region.
3. The mean values of the offsets obtained in the first step are removed from the measurement region for each of the channels.
4. The static tension values are added to the dynamic tendon signals to give total tension and all of the data is converted to full scale values.
5. Total tensions are normalised as the ratio of total tension to static tension.

$$nondimensional\ tension = \frac{total\ tension}{static\ tension}$$

Results were computed in terms of mean values, standard deviation values, spectral responses and probability density functions of the waves, the motions and tendon tensions.

7.8 Example results.

As an example, one complete set of processed results is shown for the most severe operational condition (H_s=8.46m, T_p=10.13s, wind speed=38.76m/s) with wind and wave co-linear to the model.

Detailed wave analysis is given in section 7.8.1. Section 7.8.2 and 7.8.3 present results of the motion analysis in the time and frequency domains. Then, tendon tension analysis in both the time and frequency domains is presented.

7.8.1 Wave analysis of storm condition

Figure 7.7 shows the time histories of the waves recorded during the model tests inline with the model and at the tank probe location 10m from the wavemaker.

Figure 7.8 shows the Probability Density Functions (pdf's) of wave heights obtained during the wave calibration, and those during the model test.

Figure 7.8 shows that, as expected, (section 7.2), the distribution of wave heights follows a Rayleigh distribution and that the most probable wave height is around 4m. The first plot in Figure 7.8 shows the calibration wave pdf without model in the tank. The second and the third plot show the tank wave and inline wave measured during the experiments. All of the plots show similar trends which indicate that the waves have the correct statistical properties. The similarity of results from the calibration (no model in test tank) and the tests with the model in the test tank demonstrates that the model absorbs only a small amount of energy from the waves which illustrates one of the main features, in terms of reduced motions, of the TLP structure.

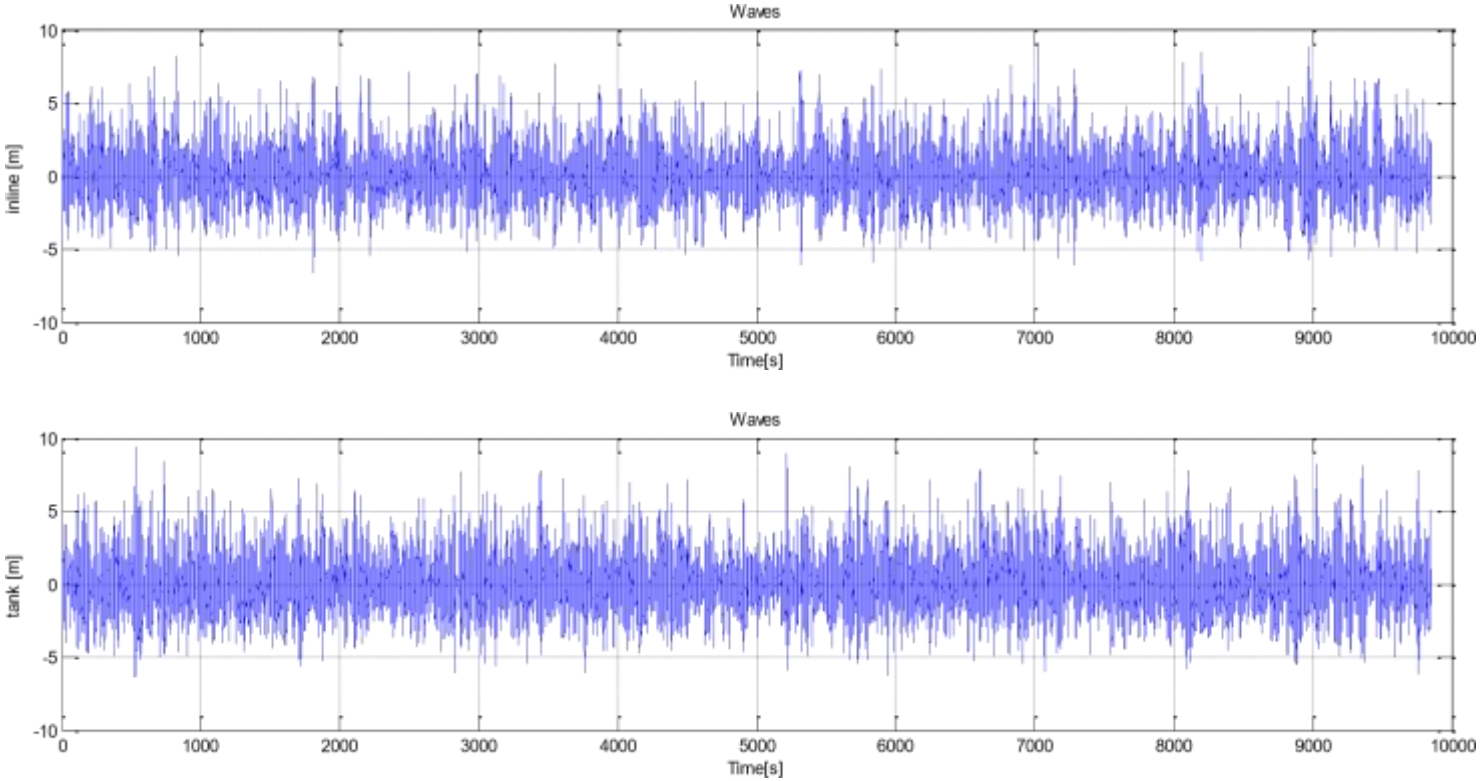

Figure 7.7 Time histories of wave heights : inline and tank probe

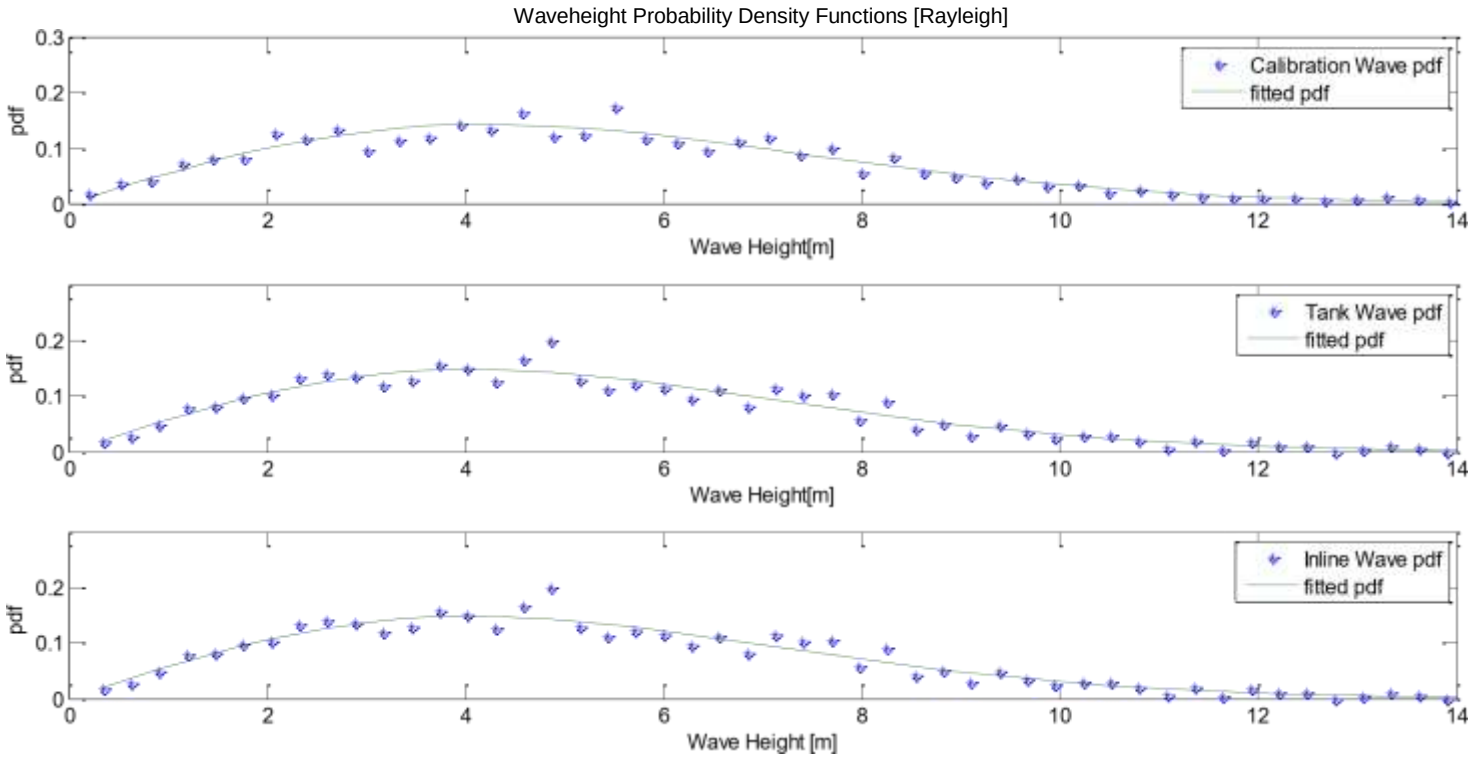

Figure 7.8 Probability density functions of wave height : calibration, tank and inline wave

Figure 7.9 shows the calculated wave spectrum from the wave calibration, and the corresponding values from the in line probe and the tank probe (as described in Chapter 4) during the model test.

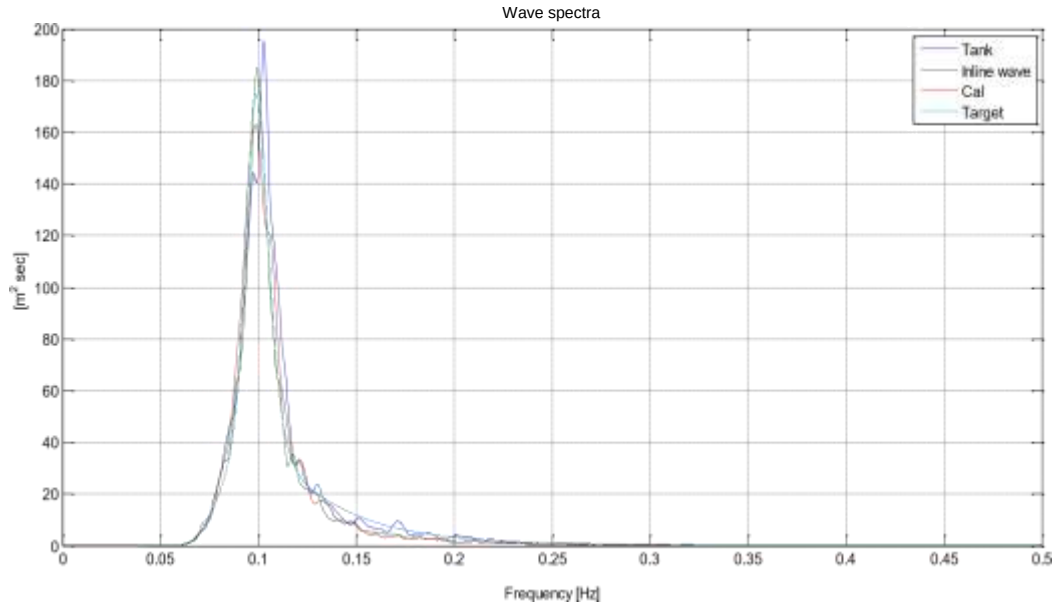

Figure 7.9 Wave spectra : Tank Probe, Inline Probe, Calibration and Target

Analysis was carried out in order to determine the statistical characteristics of the waves. Table 7.5 shows the results for the wave record during the tank calibration process and also the results for the inline and tank records measured during the tests with the FOWT. The calibration wave was measured at the location of the model but without model in tank.

Table 7.5 Wave analysis results for storm case in 0/0 heading

Parameter	Unit	Target	Calibration	Inline	Tank
$H_{(1/3)}$	m	8.46	8.420	8.191	8.598
H_s(elevation)	m	8.46	8.342	8.117	8.678
H_s(spectrum)	m	8.46	8.444	8.330	8.546
T_p	sec	10.13	10.004	9.748	10.236

It can be seen from the results in Table 7.5 that the wave measured during the tank calibration process shows good agreement to the target in terms of H_s and T_p. Figure 7.9 also shows that the shape of the spectrum obtained during the calibration process closely matches the theoretical JONSWAP spectrum. The inline probe as expected is effected by its proximity to the model whereas the tank probe shows closer agreement

with the results obtained during the wave calibration. The values of T_p for each case are approximate due to its sensitivity to the spectral estimator. Results for the other seven sea states showed similar trends (Appendix A).

7.8.2 Motion analysis of storm condition

Figure 7.10 shows the time histories of the 6-DOF motions of the floater and the corresponding pdf's are presented in Figure 7.11. A summary of the mean and standard deviation of the motions is presented in Table 7.6. The mean values and standard deviation of the surge motions are significantly higher than the other degrees of freedom as expected for this head seas case with co-linear wind direction. The FOWT drifts downwind and reaches equilibrium approximately 0.64 m from its still water value. Pitch motion is significantly larger than roll which again is to be expected for this configuration. Roll, sway and yaw mean and standard deviation values are very small. In summary, all of the TLP motions are small even for this extreme environmental test.

Table 7.6 Statistical parameters of motions in storm condition (0/0 heading)

Parameter	Roll	Pitch	Yaw	Heave	Sway	Surge
Mean	-0.0049	-0.0399	0.0309	-0.0343	-0.0081	0.6396
Standard deviation	0.0081	0.0496	0.0985	0.0492	0.0567	1.2626

Figure 7.11 shows the pdfs of the FOWT motions. All of the pdfs apart from heave show good agreement with a standard Gaussian distribution. The variation in heave is much less than would be expected in a purely Gaussian process. Heave motion is coupled with surge via the tendons. Thus it is the combination of two dependent Gaussian processes which generally give more of a Rayleigh type distribution. Surge is a function of wave elevation which is Gaussian. The nature of the pdfs obtained show close agreement to the results in Table 7.6.

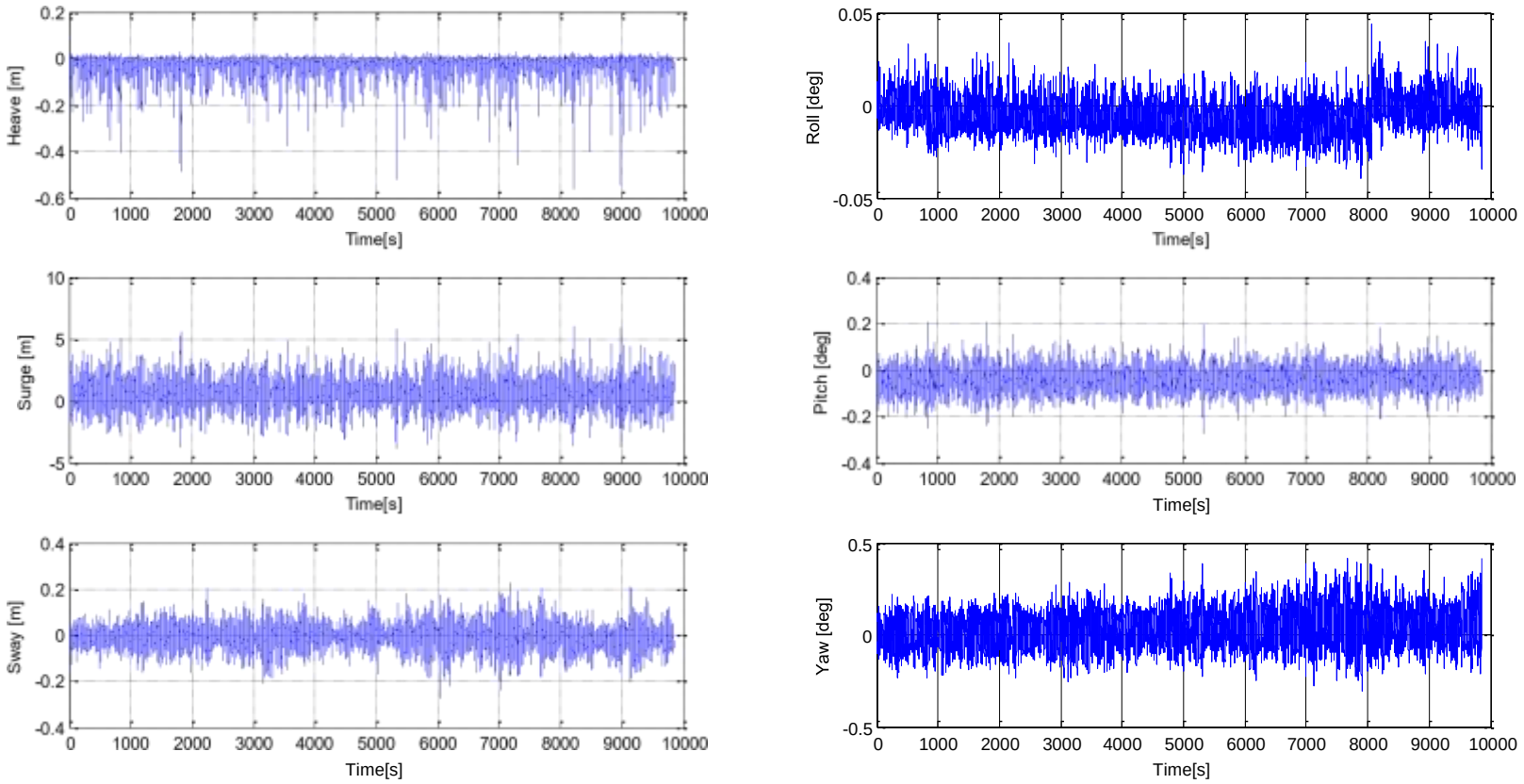

Figure 7.10 Time histories of 6 DOF motions

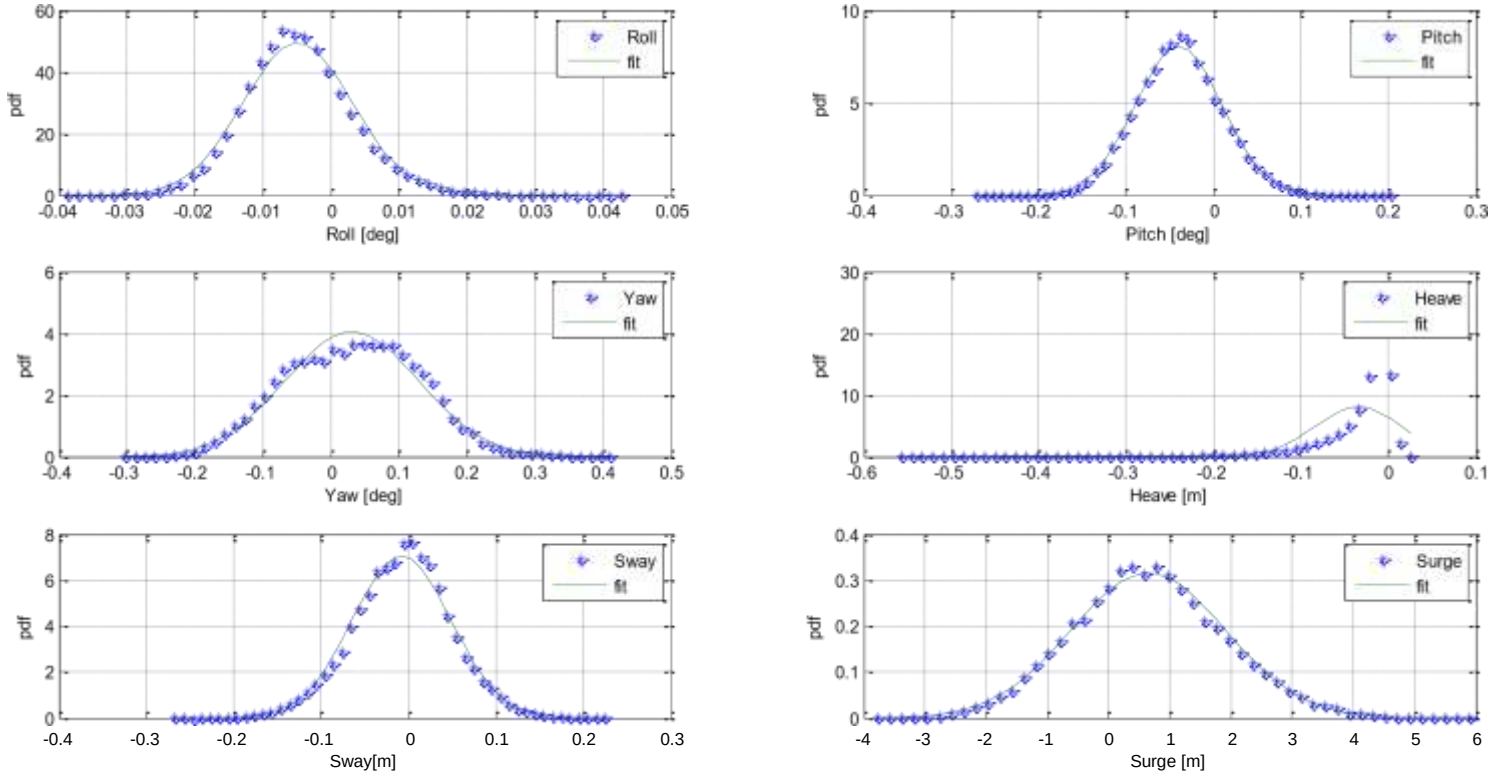

Figure 7.11 PDFs of 6 DOF motions

7.8.3 Spectral analysis of motions for storm condition

Figure 7.12 shows the motion response spectra obtained by performing a spectral analysis of the motion time histories obtained from the experiments.

The heave response spectrum shows two major peaks at approximately 0.09 and 0.19 Hz coinciding with the peak frequency of the wave spectrum and double the peak frequency. This phenomenon, caused by the interaction between the heave motion and the tendons, was also observed during the regular wave tests (see Figure 6.1).

The surge response spectrum shows two major peaks at approximately 0.09 and 0.04 Hz coinciding with the peak frequency of the wave spectrum and the surge natural frequency respectively.

The sway response spectrum like surge shows two major peaks at approximately 0.09 and 0.04 Hz but is significantly smaller. The reason behind the small sway motion observed may be due to asymmetry between the tendons, model alignment, wave alignment or possible tank side wall effects.

The roll response spectrum shows three major peaks at approximately 0.09, 0.19 and 0.42 Hz coinciding with the peak frequency of the wave spectrum, a component at double the peak frequency due to coupling between the heave motion and the tendons which is very close to the roll natural frequency.

The pitch response spectrum shows two major peaks at approximately 0.09, 0.44 Hz coinciding with the peak frequency of the wave spectrum and a component very close to the pitch natural frequency.

The yaw response spectrum shows two major peaks at approximately 0.087, 0.04 Hz coinciding with the peak frequency of the wave/yaw natural frequency and at the surge natural frequency.

Magnitudes of the motion spectra closely match the standard deviation results presented in Table 7.6.

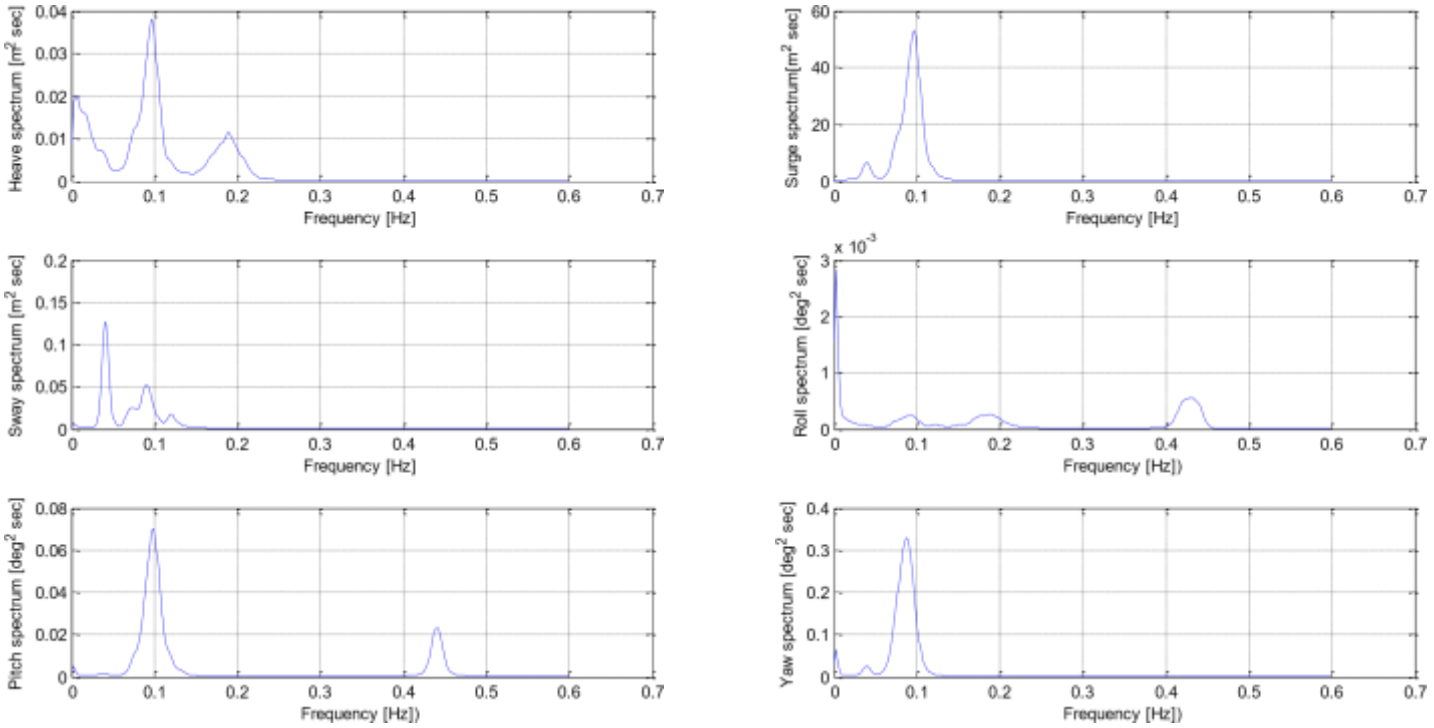

Figure 7.12 Spectral response of motions

7.8.4 Tendon tension analysis of storm condition

Non-dimensional tendon tension (section 7.7.5) values are presented in pairs in Figure 7.14. Table 7.7 shows the mean and standard deviations for each of the tendons. Tendon pairs 1 and 2 show very similar results as do tendon 5 and 6. Upstream tendons 1 and 2 show the largest mean values, downstream tendons 5 and 6 have the smallest mean values. This is probably due to the effect of trim and illustrated in Figure 7.13.

Side tendons 3 and 4 give similar trends to 7 and 8 in both mean values and standard deviations.

Table 7.7 Statistics of tendon tensions for storm case (0/0 heading) [-]

Parameter	T1	T2	T3	T4	T5	T6	T7	T8
Mean	1.15	1.15	1.03	0.98	0.85	0.86	0.98	1.02
Standard deviation	0.17	0.16	0.08	0.10	0.21	0.19	0.09	0.08

The tendon tension pdf's are shown in Figure 7.15 and all follow a Gaussian distribution. Once again tendon pair 1 and 2 gives very similar results to pair 5 and 6. The side tensions 3 and 8 are very similar to each other as are tendon pairs 4 and 7. It is likely that the variation in the pdfs of the side tensions is also due to the effect of trim. Mean tensions in tendon 3 and tendon 8 increases meanwhile the tensions in tendon 4 and tendon 7 reduce as illustrated in Figure 7.13.

During the storm condition test none of the tendons go slack as shown in Figure 7.14 and Figure 7.15. Tendon 6 experiences the lowest non-dimensional tension of approximately 0.2 i.e. 0.2 times the static tension value. The probability of this occurring is low as illustrated in the pdf's presented in Figure 7.15. The maximum non-dimensional tension is approximately 1.8 times the static tension and this peak tension is experienced by the fore aft tendons. This low probability of this level of tension is also illustrated in the pdf's as shown in Figure 7.15.

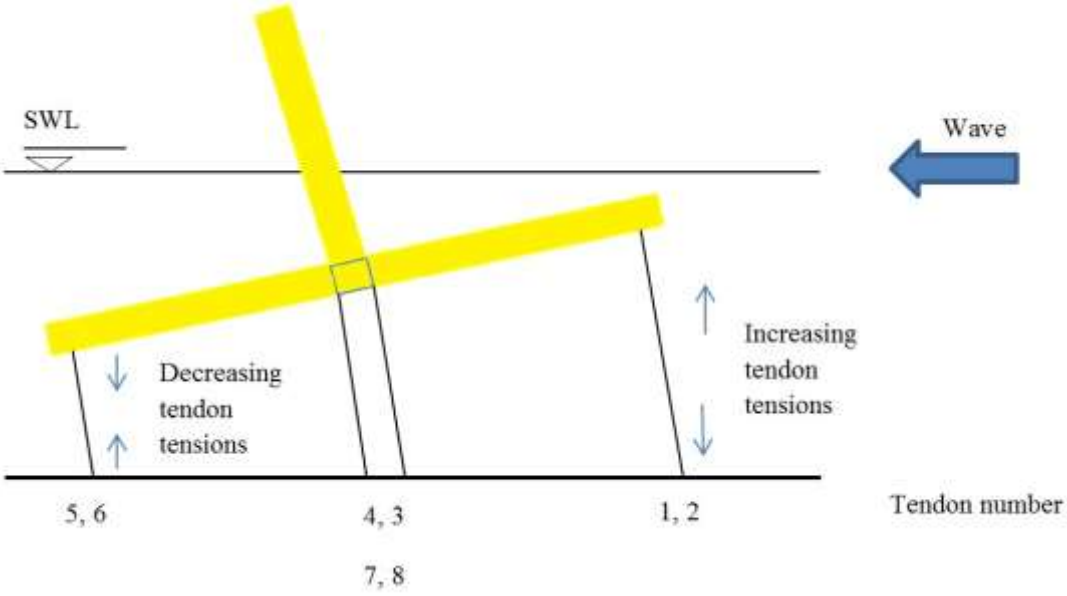

Figure 7.13 Effect of trim on tendon tension values.

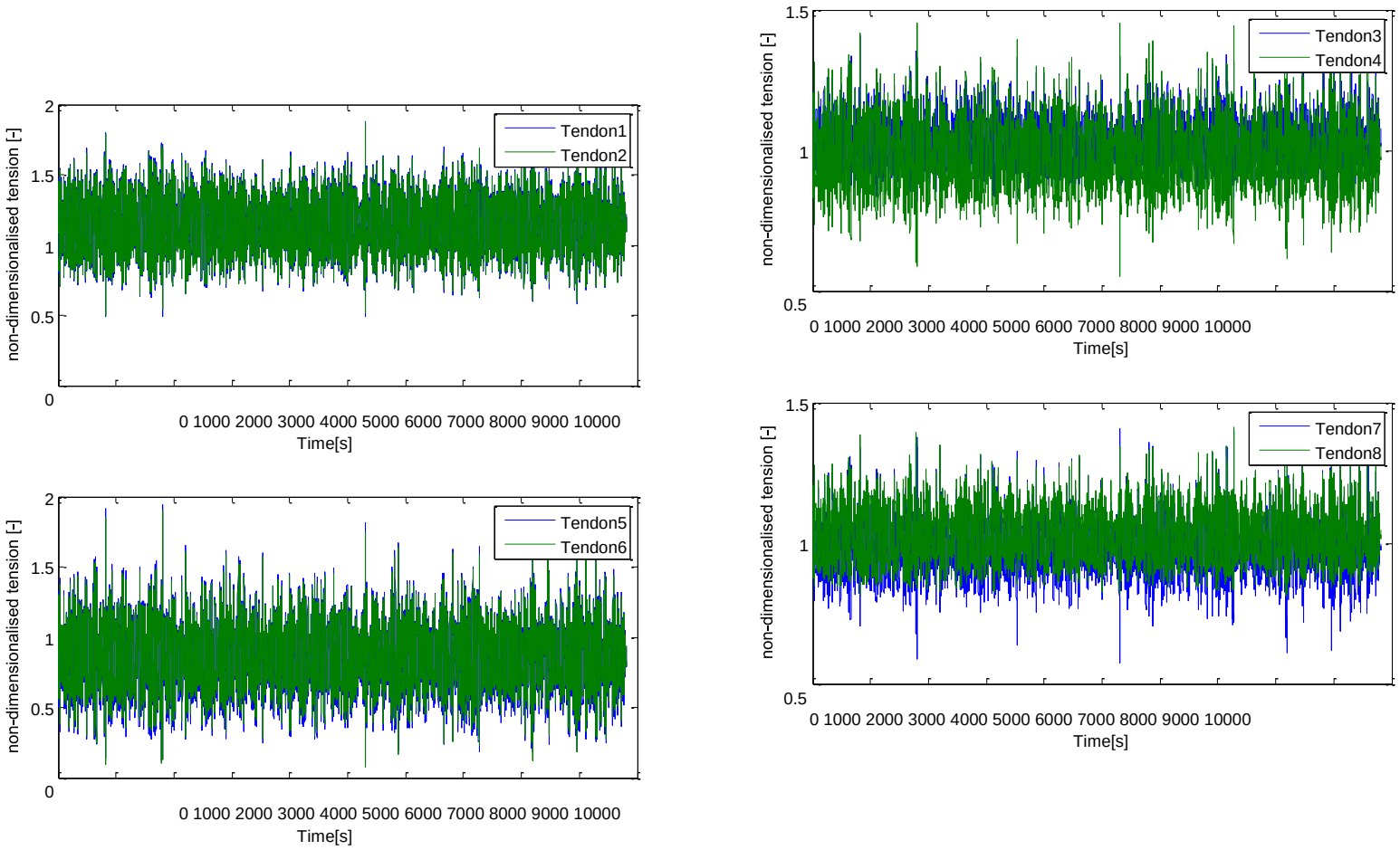

Figure 7.14 Time histories of tendon tensions

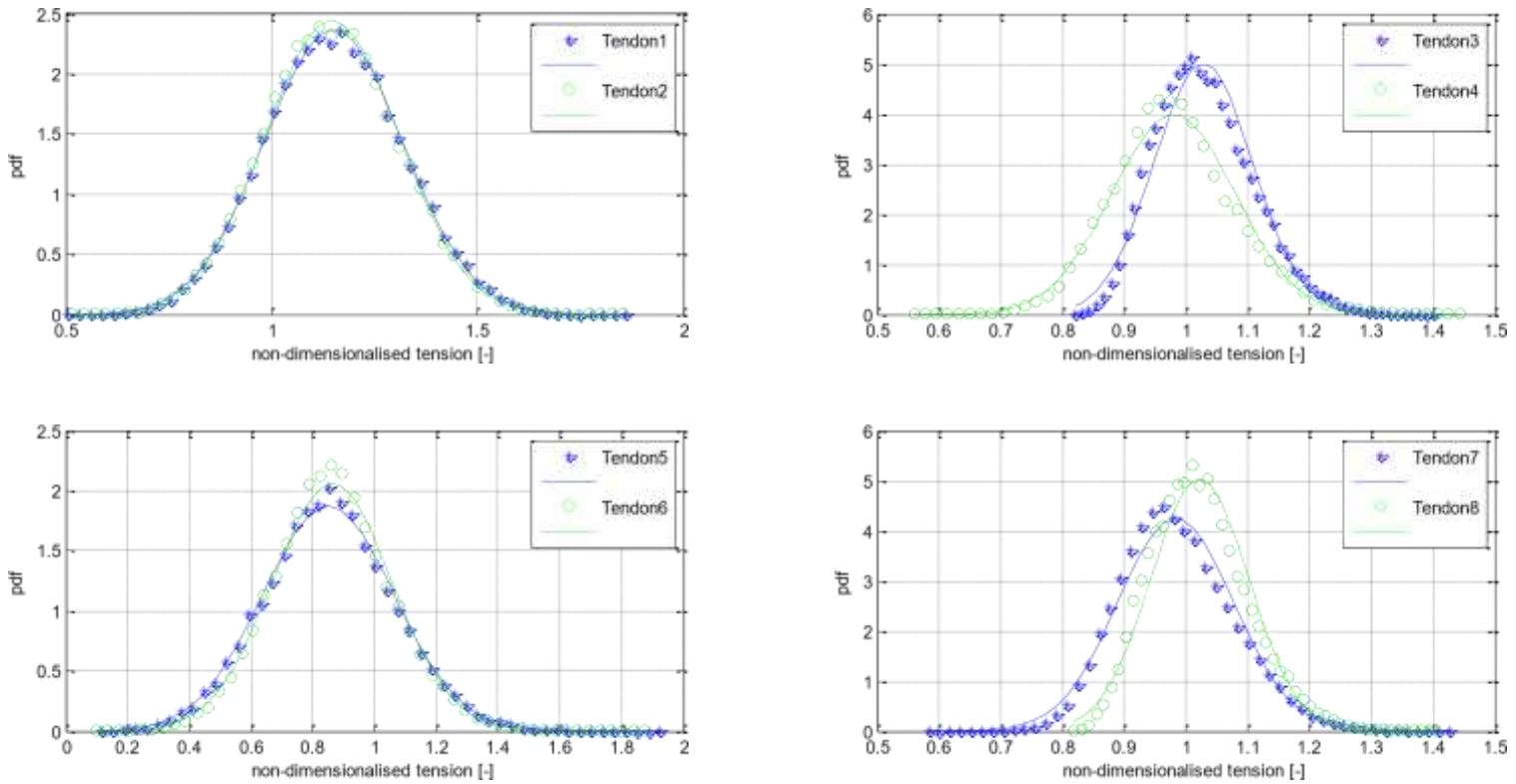

Figure 7.15 PDFs of tendon tensions

7.8.5 Spectral analysis of tendon tensions for storm condition

The non-dimensional tension response spectra for tendon pairs T1 and T2 and tendon pairs T5 and T6 each show two major peaks at approximately 0.09, 0.44 Hz coinciding with the peak frequency of the wave spectrum and a component very close to the pitch natural frequency. This is likely due to the relatively strong coupling between pitch and the forward and rear tendons.

The response spectra for tendon pairs T3 and T4 and tendon pairs T7 and T8 each have a major peak at the peak frequency of the wave spectrum. There is also a small component very close to the pitch natural frequency due to the relatively weak coupling between pitch and the side tendons.

All of the side tendons show a small response at around 0.19 Hz which is the double the wave peak frequency caused by the interaction between the heave motion and the tendons.

For all of the tendons the largest tensions coincide with the peak of the wave spectrum.

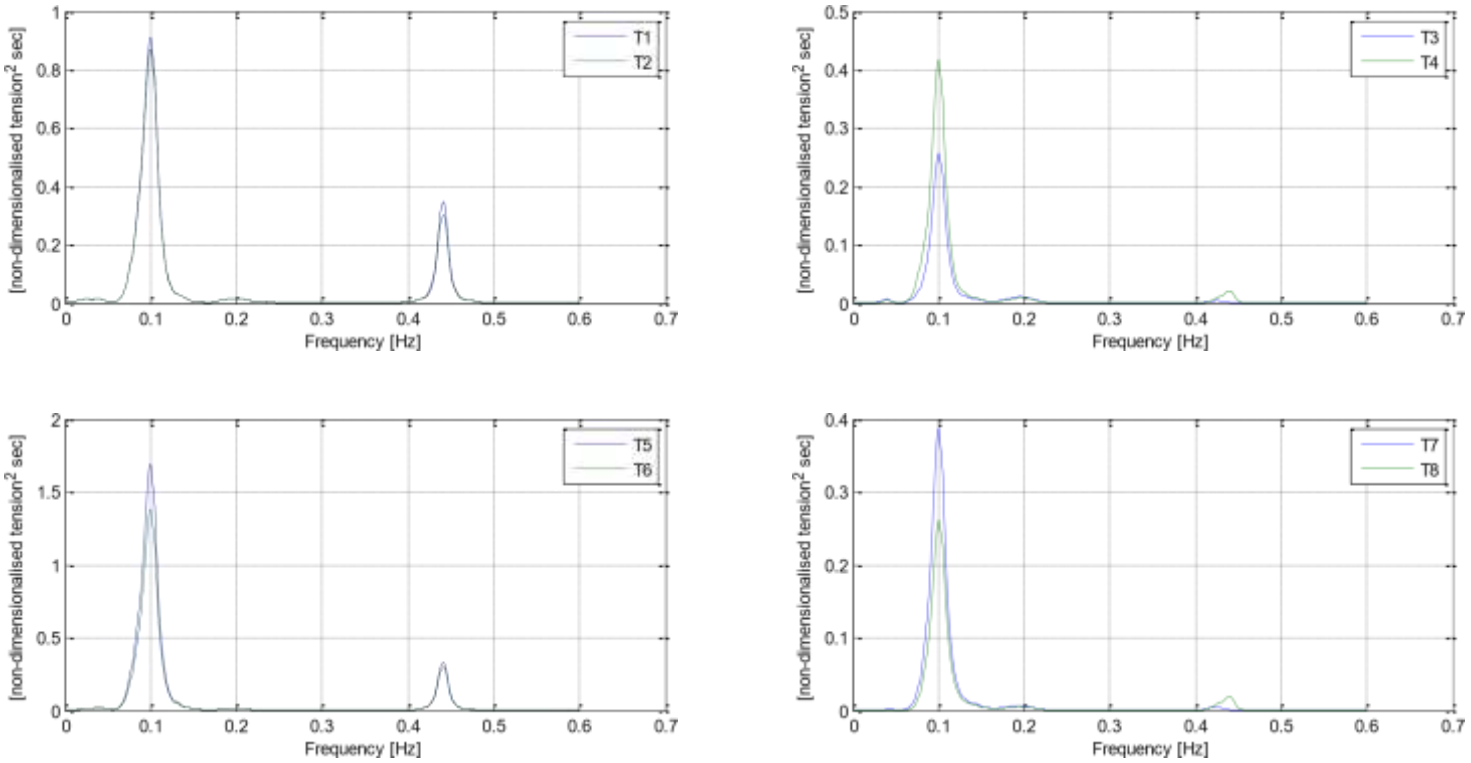

Figure 7.16 Spectral response of non-dimensional tendon tensions

7.9 Data Processing for Numerical Results

In this section data processing applied to the numerical results are presented. Initial examination of the raw data from FAST gave poor correlation with the experiment results so a spectral analysis was carried out in order to investigate the nature of the FAST outputs and the possible reasons for the poor correlation. The unprocessed motion spectra and tendon tension spectra for the storm condition are shown in Figure 7.17 and Figure 7.18. The results show large spikes appearing on the roll and pitch spectra at just over 0.5 Hz as well as a smaller response on the heave spectrum at just below 1 Hz. Further consideration of the tendon tension spectra also showed extremely large spikes occurring at these frequencies. The frequency domain investigation of other tests showed similar trends. The experimental and numerical results were processed in a similar way.

These frequencies do not coincide with the excitation or the experimental natural frequencies of the system (see Figure 7.3) and it should be noted that spikes are not observed in the experimental results, either at this frequency or at the natural frequency of the physical model in heave (which was slightly different as discussed previously). However the spike at 1Hz frequency is close to the numerical estimation of the heave natural frequency. One possible hypothesis is therefore that the platform is responding in an unrealistic manner at the natural frequency in heave due to the underestimation of damping.

In order to understand better the reason behind this a number of investigative runs carried out. A number of runs were performed with increased water depth and tendon length (up to 120m) thus changing the natural frequencies of the platform; the spikes remained at the same frequency, suggesting that the spikes may not be related to the natural frequencies. Different time steps ranging from 0.001 to 0.5 seconds also had no significant impact on the results. Variations in tendon stiffness were also shown to have no impact on the frequency of the spikes. A number of runs were carried out changing the tower properties; in particular, a flexible tower was used to check whether these spikes coincided with the tower natural period. It was found that the natural period of the tower does not coincide with the frequencies at which spikes were observed.

Spectral analysis was also carried out for results gained in the present study for the platform examined by (Matha, 2009) and similar spikes were observed at the same frequencies although the heave natural frequency in this case was found to be 0.4375 Hz (see Chapter 3), quite far from the frequency of the spikes. This suggests further that these spikes may not be related to natural frequencies. It should be noted that in the original benchmark study no spectral analysis of tendon tensions was presented. In the end, no convincing physical reason could be found to explain these results; one possible explanation is perhaps numerical stability issue or numerical modelling error. Further study should be performed in order to determine the reasons behind these spikes in FAST.

It was therefore decided to process the FAST output in order to remove these artefacts. The numerical data was subsequently processed in the time domain by a flat, pass band, high order low pass filter with a very sharp cut-off frequency at 0.45Hz. The spectral analysis of the process output is shown in Figure 7.19 and Figure 7.20. The results show that the 0.5 and 1 Hz signals have been successfully removed from the motions and tendon tensions without affecting the remaining responses at the wave frequency and the system natural frequencies apart from heave. Further investigation of the processed spectra show the motion and tendon responses give peaks at the wave excitation frequency, double this frequency and at the surge natural frequencies in a similar manner observed from the spectra obtained from the experimental results of Figure 7.12 and Figure 7.16. Therefore for the subsequent analysis, all of the numerical data was processed in this way before the next stages of analysis were performed.

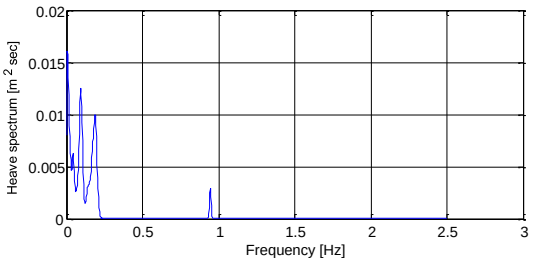

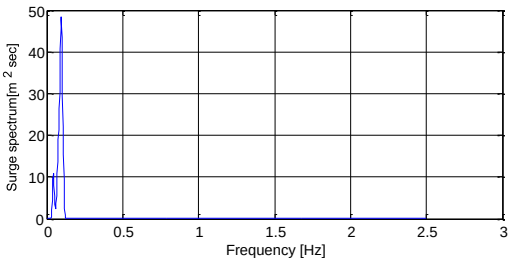

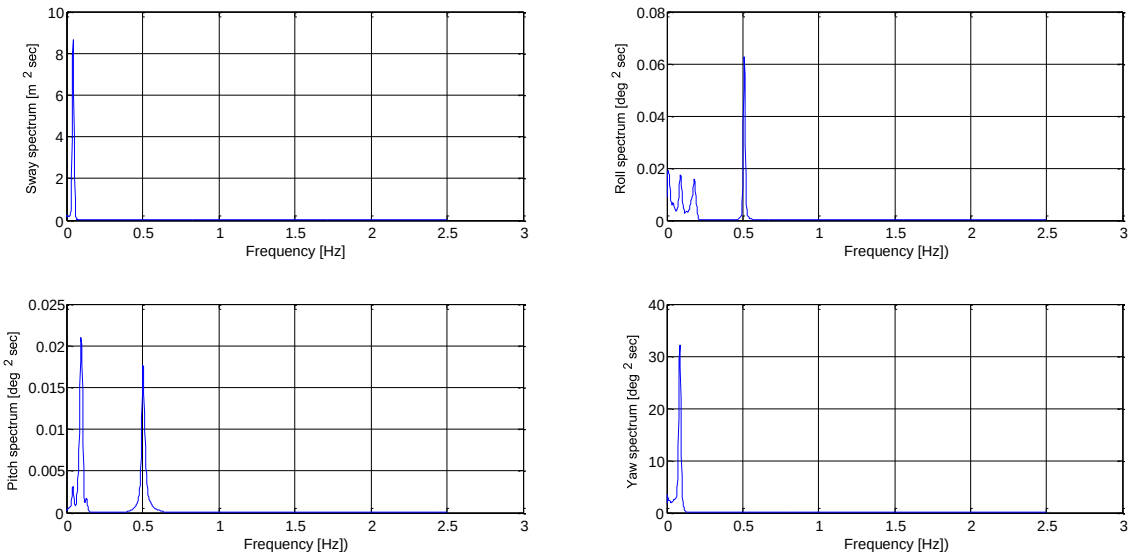

Figure 7.17 Storm condition - unprocessed motion spectra

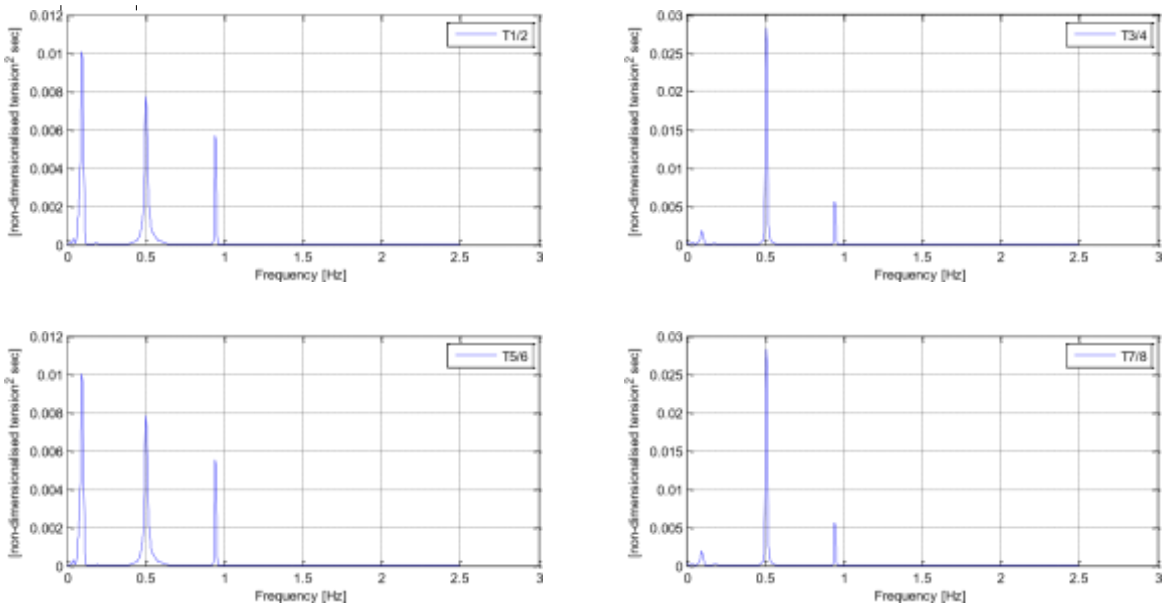

Figure 7.18 Storm condition - tendon tension spectra

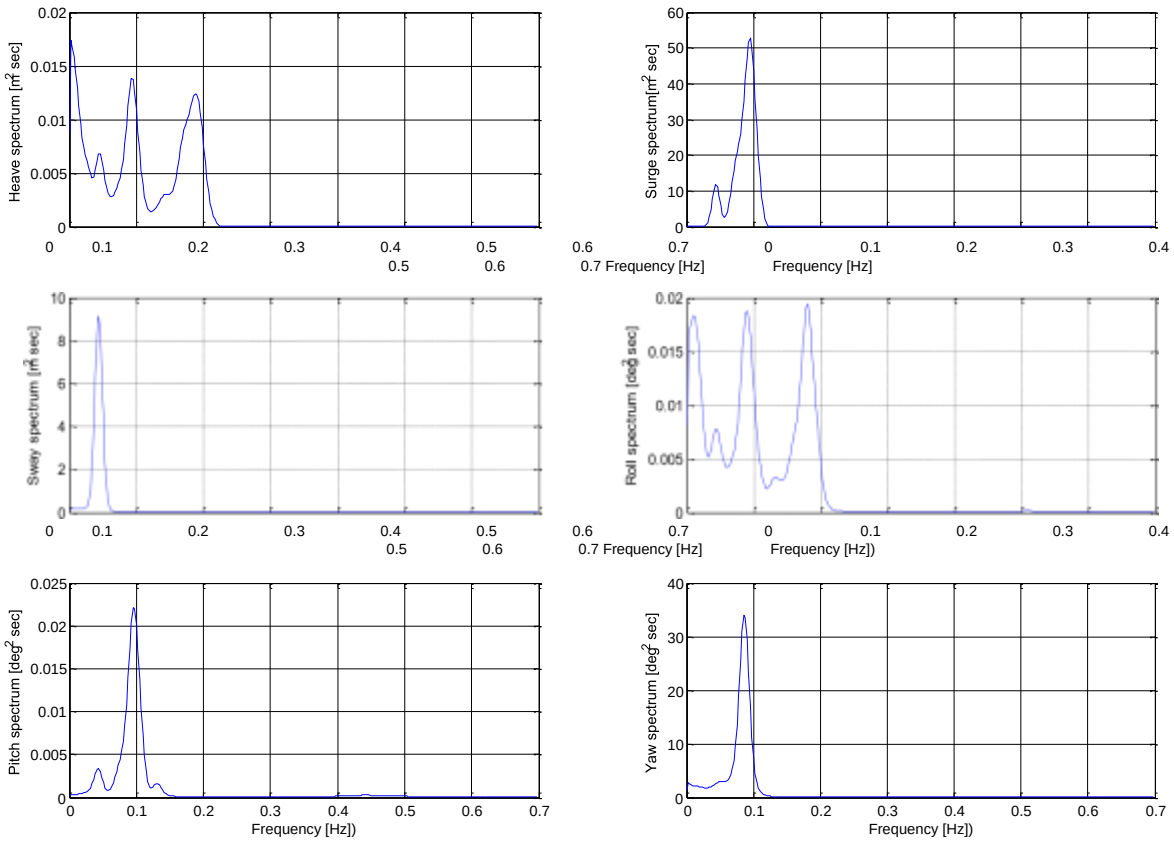

Figure 7.19 Storm condition - processed data

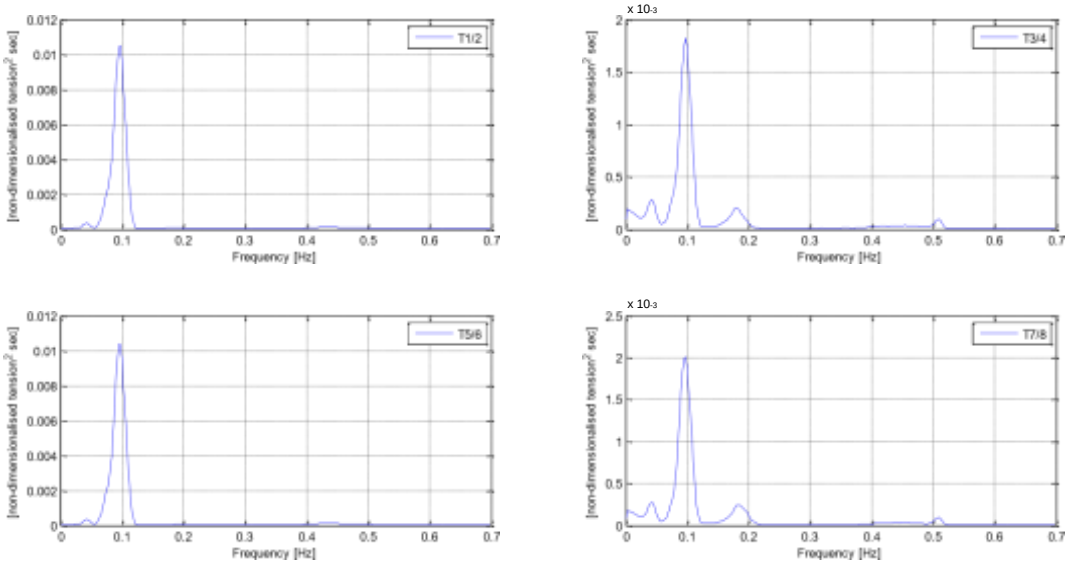

Figure 7.20 Storm condition - processed tendon tension spectra

For comparison, a selection of the storm case motion and tendon tension pdf's for the experimental and processed numerical predictions are given in the following figures.

It can be seen from the Figure 7.21 that the surge pdf's for the experiments and the processed numerical predictions give very good correlation. Heave results shown in Figure 7.22 show similar trends although the numerical predictions have an additional offset of approximately 0.1m (upwards). Calculation shows that this offset is close to the magnitude of the tendon extension due to mean load. Therefore, it is assumed that the heave results from FAST are based on the unloaded tendon length, whilst the tank results are calculated relative to the still water condition. For comparison purposes therefore, the mean tendon extension in still water should be subtracted from the FAST results. This is shown in Figure 7.23, and the agreement with the experimental results is then good.

Figure 7.24 shows the pdf of pitch motions showing good correlation with the numerical prediction with slightly higher values than those of the experiments in the region of the maximum pitch response. Pdf's of the front tension are given in Figure 7.25. The nature of the responses is similar although the numerical prediction substantially overestimates the mean value of tension. This will be discussed later in this chapter.

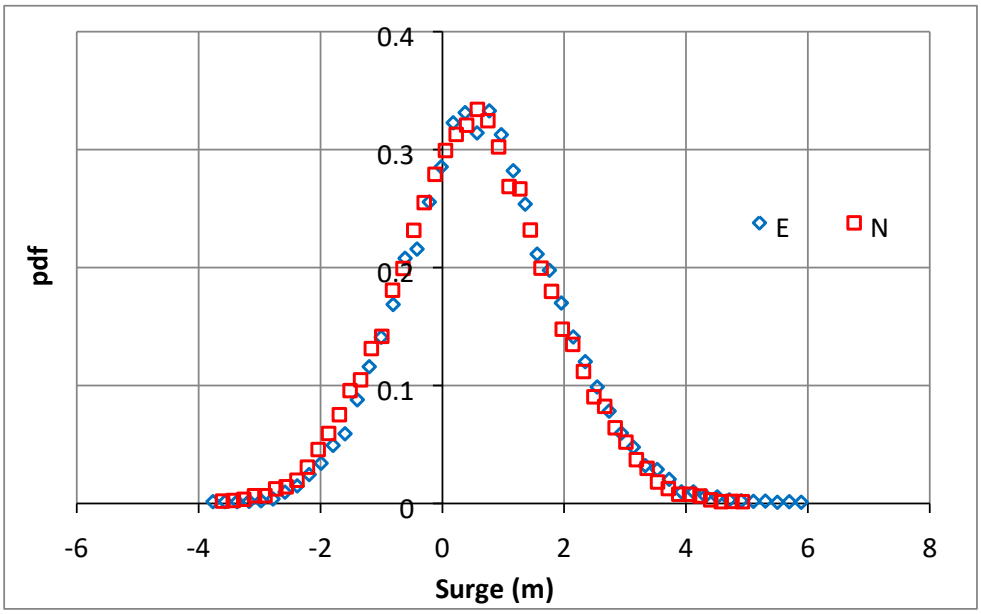

Figure 7.21 Correlation of surge motion pdf

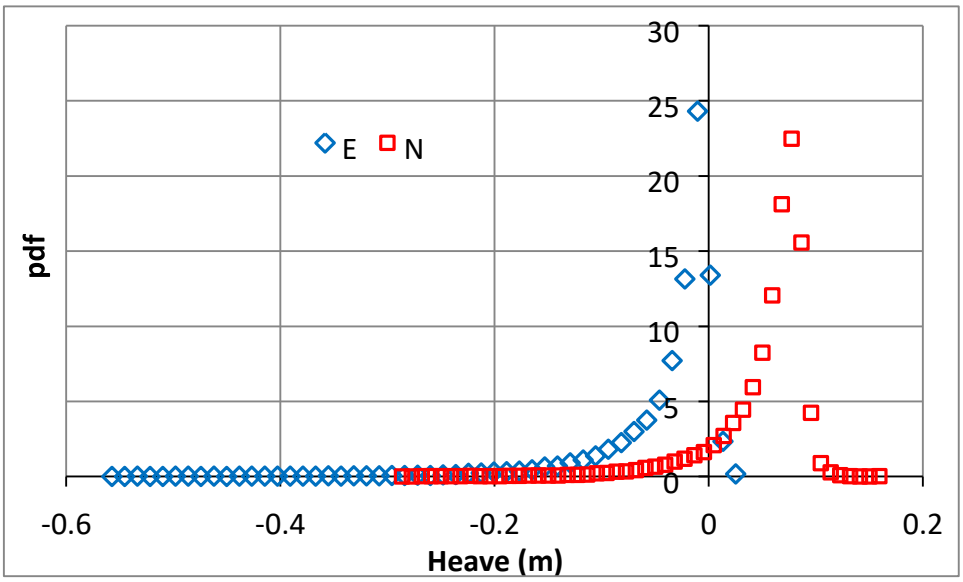

Figure 7.22 Preliminary Correlation of heave motion pdf

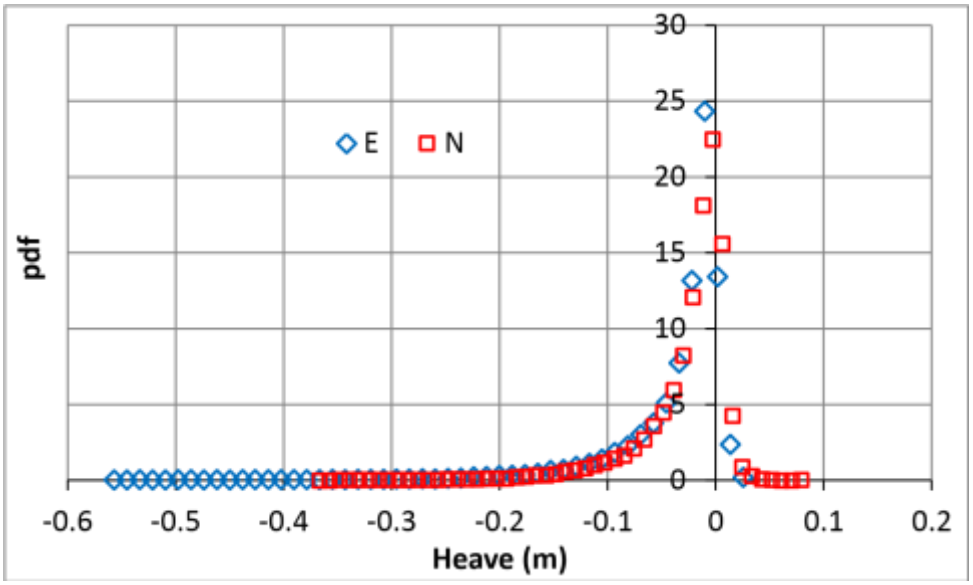

Figure 7.23 Correlation of heave motion pdf after correction for tendon extension

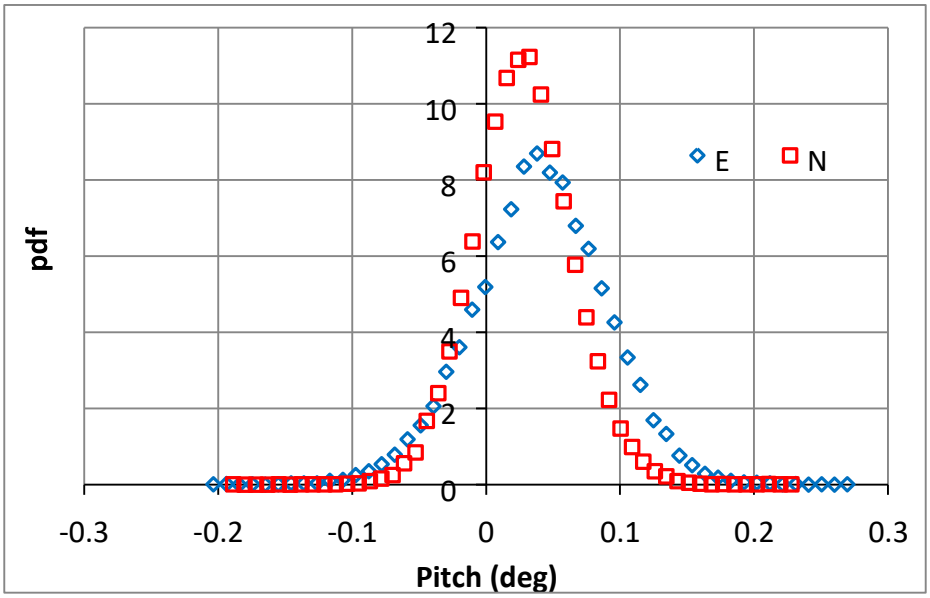

Figure 7.24 Correlation of pitch motion pdf

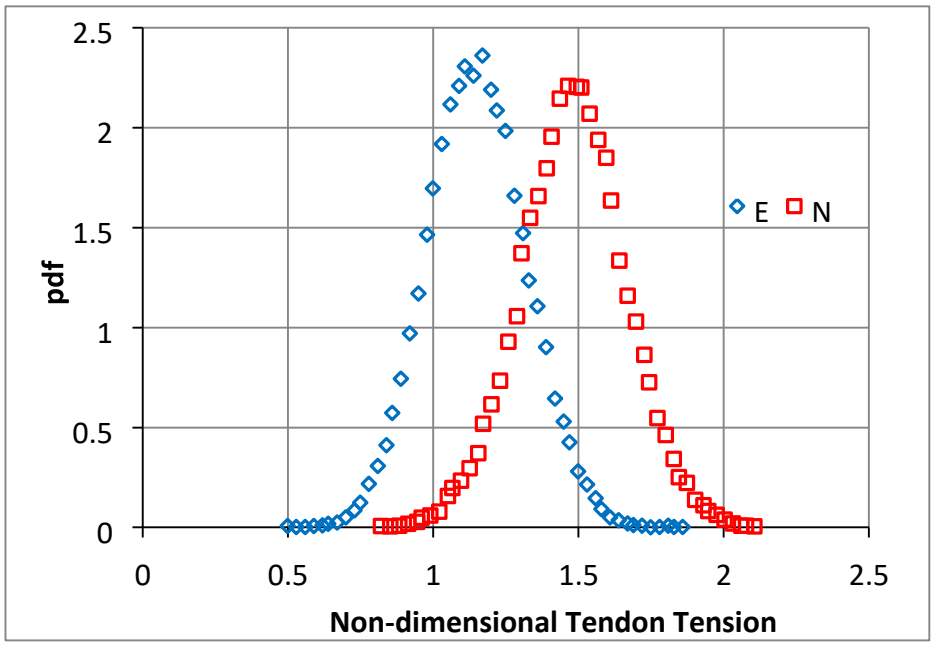

Figure 7.25 Correlation of tendon tension pdf

7.10 Experiment results and numerical correlations

In this section all of the results from the experimental campaign are presented. Comparisons between the results obtained from the experiments and the numerical study are presented for three configurations of the FOWT. The results for motions and tendon tensions are presented and the comparison between the experimental results and the numerical predictions using two wind models (turbulent, constant) are made.

In order to compare the motions and tension forces obtained from the experimental results with the numerical results, tests in irregular waves using turbulent wind model and constant wind model were also carried out using FAST code.

Some of the parameters were set up before running the simulations. *WaveMod* (Incident wave kinematics model) was taken as 2 which represents JONSWAP/Pierson-Moskowitz spectrum (irregular). *WaveHs* (Significant wave height of incident waves [meters]) and *WaveTp* (Peak spectral period of incident waves [sec]) were set up according to the sea state used for each run. Results were obtained for both flexible and rigid towers and blades; it was found that better correlation was obtained with rigid tower and blades so these results are presented here. A typical input file is shown in Appendix B.

7. 10.1 Comparisons between Experimental and Numerical results

In this section, comparisons between the results obtained from the experiments and the numerical study are presented for the three configurations of the FOWT outlined in Table 7.8. The configurations were selected in order to investigate independently the effect of the wind and wave direction on the response of the system. **Table 7.8 Comparison configurations**

Configuration	Wave direction	Wind direction	Wind model T:turbulent C:constant	
			Experiment	Numerical
1	0°	0°	T	T/C
2	0°	225°	T	T/C
3	45°	0°	T	T/C

The mean and standard deviation values of motion and tendon tensions obtained from the experiments and numerical study are presented. As it was previously described in section 7.7, the steady component (offset-measured before the wave maker has started) was subtracted from the initial value for all channels. The start and end points of the total measurement are selected. The target tension values are then added to the tendon signals. Mean is calculated for all signals between the start and end points.

7.10.1 Configuration 1 Wave direction 0° Wind direction 0°

The irregular wave tests were performed for 0°/0° wave/wind heading using five different sea states described in Table 7.9.

Table 7.9 Tests in 0/0 heading configuration

Sea State	H_s [m]	T_p[s]	Wind Speed [m/s]
N5	1.25	6.36	9.18
N2	1.50	6.61	11.40
N6	1.75	6.86	12.80
N7	2.75	7.80	16.80
N3	8.46	10.13	38.76

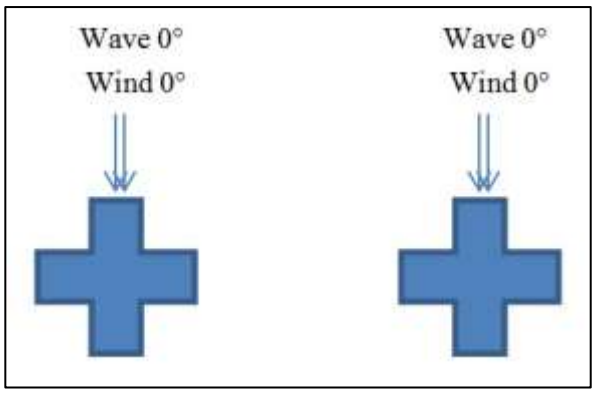

Figure 7.26 Configuration 1

7.10.1.1 Comparison of Surge Motion

The mean surge motion responses are presented in Figure 7.26. The mean values from the experiments and from the numerical predictions show very similar trends. It should be remembered that hydrodynamic drift forces are neglected in FAST, so the mean drift is only due to wind effect. Since the agreement is good with experimental results, it is suggested that the hydrodynamic drift force is small. The maximum mean surge values are obtained for H_s between 1.75-6m. In these sea states there is a reasonable amount of energy at high frequencies which cause the platform to drift down wave due to the relatively large second order drift forces. For the storm condition mean surge values are low since in this sea state the wave lengths are long and the second order drift forces are relatively small. It is interesting to note that numerical results employing the two wind models give very similar results: i.e. the turbulent effect of the wind does not affect the mean surge motion to a large extent. The numerical models and the experiments predict a maximum displacement in surge of around 1.4m. Results for surge correlation seems closer than RAOs since irregular wave frequencies are constantly changing whilst the possibility for motions to 'lock on' in a resonance type manner is possible for regular waves. Furthermore the irregular waves contain little energy at frequencies near to resonance where the discrepancies in RAOs are large.

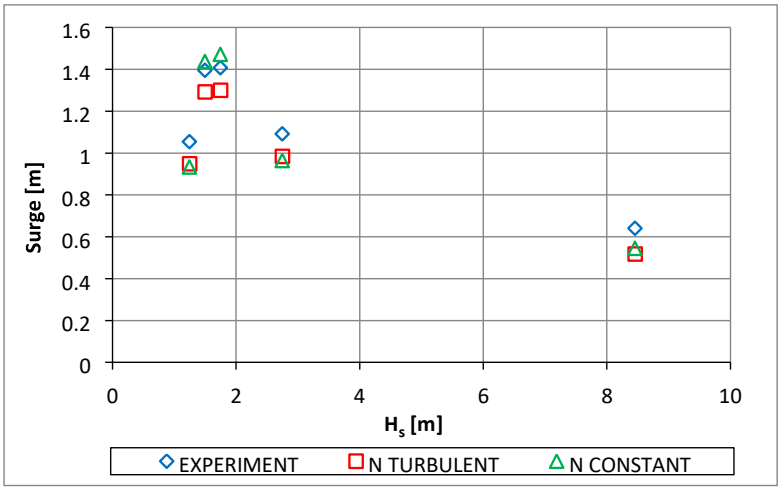

Figure 7.27 Mean value of surge motion wave 0 wind 0

Surge motion standard deviations are presented in Figure 7.28. Both numerical predictions overestimate in the region H_s=1.75 to 2.75m but give good agreement at the largest and smallest sea states. The Surge standard deviation for constant wind

model at H_s=1.75m is 0.5m higher than the turbulent wind prediction. The Turbulent wind model slightly overestimates at H_s=2.75m. Once again, perhaps surprisingly, the two wind models give similar results.

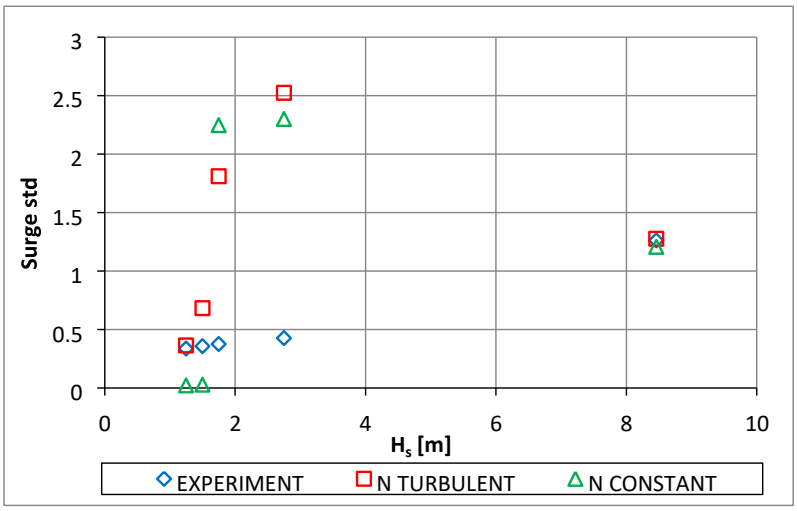

Figure 7.28 Standard deviation of surge motion wave 0 wind 0

7.10.1.2 Comparison of Heave Motion

The mean heave motion responses are presented in Figure 7.29. The experimental results show that in general the mean heave is negative i.e. the platform on average sinks slightly from its undisturbed value. The numerical predictions from both wind models show the platform rising apart from two cases and in general give similar results. The comparison of the heave motion standard deviations are presented in Figure 7.30. Both numerical prediction overestimate in the region H_s=1.75 to 2.75m but give good agreement at the largest and smallest sea states. Once again, perhaps surprisingly, the two wind models give similar results.

The most important aspect of both figures is that that the mean and standard deviation values for heave are very small for all wave conditions. Indeed, the largest mean value is less than 73mm (2mm in model scale) which casts some doubts on the accuracy of both the numerical and experimental data. For this reason the heave response of the platform will not be considered in the rest of the study.

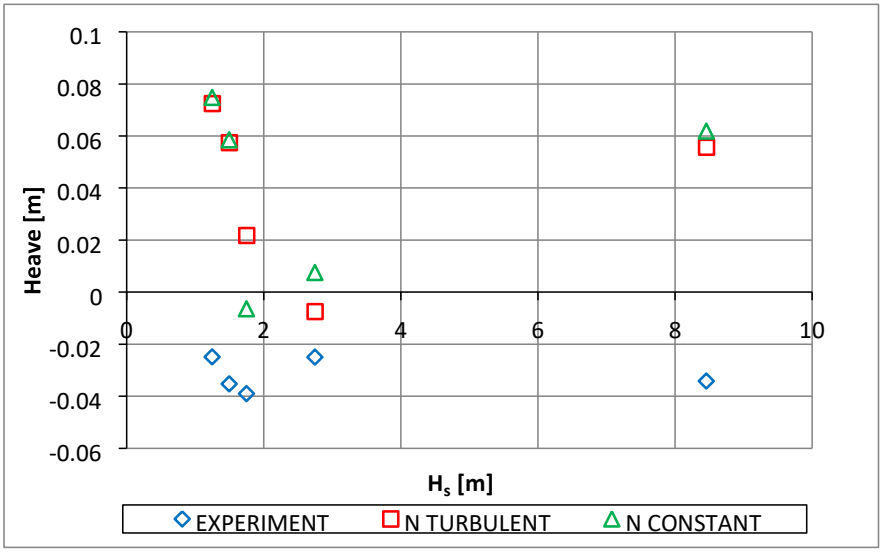

Figure 7.29 Mean value of heave motion wave 0 wind 0

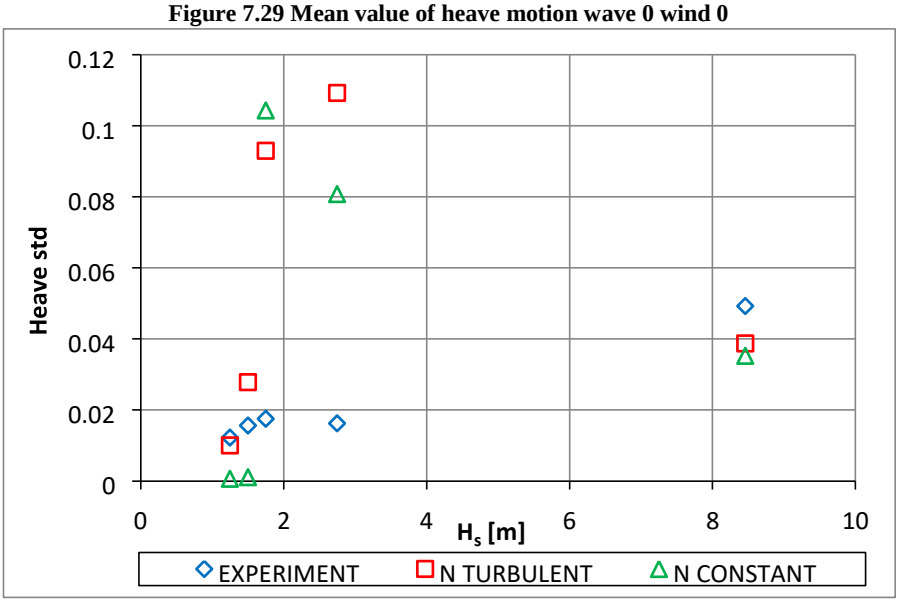

Figure 7.30 Standard deviation of heave motion wave 0 wind 0

7.10.1.3 Comparison of Pitch Motion

The mean values for pitch motions are presented in Figure 7.31. The figure shows that the mean values obtained from experiments follow a similar trend but are higher than the numerical results for all wind directions. The storm condition showed the closest agreement. Turbulent and constant wind model give very similar results.

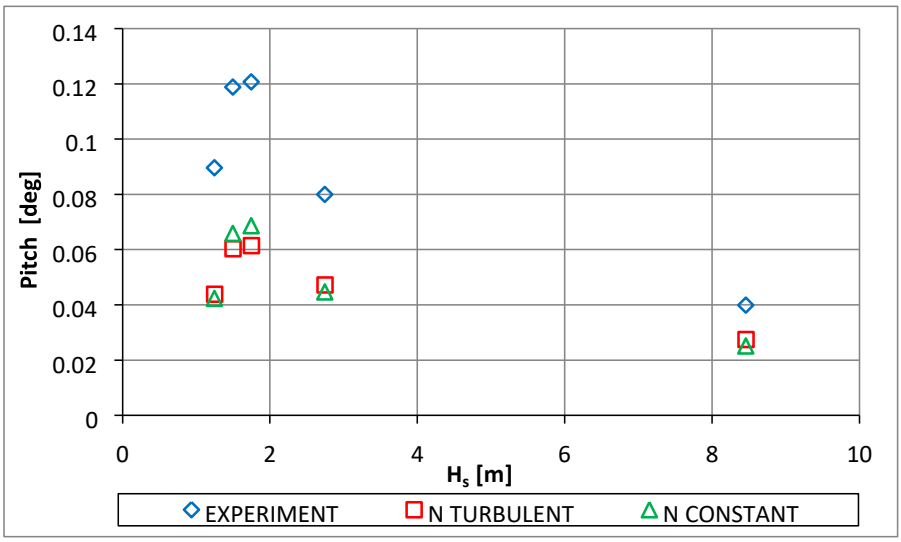

Figure 7.31 Mean value of pitch motion wave 0 wind 0

The standard deviation of pitch motions is presented in Figure 7.32. The numerical models give similar results and generally under predict the pitch standard deviation compared with the experiment results. In general the pitch motions are small.

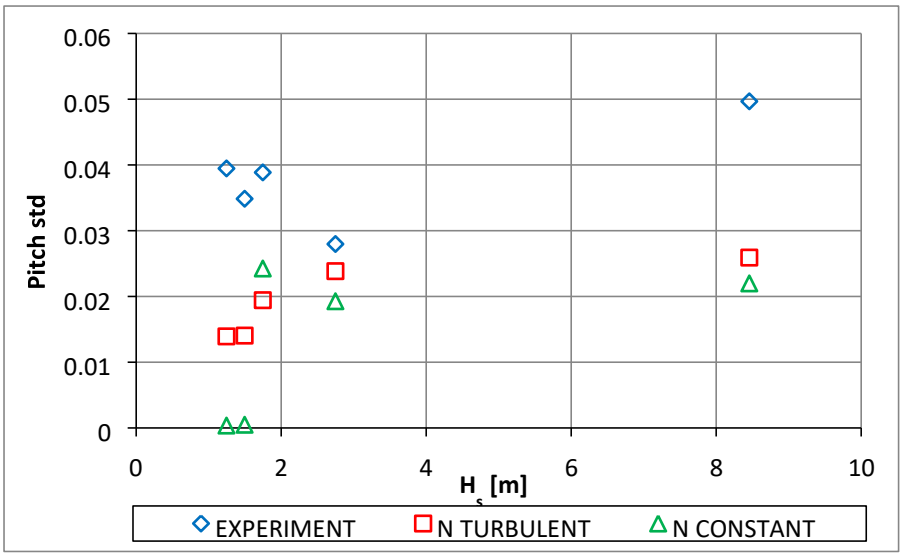

Figure 7.32 Standard deviation of pitch motion wave 0 wind 0

7.10.1.4 Comparison of Tendon tensions

In this section, comparisons of non-dimensional total tendon tensions are presented. The tendon numbering is shown in Figure 7.33. It should be noted that the average value of each pair (which gave very similar results in the experiments) are presented here. The numerical predictions do not differentiate the tendon pairs and give identical values for each pair. On the mean tension plots a tension value of 1 is equivalent to the static pre-tension.

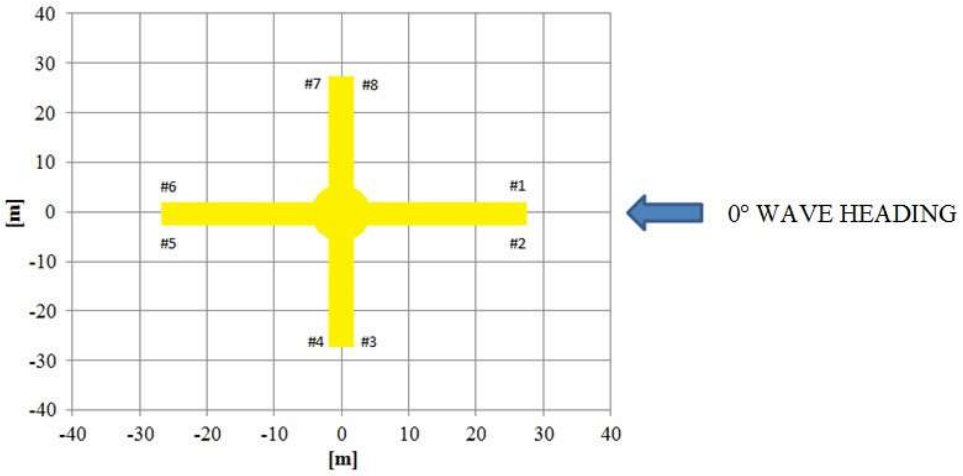

Figure 7.33 Tendon numbering

Figure 7.35 and Figure 7.35 present the mean and standard deviation results for the front (T1and T2) and back (T5 and T6) tendon tensions together. Figure 7.34 shows that the numerical results for the mean tensions are slightly higher than those obtained from the experiments. Front tendon tensions are always higher than back tendon tensions as expected furthermore front tendon tensions are greater than the mean static tension and back tensions are lower than the mean static tension. The experiment results predict an increase in forward tensions of around 40% of the static value while the numerical prediction show a 60% increase. These discrepancies in tendon tensions are broadly consistent with the discrepancies in the motions, but appear to be somewhat larger than might be expected. The standard deviation results presented in Figure 7.35 show that in general as the wave and wind energy increases the dynamic tensions increase. The trends for both the mean and standard deviation values are similar and the two wind models once again give almost identical results. Maximum static tensions occur in the region of H_s=1.75m while maximum dynamic tensions occur during the most severe environmental conditions at H_s=8.5m.

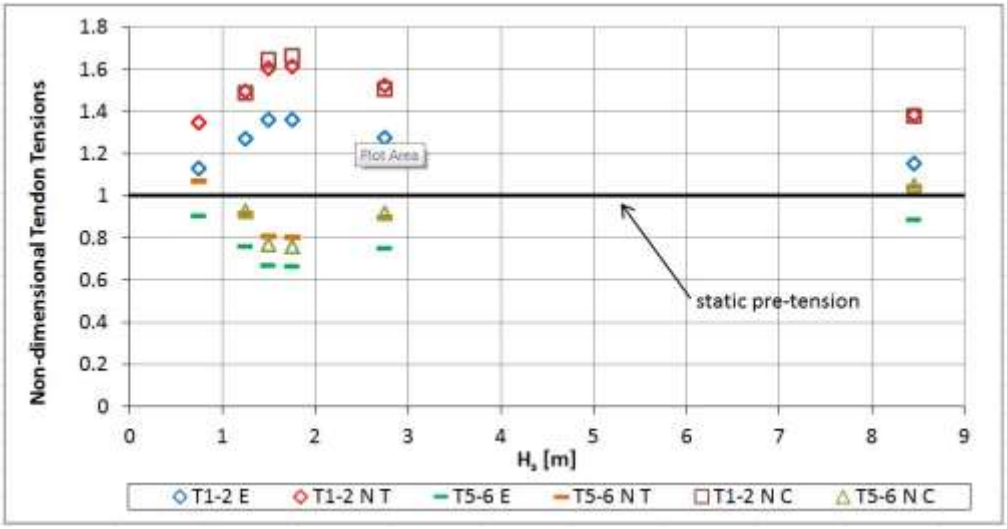

Figure 7.34 Mean tension values for front and back tendons

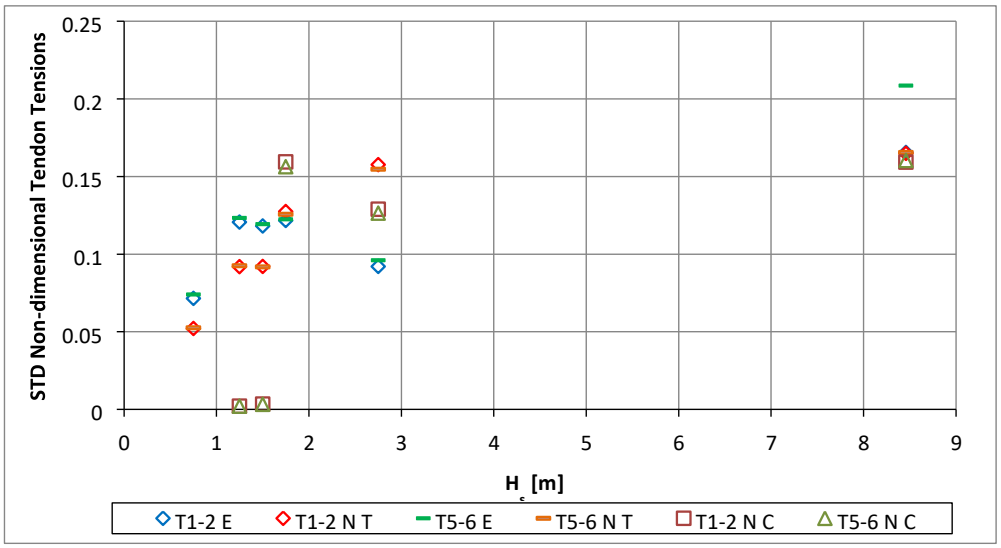

Figure 7.35 Standard deviations of tensions for front and back tendons

Figure 7.37 and Figure 7.37 present the mean and standard deviation results for the side (T3 and T4) / (T7 and T8) tendon tensions. Figure 7.36 shows once again that the numerical results for the mean tensions are higher than those obtained from the experiments. The experimental results show that the mean tensions are 1-2% higher that the static tension values with the numerical predictions 20% higher than the static values of tension. For both cases the mean side tensions are independent of wave height. The standard deviation results presented in Figure 7.37 once again show that as the wave and wind energy increases the dynamic tensions increase. The trends for both the mean and standard deviation values are similar and the two wind models once again give almost identical results.

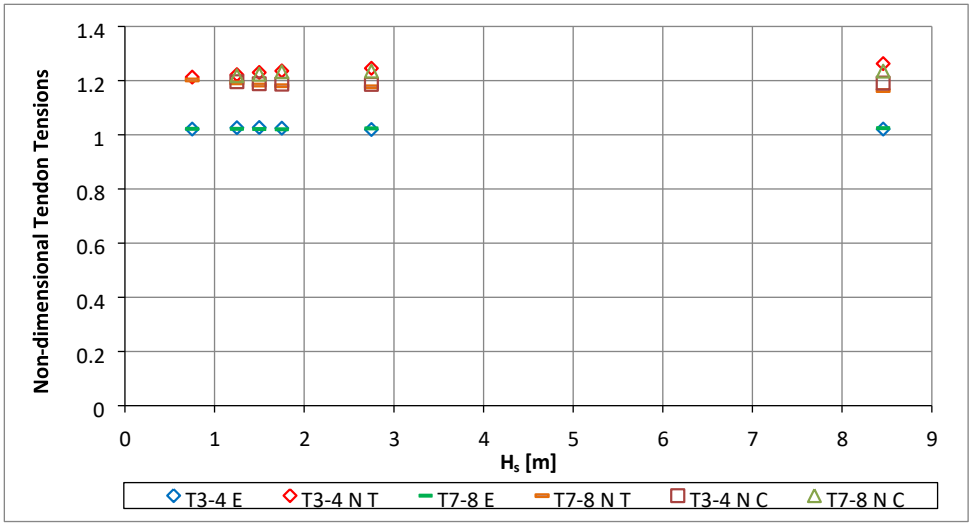

Figure 7.36 Mean tension values for side tendons

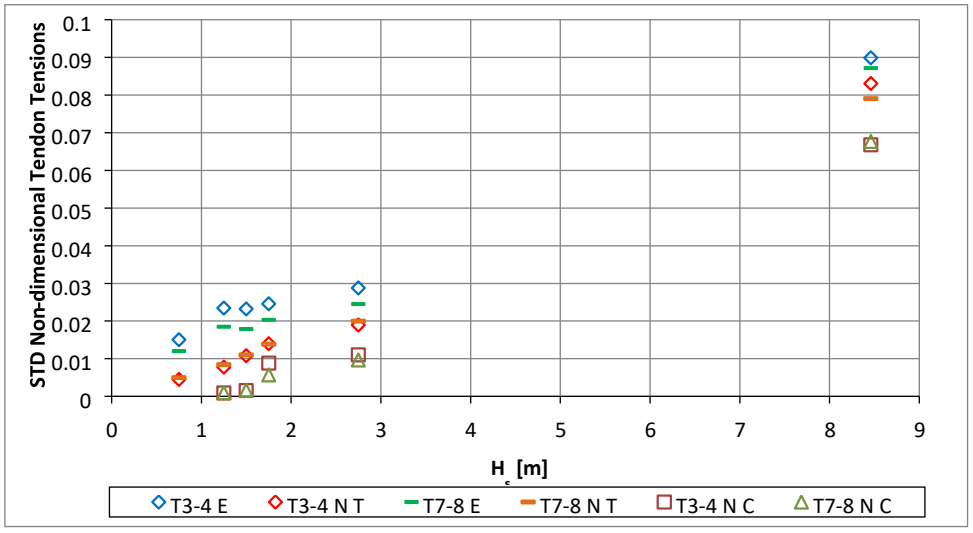

Figure 7.37 Standard deviations of tensions for side tendons

7.10.2 Configuration 2 Wave direction 0° Wind direction 225°

Irregular wave tests were performed for 0°/225° wave/wind heading using seven different sea states described in Table 7.10.

Table 7.10 Tests in 0/225 heading configuration

Sea State	H_s [m]	T_p[s]	Wind Speed [m/s]
N4	0.75	5.44	6.05
N5	1.25	6.36	9.18
N2	1.50	6.61	11.40
N6	1.75	6.86	12.80
N1	4.55	9.00	11.40
N8	6.00	10.28	25.00
N3	8.46	10.13	38.76

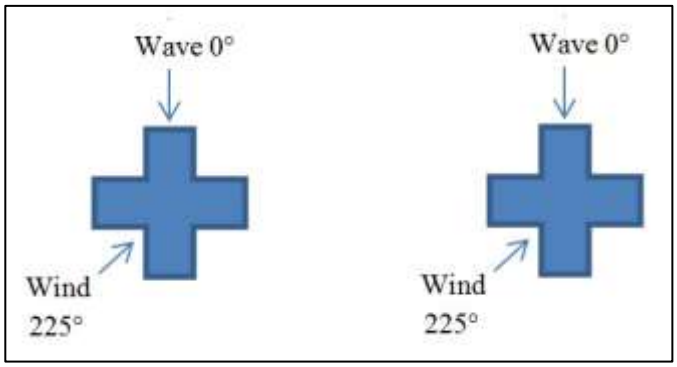

Figure 7.38 Configuration 2

7.10.2.1 Comparison of Surge Motion

The mean surge motion responses for the case of 0° head waves and 225° wind direction are presented in Figure 7.39. The mean values from the experiments and from the constant wind model numerical model show very similar trends while the turbulent model results show slightly more scatter. All of the results are negative showing that the aerodynamic force is greater than the hydrodynamic force and the platform drifts towards the direction of the incident waves. The maximum mean surge values are obtained for H_s between 1.75-4.5m. The experiments predict a maximum displacement in surge of around 1m which is lower than the 0°/0° case as expected.

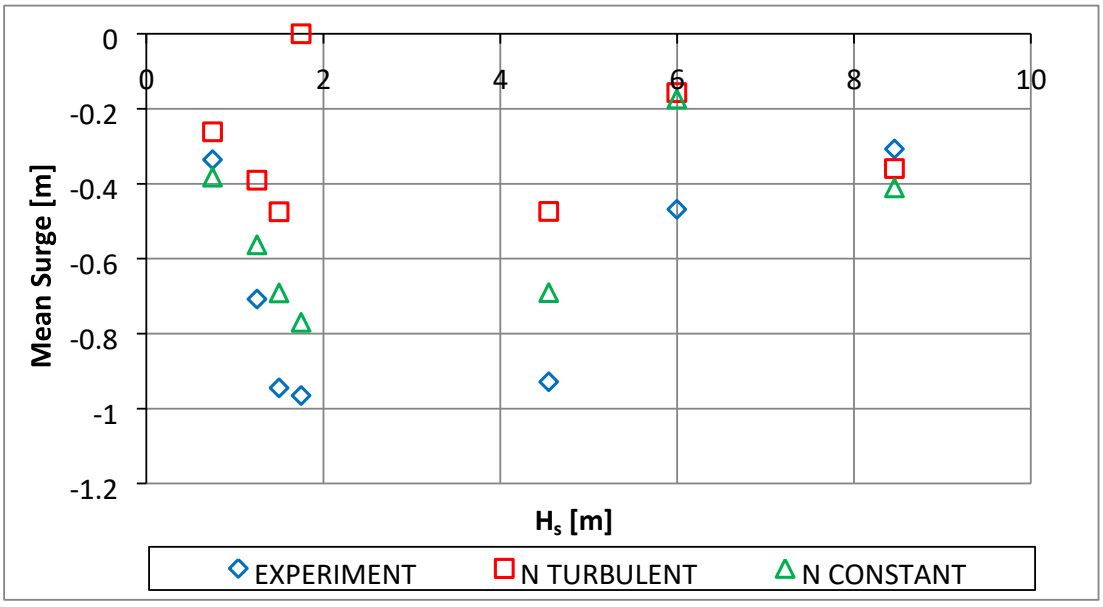

Figure 7.39 Mean value of surge motion wave 0 wind 225

The standard deviations of surge motions are presented in Figure 7.40. Both numerical predictions underestimate in the region H_s=0.75 to 1.75m. The constant wind model

gives very good agreement with the experimental results at the higher sea states while the turbulent model underpredicts. For this condition the constant wind model gives slightly better agreement with the experimental results.

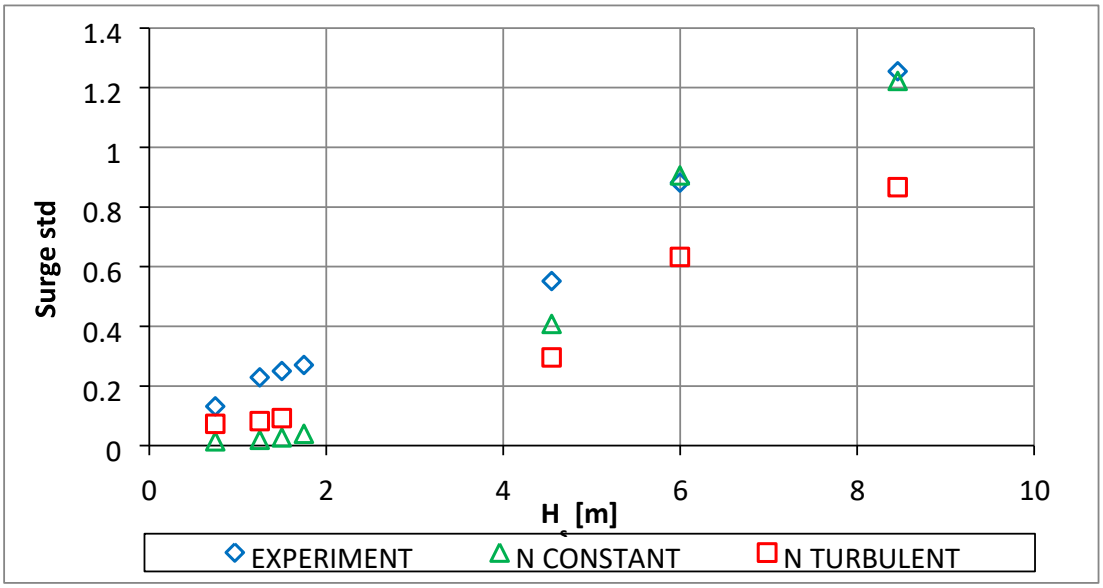

Figure 7.40 Standard deviation of surge motion wave 0 wind 225

7.10.2.3 Comparison of Pitch Motions

The mean values for pitch motions are given in Figure 7.41. The figure shows that the values obtained from experiments follow a similar trend but are less negative than the numerical results for all wind directions. All of the results are negative showing that the platform trims into the incident waves due to the aerodynamic force. The storm condition and the smallest sea state showed the closest agreement. Turbulent and constant wind models give similar results. The magnitude of the maximum trim of around 0.12 degrees is similar to that obtained on the 0°/0° case.

The mean pitch values (trim) are all relatively small.

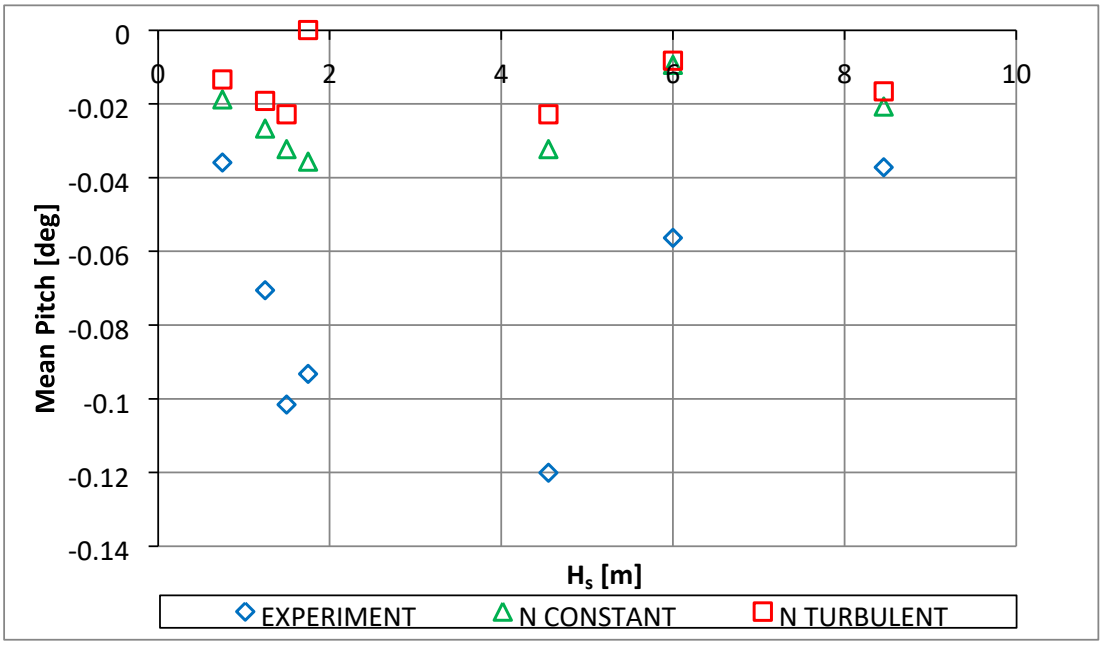

Figure 7.41 Mean value of pitch motion wave 0 wind 225

The standard deviation of pitch motions are presented in Figure 7.42. The numerical models give similar results and generally under predict the pitch standard deviation compared with the experimental results. The trend shows that the pitch motions increase at the same level of the environmental forces as expected. In general the pitch motions are small.

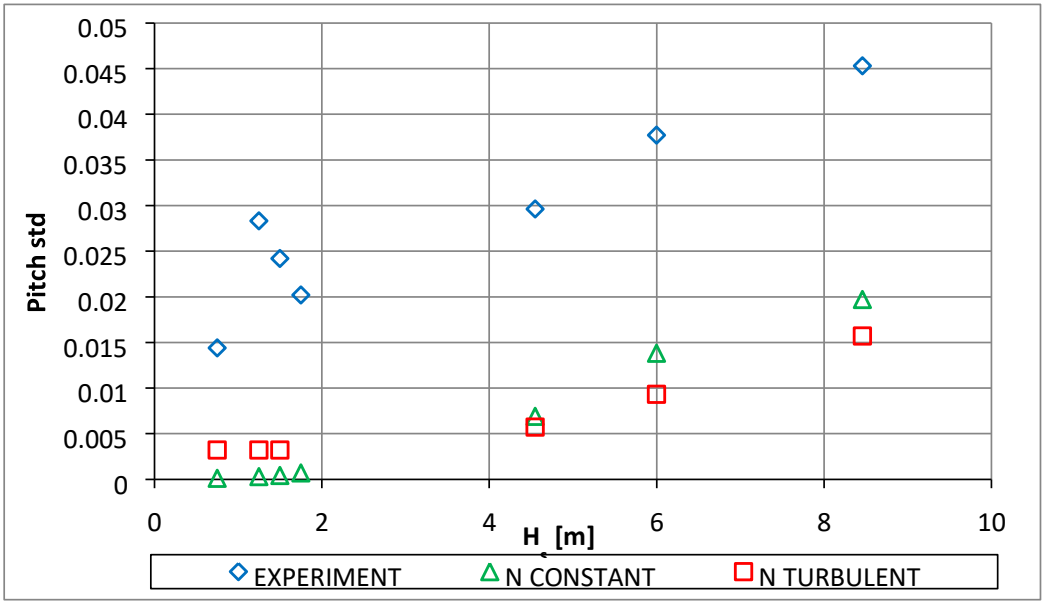

Figure 7.42 Standard deviation of pitch motion wave 0 wind 225

7.10.2.3 Comparison of Sway Motions

The mean sway motion responses are presented in Figure 7.43. The mean values from the experiments give much larger values than the numerical predictions. The trend of the mean sway being very similar to the mean surge motion showing that the aerodynamic force is dominant. The numerical predictions for both wind models give little or no mean sway for all of the sea conditions. It can be seen from the sway plots that constant wind simulations in FAST are unrealistic for sway.

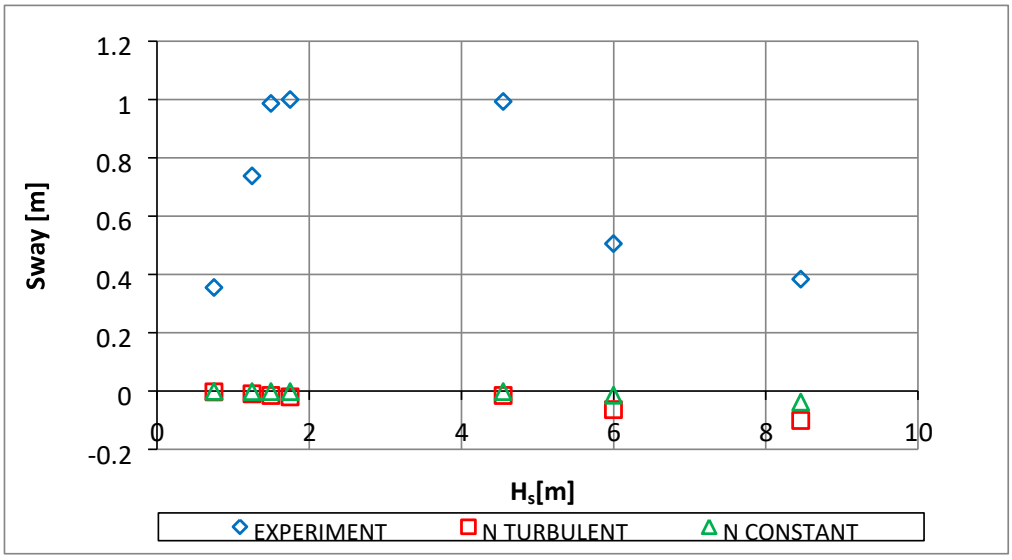

Figure 7.43 Mean value of sway motion wave 0 wind 225

The comparisons of the standard deviations for sway motions are presented in Figure 7.44. The numerical and experiment results give poor agreements for this case. The experimental values have a maximum sway around H_s=3m with the standard deviation reducing at large and small sea states. This is likely due to the first order wave forces in the larger sea states acting in the opposite direction to the aerodynamic forces. The constant wind model predicts also zero sway motion while the turbulent model predicts that the sway motions increase linearly with the sea state, neither of these scenarios is likely. Regarding turbulent wind discrepancies, sway motions are bigger that expected for larger sea states.

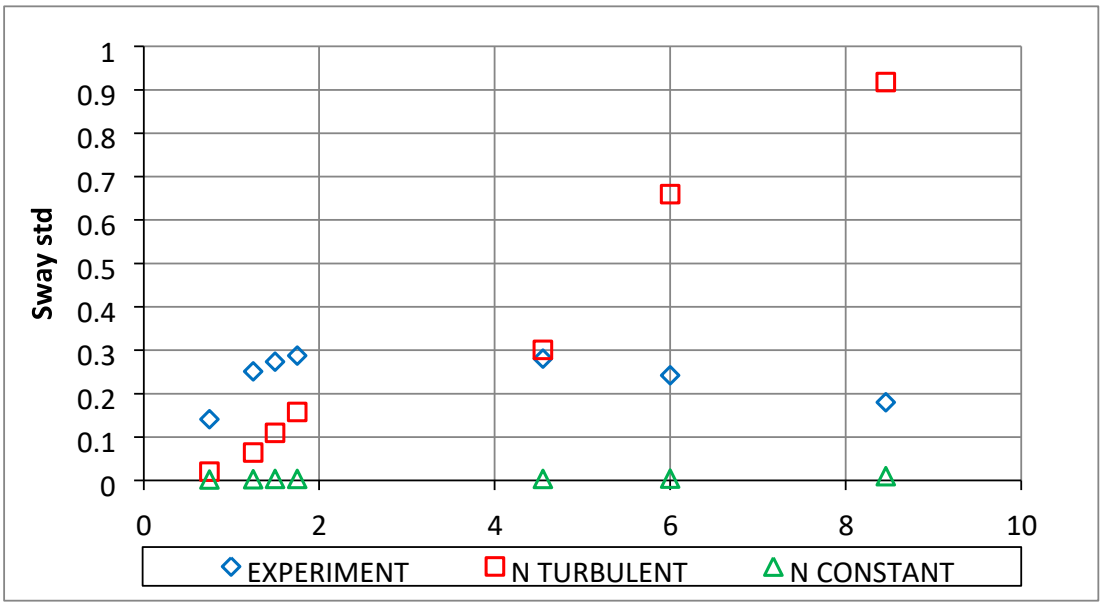

Figure 7.44 Standard deviation of surge motion wave 0 wind 225

7.10.2.4 Comparison of Roll Motions

The mean roll motion responses for the case of 0° head waves and 225° wind direction are presented in Figure 7.45. Apart from the sign change the mean roll response is very similar to the mean pitch response as obtained from the experiments showing again that the aerodynamic force is dominant. The numerical values for the mean roll are very small.

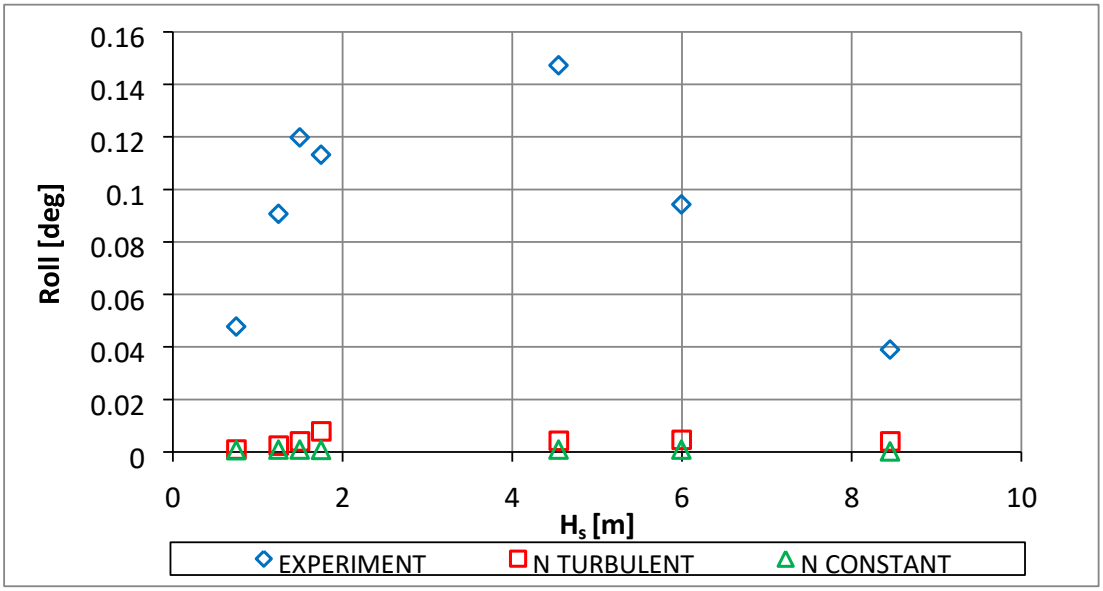

Figure 7.45 Mean value of roll motion wave 0 wind 225

The roll motion standard deviations are presented in Figure 7.46. The experimental values show a relatively constant roll angle over the range of wave conditions. The numerical values show some scatter. The values from the experiments and the numerical prediction are very small which questions the reliability of the data.

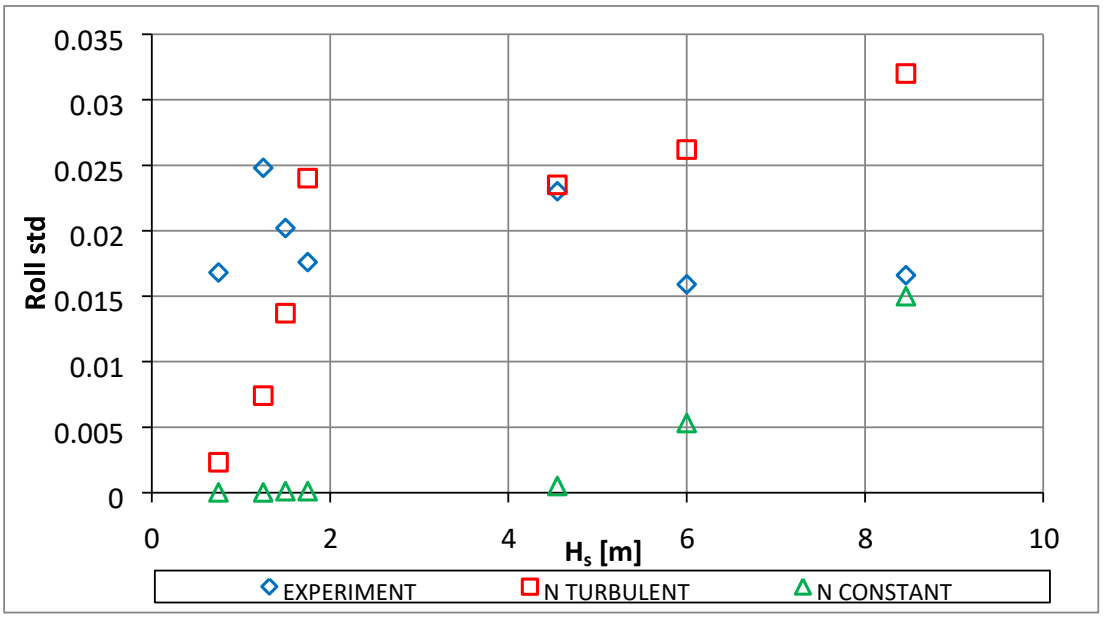

Figure 7.46 Standard deviation of roll motion wave 0 wind 225

7.10.2.5 Comparison of Tendon Tensions

Figure 7.47 and Figure 7.48 present the mean and standard deviation results for the front (T1 and T2) and back (T5 and T6) tendon tensions together. Figure 7.47 shows that the numerical results for the mean tensions are slightly higher than those obtained from the experiments. In contrast to the 0°/0° case front tendon tensions are lower than back tendon tensions as expected for this case. The maximum tendon tensions are very slightly lower than those obtained in the 0°/0° case. The standard deviation results presented in Figure 7.48 show that in general as the wave and wind energy increases the dynamic tensions increase. The trends for both the mean and standard deviation values are similar and the two wind models once again give almost identical results. Maximum mean tensions occur in the region of H_s=1.75m while maximum dynamic tensions occur in the most severe environmental conditions as expected.

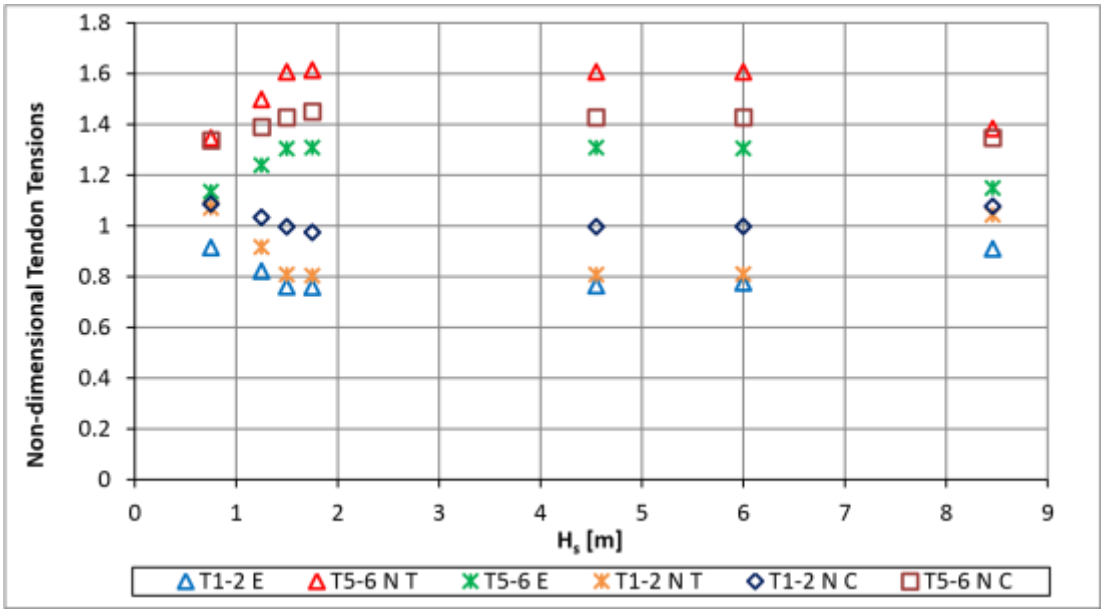

Figure 7.47 Mean tension values for front and back tendons

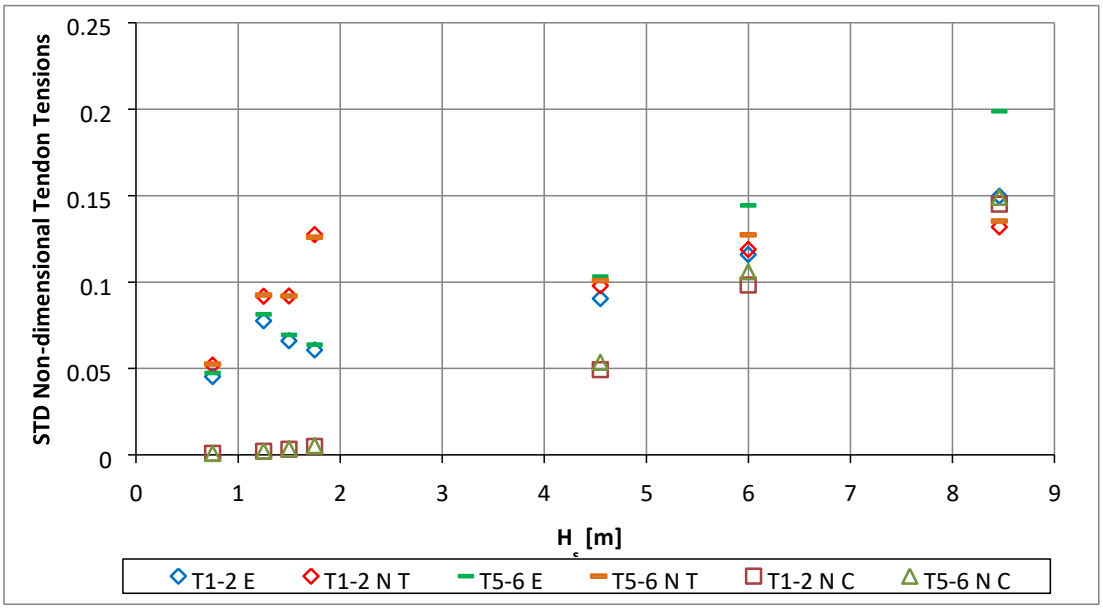

Figure 7.48 Standard deviations of tensions for front and back tendons

Figure 7.49 and Figure 7.50 present the mean and standard deviation results for the side (T3 and T4) / (T7 and T8) tendon tensions. Figure 7.49 shows that the mean tension for tendons 3 and 4 are lower than those of pair 7 and 8. The numerical predictions show that the mean side tensions are relatively independent of the wave height and have a 20% uplift from the static tension values. The standard deviation results presented in Figure 7.50 once again show that as the wave and wind energy increase the dynamic tensions increase. In this case the turbulent wind model gives

better agreement with the experimental results while the constant wind model underpredicts the side tension variations.

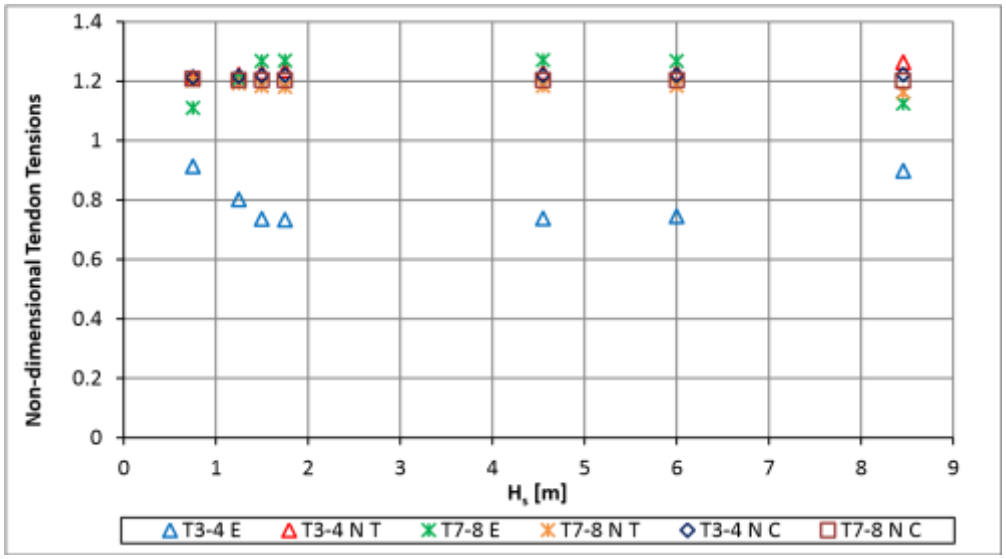

Figure 7.49 Mean tension values for side tendons

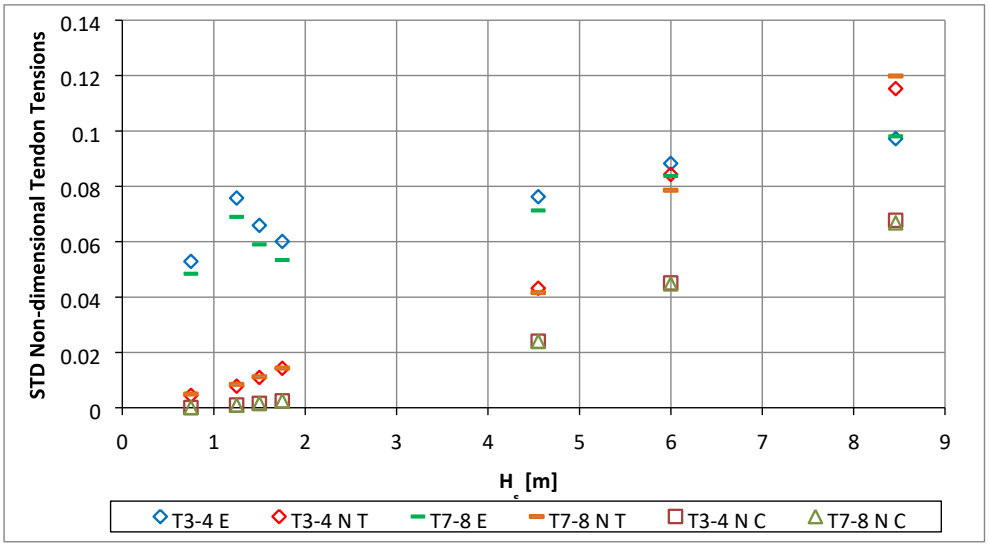

Figure 7.50 Standard deviations of tensions for side tendons

7.10.3 Wave direction 45° Wind direction 0°

The irregular wave tests were performed for 45°/0° wave/wind heading using seven different sea states described in Table 7.11. For these tests the model was rotated in the test tank by 45° as shown in Figure 7.51.

Table 7.11 Tests in 45/0 heading configuration

Sea State	H_s [m]	T_p[s]	Wind Speed [m/s]
N4	0.75	5.44	6.05
N5	1.25	6.36	9.18
N2	1.50	6.61	11.40
N6	1.75	6.86	12.80
N7	2.75	7.80	16.80
N1	4.55	9.00	11.40
N3	8.46	10.13	38.76

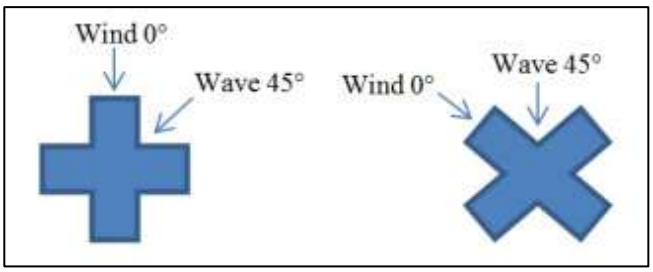

Figure 7.51 Configuration 3

7.10.3.1 Comparison of Surge Motions

The comparison of mean surge motion response for the case of 45° head waves 0° wind direction are presented in Figure 7.52. The mean values from the experiments and the turbulent wind model show very similar trends while the constant wind model over predicts. All of the results are positive showing that the platform drifts down as expected. The maximum mean surge values are obtained for H_s between 1.75-4.5m. The experiments predict a maximum displacement in surge of around 0.4m which is lower than the 0°/0° case as expected.

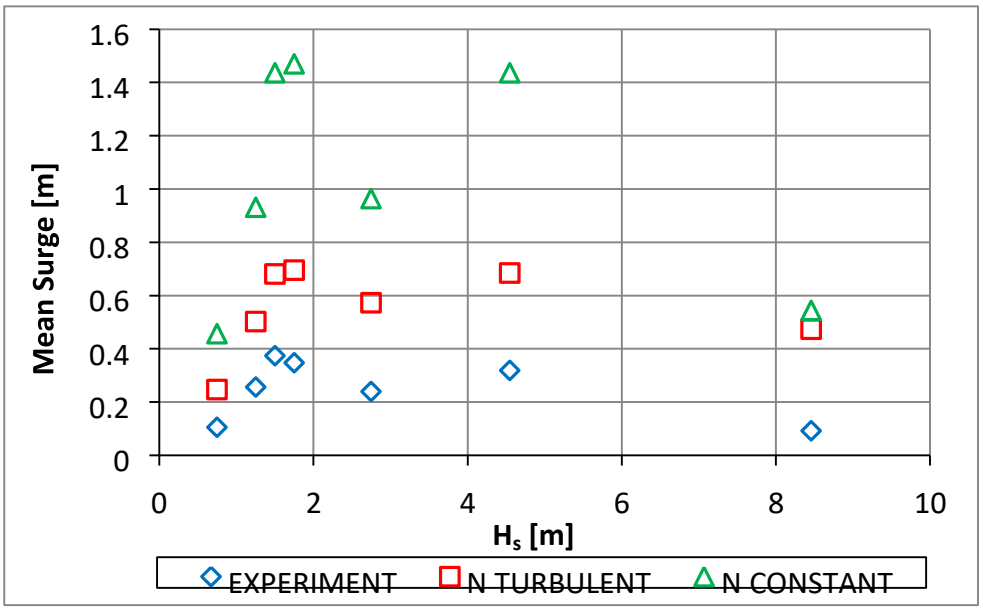

Figure 7.52 Mean value of surge motion wave 45 wind 0

The surge motion standard deviations are presented in Figure 7.53. Both numerical models give higher values in the region H_s =1.75-2.5m but otherwise they show good agreement with the experimental values. The experimental results show standard deviations increasing linearly as the wave/wind excitations increase as expected.

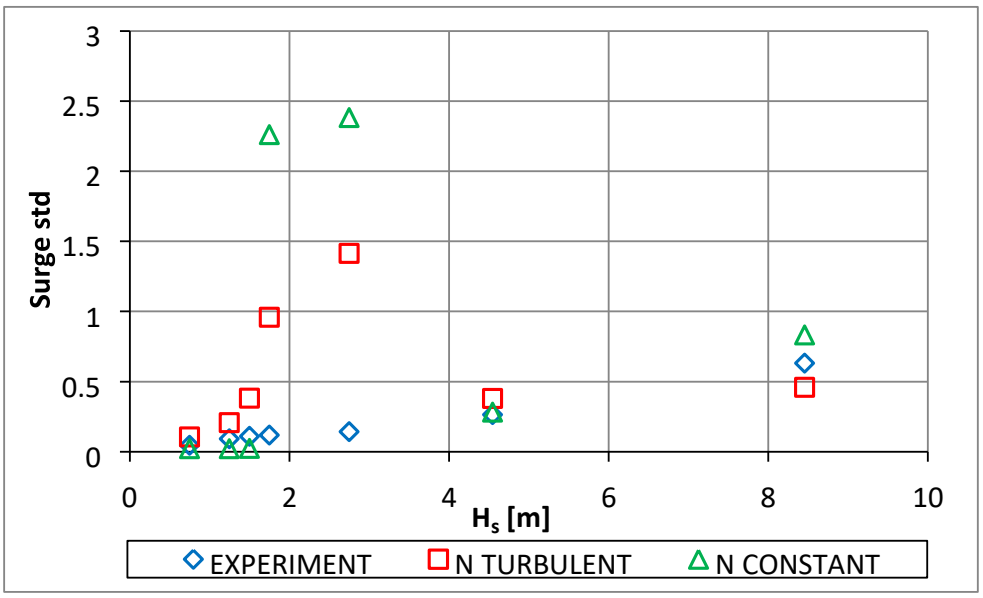

Figure 7.53 Standard deviation of surge motion wave 45 wind 0

7.10.3.2 Comparison of Pitch Motions

The mean values for the pitch motions are given in Figure 7.54. The figure shows that the mean values obtained from the experiments follow a similar trend but are higher than the numerical results for all wind directions. All of the results are positive, the

platform trims in the direction of the wind. The turbulent and constant wind models give very similar results and they are smaller than the experimental results for all sea states. The magnitude of the maximum trim is around 0.12 degrees which is similar to that obtained in the 0°/0° case. The mean pitch values are all relatively small.

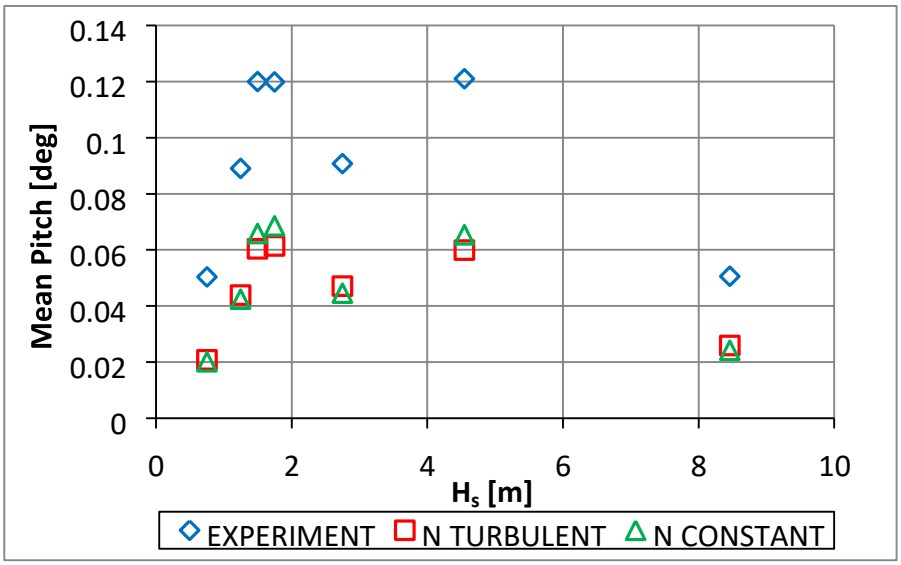

Figure 7.54 Mean value of surge motion wave 45 wind 0

The standard deviations of the pitch motions are presented in Figure 7.55. Both numerical models under predict, with the turbulent model giving closer agreement to the experimental values. The trend shows that the pitch motions generally increase at the level of the environmental forces although there is a 'flat spot' between H_s=1.5-4.5m. As with previous configurations, in general, pitch motions are small.

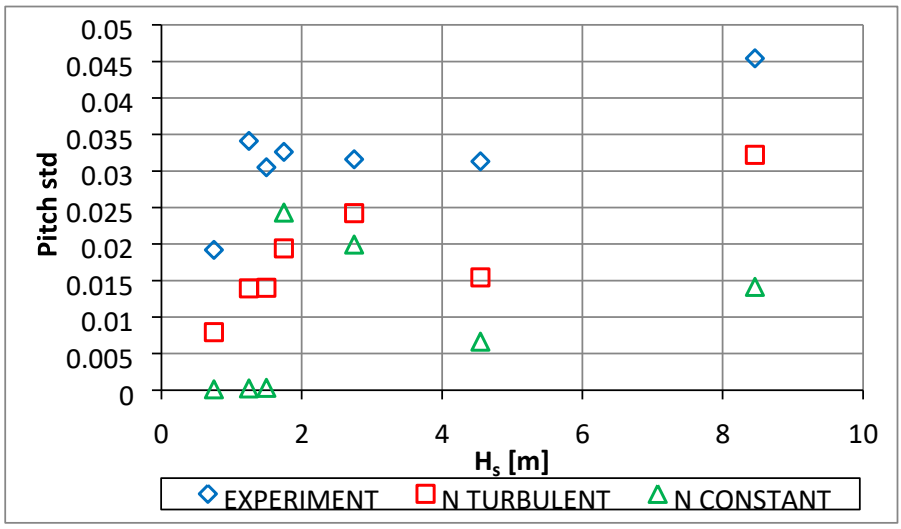

Figure 7.55 Standard deviation of pitch motion wave 45 wind 0

7.10.3.3 Comparison of Sway Motion

The sway motion responses for the case of 45° head waves and 0° wind direction are presented in Figure 7.56. The turbulent model gives good agreement with the experimental values, once again, the constant wind model fails to reliably predict the sway motions. The sway results follow the typical second order drift curve. The maximum drift is 1.4 m which is 50 % greater than the 0°/225° case as expected since the wind force and a component of the wave force act together.

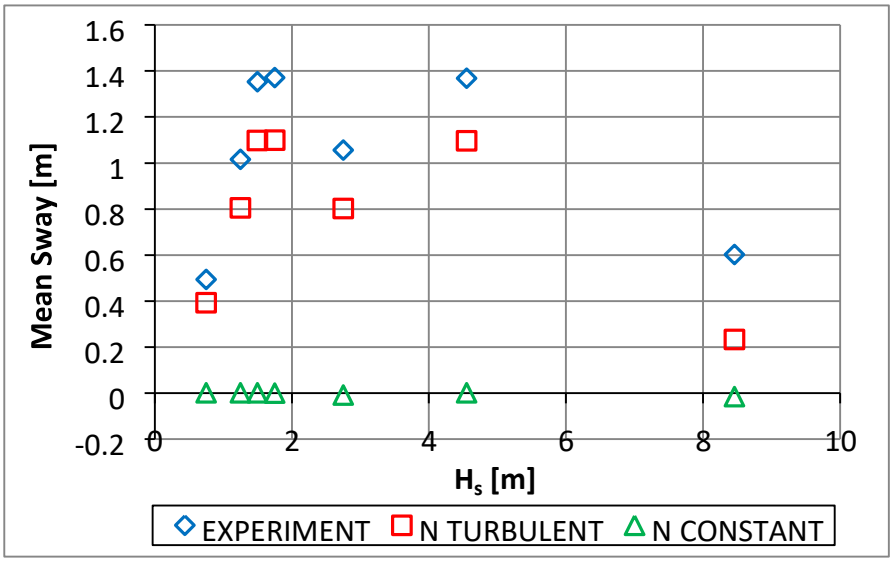

Figure 7.56 Mean value 0f sway motion wave 45 wind 0

The sway motion standard deviations are presented in Figure 7.57. The constant wind numerical and experimental results give good agreement while the turbulent wind model over predicts for H_s values between 1.75 and 2.75 m. The sway motions increase with wave/wind excitation as previously.

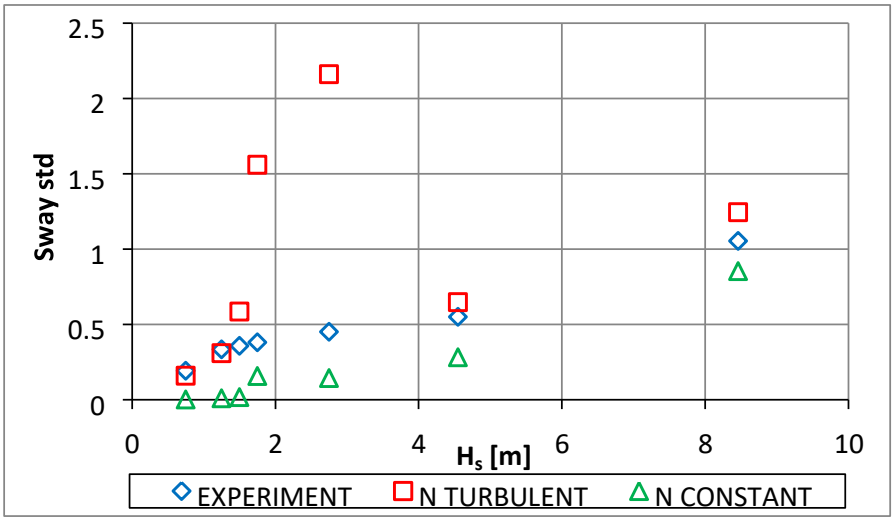

Figure 7.57 Standard deviation of sway motion wave 45 wind 0

7.10.3.4 Comparison of Roll Motions

The mean roll motion responses (heel) are presented in Figure 7.58. The numerical model gives in general good agreement but since the values from the numerical predictions and the experiments are so small then the results cannot be relied upon.

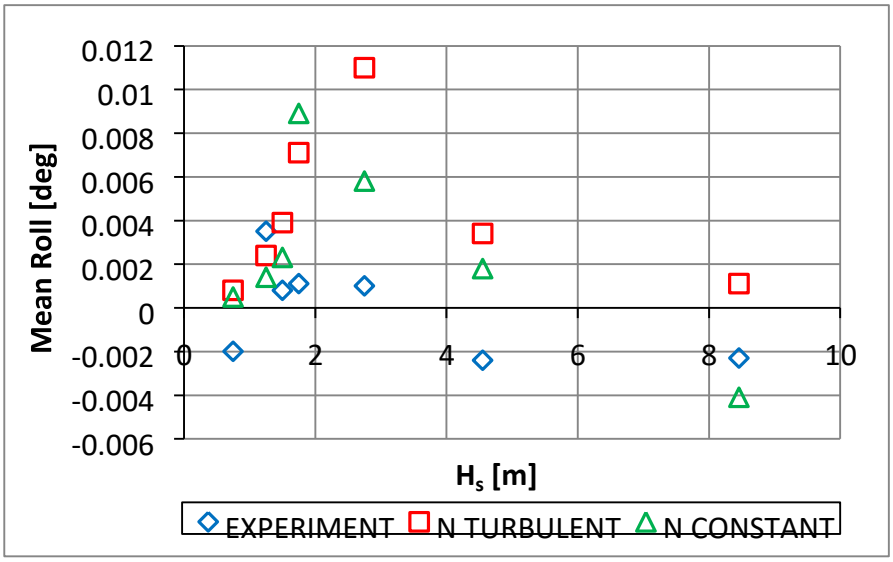

Figure 7.58 Mean value of roll motion wave 45 wind 0

The standard deviations of the roll motions are presented in Figure 7.59. They show very similar trends to the sway motion results given above. The constant wind numerical and experiment results give good agreement while the turbulent wind model over predicts for H_s values between 1.75 and 2.75 m. The roll motions increase with wave/wind excitation as previously.

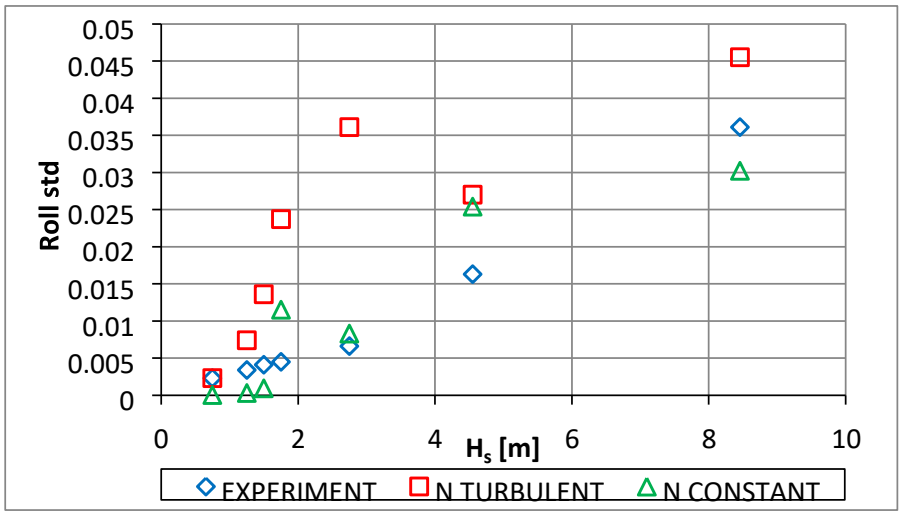

Figure 7.59 Standard deviation of roll motion wave 45 wind 0

7.10.3.5 Comparison of Tendon tensions

Figure 7.60 and Figure 7.61 present the mean and standard deviation results for the front (T1 and T2) and back (T5 and T6) tendon tensions together. Figure 7.60 shows that the numerical results for the mean tensions are slightly higher than those obtained from the experiments. As in the 0°/0° case front tendon tensions are higher than back tendon tensions as expected. The maximum tendon tensions are slightly lower than those obtained in the 0°/0° case. The standard deviation results presented in Figure 7.61 show, as in the previous two cases, that in general as the wave and wind energy increases the dynamic tensions increase. The trends for standard deviation values are similar for the turbulent wind and experiments. The constant wind model gives smaller standard deviation results. The maximum static tensions occur in the region of H_s=1.75m and H_s=4.55m while the maximum dynamic tensions occur during the most severe environmental conditions as expected.

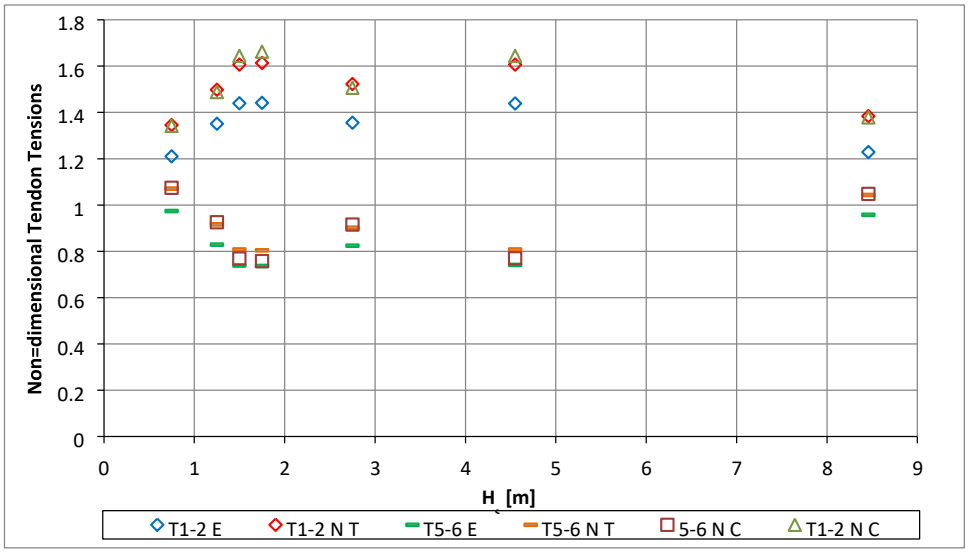

Figure 7.60 Mean tension values for front and back tensions

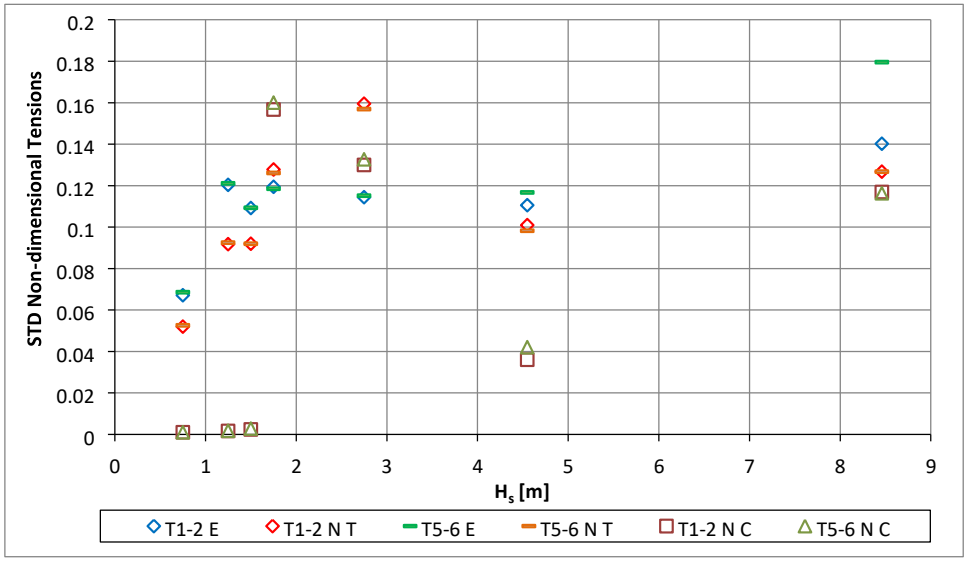

Figure 7.61 Standard deviations of tensions for front and back tendons

Figure 7.62 and Figure 7.63 present the mean and standard deviation results for the side (T3 and T4) / (T7 and T8) tendon tensions. Figure 7.62 shows that the mean tension for tendons 3 and 4 are lower that those of pair 7 and 8. The numerical predictions show that the mean side tensions are relatively independent of the wave height. The standard deviation results presented in Figure 7.63 once again show that as the wave and wind energy increases the dynamic tensions increase. The turbulent wind model gives slightly better agreement with the experimental results.

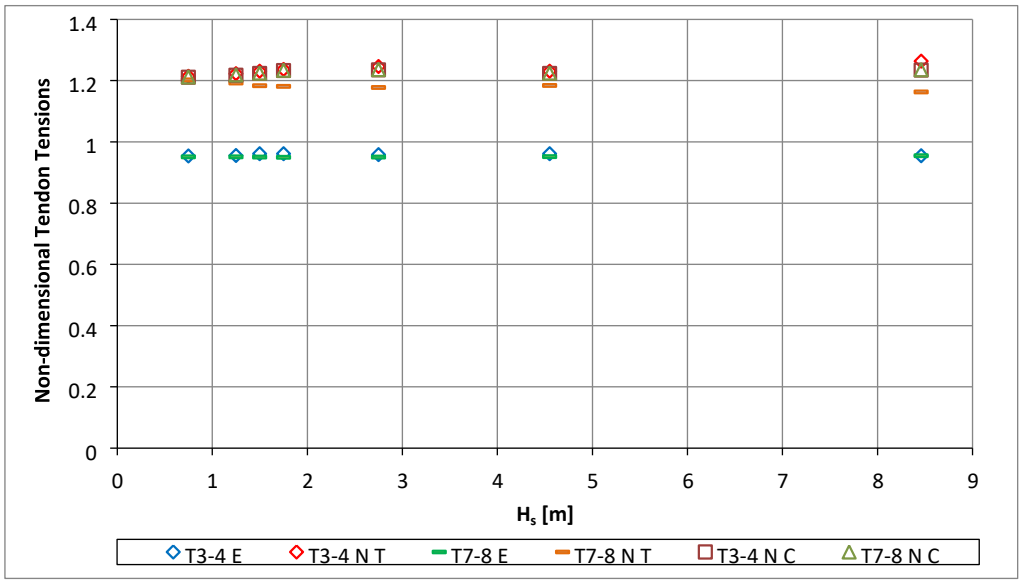

Figure 7.62 Mean tension values for side tendons

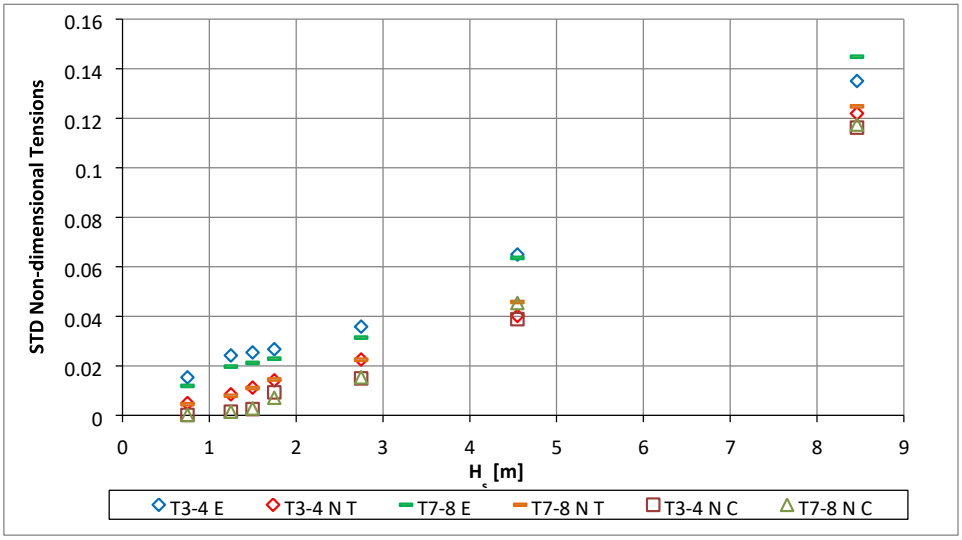

Figure 7.63 Standard deviations of tensions for side tendons

7.11 Experimental results

In this section, experimental results are presented for the four configurations of the FOWT outlined in Table 7.12. The configurations were selected in order to investigate the effect of wind on the response of the system.

Table 7.12 Experiment configurations

Configuration	Wave direction	Wind direction	Experiment Wind Model
4	45°	0°	T
5	45°	45°	T
6	45°	-45°	T
7	45°	225°	T

Mean values and standard deviation values of motion and tendon are presented.

7.11.1 Description of configurations and test matrix

In this section all configurations used in the experiments to investigate the wind impact on the system are described. As was previously mentioned in section 7.10.3, the irregular wave tests were carried out for 45°/0° wave/wind heading using seven different sea-states described in Table 7.13 and the model configuration is given in Figure 7.64.

Table 7.13 Tests in 45/0 configuration

Sea State	H_s [m]	T_p[s]	Wind Speed [m/s]
N4	0.75	5.44	6.05
N5	1.25	6.36	9.18
N2	1.50	6.61	11.40

N6	1.75	6.86	12.80
N7	2.75	7.80	16.80
N1	4.55	9.00	11.40
N3	8.46	10.13	38.76

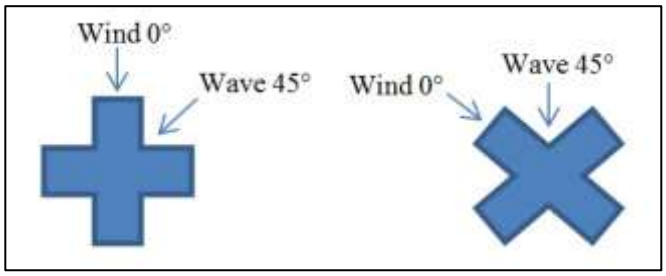

Figure 7.64 Configuration 4

The irregular wave tests were carried out for 45°/45° wave/wind heading using three different sea states described in Table 7.14 and the model configuration is given in Figure 7.65.

Table 7.14 Tests in 45/45 configuration

Sea State	H_s [m]	T_p[s]	Wind Speed [m/s]
N4	0.75	5.44	6.05
N5	1.25	6.36	9.18
N6	1.75	6.86	12.80

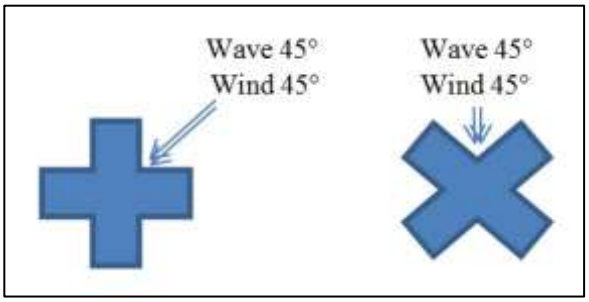

Figure 7.65 Configuration 5

The irregular wave tests were performed for 45°/-45° wave/wind heading angles using six different sea states as described in Table 7.15 and the model configuration is given in Figure 7.66.

Table 7.15 Tests in 45/-45 configuration

Sea State	H_s [m]	T_p[s]	Wind Speed [m/s]
N5	1.25	6.36	9.18
N2	1.50	6.61	11.40
N6	1.75	6.86	12.80
N7	2.75	7.80	16.80
N8	6.00	10.28	25.00
N3	8.46	10.13	38.76

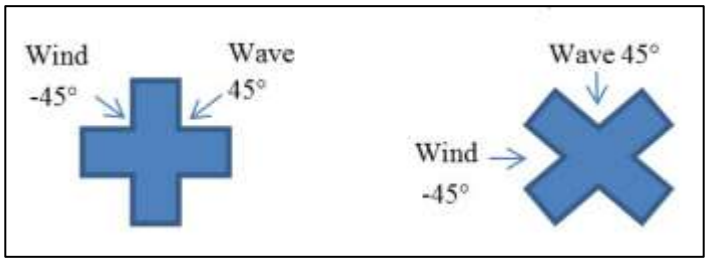

Figure 7.66 Configuration 6

The irregular wave tests were performed for 45°/225° wave/wind heading using five different sea states as described in Table 7.16 and the model configuration is given in Figure 7.67.

Table 7.16 Tests in 45/225 configuration

Sea State	H_s [m]	T_p[s]	Wind Speed [m/s]
N4	0.75	5.44	6.05
N5	1.25	6.36	9.18
N6	1.75	6.86	12.80
N8	6.00	10.28	11.40
N3	8.46	10.13	38.76

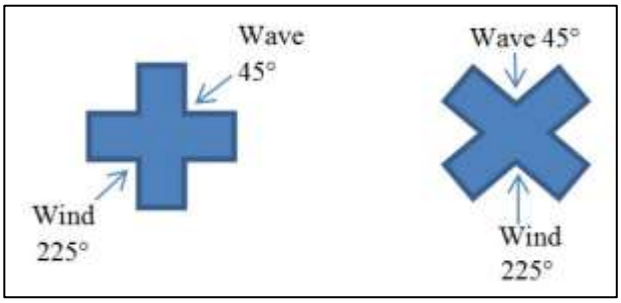

Figure 7.67 Configuration 7

7.11.2 Comparison of Surge Motions

The comparison of the mean surge motion response for the case of 45° head waves are presented in Figure 7.68. The mean surge values obtained from 45°/-45° configuration are higher than other configurations apart from when H_s=6m. In general, the mean surge values show very similar trends in all wind directions. The maximum mean surge values are obtained for H_s between 1.75-6m in the case of 45°/-45°, 45°/225°. It is interesting to note that the wind direction of -45° affects the mean values most. The experiments for 45°/-45° configuration predict a maximum displacement in surge of around 1.2m. It should be noted that the maximum difference between 45°/0° and 45°/-45° configuration is due to the wind direction and it is 0.8m at Hs= 1.75m. The minimum mean surge response occurs for the 45°/0° case.

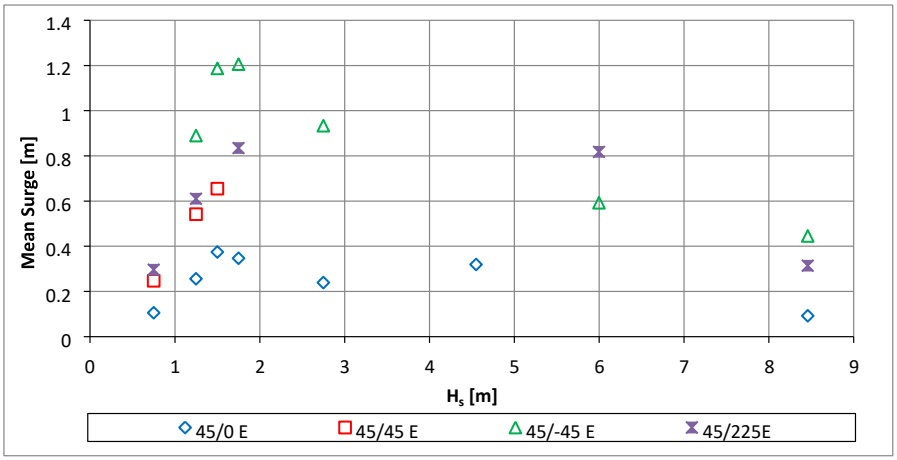

Figure 7.68 Comparison of mean surge values

The standard deviations for surge motions are presented in Figure 7.69. As the sea state increases, the energy increases as expected. Once again, 45°/-45° configuration gives higher standard deviation values and the minimum surge response occurs for the 45°/0° case.

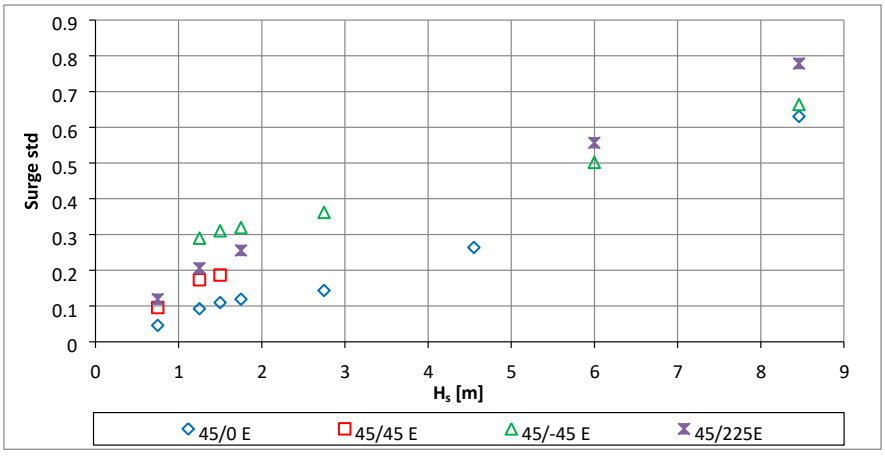

Figure 7.69 Comparison of standard deviation values for surge motion

7.11.3 Comparison of Pitch Motions

The mean values for mean pitch (trim) motions are given in Figure 7.70. The figure shows that the mean values obtained from all configurations follow a similar trend but are lower for 45°/-45° configuration than other wind directions. The maximum mean pitch obtained from experiments is around 0.12 degrees.

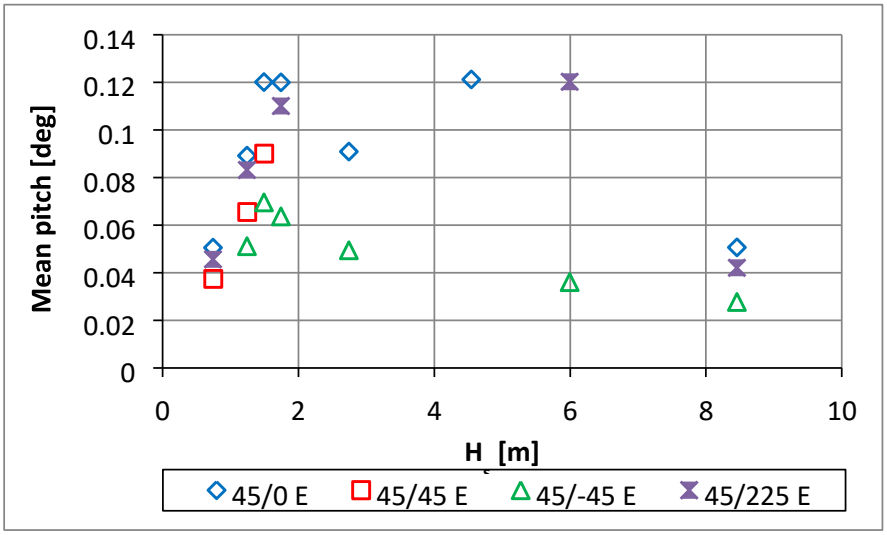

Figure 7.70 Comparison of mean pitch values

The standard deviations of pitch motions are presented in Figure 7.71. All configurations give similar results and 45°/-45° configuration generally under predict the pitch standard deviation for smaller sea states compared with the other configurations. It should be noted again that, in general, the pitch motions are very small.

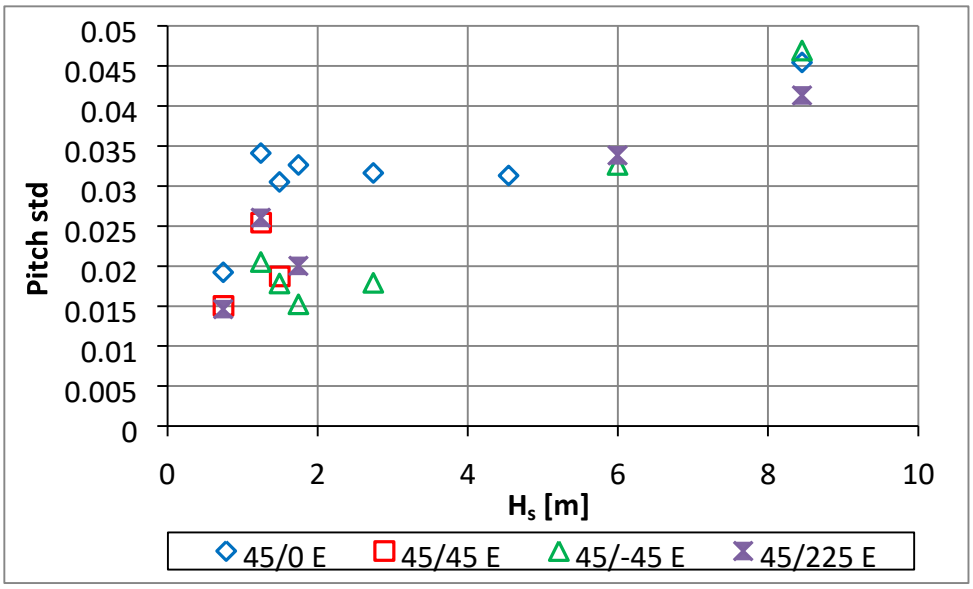

Figure 7.71 Comparison of standard deviation values for pitch motion

7.11.4 Comparison of Sway Motion

The mean sway motion responses for the case of 45° head waves and different wind directions are presented in Figure 7.72. The mean values from the experiments give similar trends and the three configurations are in the same direction. For the 45°/225° configuration the platform drifts toward the waves indicating that the wind force is greater than the wave force for all the sea-states. The 45°/0° and 45°/45° configurations give the largest sideways drift of just under 1.5m.

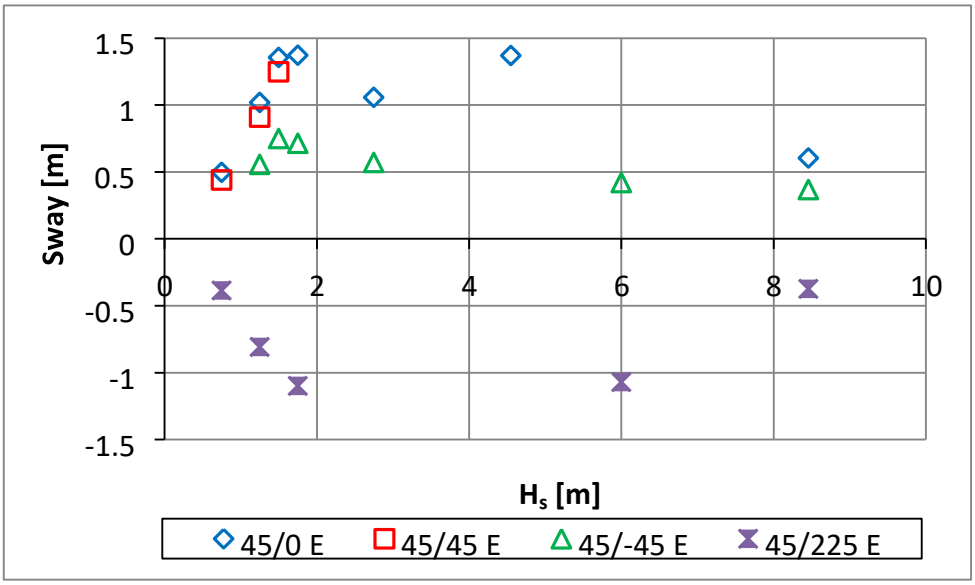

Figure 7.72 Comparison of mean sway values

The standard deviations for the sway motions are presented in Figure 7.73. All configurations give similar trends which increase with the environmental forces as

expected showing the insensitivity of the platform sway motions to changing wind direction.

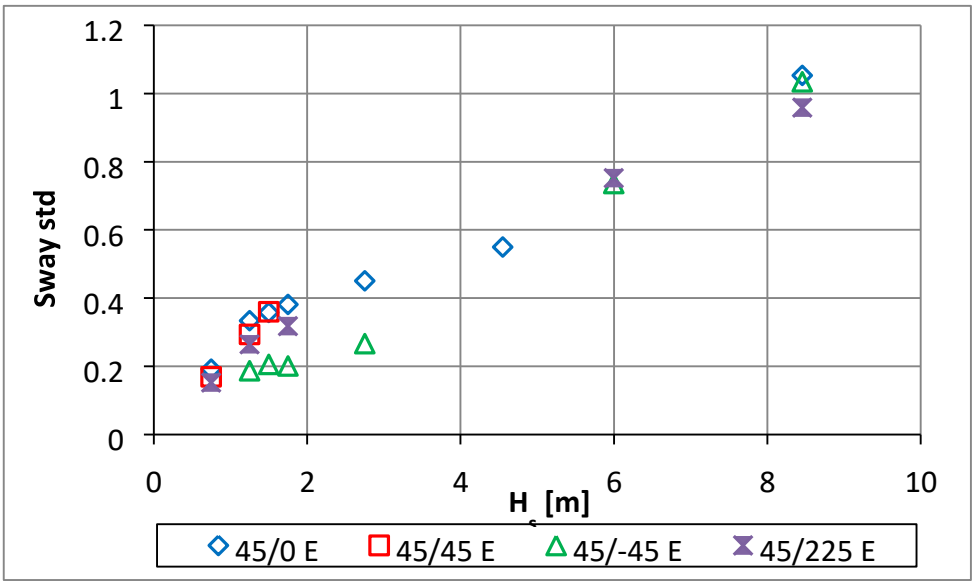

Figure 7.73 Comparison of standard deviation values for sway motion

7.11.5 Comparison of Roll Motions

The mean roll motion responses for the case of 45° head waves and different wind directions are presented in Figure 7.74. Apart from the configuration of 45°/225° all roll mean values are small. For configuration 45°/225° the platform trims toward the waves due to the dominant wind force. The maximum heel angle was just under 1.2 degrees. The comparison of figures 7.96 and 7.98 shows that there is a strong correlation between mean sway and mean roll.

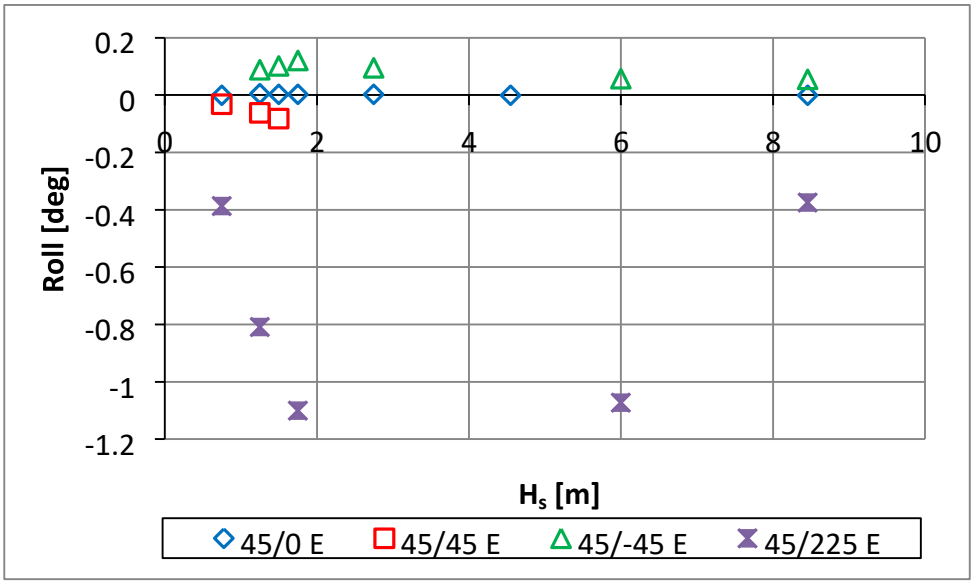

Figure 7.74 Comparison of mean roll values

The standard deviations for roll are presented in Figure 7.75. Apart from configuration 45°/225° all the remaining configurations show an insignificant roll response over the range of wave conditions.

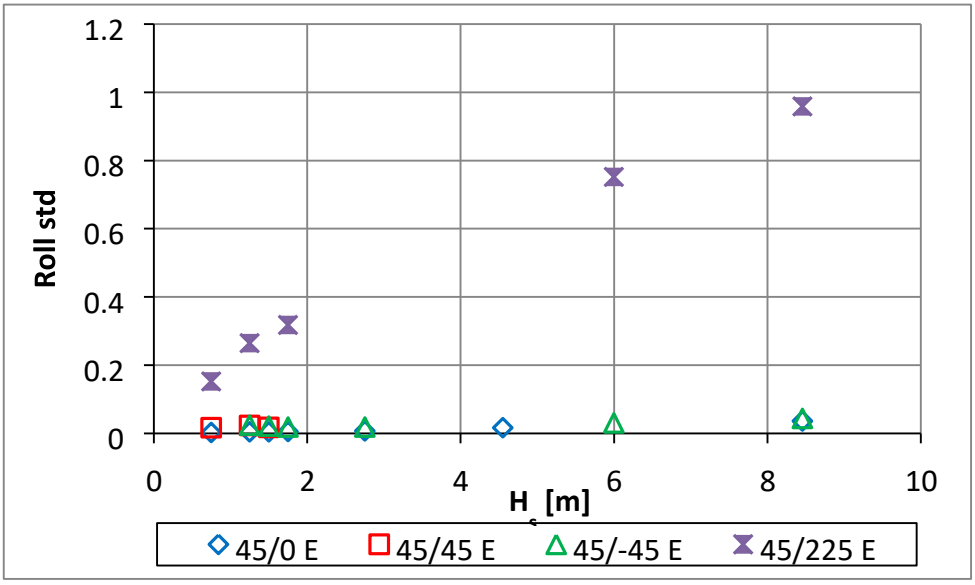

Figure 7.75 Comparison of standard deviation values for roll motion

7.11.6 Comparison of Tendon Tensions

Figure 7.76 and Figure 7.77 present the mean and standard deviation results for the front (T1 and T2) and back (T5 and T6) tendon tensions. Figure 7.76 shows that the results for the mean tensions in the case of 45°/225° are opposite than the others.

Apart from 45°/225° configuration, front tendon tensions are always higher than back tendon tensions as expected. The maximum front tendon tensions are very slightly higher than those obtained in the 45°/0° case. The standard deviation results presented in Figure 7.77 show that in general as the wave and wind energy increases the dynamic tensions increase. The trends for the standard deviation values are similar for 45°/45°, 45°/-45°, 45°/225° configurations. Maximum mean tensions occur in the region of H_s=1.75m and H_s=4.55m while maximum dynamic tensions occur at the most severe environmental conditions as expected.

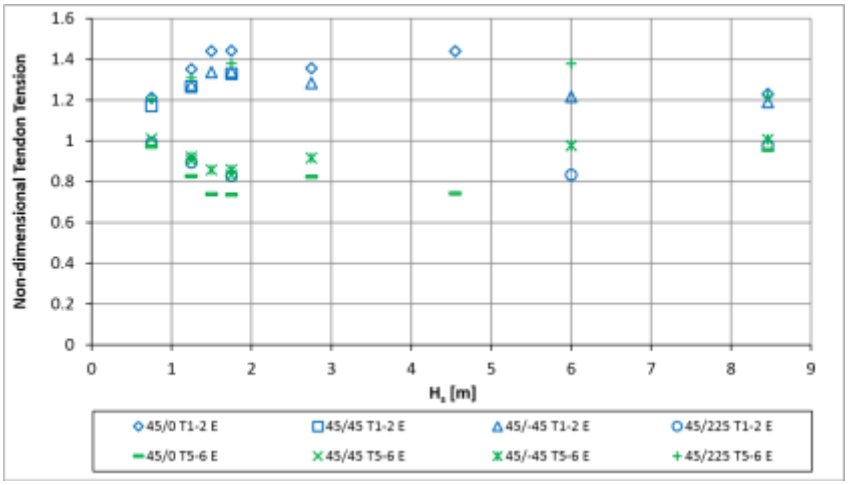

Figure 7.76 Mean tension values for front and back tendons

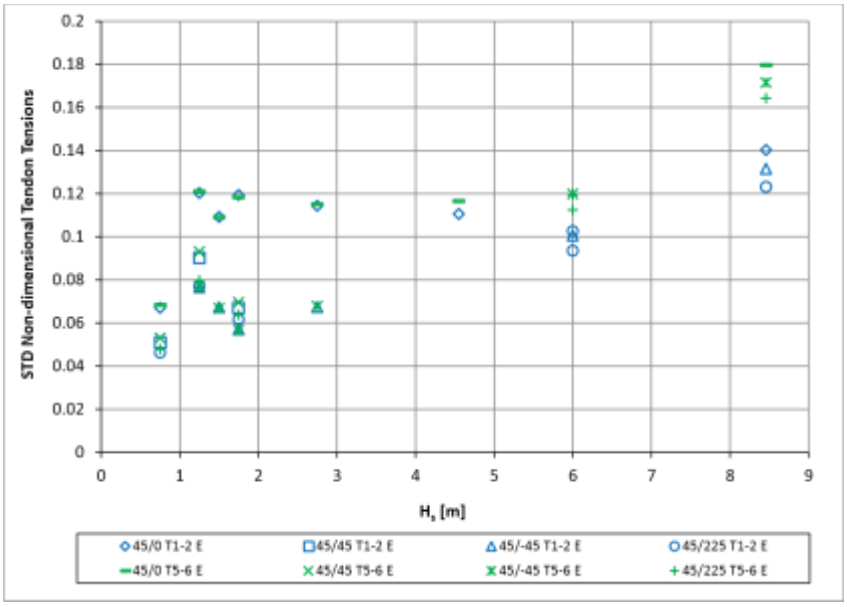

Figure 7.77 Standard deviations of tensions for front and back tendons

Figure 7.78 and Figure 7.79 present the mean and standard deviation results for the side (T3 and T4) / (T7 and T8) tendon tensions. Figure 7.78 shows that the mean tension forces for tendons 3 and 4 are almost identical with those of pair 7 and 8 except when H_s=2.75m and H_s=6m. The standard deviation results presented in Figure 7.79 once again show that as the wave and wind energy increases the dynamic tensions increase. In this case the 45°/0° configuration gives slightly different trend at the smaller sea states while all the remaining configurations give similar trends.

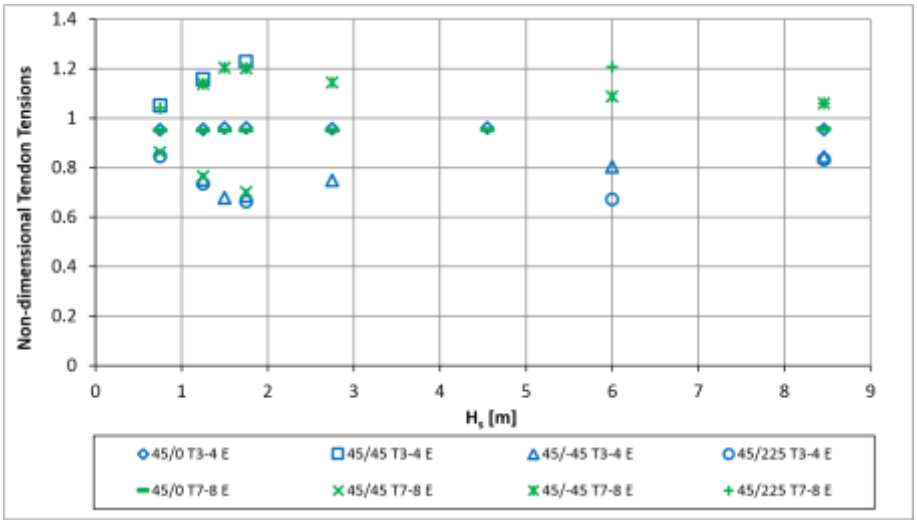

Figure 7.78 Mean tension values for side tendons

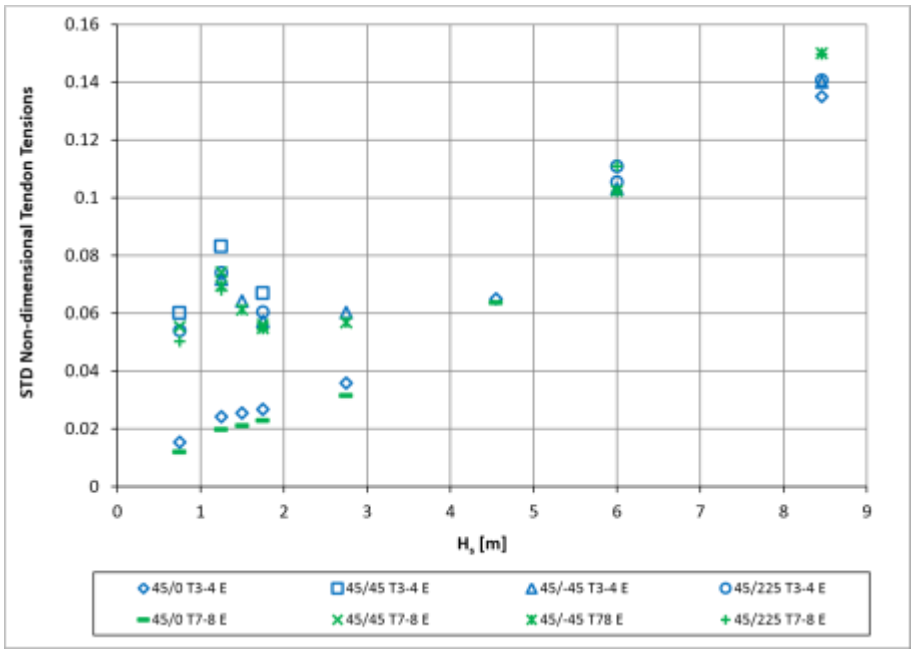

Figure 7.79 Standard deviation of tensions for side tendons

7.12 Conclusions

This chapter described the experimental results and numerical predictions of the hydrodynamic performance of the FOWT in realistic environmental conditions. The details of the wind and wave models used in the investigation were given. Data processing of experimental results and numerical results were presented. One complete set of detailed results were presented for the most severe operational condition.

The experimental results showed that for all environmental conditions the motions of the platform are generally small. The most significant responses were found as the first and second order surge motions.

The case 0°/0° gave the largest mean surge responses with the platform drifting 1.4m down wave whilst the smallest response occurred for the 45°/0° case (0.4m). In general the largest mean surge responses occurred at H_s values of 1.5m to 1.75m. 0°/0° and 0°/225° cases gave the largest first order surge response (~1.2m) whilst the smallest responses occurred for the 45°/0° case (0.05m). The largest responses occurred in the largest sea states.

For all of the configurations tested the tendons facing the incoming waves experienced the largest mean tensions apart from the 0°/225° case when the rear tendons gave the largest mean tension. For all the cases the side tendons gave the mean tension values between those of the front and rear tendon tensions. The lowest mean tensions were observed in the rear tendons for the 0°/0° case. The highest mean tensions were observed in the front tendons for the 45°/0° case.

For all of the configurations tested the front and rear tendons gave similar values of dynamic tensions. The mean values of the side tensions were also similar to one another although the values were generally smaller than those found in the front and rear tendons. The lowest dynamic tensions were generally observed in the side tendons. The highest dynamic tensions were observed in the rear tendons for the 0°/0° case. The largest dynamic tensions occurred in the highest sea states.

The unprocessed numerical output showed large spikes at frequencies higher than any of the physical processes. No reasons apart from possible numerical instability could be found to explain this behaviour. In general, modelling of tendons could be enhanced in FAST by modifying the source code or potentially using updated version (i.e.FASTv8). Alternatively, the mooring system could be modelled using different software. It would be also useful to run FAST using additional damping values to determine the effect of viscous damping on the results for this structure.

In general comparisons of the experimental results with the numerical predictions were inconsistent whereby some cases gave very good agreement while in other cases agreement was poor.

The best correlation was obtained for the 0°/0° case with the mean values of surge from the experiments and the numerical predictions using both wind models giving very similar results. For the dynamic surge responses the agreement was also good apart from the cases when H_s=1.75 and 2.75m where both numerical models overestimated. All the results for the tendon tensions showed good agreement.

For the 0°/225° case the mean values of surge motions from the experiments and the constant wind numerical predictions were very similar. The turbulent model whilst following the correct trend tended to underestimate the mean surge response. For the dynamic surge responses the agreement was also good although the turbulent model slightly under predicted the first order surge motions. For this condition all the results for the mean tendon tensions showed good agreement whilst for the dynamic tensions the turbulent model gives good agreement with the experimental results. The constant wind model showed the correct trend but under predicted the dynamic tensions.

For the 45°/0° case the trend in the mean values of surge motions from the experiments and the numerical predictions were very similar, the turbulent model providing the best agreement with the experiment results. For the first order surge motion responses the agreement was also good although both numerical models overestimated when H_s=1.75 and 2.75m. For this condition all the results for the mean tendon tensions showed good agreement. For dynamic tensions the turbulent model gave good agreement with the experimental results. The constant wind model while showing the correct trend under predicted the dynamic tensions similar to the 0°/225° case.

Chapter 8

Discussion and Conclusions

This chapter provides a summary of the main results presented in this thesis, and describes how the research aims and objectives have been met. Following this, a brief discussion on the proposed FOWT is presented. Finally, recommendations are given for areas of future research.

8.1 Discussion

The first research aim listed in Chapter 1 was as follows:

- *To review the available literature on numerical and experiment methodologies for the prediction of the performance of floating wind turbine systems.*

Chapter 2 addressed this by presenting an overview of numerical and experimental methods, from the linear frequency-domain approach to state-of-the-art fully coupled analysis methods (time domain simulation methods). A discussion of each method's strengths and weaknesses was also provided. The chapter also provided a review of physical modelling of FOWTs, prediction of hydrodynamic behaviour of FOWTs using experimental and numerical methods, offshore floating renewable energy developments, classification of offshore wind turbines. This study highlighted the advantages of the TLP as a reliable and low cost solution for offshore wind. The chapter highlighted the necessity of employing time domain methods due to the complex interaction between the system and the environment. It also highlighted the challenges of performing accurate experimental investigation of FOWTs.

The second research aim listed in Chapter 1 was as follows:

- *To describe the state of the art numerical tools used in this research and provide results of a program testing study*

In Chapter 3 the 'Numerical investigation of the TLP' the theoretical background of the numerical programmes was presented along with their assumptions and limitations. It was shown that due to the nonlinear nature of the FOWT a time domain approach is required. It was also shown that as well as the hydrodynamic loading it is also important to correctly model the aerodynamic loads in order to take into account the strong interaction between the aerodynamic loads and the platform response. As was demonstrated in the irregular wave cases in particular the 0°/225° condition which showed the strong influence of the wind direction on the mean surge of the platform. It was also evident from these tests that variations in wave direction have less effect on the platform response than changes in wind direction.

The results of a correlation study using the MIT/NREL TLP floater carrying the NREL offshore 5 MW baseline wind turbine were presented and it was demonstrated that the results from the study were comparable to those from the NREL study. This provided confidence that the modelling procedure for the FOWT was correct.

The third research aim listed in Chapter 1 was as follows:

- *To present the experimental arrangement and test procedure for TLP wind turbine*

The experimental methodology used to investigate the hydrodynamic performance of the TLP type wind turbine was presented in Chapter 4. Model design and construction, scaling, ballasting, instrumentation, instrument calibration, wave calibration, tendon setup and calibration were presented. An overview of the rational for the test matrix was given. The procedure for carrying out the experiments was described. The calibration and model preparation results showed the fidelity of the model and the instruments used for this study.

This chapter highlighted the practical challenges relating to scaling of the mass properties of the FOWT and physical modelling of the tendons. Although some difficulties were encountered in correctly modelling KG and the inertias of the FOWT model, the natural periods of the entire system agreed with the similar studies (Rodriguez et al., 2014). In hindsight the problems encountered with correctly setting the mass properties of the model could have been mitigated by constructing the model from a lighter weight material although the all-aluminium construction produced a model which just met the criteria for model stiffness. It is therefore recommended that for future work of this nature the model construction and the materials selected should be considered with great care. The system developed to rotate the model in order to represent the different wave directions proved to be easy to use and was found to only slightly affect the target values for the static tension of the tendons as the model was rotated.

The fourth research aim listed in Chapter 1 was as follows:

- *To determine the hydrodynamic properties of the FOWT concept and investigate the effect of wind by performing free oscillation tests using numerical and experimental methods*

The method to obtain the natural periods of the FOWT from experiments was presented in Chapter 5 and the results were compared to numerical predictions.

The repeatability of the natural period was found to be extremely good for surge in the no wind and predefined thrust cases. The natural periods in surge with Software in the loop and in yaw were not as consistent as in the no wind condition. Heave and pitch natural period values were widely scattered due to the difficulties of performing these tests. As expected the virtual mass values closely followed the trends observed in the natural frequency results.

Damping values were found to be less repeatable than the natural periods of the system. Results for surge no wind and with predefined thrust had standard deviations of less than 5%. High scattered results were observed for surge with SIL, which may be due to controller instability. The standard deviation obtained from the yaw tests was high, but the results were acceptable. Results for heave and pitch were unreliable.

The results from the numerical study showed good correlation in surge with the experimental values. Comparison of pitch and heave proved much more problematic. In general the numerical predictions underestimated the values of damping obtained from the experiments with surge providing the closest correlation while heave and pitch damping coefficients obtained from numerical predictions were found to be unreasonably small. This may explain to some extent the general nature of the motion numerical predictions which showed that the surge predictions usually provided the closest match to those measured in the experimental study. The surge, heave and pitch natural periods obtained from the measurements closely matched those obtained from the numerical predictions. This shows that the added mass values used in the numerical study were consistent with those measured in the experiments.

The fifth research aim listed in Chapter 1 was as follows:

- *To investigate the platform behaviour in regular waves and simulated wind conditions using a Software In the Loop (SIL) system and compare with numerical predictions.*

The main results found from this study showed that the surge responses of the FOWT dominate all of the motion responses. The surge responses for the case with no wind are larger than those obtained with either of the wind simulated cases. The effect of wave heading has only a small effect on the motion responses as also found in (Rodriguez et al., 2014).

The largest dynamic tensions were observed for the down wave tendons (5 and 6) with the side tendons showing the smallest variation. The maximum tensions coincided with the maximum surge motion at a period of around 24s which is quite close to previously published results reported in (Rodriguez et al., 2014) . The effect of the wind model did not significantly affect the dynamic tensions while the wave heading had a significant effect.

Motion RAO's and tension transfer functions obtained from the experimental results were compared to those from the numerical results for 0° head seas and no wind cases. In general good correlation was evident over the 5-20 sec wave period whilst the numerical responses over predicted in the region of the surge natural period.

The sixth research aim listed in Chapter 1 was :

- *To characterise the design performance of the FOWT in terms of hydrodynamic responses to realistic environmental loading using numerical and experimental methods.*

The experimental results and comparison of numerical predictions of the performance of the FOWT in realistic environmental conditions were presented in Chapter 7. The details of the wave and wind (turbulent and constant wind speed) models used in the investigation were provided. Detailed results were presented for the most severe operational condition.

The experimental results showed that for all environmental conditions the motions of the platform are generally small. Surge, heave, sway, pitch, roll and yaw natural frequencies are outside the range of all of the wave and wind spectra with only yaw overlapping slightly. The most significant responses were found in the first and second order surge motions. Depending on the wind direction the platform was observed to drift both up wave and down wave illustrating the significant contribution of the aerodynamic loading to the overall hydrodynamic response.

The case with co linear wind and waves (0°/0°) gave the largest mean surge response whilst the smallest response occurred for the 45°/0° case. In general the largest mean surge response (drift) occurred at H_s values of 1.5m to 1.75m whilst the largest first order responses were observed in the largest sea states.

For all of the configurations tested the tendons facing the incoming waves generally experienced the largest mean tensions as was found in the regular wave tests. For the 0°/225° case the rear tendons give the largest mean tension, the aerodynamic loading being dominant for this condition. The lowest mean tensions were observed in the rear tendons for the 0°/0° case. The highest mean tensions were observed in the front tendons for the 45°/0° case.

For all of the configurations tested the front and rear tendons gave similar values of dynamic tension. The side tensions were also similar to one another although the values were generally smaller and those found in the front and rear tendons. The lowest dynamic tensions were generally observed in the side tendons. The highest dynamic tensions were observed in the rear tendons for the 0°/0° case. The dynamic tensions increased with increasing environmental conditions. For all of the cases investigated none of the tendons approached a slack condition. The maximum tension (mean + dynamic) occurring during the 0°/0° H_s = 1.75m condition is well below the maximum tendon breaking strength.

Problems were identified with the nature of the numerical predictions. Peak values of the pdf's obtained from the numerical predictions were much larger than those obtained from the experiments. Furthermore, the bandwidth of the numerical pdf's was much narrower than those obtained from the experiments. The frequency analysis of the numerical outputs showed that for every case large spikes were observed at frequencies higher than any of the physical processes involved. A significant processing was required before the analysis of the numerical output could be carried out. No convincing explanation of this unusual behaviour apart from possible numerical instability could be found.

Even after processing in general comparisons of the experiment results with the numerical predictions were inconsistent. The best correlation was obtained for the 0°/0° case with mean values of surge from the experiments and the numerical predictions using both wind models giving very similar results. For dynamic surge the agreement was also good apart from the cases H_s=1.75 and 2.75m where both numerical models overestimated. All the results for the tendon tensions showed good agreement.

For the 0°/225° case the mean values of surge from the experiments and the constant wind numerical predictions were very similar. The turbulent model whilst following the correct trend tended to underestimate the mean surge response. For the dynamic surge the agreement was also good although the turbulent model slightly under predicted the first order surge motions. Results for the mean tendon tensions showed good agreement while for the dynamic tension the turbulent model gave better agreement with the experimental results. The constant wind model showed the correct trend but under predicted the dynamic tensions.

For the 45°/0° case the trend in the mean values of the surge motions as obtained from the experiments and the numerical predictions were very similar, the turbulent model providing the best agreement with the experiment results. For the first order surge motion the agreement was also good although both numerical models again overestimated for H_s=1.75 and 2.75m. For this condition all the results for the mean tendon tensions showed good agreement. For dynamic tensions the turbulent model gave good agreement with the experimental results. The constant wind model while showing the correct trend under predicted the dynamic tensions similar to the 0°/225° case.

Although a large number of tests carried out within the framework of this study, no tests were performed in irregular waves without wind. It would be worthwhile to carry out irregular wave test without wind in order to assess the breakdown between aero- and hydrodynamic effects, and hence explain possible problematic cases. It should be definitely considered for further experimental study.

8.2 Conclusions

This thesis describes the characterisation of a FOWT using two different approaches: experimental and numerical. The major contribution of the study consisted of an extensive experimental investigation of a state-of-the art FOWT concept. The results drawn from this work were summarised and discussed in detail in the previous section.

The experimental and numerical results showed that for all the environmental conditions investigated the motions of the platform are generally small. All of the platform natural frequencies were found to be outside the range of all of the wave and wind spectra. The most significant responses were found to be the first and second order surge responses.

For all of the cases investigated none of the tendons approached a slack condition and the maximum tension measured was well below the maximum tendon breaking strength.

The wind direction was found to have a significant contribution to the overall hydrodynamic response of the platform. This shows the important influence of the SIL system on the platform response. The variations in wave directions were found to have less effect on the platform responses than changes in the wind direction.

Difficulties encountered in correctly modelling the KG and the inertias of the FOWT model, were due to the large mass of the un-ballasted model. It is recommended that for future work the model construction and the materials selected should be considered with great care.

The numerical predictions underestimated the values of damping obtained from the experiments while surge, heave and pitch natural periods obtained from the experimental measurements closely matched those obtained from the numerical predictions.

This research has shown that, at present, experiments are essential in order to characterise the hydrodynamic performance of FOWTs. In some cases the numerical predictions were very close to the results obtained from the experiments but in other cases the numerical model failed to accurately predict the platform responses. Some aspects of the experimental study were also problematic, in particular obtaining the correct mass properties whilst insuring adequate model stiffness in the roll and pitch axes. The experimental study also proved to be a very time consuming process compared to the numerical predictions.

During this study it was found that, without a doubt, the preparation of the experimental campaign requires a great deal of attention and planning. The most challenging of these being the preparation of the model, the calibration of the instrument systems and processing the vast amount of data gathered from the tank. In addition to this for such a long testing campaign the use of daily system checks is an equally important factor to ensure some control over the quality of the measurements.

Numerical methods can be used to obtain results in a much shorter time compared to experimental methods but a number of problems were encountered with the numerical approach. These included the spikes evident in the spectral analysis of the unprocessed numerical results which could not be convincingly explained. The results from the two different wind models could be inconsistent. For some cases neither of the numerical models agreed with the experiment results. The largest responses of the FOWT was in surge and for most of the cases investigated the numerical predictions were reasonably good agreement with the measurements obtained from the experiments.

8.3 Recommendations for Future Research

Recommendations for further studies relating to the work presented in this thesis are briefly outlined below.

- Given the over prediction of many of the dynamic responses observed in the regular and irregular studies by FAST, the damping model employed needs to be investigated in detail.

- The use of turbulent and constant wind models should be investigated further in order to understand why these models give inconsistent results in some cases.

- The numerical study should also be extended to investigate the reasons for the unusual spikes obtained in the unprocessed FAST output files. For example effects of water depth, tendon stiffness and hydrodynamic coefficients on the nature of the numerical predictions should be investigated.

- For this study the mooring line tensions were calculated internally in FAST. The complex TLP mooring system could be modelled using an appropriate numerical simulation tool such as Orcaflex to replace the simplified mooring line module used in the numerical predictions.

- The results have shown the importance of the aerodynamic loading in the response of the platform. Investigation into the performance of the SIL system is required in order to ensure that the system is operating correctly. The study should be extended to investigate the effect of other parameters, such as control stability.

References

2015. Special Issue : World Wind Energy Report 2014.

February 2016. Wind in Power : 2015 European Statistics. The European Wind Energy Association

BAYATI, I., BELLOLI, M., FERRARI, D., FOSSATI, F. & GIBERTI, H. 2014. Design of a 6-DoF robotic platform for wind tunnel tests of floating wind turbines. *Energy Procedia,* 53**,** 313-323.

BIRAN, A. & PULIDO, R. L. 2014. *Ship Hydrostatics and Stability*, Elsevier, Second Edition.

BOSSANYI, E. A. December, 2003. GH Bladed Theory Manual. Issue No. 12, 282/BR/009, Bristol, UK: Garrad Hassan and Partners Limited.

BUTTERFIELD, S., MUSIAL, W. & JONKMAN, J. October 2007. Overview of Offshore Wind Technology. *Chinese Renewable Energy Industry Association WindPower Shanghai Conference.* Shanghai, China.

BUTTERFIELD, S., MUSIAL, W., JONKMAN, J. & SCLAVOUNOS, P. 2007. Engineering Challenges for Floating Offshore Wind Turbines. *Offshore Wind Conference* Copenhagen, Denmark.

ÇENGEL, Y. A. & CIMBALA, J. M. 2006. *Fluid Mechanics : fundamentals and applications* 1st Edition. New York : McGraw-Hill.

CERMELLI, C., RODDIER, D. & AUBAULT, A. Windfloat: a floating foundation for offshore wind turbines, Part II: Hydrodynamic analysis. 28th International Conference on Ocean, Offshore and Arctic Engineering OMAE2009, 2009 Honolulu, HI, USA.

CHENG, P. W. 2002. *A Reliability Based Design Methodology for Extreme Responses of Offshore Wind Turbines.* PhD Dissertation, Wind Energy Research Institute, Delft University of Technology, Delft, The Netherlands.

CHRISTENSEN, B. 2009. Danish Windmill Production before and after Poul La Cour - and the first golden age of wind power 1906-1920 in Wind Power - the Danish Way, Poul La Cour Foundation, Askov, Denmark.

CHUJO, T., MINAMI, Y., ISHIDA, S., NIMURA, T. & INOUE, S. Model Experiments on the motion of a spar type floating wind turbine in wind and waves. 30th International Conference on Ocean, Offshore and Arctic Engineering, OMAE2011, June 19-24,2011 2011 Rotterdam, The Netherlands.

DAY, A. H., BABARIT, A., FONTAINE, A., HE, Y. P., KRASKOWSKI, M., MURAI, M., PENESIS, I., SALVATORE, F. & SHIN, H. 2015. Hydrodynamic modelling of marine renewable energy devices: A state of the art review. *Ocean Engineering,* 108**,** 46-69.

DNV-OS-J103 Design of Floating Wind Turbines. . Technical Report, Det Norske Veritas AS, June 2013. Offshore Standard.

ESTEBAN, M. D., DIEZ, J. J., LÓPEZ, J. S. & NEGRO, V. 2011. Why offshore wind energy? *Renewable Energy,* 36**,** 444-450.

FALTINSEN, O. M. 1990. *Sea Loads on Ships and Offshore Structures,* Cambridge University Press, Cambridge, UK.

FUKUSHIMA-FORWARD. 2013. Fukushima Floating Offshore Wind Farm Demonstration Project (Fukushima FORWARD).

GOUPEE, A. J., KOO, B., KIMBALL, R. W., LAMBRAKOS, K. F. & DAGHER, H. J. 2012. Experimental Comparison of Three Floating Wind Turbine Concepts. *OMAE 2012.* Rio de Janeiro, Brazil.

HENDERSON, A. R., MORGAN, C. S., SMITH, B., SORENSEN, H. C., BARTHELMIE, R. J. & BOESMANS, B. 2003. Offshore Wind Enegy in Europe, A Review of the State-of-the-Art. *Wind Energy,* 6**,** 35-52.

HOUSNER, G. W. 1963. Dynamic analysis of fluids in containers subjected to acceleration. *Nuclear Reactors and Earthquakes, Report No. TID 7024, US Atomic Energy Commission, Washington, DC.*

HTTP://SEATWIRL.COM/. *Sea Twirl, Sweeden (Spar)* [Online].

HTTP://WWW.BLUEHGROUP.COM. *Blue H, Netherlands (TLP)* [Online].
HTTP://WWW.DEEPCWIND.ORG. *DeepCwind VolturnUS (US) (Semisubmersible)* [Online].
HTTP://WWW.FLOATINGPOWERPLANT.COM. *Poseidon, Denmark (Semisubmersible)* [Online].
HTTP://WWW.GICON.DE. *GICON-SOF,Germany (TLP)* [Online].
HTTP://WWW.GUSTOMSC.COM. *Gusto Trifloater, Netherlands* [Online].
HTTP://WWW.HYPERWIND.EU/. *HiRR Wind, Spain (Semisubmersible)* [Online].
HTTP://WWW.IDEOL-OFFSHORE.COM. *IDEOL, France (Floater)* [Online].
HTTP://WWW.JMUC.CO.JP. *Japan Marine United (formerly IHI) (Advanced Spar)* [Online].
HTTP://WWW.KYOTO-U.AC.JP. *Kabashima Island, Kyushu* [Online].
HTTP://WWW.MARUBENI.COM. *Marubeni ; Mitsubishi Heavy Industries* [Online].
HTTP://WWW.MES.CO.JP. *Mitsui Zosen (Semisubmersible)* [Online].
HTTP://WWW.MHI.CO.JP. *Mitsubishi Heavy Industries (Semisubmersible)* [Online].
HTTP://WWW.MODEC.COM. *MODEC (Mitsui Ocean Development & Engineering Company) (Floater)* [Online].
HTTP://WWW.NASS-ET-WIND.COM. *Windflo, France (Floater)* [Online].
HTTP://WWW.NAUTICAWINDPOWER.COM/. *Nautica Windpoer AFT (US)* [Online].
HTTP://WWW.NMRI.GO.JP. *National Maritime Research Institute of Japan (Spar)* [Online].
HTTP://WWW.PRINCIPLEPOWERINC.COM. *WindFloat (US/Portugal) (Semisubmersible)* [Online].
HTTP://WWW.RIAM.KYUSHU-U.AC.JP. *Wind Lens, Kyushu* [Online].
HTTP://WWW.SHIMZ.CO.JP. *Shimizu Corporation* [Online].
HTTP://WWW.STATOIL.COM. *Statoil Hywind, Norway (Spar)* [Online].
HTTP://WWW.SWAY.NO/. *Changing The Future of Wind Power, SWAY Concept* [Online]. [Accessed 30/05/2016.
HTTP://WWW.TECHNIP.COM. *Vertiwind, France (Floater)* [Online].
IBERDROLA ENGINEERING & CONSTRUCTION, U. O. S., ORE CATAPULT 2014. TLPWIND UK : "Driving down the cost of offshore wind in UK waters" Deliverable D2.1 Site Selection & Characterisation.
IEC 2009. Wind turbines standard 61400-3. International Electrotechnical Commission.
JONKMAN, B. J. Revised August 26, 2009. TurbSIM User's Guide : Version 1.50. National Renewable Energy Laboratory, Colorado, U.S.
JONKMAN, J. Technical Report, May 2010. Definition of the Floating System for Phase IV of OC3. National Renewable Energy Laboratory (NREL), Golden, CO.
JONKMAN, J., BUTTERFIELD, S., MUSIAL, W. & SCOTT, G. 2009. Definition of a 5-MW Reference Wind Turbine for Offshore System Development. National Renewable Energy Laboratory, Golden, CO.

JONKMAN, J. & MATHA, D. March, 2010. A Quantitative Comparison of the Response of Three Floating Platforms. *European Offshore Wind Conference and Exhibition.* Stockholm, Sweeden.

JONKMAN, J. & MUSIAL, W. 2010. Offshore Code Comparison Collaboration (OC3) for IEA Task 23 Offshore Wind Technology and Deployment. NREL.

JONKMAN, J. & MUSIAL, W. Technical Report, 2010. IEA Wind Task 23 Offshore Wind Technology and Deployment.

JONKMAN, J. M. 2007. *Dynamics Modeling and Loads Analysis of an Offshore Floating Wind Turbine.* PhD Thesis, University of Colorado, Boulder, CO, USA.

JOSELIN HERBERT, G. M., INIYAN, S., SREEVALSAN, E. & RAJAPANDIAN, S. 2007. A Review of Wind Energy Technologies. *Renewable and Sustainable Energy Reviews,* 11**,** 1117-1145.

KALDELLIS, J. K. & KAPSALI, M. 2013. Shifting towards offshore wind energy—Recent activity and future development. *Energy Policy,* 53**,** 136148.

KALDELLIS, J. K., KAPSALI, M. & KATSANOU, E. 2012. Renewable energy applications in Greece—What is the public attitude? *Energy Policy,* 42**,** 37-48.

LEE, H. T., CHEN, S. H. & KANG, H. Y. 2004. A study of Generalised Reduced Gradient Method with Different Search Directions. 1**,** 25-38.

LONGUET-HIGGINS, M. S. 1952. On the statistical distribution of the heights of sea waves. *Journal of Marine Research,* 11**,** 245-266.

M.ST.DENIS & W.J.PIERSON 1953. On the motion of ships in confused seas. *TRANS. SNAME,* 61.

MARTIN, H. R., KIMBALL, R. W., VISELLI, A. M. & GOUPEE, A. J. 2012. Methodology for wind/wave basin testing of floating offshore wind turbines. *OMAE 2012.* Rio de Janeiro, Brazil.

MATHA, D. 2009. *Model Development and Loads Analysis of an Offshore Wind Turbine on a Tension Leg Platform, with Comparison to Other Floating Turbine Concepts.* Thesis M.E., University of Colorado, Boulder.

MIT. 1998. *WAMIT User Manual* [Online]. WAMIT, Inc. MA, USA.

NIELSEN, F. G., ARGYRIADIS, K., FONSECA, N., LE BOULLUEC, M., LIU, P., SUZUKI, H., SIRKAR, J., TARP-JOHANSEN, N. J., TURNOCK, S. R., WAEGTER, J. & ZONG, Z. 2009. Ocean, Wind and wave energy utilisation. *17th International Ship and Offshore Structures Congress.* Seoul, Korea.

PEREZ, L. R. 2014. *Design, Testing and Validation of a Scale Model Semisubmersible Offshore Wind Turbine Under Regular/Irregular Waves and Wind Loads.* Master of Science, University of Strathclyde.

PRYOR, S. C. & BARTHELMIE, R. J. 2001. Comparison of potential power production at on- and offshore sites. *Wind Energy,* 4**,** 173-181.

RAO, N. 2004. *Mechanical Vibrations*, Fourth Edition NJ, USA : Pearson Education, Inc.

REPORT, T. May 2013. An Overview - Floating Offshore Wind Foundations : Industry Consortia and Projects in the United States, Europe and Japan Main(e) International Consulting LLC.

RIDDER, E., OTTO, W. & ZONDERVAN, G. J. 2013. State of the art model testing techniques for floating wind turbines.

RODDIER, D., CERMELLI, C., AUBAULT, A. & WEINSTEIN, A. 2010. WindFloat: A floating foundation for offshore wind turbines. *Journal of Renewable and Sustainable Energy,* 2.

RODRIGUEZ, R. Z., ALONSO, P. G., LOPEZ, J. A., MARTIN, V. D., DINOI, P., SIMOS, A. N. & IGLESIAS, A. S. 2014. Model Scale Analysis of a TLP Floating Offshore Wind Turbine. *OMAE2014.* San Francisco, California, USA.

S.K.CHAKRABARTI 1987. *Hydrodynamics of Offshore Structures*, Computational Mechanics Publications Springer-Verlag.

SAJJADI, S. G. & HUNT, J. 2003. Wind Over Waves II: Forecasting and Fundamentals of Applications. Horwood Publishing Limited.

SHIN, H., KIM, B., DAM, P. T. & JUNG, K. Motion of OC4 5MW Semisubmersible Offshore Wind Turbine in irregular waves. 32nd International Conference on Ocean Offshore & Arctic Engineering, OMAE2013-10463, 2013 Nantes, France.

TRACY, C. 2007. *Parametric Design of Floating Wind Turbines.* Master of Science, Massachusetts Institute of Technology (MIT).

WALTER MUSIAL, N. & BONNIE RAM, E. September 2010. Large-Scale Offshore Wind Power in the United States NREL.

WANG, C. M., UTSUNOMIYA, T., WEE, S. C. & CHOO, Y. S. 2010. Research on floating wind turbines : a literature survey. *The IES Journal Part A : Civil and Structural Engineering,* 3**,** 267-277.

WATSON, G., HILL, B., COURTNEY, F., GOLDMAN, P., CALVERT, S., THRESHER, R., ASSIMAKOPOULOS, E., LYONS, J. & BELL, B. 2005. A Framework for Offshore Wind Energy Development in the United States. Massachussetts Technology Collaborative (MIT), U.S. Department of Energy and GE.

WAYMAN, E., SCLAVOUNOS, P., BUTTERFIELD, S., JONKMAN, J. & MUSIAL, W. 2006. Coupled dynamic modeling of floating wind turbine systems. *Offshore Technology Conference* Houston, Texas.

WWW.WINDSEA.NO. 2016. *WindSea* [Online].

Appendix A

In the following graphs wave spectra and probability density functions of wave heights for each sea state are presented.

A.1 Sea State N4

Table A 1 Wave analysis results for sea state N4

Parameter	Unit	Target	Calibration	Inline	Tank
	m				
	m				
	m				
T_p	sec	5.44	5.290	5.847	5.071
0.75		0.729	0.671	0.733	
H_s(spectrum)		0.75	0.727	0.673	0.721

$H_{(1/3)}$ 0.75
0.708 0.650
0.711
H_s(elevation)

Wave spectra

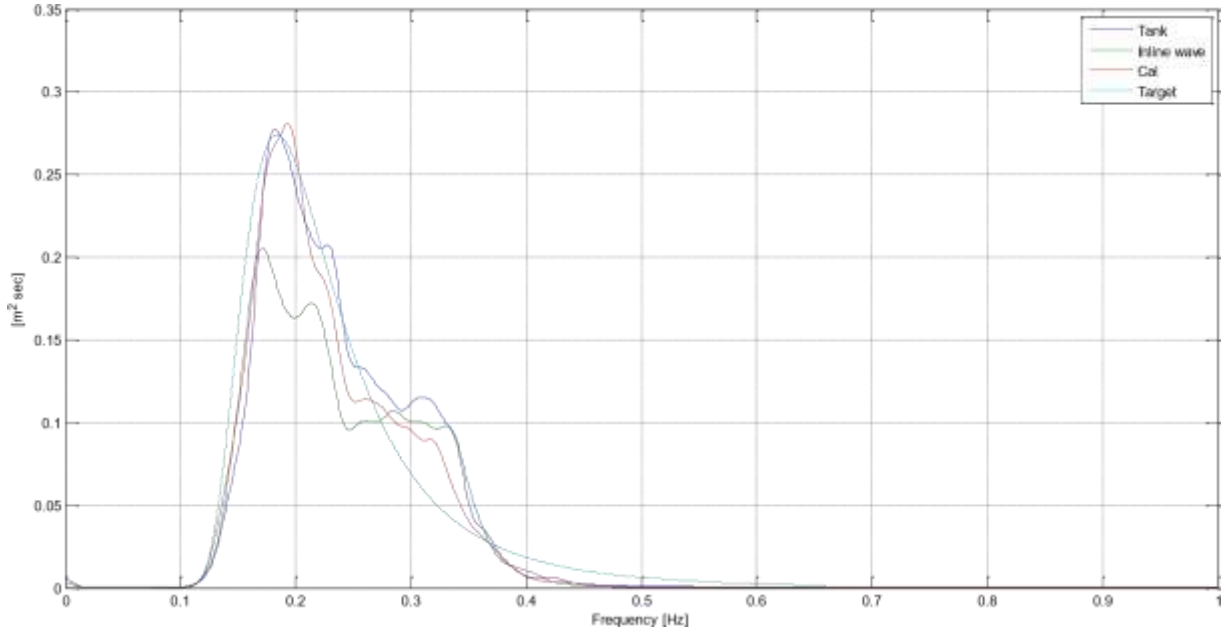

Figure A 1 Wave spectra : Tank Probe, Inline Probe, Calibration and Target for sea state N4

Waveheight Probability Density Functions [Rayleigh]

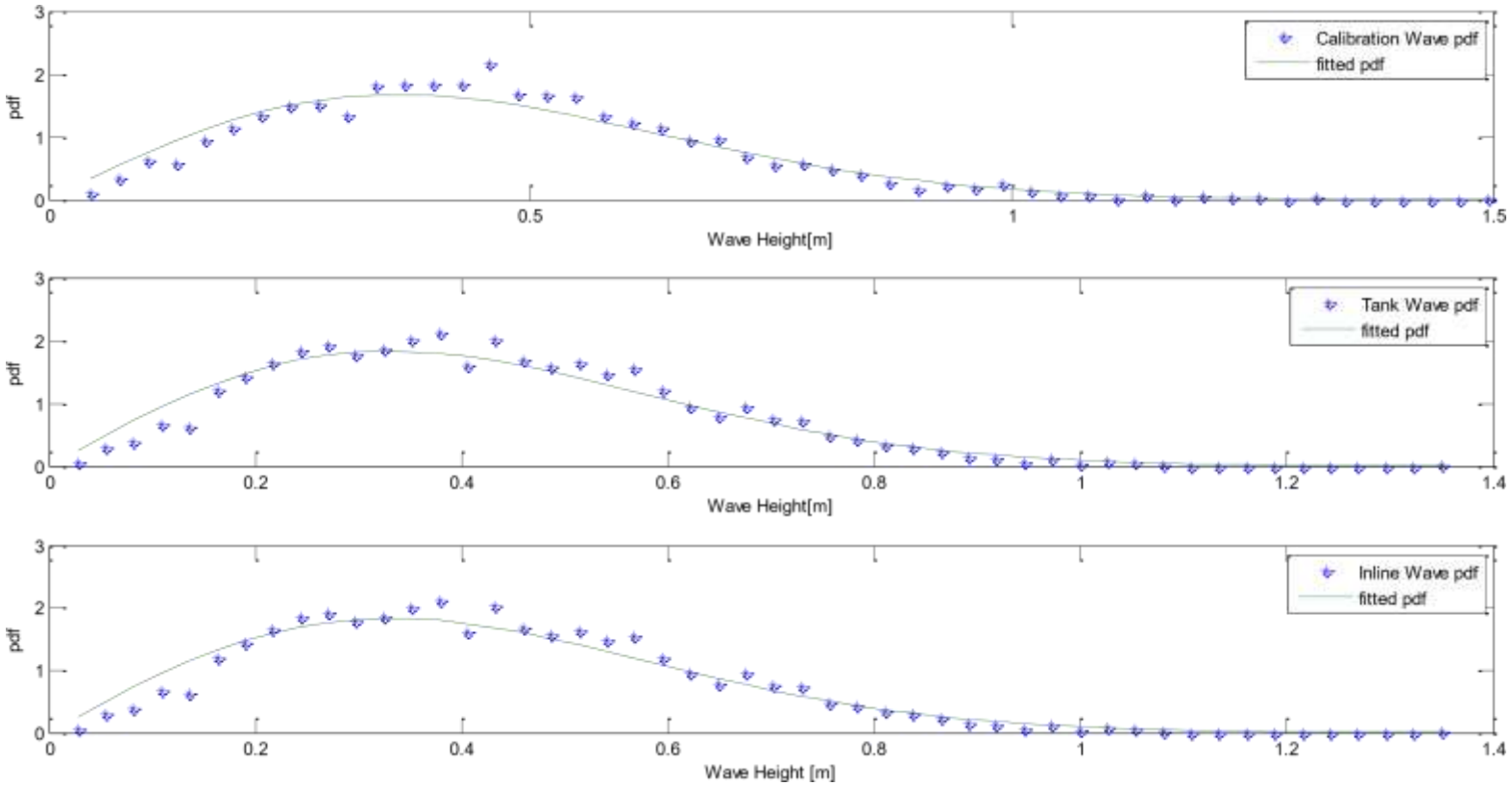

Figure A 2 Probability density functions of wave height : calibration, tank and inline wave for sea state N4

A.2 Sea State N5

Table A 2 Wave analysis results for sea state N5

Parameter	Unit	Target	Calibration	Inline	Tank
	m				
	m				
	m				
T_p	sec	6.36	5.464	6.134	5.680

1.194

1.25 1.235 1.226 1.235

$H_{(1/3)}$ 1.25
1.199 1.167

H_s(elevation)
1.25 1.225
1.212 1.228

H_s(spectrum)

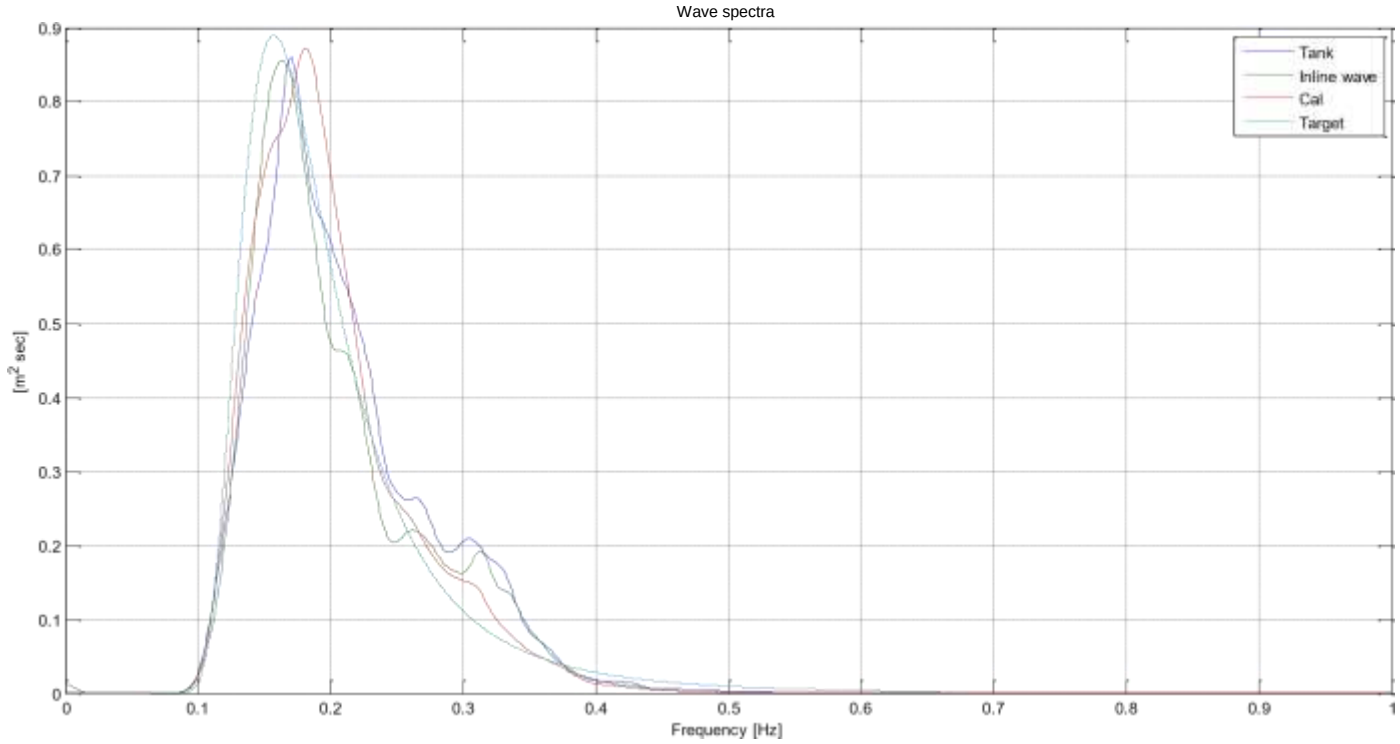

Figure A 3 Wave spectra : Tank Probe, Inline Probe, Calibration and Target for sea state N5

Waveheight Probability Density Functions [Rayleigh]

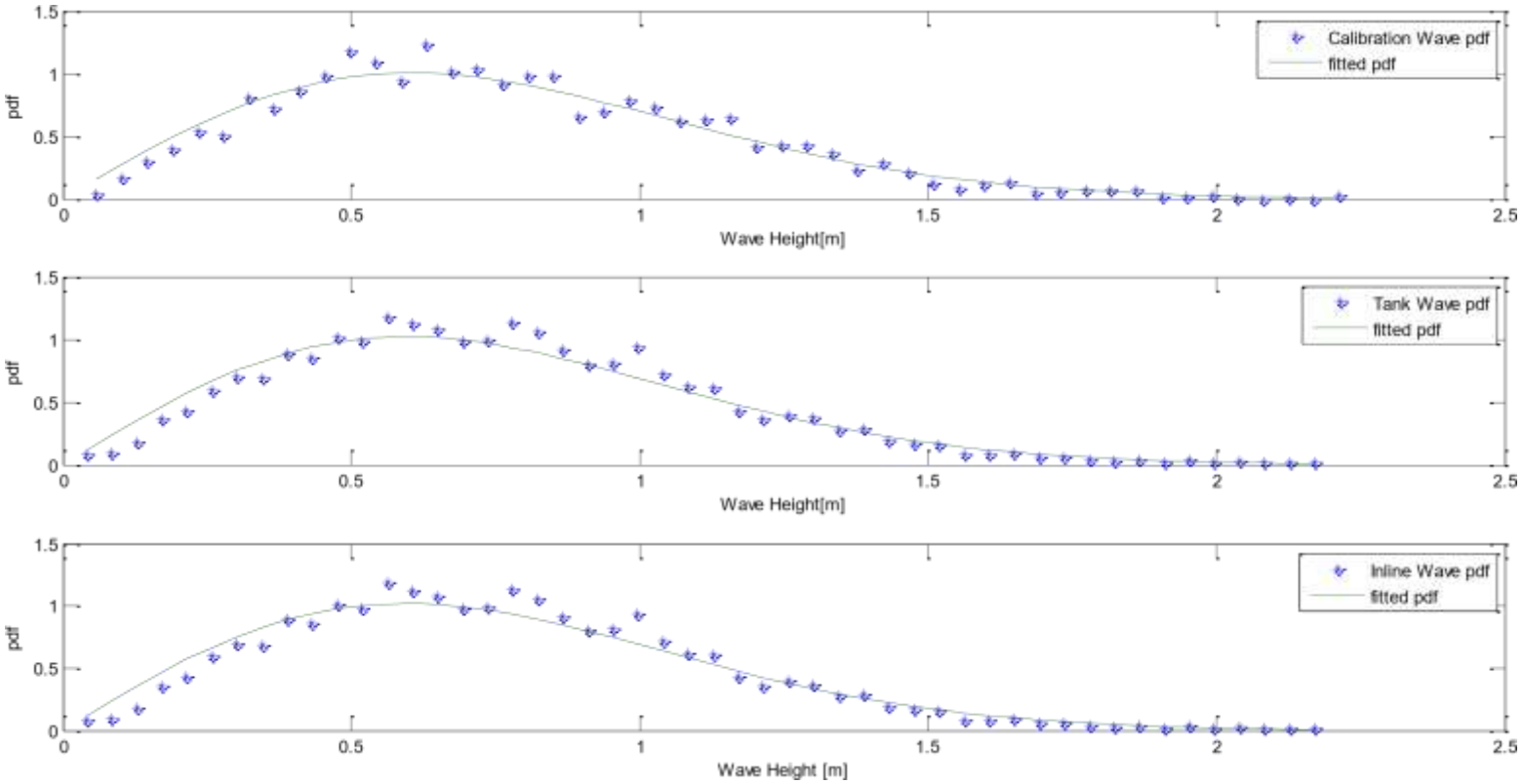

Figure A 4 Probability density functions of wave height : calibration, tank and inline wave for sea state N5

A.3 Sea State N2

Table A 3 Wave analysis results for sea state N2

Parameter	Unit	Target	Calibration	Inline	Tank
	m				
	m				
T_p	sec	6.61	5.547	6.193	5.730
	1.415				
H_s(elevation)		1.50	1.463	1.446	1.460
H_s(spectrum)		1.50	1.487	1.446	1.471

$H_{(1/3)}$
m
1.50
1.418
1.406

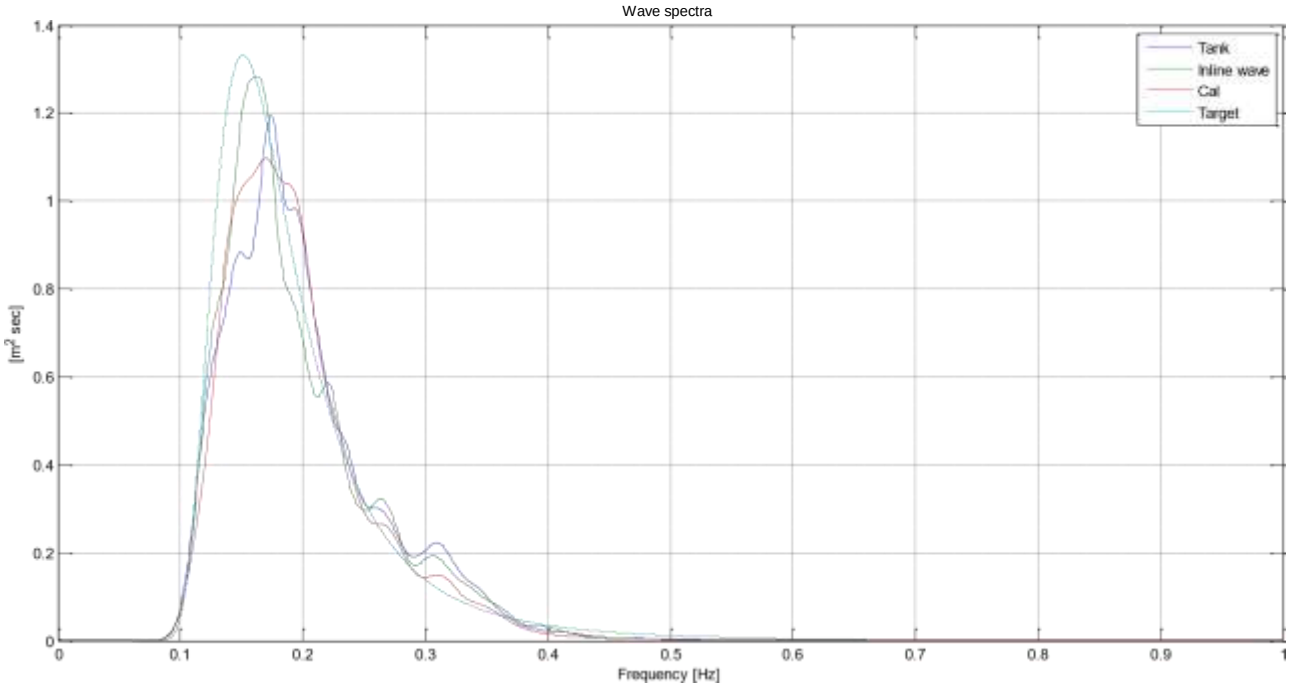

Figure A 5 Wave spectra : Tank Probe, Inline Probe, Calibration and Target for sea state N2

Waveheight Probability Density Functions [Rayleigh]

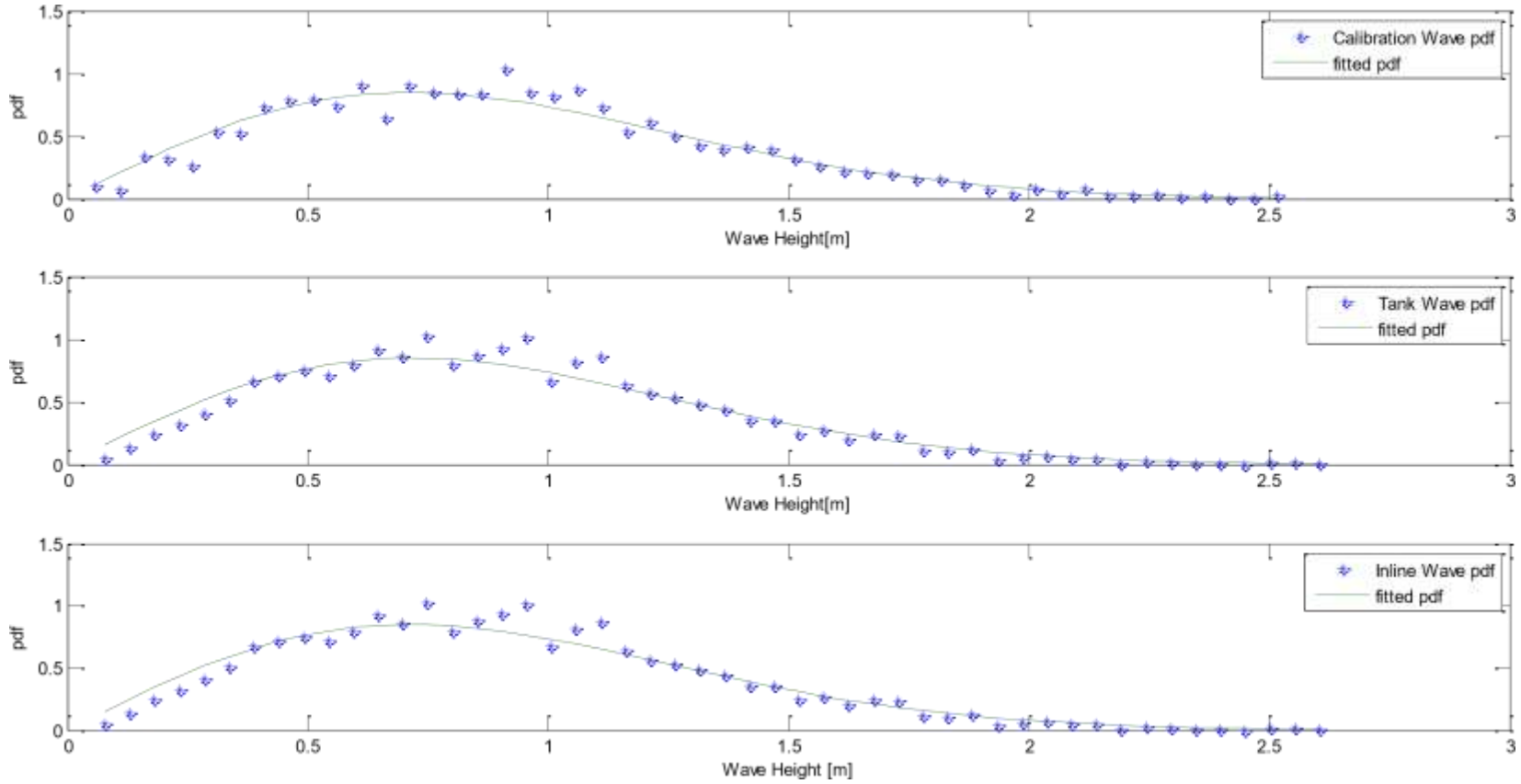

Figure A 6 Probability density functions of wave height : calibration, tank and inline wave for sea state N2

A.4 Sea State N6

Table A 4 Wave analysis results for sea state N6

Parameter	Unit	Target	Calibration	Inline	Tank
$H_{(1/3)}$	m				
	m				1.75
T_p	sec	6.86	5.790	6.025	5.662
					1.678
	1.629				1.720
H_s(elevation)		1.75	1.703	1.757	1.661
H_s(spectrum)		1.75	1.683	1.752	1.625

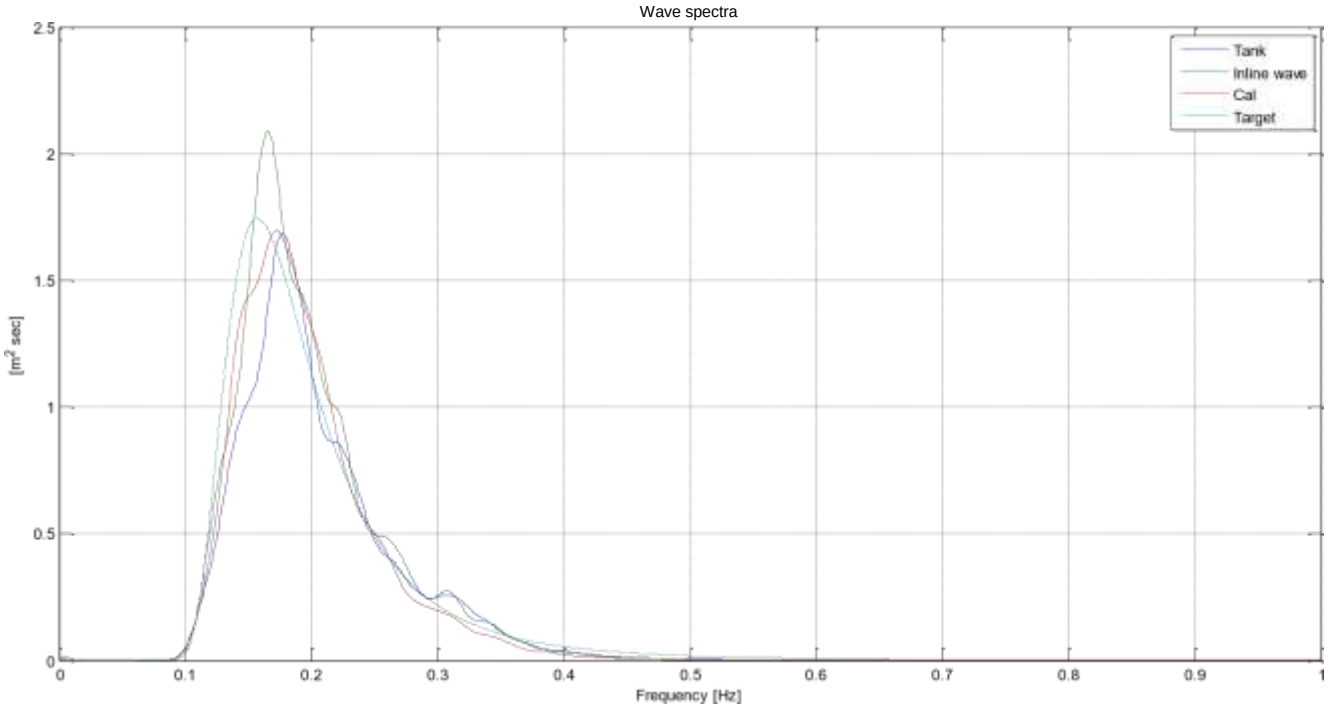

Figure A 7 Wave spectra : Tank Probe, Inline Probe, Calibration and Target for sea state N6

Waveheight Probability Density Functions [Rayleigh]

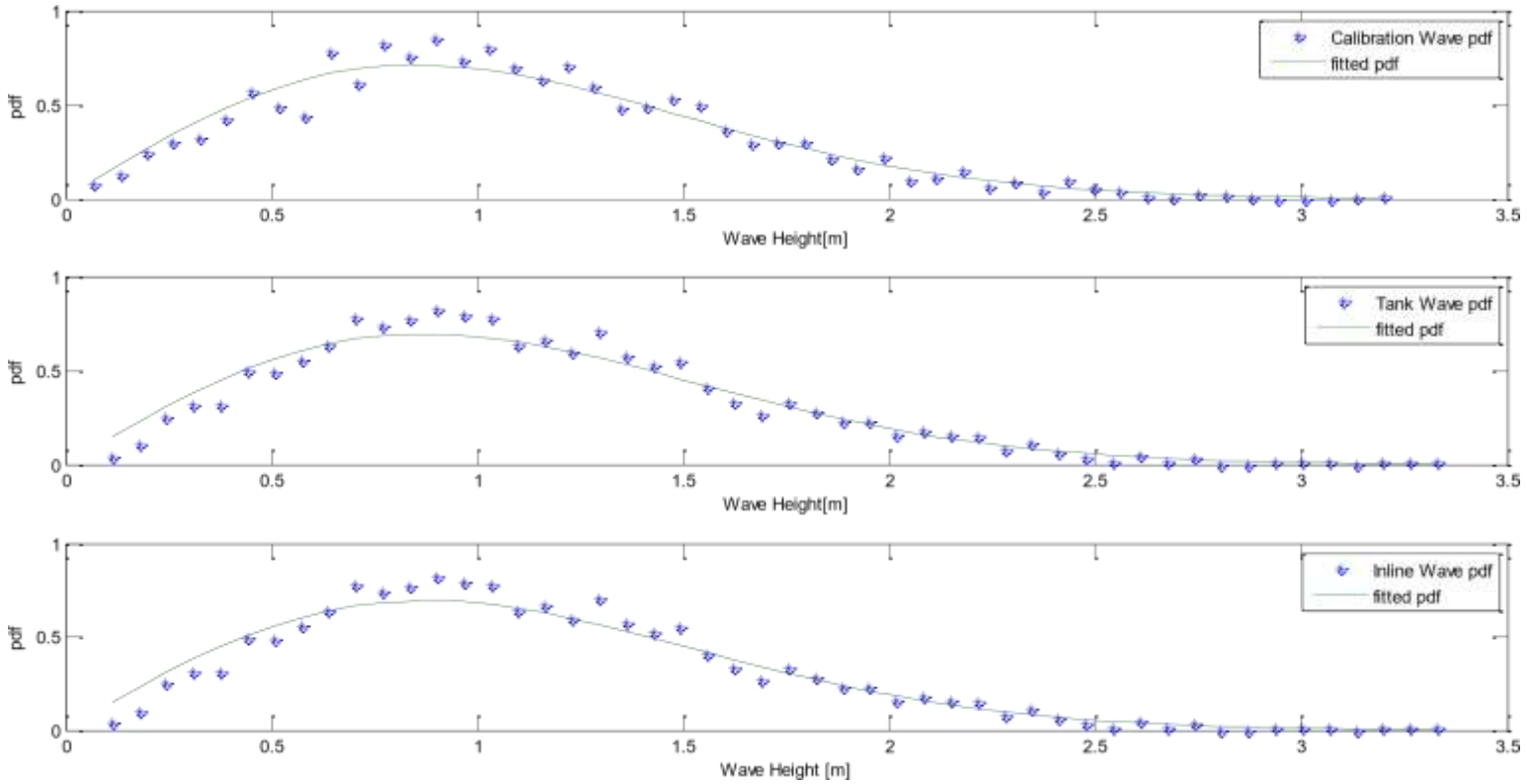

Figure A 8 Probability density functions of wave height : calibration, tank and inline wave for sea state N6

A.5 Sea State N7

Table A 5 Wave analysis results for sea state N7

Parameter	Unit	Target	Calibration	Inline	Tank
	m				
	m				
	m				
T_p	sec	7.80	2.689	2.768	2.647
H_s(elevation)		2.75	2.726	2.716	2.665
H_s(spectrum)		2.75	7.690	7.499	8.095

Wave spectra

$H_{(1/3)}$
2.75
2.689
2.768
2.647

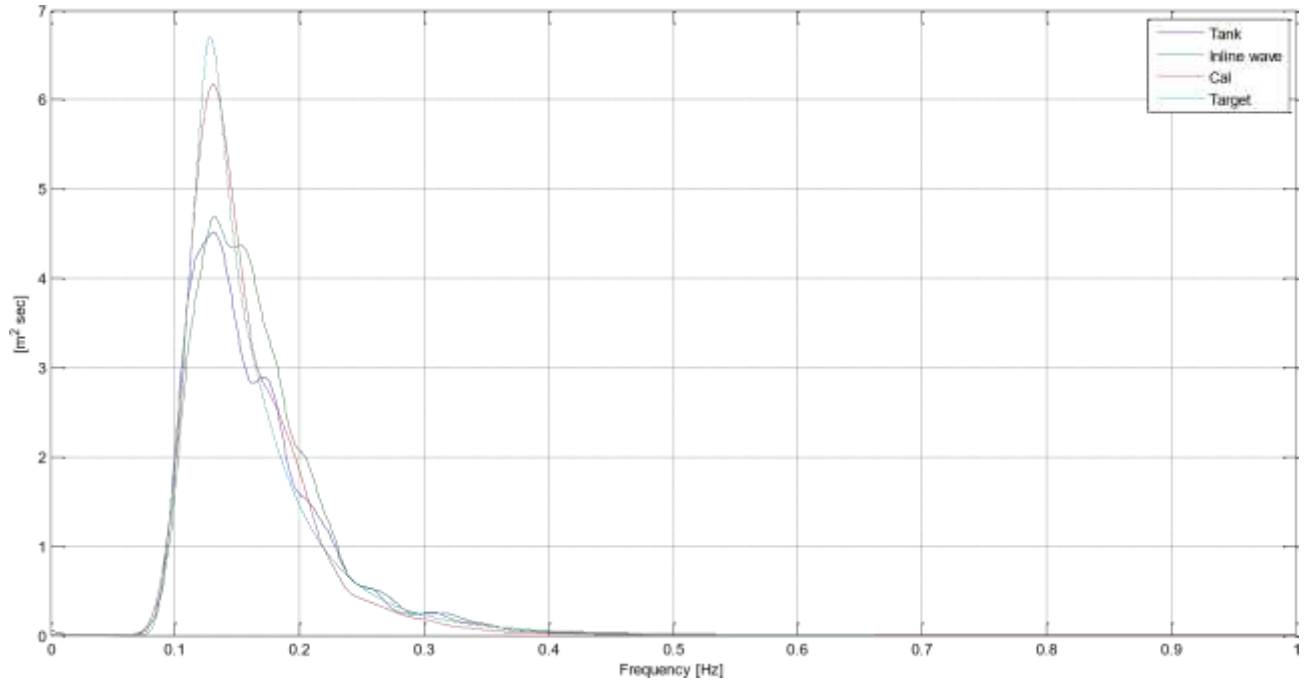

Figure A 9 Wave spectra : Tank Probe, Inline Probe, Calibration and Target for sea state N7

Waveheight Probability Density Functions [Rayleigh]

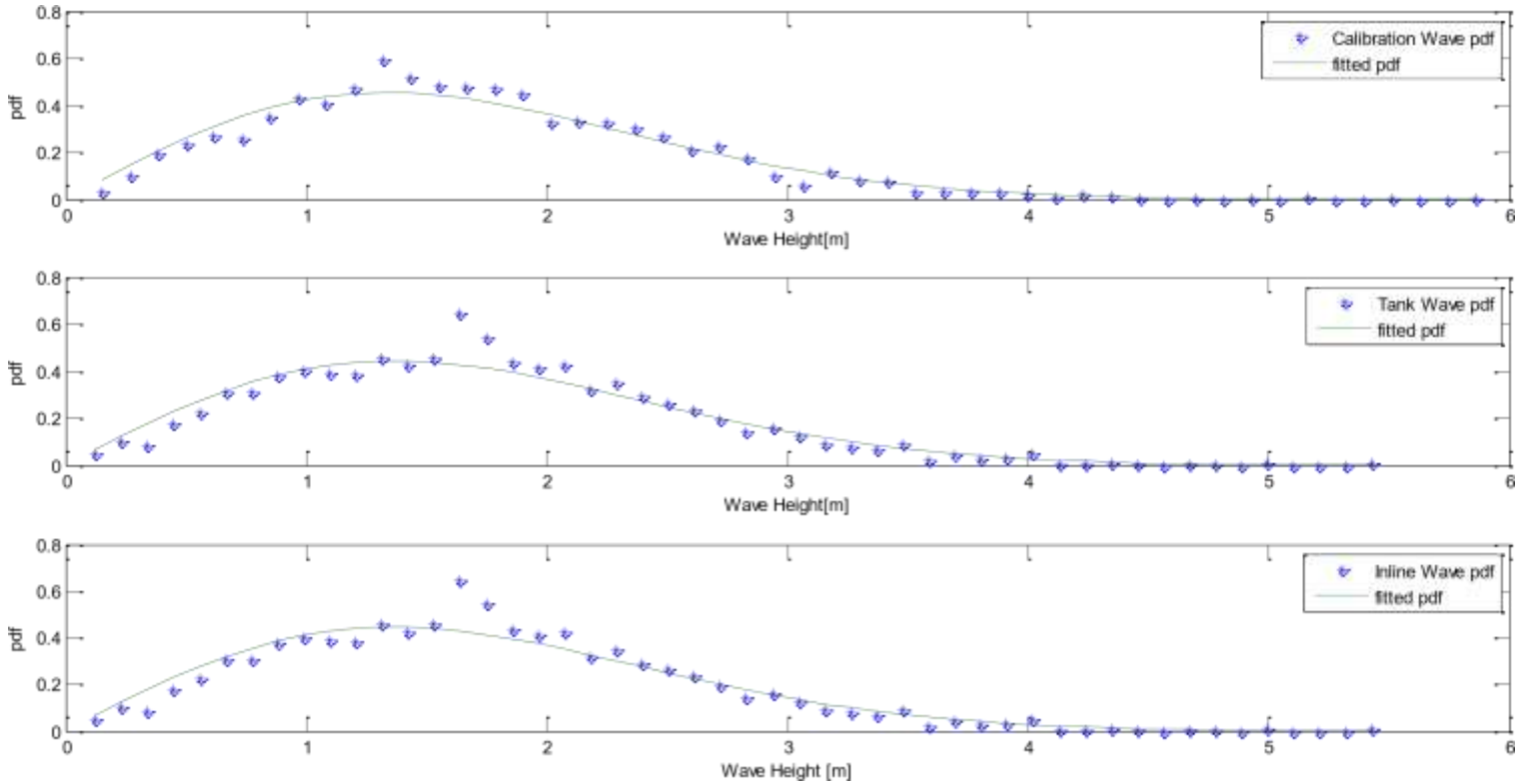

Figure A 10 Probability density functions of wave height : calibration, tank and inline wave for sea state N7

A.6 Sea State N1

Table A 6 Wave analysis results for sea state N1

Parameter	Unit	Target	Calibration	Inline	Tank
	m				
	m				
	m				
T_p	sec	9.00	8.805	8.736	8.863
H_s(elevation)		4.55	4.632	4.434	4.688
H_s(spectrum)		4.55	4.602	4.625	4.643

$H_{(1/3)}$
4.55
4.603
4.377
4.581

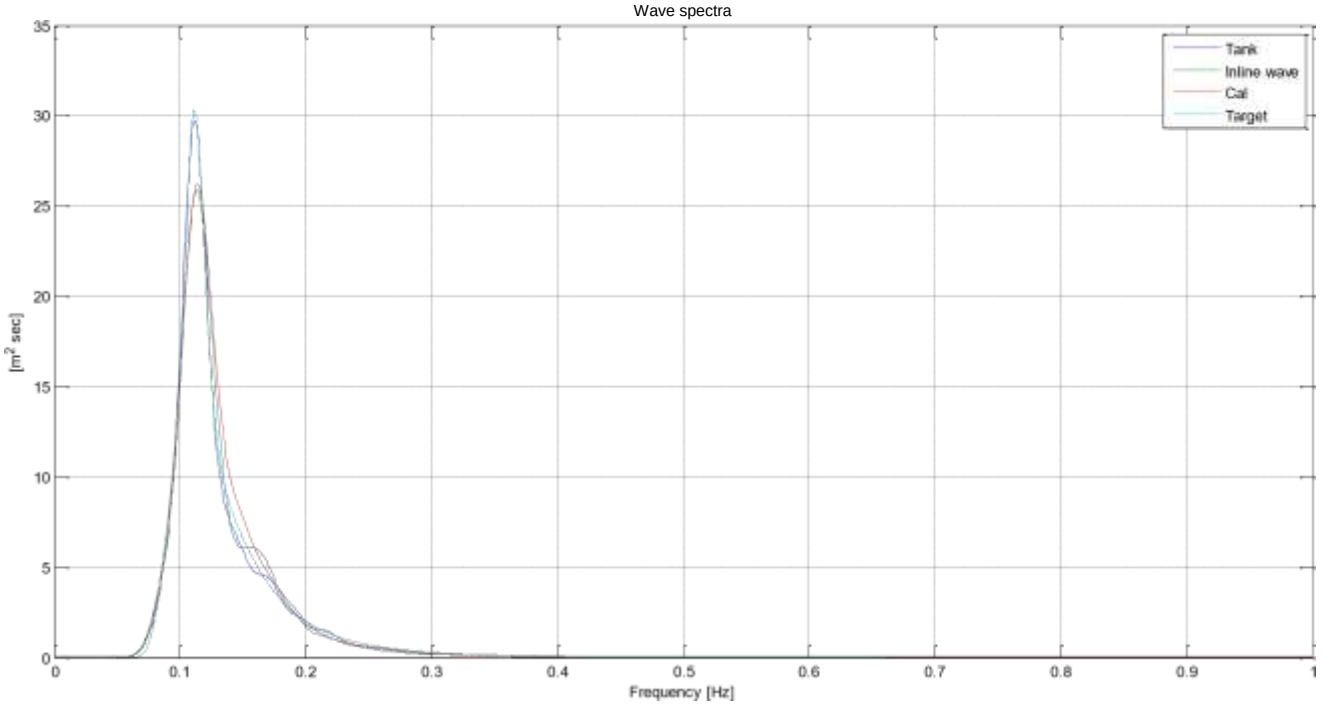

Figure A 11 Wave spectra : Tank Probe, Inline Probe, Calibration and Target for sea state N1

Waveheight Probability Density Functions [Rayleigh]

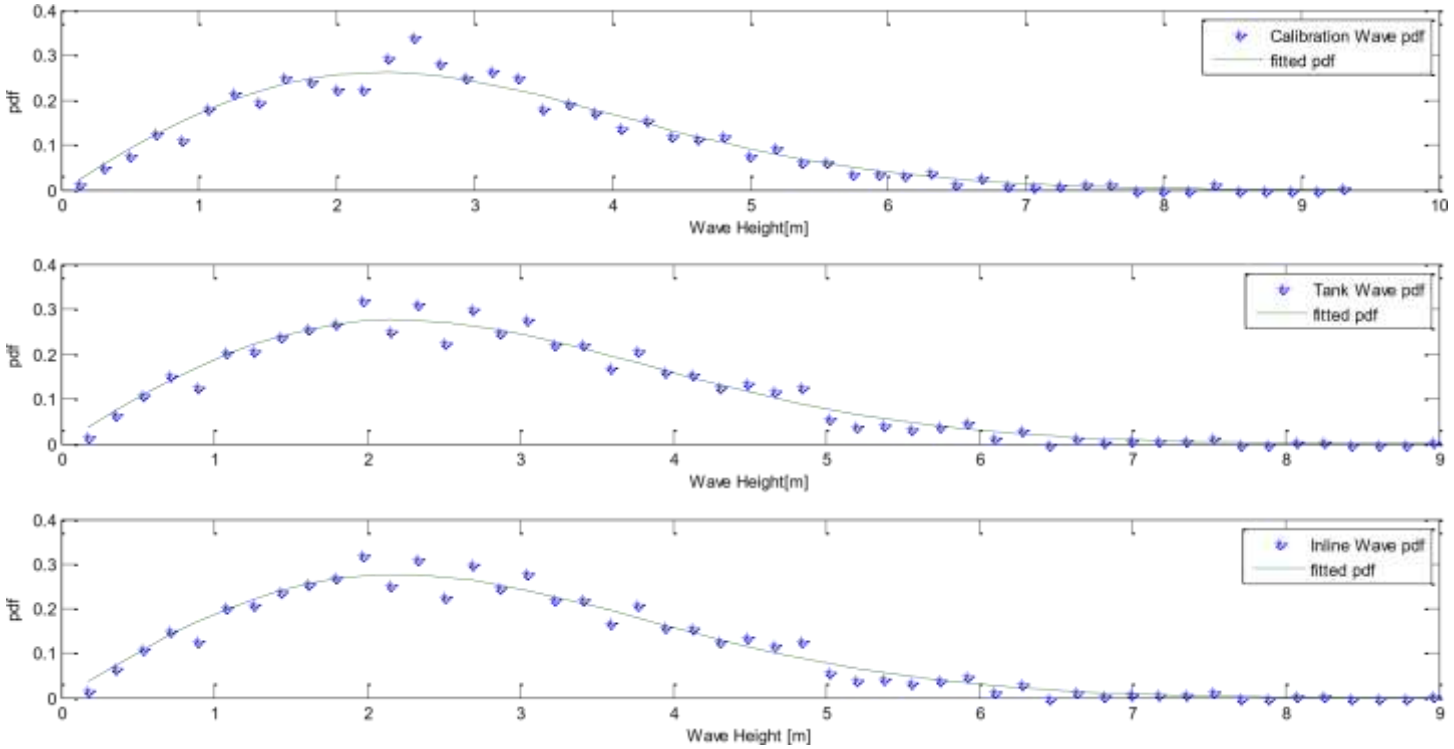

Figure A 12 Probability density functions of wave height : calibration, tank and incline wave for sea state N1

A.7 Sea State N8

Table A 7 Wave analysis results for sea state N8

Parameter	Unit	Target	Calibration	Inline	Tank
	m				
	m				
	m				
T_p	sec	10.28	6.018	5.867	6.089
H_s(elevation)		6.00	5.891	5.793	6.23
H_s(spectrum)		6.00	10.157	10.064	9.822

$H_{(1/3)}$
6.00
6.018
5.867
6.089

Wave spectra

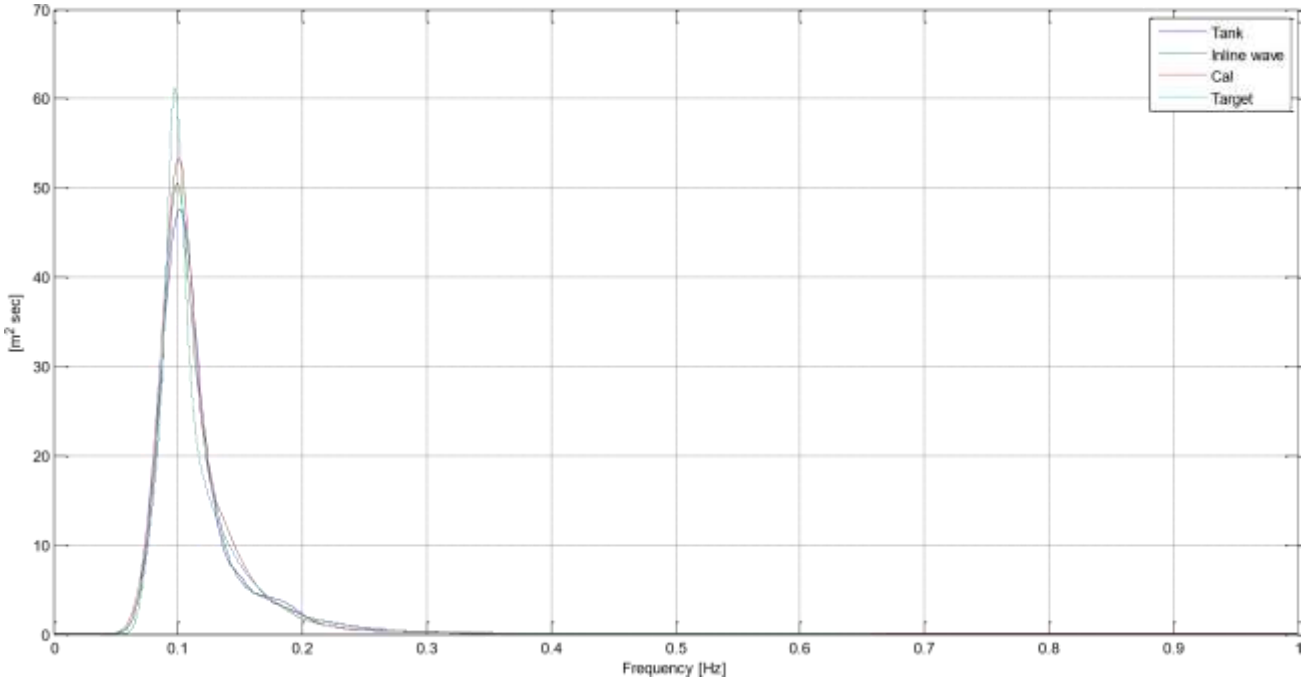

Figure A 13 Wave spectra : Tank Probe, Inline Probe, Calibration and Target for sea state N8

Waveheight Probability Density Functions [Rayleigh]

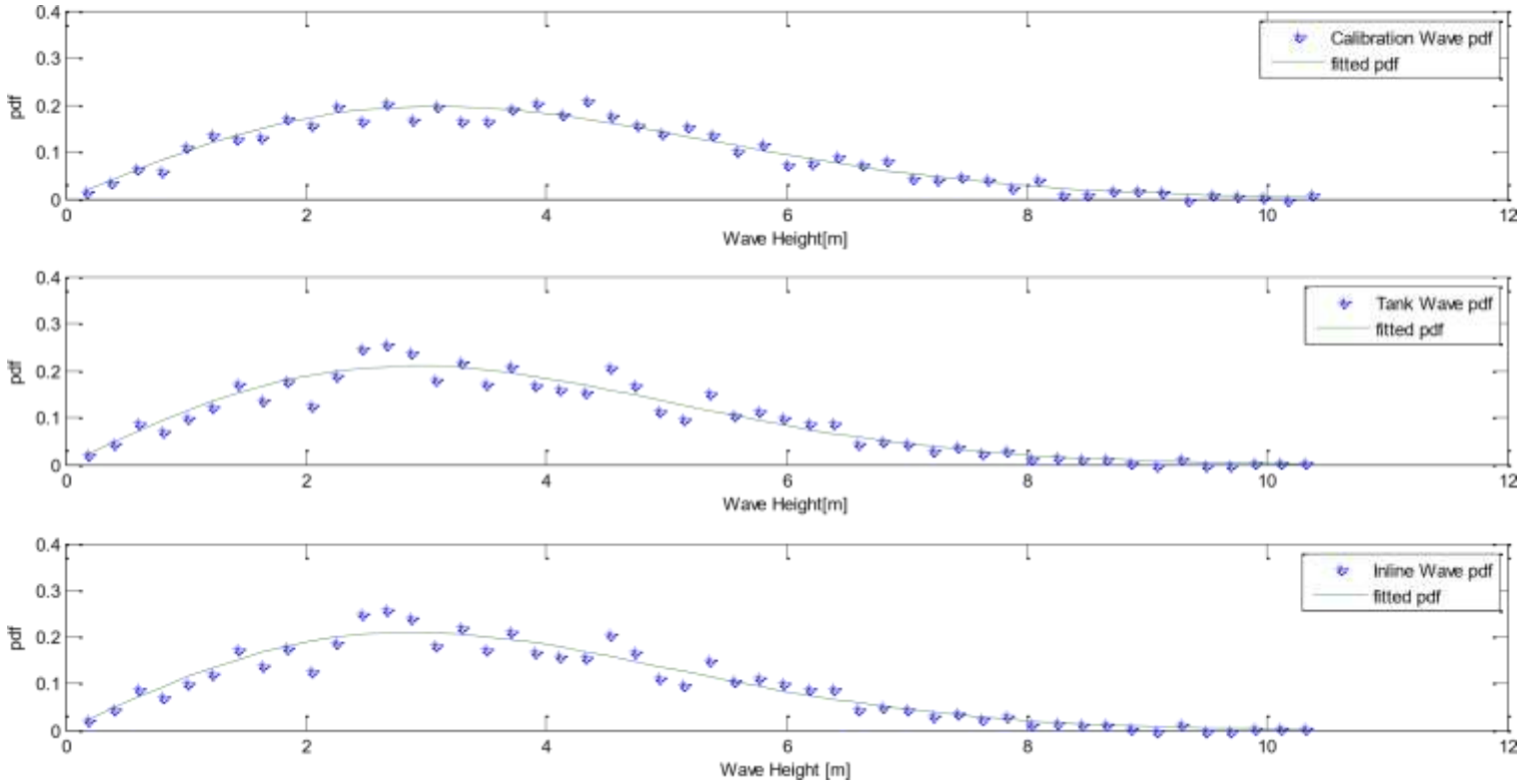

Figure A 14 Probability density functions of wave height : calibration, tank and incline wave for sea state N8

Appendix B

B.1 FAST Files for Free Oscillation Test (no wind condition) – Platform File

Note that some confidential data in these files has been written here as "XXX"

FAST PLATFORM FILE ----------

NREL 5.0 MW offshore baseline floating platform input properties for the TLP.

---------- FEATURE FLAGS (CONT) ----------

True PtfmSgDOF - Platform horizontal surge translation DOF (flag)

True PtfmSwDOF - Platform horizontal sway translation DOF (flag)

True PtfmHvDOF - Platform vertical heave translation DOF (flag)

True PtfmRDOF - Platform roll tilt rotation DOF (flag)

True PtfmPDOF - Platform pitch tilt rotation DOF (flag)

True PtfmYDOF - Platform yaw rotation DOF (flag)

---------- INITIAL CONDITIONS (CONT) ----------

1.0 PtfmSurge - Initial or fixed horizontal surge translational displacement of platform (meters)

0.0 PtfmSway - Initial or fixed horizontal sway translational displacement of platform (meters)

0.0 PtfmHeave - Initial or fixed vertical heave translational displacement of platform (meters)

0.0 PtfmRoll - Initial or fixed roll tilt rotational displacement of platform (degrees)

0.0 PtfmPitch - Initial or fixed pitch tilt rotational displacement of platform (degrees)

0.0 PtfmYaw - Initial or fixed yaw rotational displacement of platform (degrees)

---------- TURBINE CONFIGURATION (CONT) ----------

-16.50 TwrDraft - Downward distance from the ground level [onshore] or MSL [offshore] to the tower base platform connection (meters)

30.625 PtfmCM - Downward distance from the ground level [onshore] or MSL [offshore] to the platform CM (meters)

0.0 PtfmRef - Downward distance from the ground level [onshore] or MSL [offshore] to the platform reference point (meters)

---------- MASS AND INERTIA (CONT) ----------

XXX PtfmMass - Platform mass (kg)

XXX PtfmRIner - Platform inertia for roll tilt rotation about the platform CM (kg m^2)

XXX PtfmPIner - Platform inertia for pitch tilt rotation about the platform CM (kg m^2)

XXX PtfmYIner - Platfrom inertia for yaw rotation about the platform CM (kg m^2)

---------- PLATFORM (CONT) ----------

FltngPtfmLd PtfmLdMod - Platform loading model {0: none, 1: user-defined from routine UserPtfmLd} (switch)

"HydroData\tlpmit" WAMITFile - Root name of WAMIT output files containing the linear, nondimensionalized, hydrostatic restoring matrix (.hst extension), frequency-dependent hydrodynamic added mass matrix and damping matrix (.1 extension), and frequency- and

directiondependent wave excitation force vector per unit wave amplitude (.3 extension) (quoted string) [MAKE SURE THE FREQUENCIES INHERENT IN THESE WAMIT FILES SPAN THE PHYSICALLY-SIGNIFICANT RANGE OF FREQUENCIES FOR THE GIVEN PLATFORM; THEY MUST CONTAIN THE ZERO- AND INFINITE-FREQUENCY LIMITS!]

XXX PtfmVol0 - Displaced volume of water when the platform is in its undisplaced position (m^3) [USE THE SAME VALUE COMPUTED BY WAMIT AS OUTPUT IN THE .OUT FILE!]

100 PtfmNodes - Number of platform nodes used in calculation of viscous drag term from Morison's equation (-)

35.50 PtfmDraft - Effective platform draft in calculation of viscous drag term from Morison's equation (meters)

5.59 PtfmDiam - Effective platform diameter in calculation of viscous drag term from Morison's equation (meters) NOTE: THIS WAS CHOSEN TO GIVE THE SAME CROSS-SECTIONAL AREA AS THE SQUARE BARGE!

0.6 PtfmCD - Effective platform normalized hydrodynamic viscous drag coefficient in calculation of viscous drag term from Morison's equation (-)

60.0 RdtnTMax - Analysis time for wave radiation kernel calculations (sec) [determines RdtnDOmega=Pi/RdtnTMax in the cosine transform] [MAKE SURE THIS IS LONG ENOUGH FOR THE RADIATION IMPULSE RESPONSE FUNCTIONS TO DECAY TO NEARZERO FOR THE GIVEN PLATFORM!]

0.025 RdtnDT - Time step for wave radiation kernel calculations (sec) [DT<=RdtnDT<=0.1 recommended] [determines RdtnOmegaMax=Pi/RdtnDT in the cosine transform]

---------- MOORING LINES ----------

8 NumLines - Number of mooring lines (-)

1 LineMod - Mooring line model {1: standard quasi-static, 2: user-defined from routine UserLine} (switch) [used only when NumLines>0]

LRadAnch LAngAnch LDpthAnch LRadFair LAngFair LDrftFair LUnstrLen LDiam LMassDen LEAStff LSeabedCD LTenTol [used only when NumLines>0 and LineMod=1]

(m)	(deg)	(m)	(m)	(deg)	(m)	(m)	(m)	(kg/m)	(N)	(-)	(-)	[used only when NumLines>0 and LineMod=1]
27.50	0.0	70.0	27.50	0.0	35.50	34.50	0.09	43.1	XXX	-1.0	0.00001	
27.50	90.0	70.0	27.50	90.0	35.50	34.50	0.09	43.1	XXX	-1.0	0.00001	
27.50	180.0	70.0	27.50	180.0	35.50	34.50	0.09	43.1	XXX	-1.0	0.00001	
27.50	270.0	70.0	27.50	270.0	35.50	34.50	0.09	43.1	XXX	-1.0	0.00001	
27.50	0.0	70.0	27.50	0.0	35.50	34.50	0.09	43.1	XXX	-1.0	0.00001	
27.50	90.0	70.0	27.50	90.0	35.50	34.50	0.09	43.1	XXX	-1.0	0.00001	
27.50	180.0	70.0	27.50	180.0	35.50	34.50	0.09	43.1	XXX	-1.0	0.00001	
27.50	270.0	70.0	27.50	270.0	35.50	34.50	0.09	43.1	XXX	-1.0	0.00001	

---------- WAVES ----------

1025.0 WtrDens - Water density (kg/m^3)

70.0 WtrDpth - Water depth (meters) [USE THE SAME VALUE SPECIFIED IN THE WAMIT .POT FILE!]

0 WaveMod - Incident wave kinematics model {0: none=still water, 1: plane progressive (regular), 1: JONSWAP/Pierson-Moskowitz spectrum (irregular), 3: user-defind spectrum from routine UserWaveSpctrm (irregular)} (switch)

6000.0 WaveTMax - Analysis time for incident wave calculations (sec) [unused when WaveMod=0] [determines WaveDOmega=2Pi/WaveTMax in the IFFT]

0.25 WaveDT - Time step for incident wave calculations (sec) [unused when WaveMod=0] [0.1<=WaveDT<=1.0 recommended] [determines WaveOmegaMax=Pi/WaveDT in the IFFT]

1.5 WaveHs - Significant wave height of incident waves (meters) [used only when WaveMod=1 or 2]

6.61 WaveTp - Peak spectral period of incident waves (sec) [used only when WaveMod=1 or 2]

DEFAULT WavePkShp - Peak shape parameter of incident wave spectrum (-) or DEFAULT (unquoted string) [used only when WaveMod=2] [use 1.0 for Pierson-Moskowitz]

0.0 WaveDir - Incident wave propagation heading direction (degrees) [unused when WaveMod=0]

123456789 WaveSeed(1) - First random seed of incident waves [-2147483648 to 2147483647] (-) [unused when WaveMod=0]

1011121314 WaveSeed(2) - Second random seed of incident waves [-2147483648 to 2147483647] (-) [unused when WaveMod=0]

---------- CURRENT ----------

0 CurrMod - Current profile model {0: none=no current, 1: standard, 2: user-defined from routine UserCurrent} (switch)

0.0 CurrSSV0 - Sub-surface current velocity at still water level (m/s) [used only when CurrMod=1]

DEFAULT CurrSSDir - Sub-surface current heading direction (degrees) or DEFAULT (unquoted string) [used only when CurrMod=1]

20.0 CurrNSRef - Near-surface current reference depth (meters) [used only when CurrMod=1]

0.0 CurrNSV0 - Near-surface current velocity at still water level (m/s) [used only when CurrMod=1]

0.0 CurrNSDir - Near-surface current heading direction (degrees) [used only when CurrMod=1]

0.0 CurrDIV - Depth-independent current velocity (m/s) [used only when CurrMod=1]

0.0 CurrDIDir - Depth-independent current heading direction (degrees) [used only when CurrMod=1]

---------- OUTPUT (CONT) ----------

1 NWaveKin - Number of points where the incident wave kinematics can be output [0 to 9] (-)

100 WaveKinNd - List of platform nodes that have wave kinematics sensors [1 to PtfmNodes] (-) [unused if NWaveKin=0]

B.2 FAST Files for Free Oscillation Test (no wind condition) – *.fst* File

FAST INPUT FILE ---------- NREL

5.0 MW Baseline Wind Turbine for Use in Offshore Analysis.

Properties from Dutch Offshore Wind Energy Converter (DOWEC) 6MW Pre-Design (10046_009.pdf) and REpower 5M 5MW (5m_uk.pdf); Compatible with FAST v6.0.

---------- SIMULATION CONTROL ----------

False Echo - Echo input data to "echo.out" (flag)

1 ADAMSPrep - ADAMS preprocessor mode {1: Run FAST, 2: use FAST as a preprocessor to create an ADAMS model, 3: do both} (switch)

1 AnalMode - Analysis mode {1: Run a time-marching simulation, 2: create a periodic linearized model} (switch)

3 NumBl - Number of blades (-)

800.0 TMax - Total run time (s)

0.01 DT - Integration time step (s)

---------- TURBINE CONTROL ----------

0 YCMode - Yaw control mode {0: none, 1: user-defined from routine UserYawCont, 2: user-defined from Simulink} (switch)

9999.9 TYCOn - Time to enable active yaw control (s) [unused when YCMode=0]

0 PCMode - Pitch control mode {0: none, 1: user-defined from routine PitchCntrl, 2: user-defined from Simulink} (switch)

0.0 TPCOn - Time to enable active pitch control (s) [unused when PCMode=0]

2 VSContrl - Variable-speed control mode {0: none, 1: simple VS, 2: user-defined from routine UserVSCont, 3: user-defined from Simulink} (switch)

9999.9 VS_RtGnSp - Rated generator speed for simple variable-speed generator control (HSS side) (rpm) [used only when VSContrl=1]

9999.9 VS_RtTq - Rated generator torque/constant generator torque in Region 3 for simple variable-speed generator control (HSS side) (Nm) [used only when VSContrl=1]

9999.9 VS_Rgn2K - Generator torque constant in Region 2 for simple variable-speed generator control (HSS side) (N-m/rpm^2) [used only when VSContrl=1]

9999.9 VS_SlPc - Rated generator slip percentage in Region 2 1/2 for simple variable-speed generator control (%) [used only when VSContrl=1]

2 GenModel - Generator model {1: simple, 2: Thevenin, 3: user-defined from routine UserGen} (switch) [used only when VSContrl=0]

True GenTiStr - Method to start the generator {T: timed using TimGenOn, F: generator speed using SpdGenOn} (flag)

True GenTiStp - Method to stop the generator {T: timed using TimGenOf, F: when generator power = 0} (flag)

9999.9 SpdGenOn - Generator speed to turn on the generator for a startup (HSS speed) (rpm) [used only when GenTiStr=False]

0.0 TimGenOn - Time to turn on the generator for a startup (s) [used only when GenTiStr=True]

9999.9 TimGenOf - Time to turn off the generator (s) [used only when GenTiStp=True]

1 HSSBrMode - HSS brake model {1: simple, 2: user-defined from routine UserHSSBr} (switch)

9999.9 THSSBrDp - Time to initiate deployment of the HSS brake (s)

9999.9 TiDynBrk - Time to initiate deployment of the dynamic generator brake [CURRENTLY IGNORED] (s)

9999.9 TTpBrDp(1) - Time to initiate deployment of tip brake 1 (s)

9999.9 TTpBrDp(2) - Time to initiate deployment of tip brake 2 (s)

9999.9 TTpBrDp(3) - Time to initiate deployment of tip brake 3 (s) [unused for 2 blades]

9999.9 TBDepISp(1) - Deployment-initiation speed for the tip brake on blade 1 (rpm)

9999.9 TBDepISp(2) - Deployment-initiation speed for the tip brake on blade 2 (rpm)

9999.9 TBDepISp(3) - Deployment-initiation speed for the tip brake on blade 3 (rpm) [unused for 2 blades]

9999.9 TYawManS - Time to start override yaw maneuver and end standard yaw control (s)

9999.9 TYawManE - Time at which override yaw maneuver reaches final yaw angle (s)

0.0 NacYawF - Final yaw angle for yaw maneuvers (degrees)

9999.9 TPitManS(1) - Time to start override pitch maneuver for blade 1 and end standard pitch control (s)

9999.9 TPitManS(2) - Time to start override pitch maneuver for blade 2 and end standard pitch control (s)

9999.9 TPitManS(3) - Time to start override pitch maneuver for blade 3 and end standard pitch control (s) [unused for 2 blades]

9999.9 TPitManE(1) - Time at which override pitch maneuver for blade 1 reaches final pitch (s)

9999.9 TPitManE(2) - Time at which override pitch maneuver for blade 2 reaches final pitch (s)

9999.9 TPitManE(3) - Time at which override pitch maneuver for blade 3 reaches final pitch (s) [unused for 2 blades]

90.0 BlPitch(1) - Blade 1 initial pitch (degrees)

90.0 BlPitch(2) - Blade 2 initial pitch (degrees)

90.0 BlPitch(3) - Blade 3 initial pitch (degrees) [unused for 2 blades]

0.0 B1PitchF(1) - Blade 1 final pitch for pitch maneuvers (degrees)

0.0 B1PitchF(2) - Blade 2 final pitch for pitch maneuvers (degrees)

0.0 B1PitchF(3) - Blade 3 final pitch for pitch maneuvers (degrees) [unused for 2 blades]

---------- ENVIRONMENTAL CONDITIONS ----------

9.80665 Gravity - Gravitational acceleration (m/s^2)

---------- FEATURE FLAGS ----------

True FlapDOF1 - First flapwise blade mode DOF (flag)

True FlapDOF2 - Second flapwise blade mode DOF (flag)

```
True        EdgeDOF     - First edgewise blade mode DOF (flag)
False       TeetDOF     - Rotor-teeter DOF (flag) [unused for 3 blades]
False       DrTrDOF     - Drivetrain rotational-flexibility DOF (flag)
False       GenDOF      - Generator DOF (flag)
True        YawDOF      - Yaw DOF (flag)
True        TwFADOF1    - First fore-aft tower bending-mode DOF (flag)
True        TwFADOF2    - Second fore-aft tower bending-mode DOF (flag)
True        TwSSDOF1    - First side-to-side tower bending-mode DOF (flag)
True        TwSSDOF2    - Second side-to-side tower bending-mode DOF (flag)
True        CompAero    - Compute aerodynamic forces (flag)
False       CompNoise   - Compute aerodynamic noise (flag)
---------------------- INITIAL CONDITIONS ---------------------------------
  0.0       OoPDefl     - Initial out-of-plane blade-tip displacement (meters)
  0.0       IPDefl      - Initial in-plane blade-tip deflection (meters)
  0.0       TeetDefl    - Initial or fixed teeter angle (degrees) [unused for 3 blades]
  0.0       Azimuth     - Initial azimuth angle for blade 1 (degrees)
```

0.0 RotSpeed - Initial or fixed rotor speed (rpm)

0.0 NacYaw - Initial or fixed nacelle-yaw angle (degrees)

0.0 TTDspFA - Initial fore-aft tower-top displacement (meters)

0.0 TTDspSS - Initial side-to-side tower-top displacement (meters)

---------- TURBINE CONFIGURATION ----------

63.0 TipRad - The distance from the rotor apex to the blade tip (meters)

1.5 HubRad - The distance from the rotor apex to the blade root (meters)

1 PSpnElN - Number of the innermost blade element which is still part of the pitchable portion of the blade for partial-span pitch control [1 to BldNodes] [CURRENTLY IGNORED] (-)

0.0 UndSling - Undersling length [distance from teeter pin to the rotor apex] (meters) [unused for 3 blades]

0.0 HubCM - Distance from rotor apex to hub mass [positive downwind] (meters)

-5.01910 OverHang - Distance from yaw axis to rotor apex [3 blades] or teeter pin [2 blades] (meters)

1.9 NacCMxn - Downwind distance from the tower-top to the nacelle CM (meters)

0.0 NacCMyn - Lateral distance from the tower-top to the nacelle CM (meters)

1.75 NacCMzn - Vertical distance from the tower-top to the nacelle CM (meters)

87.6 TowerHt - Height of tower above ground level [onshore] or MSL [offshore] (meters)

1.96256 Twr2Shft - Vertical distance from the tower-top to the rotor shaft (meters)

16.50 TwrRBHt - Tower rigid base height (meters)

-5.0 ShftTilt - Rotor shaft tilt angle (degrees)

0.0 Delta3 - Delta-3 angle for teetering rotors (degrees) [unused for 3 blades]

-2.5 PreCone(1) - Blade 1 cone angle (degrees)

-2.5 PreCone(2) - Blade 2 cone angle (degrees)

-2.5 PreCone(3) - Blade 3 cone angle (degrees) [unused for 2 blades]

0.0 AzimB1Up - Azimuth value to use for I/O when blade 1 points up (degrees)

---------- MASS AND INERTIA ----------

0.0 YawBrMass - Yaw bearing mass (kg)

XXX NacMass - Nacelle mass (kg)

XXX HubMass - Hub mass (kg)

0.0 TipMass(1) - Tip-brake mass, blade 1 (kg)

0.0 TipMass(2) - Tip-brake mass, blade 2 (kg)

0.0 TipMass(3) - Tip-brake mass, blade 3 (kg) [unused for 2 blades]

2607.89E3 NacYIner - Nacelle inertia about yaw axis (kg m^2)

534.116 GenIner - Generator inertia about HSS (kg m^2)

115.926E3 HubIner   - Hub inertia about rotor axis [3 blades] or teeter axis [2 blades] (kg m^2)

---------- DRIVETRAIN ----------

100.0   GBoxEff   - Gearbox efficiency (%)

94.4   GenEff   - Generator efficiency [ignored by the Thevenin and user-defined generator models] (%)   97.0

GBRatio   - Gearbox ratio (-)

False   GBRevers   - Gearbox reversal {T: if rotor and generator rotate in opposite directions} (flag)

28.1162E3 HSSBrTqF   - Fully deployed HSS-brake torque (N-m)

0.6   HSSBrDT   - Time for HSS-brake to reach full deployment once initiated (sec) [used only when HSSBrMode=1]

DynBrkFi   - File containing a mech-gen-torque vs HSS-speed curve for a dynamic brake [CURRENTLY IGNORED] (quoted string)

867.637E6 DTTorSpr   - Drivetrain torsional spring (N-m/rad)

6.215E6 DTTorDmp   - Drivetrain torsional damper (N-m/(rad/s))

---------- SIMPLE INDUCTION GENERATOR ----------

9999.9   SIG_SlPc   - Rated generator slip percentage (%) [used only when VSContrl=0 and GenModel=1]

9999.9   SIG_SySp   - Synchronous (zero-torque) generator speed (rpm) [used only when VSContrl=0 and GenModel=1]

9999.9   SIG_RtTq   - Rated torque (N-m) [used only when VSContrl=0 and GenModel=1]

9999.9   SIG_PORt   - Pull-out ratio (Tpullout/Trated) (-) [used only when VSContrl=0 and GenModel=1]

---------- THEVENIN-EQUIVALENT INDUCTION GENERATOR ----------

9999.9 TEC_Freq - Line frequency [50 or 60] (Hz) [used only when VSContrl=0 and GenModel=2]

9998 TEC_NPol - Number of poles [even integer > 0] (-) [used only when VSContrl=0 and GenModel=2]

9999.9 TEC_SRes - Stator resistance (ohms) [used only when VSContrl=0 and GenModel=2]

9999.9 TEC_RRes - Rotor resistance (ohms) [used only when VSContrl=0 and GenModel=2]

9999.9 TEC_VLL - Line-to-line RMS voltage (volts) [used only when VSContrl=0 and GenModel=2]

9999.9 TEC_SLR - Stator leakage reactance (ohms) [used only when VSContrl=0 and GenModel=2]

9999.9 TEC_RLR - Rotor leakage reactance (ohms) [used only when VSContrl=0 and GenModel=2]

9999.9 TEC_MR - Magnetizing reactance (ohms) [used only when VSContrl=0 and GenModel=2]

---------- PLATFORM ----------

3 PtfmModel - Platform model {0: none, 1: onshore, 2: fixed bottom offshore, 3: floating offshore} (switch)

"NRELOffshrBsline5MW_Platform_TLP.dat" PtfmFile - Name of file containing platform properties (quoted string) [unused when PtfmModel=0]

---------- TOWER ----------

20 TwrNodes - Number of tower nodes used for analysis (-)

"NRELOffshrBsline5MW_Tower_TLP.dat" TwrFile - Name of file containing tower properties (quoted string)

---------- NACELLE-YAW ----------

9028.32E6 YawSpr   - Nacelle-yaw spring constant (N-m/rad)

 19.16E6   YawDamp   - Nacelle-yaw damping constant (N-m/(rad/s))

  0.0   YawNeut   - Neutral yaw position--yaw spring force is zero at this yaw (degrees)

---------------------- FURLING --

False   Furling   - Read in additional model properties for furling turbine (flag)

            FurlFile   - Name of file containing furling properties (quoted string) [unused when Furling=False]

---------------------- ROTOR-TEETER ---

0   TeetMod   - Rotor-teeter spring/damper model {0: none, 1: standard, 2: user-defined from routine UserTeet} (switch) [unused for 3 blades]

  0.0   TeetDmpP   - Rotor-teeter damper position (degrees) [used only for 2 blades and when TeetMod=1]

  0.0   TeetDmp   - Rotor-teeter damping constant (N-m/(rad/s)) [used only for 2 blades and when TeetMod=1]

  0.0   TeetCDmp   - Rotor-teeter rate-independent Coulomb-damping moment (N-m) [used only for 2 blades and when TeetMod=1]

  0.0   TeetSStP   - Rotor-teeter soft-stop position (degrees) [used only for 2 blades and when TeetMod=1]

  0.0   TeetHStP   - Rotor-teeter hard-stop position (degrees) [used only for 2 blades and when TeetMod=1]

  0.0   TeetSSSp   - Rotor-teeter soft-stop linear-spring constant (N-m/rad) [used only for 2 blades and when TeetMod=1]

  0.0   TeetHSSp   - Rotor-teeter hard-stop linear-spring constant (N-m/rad) [used only for 2 blades and when TeetMod=1]

---------------------- TIP-BRAKE --

0.0 TBDrConN - Tip-brake drag constant during normal operation, Cd*Area (m^2)

0.0 TBDrConD - Tip-brake drag constant during fully-deployed operation, Cd*Area (m^2)

0.0 TpBrDT - Time for tip-brake to reach full deployment once released (sec)

---------- BLADE ----------

"NRELOffshrBsline5MW_Blade.dat" BldFile(1) - Name of file containing properties for blade 1 (quoted string)

"NRELOffshrBsline5MW_Blade.dat" BldFile(2) - Name of file containing properties for blade 2 (quoted string)

"NRELOffshrBsline5MW_Blade.dat" BldFile(3) - Name of file containing properties for blade 3 (quoted string) [unused for 2 blades] ----------

------- AERODYN ----------

"NRELOffshrBsline5MW_AeroDyn.ipt" ADFile - Name of file containing AeroDyn input parameters (quoted string) ----------

NOISE ----------

NoiseFile - Name of file containing aerodynamic noise input parameters (quoted string) [used only when CompNoise=True] ----------

ADAMS ----------

"NRELOffshrBsline5MW_ADAMSSpecific.dat" ADAMSFile - Name of file containing ADAMS-specific input parameters (quoted string) [unused when ADAMSPrep=1]

---------- LINEARIZATION CONTROL ----------

"NRELOffshrBsline5MW_Linear.dat" LinFile - Name of file containing FAST linearization parameters (quoted string) [unused when AnalMode=1]

---------------------- OUTPUT -- True

SumPrint   - Print summary data to "<RootName>.fsm" (flag)

True   TabDelim   - Generate a tab-delimited tabular output file. (flag)

"ES10.3E2" OutFmt - Format used for tabular output except time. Resulting field should be 10 characters. (quoted string) [not checked for validity!]

1.0   TStart   - Time to begin tabular output (s)

1.0   DecFact   - Decimation factor for tabular output {1: output every time step} (-)

1.0   SttsTime   - Amount of time between screen status messages (sec)

-3.09528 NcIMUxn   - Downwind distance from the tower-top to the nacelle IMU (meters)

0.0   NcIMUyn   - Lateral distance from the tower-top to the nacelle IMU (meters)

2.23336 NcIMUzn   - Vertical distance from the tower-top to the nacelle IMU (meters)

1.912   ShftGagL   - Distance from rotor apex [3 blades] or teeter pin [2 blades] to shaft strain gages [positive for upwind rotors] (meters)

1   NTwGages   - Number of tower nodes that have strain gages for output [0 to 9] (-)

10   TwrGagNd   - List of tower nodes that have strain gages [1 to TwrNodes] (-) [unused if NTwGages=0]

1   NBlGages   - Number of blade nodes that have strain gages for output [0 to 9] (-)

9   BldGagNd   - List of blade nodes that have strain gages [1 to BldNodes] (-) [unused if NBlGages=0]

         OutList   - The next line(s) contains a list of output parameters. See OutList.txt for a listing of available output channels, (-)

"WindVxi , WindVyi , WindVzi" - Longitudinal, lateral, and vertical wind speeds

"WaveElev" - Wave elevation at the platform reference point

"Wave1Vxi , Wave1Vyi , Wave1Vzi" - Longitudinal, lateral, and vertical wave particle velocities at platform node 1 (approx. platform reference point)

"Wave1Axi , Wave1Ayi , Wave1Azi" - Longitudinal, lateral, and vertical wave particle accelerations at platform node 1 (approx. platform reference point)

"GenPwr , GenTq" - Electrical generator power and torque

"HSSBrTq" - High-speed shaft brake torque

"BldPitch1, BldPitch2, BldPitch3" - Pitch angles for blades 1, 2, and 3

"Azimuth" - Blade 1 azimuth angle

"RotSpeed , GenSpeed" - Low-speed shaft and high-speed shaft speeds

"NacYaw , NacYawErr" - Nacelle yaw angle and nacelle yaw error estimate

"OoPDefl1 , IPDefl1 , TwstDefl1" - Blade 1 out-of-plane and in-plane deflections and tip twist

"OoPDefl2 , IPDefl2 , TwstDefl2" - Blade 2 out-of-plane and in-plane deflections and tip twist

"OoPDefl3 , IPDefl3 , TwstDefl3" - Blade 3 out-of-plane and in-plane deflections and tip twist

"TwrClrnc1, TwrClrnc2, TwrClrnc3" - Tip-to-tower clearance estimate for blades 1, 2, and 3

"NcIMUTAxs, NcIMUTAys, NcIMUTAzs" - Nacelle IMU translational accelerations (absolute) in the nonrotating, shaft coordinate system

"TTDspFA , TTDspSS , TTDspTwst"	- Tower fore-aft and side-to-side displacements and top twist
"PtfmSurge, PtfmSway , PtfmHeave"	- Platform translational surge, sway, and heave displacements
"PtfmRoll , PtfmPitch, PtfmYaw"	- Platform rotational roll, pitch and yaw displacements
"PtfmTAxt , PtfmTAyt , PtfmTAzt"	- Platform translation accelerations (absolute) in the tower-base coordinate system
"RootFxc1 , RootFyc1 , RootFzc1"	- Out-of-plane shear, in-plane shear, and axial forces at the root of blade 1
"RootMxc1 , RootMyc1 , RootMzc1"	- In-plane bending, out-of-plane bending, and pitching moments at the root of blade 1
"RootFxc2 , RootFyc2 , RootFzc2"	- Out-of-plane shear, in-plane shear, and axial forces at the root of blade 2
"RootMxc2 , RootMyc2 , RootMzc2"	- In-plane bending, out-of-plane bending, and pitching moments at the root of blade 2
"RootFxc3 , RootFyc3 , RootFzc3"	- Out-of-plane shear, in-plane shear, and axial forces at the root of blade 3
"RootMxc3 , RootMyc3 , RootMzc3"	- In-plane bending, out-of-plane bending, and pitching moments at the root of blade 3
"Spn1MLxb1, Spn1MLyb1, Spn1MLzb1"	- Blade 1 local edgewise bending, flapwise bending, and pitching moments at span station 1 (approx. 50% span)
"Spn1MLxb2, Spn1MLyb2, Spn1MLzb2"	- Blade 2 local edgewise bending, flapwise bending, and pitching moments at span station 1 (approx. 50% span)
"Spn1MLxb3, Spn1MLyb3, Spn1MLzb3"	- Blade 3 local edgewise bending, flapwise bending, and pitching moments at span station 1 (approx. 50% span)
"RotThrust, LSSGagFya, LSSGagFza"	- Rotor thrust and low-speed shaft 0- and 90-rotating shear forces at the main bearing

"RotTorq , LSSGagMya, LSSGagMza" - Rotor torque and low-speed shaft 0- and 90-rotating bending moments at the main bearing "YawBrFxp , YawBrFyp , YawBrFzp" - Fore-aft shear, side-to-side shear, and vertical forces at the top of the tower (not rotating with nacelle yaw)

"YawBrMxp , YawBrMyp , YawBrMzp" - Side-to-side bending, fore-aft bending, and yaw moments at the top of the tower (not rotating with nacelle yaw)

"TwrBsFxt , TwrBsFyt , TwrBsFzt" - Fore-aft shear, side-to-side shear, and vertical forces at the base of the tower (platform)

"TwrBsMxt , TwrBsMyt , TwrBsMzt" - Side-to-side bending, fore-aft bending, and yaw moments at the base of the tower (platform)

"TwHt1MLxt, TwHt1MLyt, TwHt1MLzt" - Local side-to-side bending, fore-aft bending, and yaw moments at tower gage 1 (approx. 50% elevation)

"Fair1Ten , Fair1Ang , Anch1Ten , Anch1Ang" - Line 1 fairlead and anchor effective tensions and vertical angles

"Fair2Ten , Fair2Ang , Anch2Ten , Anch2Ang" - Line 2 fairlead and anchor effective tensions and vertical angles

"Fair3Ten , Fair3Ang , Anch3Ten , Anch3Ang" - Line 3 fairlead and anchor effective tensions and vertical angles

"Fair4Ten , Fair4Ang , Anch4Ten , Anch4Ang" - Line 4 fairlead and anchor effective tensions and vertical angles

"Fair5Ten , Fair5Ang , Anch5Ten , Anch5Ang" - Line 5 fairlead and anchor effective tensions and vertical angles

"Fair6Ten , Fair6Ang , Anch6Ten , Anch6Ang" - Line 6 fairlead and anchor effective tensions and vertical angles

"Fair7Ten , Fair7Ang , Anch7Ten , Anch7Ang" - Line 7 fairlead and anchor effective tensions and vertical angles

"Fair8Ten , Fair8Ang , Anch8Ten , Anch8Ang" - Line 8 fairlead and anchor effective tensions and vertical angles

"TipSpdRat, RotCp , RotCt , RotCq" - Rotor tip speed ratio and power, thrust, and torque coefficients

B.3 FAST Files for Test in Regular Wave (no wind condition) – Platform File

FAST PLATFORM FILE ----------

NREL 5.0 MW offshore baseline floating platform input properties for the TLP.

---------- FEATURE FLAGS (CONT) ----------

True PtfmSgDOF - Platform horizontal surge translation DOF (flag)

True PtfmSwDOF - Platform horizontal sway translation DOF (flag)

True PtfmHvDOF - Platform vertical heave translation DOF (flag)

True PtfmRDOF - Platform roll tilt rotation DOF (flag)

True PtfmPDOF - Platform pitch tilt rotation DOF (flag)

True PtfmYDOF - Platform yaw rotation DOF (flag)

---------- INITIAL CONDITIONS (CONT) ----------

0.0 PtfmSurge - Initial or fixed horizontal surge translational displacement of platform (meters)

0.0 PtfmSway - Initial or fixed horizontal sway translational displacement of platform (meters)

0.0 PtfmHeave - Initial or fixed vertical heave translational displacement of platform (meters)

0.0 PtfmRoll - Initial or fixed roll tilt rotational displacement of platform (degrees)

0.0 PtfmPitch - Initial or fixed pitch tilt rotational displacement of platform (degrees)

0.0 PtfmYaw - Initial or fixed yaw rotational displacement of platform (degrees)

---------- TURBINE CONFIGURATION (CONT) ----------

-16.50 TwrDraft - Downward distance from the ground level [onshore] or MSL [offshore] to the tower base platform connection (meters)

30.625 PtfmCM - Downward distance from the ground level [onshore] or MSL [offshore] to the platform CM (meters)

0.0 PtfmRef - Downward distance from the ground level [onshore] or MSL [offshore] to the platform reference point (meters)

---------- MASS AND INERTIA (CONT) ----------

XXX PtfmMass - Platform mass (kg)

XXX PtfmRIner - Platform inertia for roll tilt rotation about the platform CM (kg m^2)

XXX PtfmPIner - Platform inertia for pitch tilt rotation about the platform CM (kg m^2)

XXX PtfmYIner - Platfrom inertia for yaw rotation about the platform CM (kg m^2)

---------- PLATFORM (CONT) ----------

FltngPtfmLd PtfmLdMod - Platform loading model {0: none, 1: user-defined from routine UserPtfmLd} (switch)

"HydroData\tlpmit" WAMITFile - Root name of WAMIT output files containing the linear, nondimensionalized, hydrostatic restoring matrix (.hst extension), frequency-dependent hydrodynamic added mass matrix and damping matrix (.1 extension), and frequency- and directiondependent wave excitation force vector per unit wave amplitude (.3 extension) (quoted string) [MAKE SURE THE FREQUENCIES INHERENT IN THESE WAMIT FILES SPAN THE PHYSICALLY-SIGNIFICANT RANGE OF FREQUENCIES FOR THE GIVEN PLATFORM; THEY MUST CONTAIN THE ZERO- AND INFINITE-FREQUENCY LIMITS!]

XXX PtfmVol0 - Displaced volume of water when the platform is in its undisplaced position (m^3) [USE THE SAME VALUE COMPUTED BY WAMIT AS OUTPUT IN THE .OUT FILE!]

100 PtfmNodes - Number of platform nodes used in calculation of viscous drag term from Morison's equation (-)

35.50 PtfmDraft - Effective platform draft in calculation of viscous drag term from Morison's equation (meters)

5.59 PtfmDiam - Effective platform diameter in calculation of viscous drag term from Morison's equation (meters) NOTE: THIS WAS CHOSEN TO GIVE THE SAME CROSS-SECTIONAL AREA AS THE SQUARE BARGE!

0.6 PtfmCD - Effective platform normalized hydrodynamic viscous drag coefficient in calculation of viscous drag term from Morison's equation (-)

60.0 RdtnTMax - Analysis time for wave radiation kernel calculations (sec) [determines RdtnDOmega=Pi/RdtnTMax in the cosine transform] [MAKE SURE THIS IS LONG ENOUGH FOR THE RADIATION IMPULSE RESPONSE FUNCTIONS TO DECAY TO NEARZERO FOR THE GIVEN PLATFORM!]

0.025 RdtnDT - Time step for wave radiation kernel calculations (sec) [DT<=RdtnDT<=0.1 recommended] [determines RdtnOmegaMax=Pi/RdtnDT in the cosine transform]

---------- MOORING LINES ----------

8 NumLines - Number of mooring lines (-)

1 LineMod - Mooring line model {1: standard quasi-static, 2: user-defined from routine UserLine} (switch) [used only when NumLines>0]

LRadAnch LAngAnch LDpthAnch LRadFair LAngFair LDrftFair LUnstrLen LDiam LMassDen LEAStff LSeabedCD LTenTol [used only when NumLines>0 and LineMod=1]

(m) (deg) (m) (m) (deg) (m) (m) (m) (kg/m) (N) (-) (-) [used only when NumLines>0 and LineMod=1]

27.50	0.0	70.0	27.5	0.0	35.50	34.50	0.09	43.1	XXX	-1.0	0.00001
27.50	90.0	70.0	27.5	90.0	35.50	34.50	0.09	43.1	XXX	-1.0	0.00001
27.50	180.0	70.0	27.5	180.0	35.50	34.50	0.09	43.1	XXX	-1.0	0.00001
27.50	270.0	70.0	27.5	270.0	35.50	34.50	0.09	43.1	XXX	-1.0	0.00001
27.50	0.0	70.0	27.5	0.0	35.50	34.50	0.09	43.1	XXX	-1.0	0.00001
27.50	90.0	70.0	27.5	90.0	35.50	34.50	0.09	43.1	XXX	-1.0	0.00001
27.50	180.0	70.0	27.5	180.0	35.50	34.50	0.09	43.1	XXX	-1.0	0.00001
27.50	270.0	70.0	27.5	270.0	35.50	34.50	0.09	43.1	XXX	-1.0	0.00001

---------- WAVES ----------

1025.0 WtrDens - Water density (kg/m^3)

70.0 WtrDpth - Water depth (meters) [USE THE SAME VALUE SPECIFIED IN THE WAMIT .POT FILE!]

1 WaveMod - Incident wave kinematics model {0: none=still water, 1: plane progressive (regular), 2: JONSWAP/Pierson-Moskowitz spectrum (irregular), 3: user-defind spectrum from routine UserWaveSpctrm (irregular)} (switch)

9999.999 WaveTMax - Analysis time for incident wave calculations (sec) [unused when WaveMod=0] [determines WaveDOmega=2Pi/WaveTMax in the IFFT]

0.25 WaveDT - Time step for incident wave calculations (sec) [unused when WaveMod=0] [0.1<=WaveDT<=1.0 recommended] [determines WaveOmegaMax=Pi/WaveDT in the IFFT]

2.0 WaveHs - Significant wave height of incident waves (meters) [used only when WaveMod=1 or 2]

```
   8.0      WaveTp      - Peak spectral period of incident waves (sec) [used only when WaveMod=1 or 2]
DEFAULT  WavePkShp   - Peak shape parameter of incident wave spectrum (-) or DEFAULT (unquoted string) [used only when WaveMod=2] [use
1.0 for Pierson-Moskowitz]
   0.0          WaveDir     - Incident wave propagation heading direction (degrees) [unused when WaveMod=0]
123456789   WaveSeed(1) - First  random seed of incident waves [-2147483648 to 2147483647] (-) [unused when WaveMod=0]
1011121314  WaveSeed(2) - Second random seed of incident waves [-2147483648 to 2147483647] (-) [unused when WaveMod=0]
---------------------- CURRENT ------------------------------------------------
0         CurrMod     - Current profile model {0: none=no current, 1: standard, 2: user-defined from routine UserCurrent} (switch)
   0.0      CurrSSV0    - Sub-surface current velocity at still water level (m/s) [used only when CurrMod=1]
DEFAULT  CurrSSDir   - Sub-surface current heading direction (degrees) or DEFAULT (unquoted string) [used only when CurrMod=1]
  20.0      CurrNSRef   - Near-surface current reference depth (meters) [used only when CurrMod=1]
   0.0      CurrNSV0    - Near-surface current velocity at still water level (m/s) [used only when CurrMod=1]
   0.0      CurrNSDir   - Near-surface current heading direction (degrees) [used only when CurrMod=1]
   0.0      CurrDIV     - Depth-independent current velocity (m/s) [used only when CurrMod=1]
   0.0      CurrDIDir   - Depth-independent current heading direction (degrees) [used only when CurrMod=1]
---------------------- OUTPUT (CONT) ------------------------------------------
1         NWaveKin    - Number of points where the incident wave kinematics can be output [0 to 9] (-)
```

100 WaveKinNd - List of platform nodes that have wave kinematics sensors [1 to PtfmNodes] (-) [unused if NWaveKin=0]

B.4 FAST Files for Test in Regular Wave (no wind condition) – *.fst* File

FAST INPUT FILE ---------- NREL

5.0 MW Baseline Wind Turbine for Use in Offshore Analysis.

Properties from Dutch Offshore Wind Energy Converter (DOWEC) 6MW Pre-Design (10046_009.pdf) and REpower 5M 5MW (5m_uk.pdf); Compatible with FAST v6.0.

---------- SIMULATION CONTROL ----------

False Echo - Echo input data to "echo.out" (flag)

1 ADAMSPrep - ADAMS preprocessor mode {1: Run FAST, 2: use FAST as a preprocessor to create an ADAMS model, 3: do both} (switch)

1 AnalMode - Analysis mode {1: Run a time-marching simulation, 2: create a periodic linearized model} (switch)

3 NumBl - Number of blades (-)

9999.999 TMax - Total run time (s)

0.01 DT - Integration time step (s)

---------- TURBINE CONTROL ----------

0 YCMode - Yaw control mode {0: none, 1: user-defined from routine UserYawCont, 2: user-defined from Simulink} (switch)

9999.9 TYCOn - Time to enable active yaw control (s) [unused when YCMode=0]

0 PCMode - Pitch control mode {0: none, 1: user-defined from routine PitchCntrl, 2: user-defined from Simulink} (switch)

0.0 TPCOn - Time to enable active pitch control (s) [unused when PCMode=0]

2 VSContrl - Variable-speed control mode {0: none, 1: simple VS, 2: user-defined from routine UserVSCont, 3: user-defined from Simulink} (switch)

9999.9 VS_RtGnSp - Rated generator speed for simple variable-speed generator control (HSS side) (rpm) [used only when VSContrl=1]

9999.9 VS_RtTq - Rated generator torque/constant generator torque in Region 3 for simple variable-speed generator control (HSS side) (Nm) [used only when VSContrl=1]

9999.9 VS_Rgn2K - Generator torque constant in Region 2 for simple variable-speed generator control (HSS side) (N-m/rpm^2) [used only when VSContrl=1]

9999.9 VS_SlPc - Rated generator slip percentage in Region 2 1/2 for simple variable-speed generator control (%) [used only when VSContrl=1]

2 GenModel - Generator model {1: simple, 2: Thevenin, 3: user-defined from routine UserGen} (switch) [used only when VSContrl=0]

True GenTiStr - Method to start the generator {T: timed using TimGenOn, F: generator speed using SpdGenOn} (flag)

True GenTiStp - Method to stop the generator {T: timed using TimGenOf, F: when generator power = 0} (flag)

9999.9 SpdGenOn - Generator speed to turn on the generator for a startup (HSS speed) (rpm) [used only when GenTiStr=False]

0.0 TimGenOn - Time to turn on the generator for a startup (s) [used only when GenTiStr=True] 9999.9

TimGenOf - Time to turn off the generator (s) [used only when GenTiStp=True]

```
  1        HSSBrMode   - HSS brake model {1: simple, 2: user-defined from routine UserHSSBr} (switch)
9999.9     THSSBrDp    - Time to initiate deployment of the HSS brake (s)
9999.9     TiDynBrk    - Time to initiate deployment of the dynamic generator brake [CURRENTLY IGNORED] (s)
9999.9     TTpBrDp(1)  - Time to initiate deployment of tip brake 1 (s)
9999.9     TTpBrDp(2)  - Time to initiate deployment of tip brake 2 (s)
9999.9     TTpBrDp(3)  - Time to initiate deployment of tip brake 3 (s) [unused for 2 blades]
9999.9     TBDepISp(1) - Deployment-initiation speed for the tip brake on blade 1 (rpm)
9999.9     TBDepISp(2) - Deployment-initiation speed for the tip brake on blade 2 (rpm)
9999.9     TBDepISp(3) - Deployment-initiation speed for the tip brake on blade 3 (rpm) [unused for 2 blades]
9999.9     TYawManS    - Time to start override yaw maneuver and end standard yaw control (s)
9999.9     TYawManE    - Time at which override yaw maneuver reaches final yaw angle (s)
  0.0      NacYawF     - Final yaw angle for yaw maneuvers (degrees)
9999.9     TPitManS(1) - Time to start override pitch maneuver for blade 1 and end standard pitch control (s)
9999.9     TPitManS(2) - Time to start override pitch maneuver for blade 2 and end standard pitch control (s)
9999.9     TPitManS(3) - Time to start override pitch maneuver for blade 3 and end standard pitch control (s) [unused for 2 blades]
9999.9     TPitManE(1) - Time at which override pitch maneuver for blade 1 reaches final pitch (s)
```

9999.9 TPitManE(2) - Time at which override pitch maneuver for blade 2 reaches final pitch (s)

9999.9 TPitManE(3) - Time at which override pitch maneuver for blade 3 reaches final pitch (s) [unused for 2 blades]

20.0 BlPitch(1) - Blade 1 initial pitch (degrees)

20.0 BlPitch(2) - Blade 2 initial pitch (degrees)

20.0 BlPitch(3) - Blade 3 initial pitch (degrees) [unused for 2 blades]

90.0 B1PitchF(1) - Blade 1 final pitch for pitch maneuvers (degrees)

90.0 B1PitchF(2) - Blade 2 final pitch for pitch maneuvers (degrees)

90.0 B1PitchF(3) - Blade 3 final pitch for pitch maneuvers (degrees) [unused for 2 blades]

---------- ENVIRONMENTAL CONDITIONS ----------

9.80665 Gravity - Gravitational acceleration (m/s^2)

---------- FEATURE FLAGS ----------

False FlapDOF1 - First flapwise blade mode DOF (flag)

False FlapDOF2 - Second flapwise blade mode DOF (flag)

False EdgeDOF - First edgewise blade mode DOF (flag)

False TeetDOF - Rotor-teeter DOF (flag) [unused for 3 blades]

False DrTrDOF - Drivetrain rotational-flexibility DOF (flag)

False GenDOF - Generator DOF (flag)

True YawDOF - Yaw DOF (flag)

False TwFADOF1 - First fore-aft tower bending-mode DOF (flag)

False TwFADOF2 - Second fore-aft tower bending-mode DOF (flag)

False TwSSDOF1 - First side-to-side tower bending-mode DOF (flag)

False TwSSDOF2 - Second side-to-side tower bending-mode DOF (flag)

True CompAero - Compute aerodynamic forces (flag)

False CompNoise - Compute aerodynamic noise (flag)

---------- INITIAL CONDITIONS ----------

0.0 OoPDefl - Initial out-of-plane blade-tip displacement (meters)

0.0 IPDefl - Initial in-plane blade-tip deflection (meters)

0.0 TeetDefl - Initial or fixed teeter angle (degrees) [unused for 3 blades]

0.0 Azimuth - Initial azimuth angle for blade 1 (degrees)

0.0 RotSpeed - Initial or fixed rotor speed (rpm)

0.0 NacYaw - Initial or fixed nacelle-yaw angle (degrees)

0.0 TTDspFA - Initial fore-aft tower-top displacement (meters)

0.0 TTDspSS - Initial side-to-side tower-top displacement (meters) ---------- TURBINE CONFIGURATION ----------

63.0 TipRad - The distance from the rotor apex to the blade tip (meters)

1.5 HubRad - The distance from the rotor apex to the blade root (meters)

1 PSpnElN - Number of the innermost blade element which is still part of the pitchable portion of the blade for partial-span pitch control [1 to BldNodes] [CURRENTLY IGNORED] (-)

0.0 UndSling - Undersling length [distance from teeter pin to the rotor apex] (meters) [unused for 3 blades]

0.0 HubCM - Distance from rotor apex to hub mass [positive downwind] (meters)

-5.01910 OverHang - Distance from yaw axis to rotor apex [3 blades] or teeter pin [2 blades] (meters)

1.9 NacCMxn - Downwind distance from the tower-top to the nacelle CM (meters)

0.0 NacCMyn - Lateral distance from the tower-top to the nacelle CM (meters)

1.75 NacCMzn - Vertical distance from the tower-top to the nacelle CM (meters)

87.6 TowerHt - Height of tower above ground level [onshore] or MSL [offshore] (meters)

1.96256 Twr2Shft - Vertical distance from the tower-top to the rotor shaft (meters)

16.50 TwrRBHt - Tower rigid base height (meters)

-5.0 ShftTilt - Rotor shaft tilt angle (degrees)

0.0 Delta3 - Delta-3 angle for teetering rotors (degrees) [unused for 3 blades]

-2.5 PreCone(1) - Blade 1 cone angle (degrees)

-2.5 PreCone(2) - Blade 2 cone angle (degrees)

-2.5 PreCone(3) - Blade 3 cone angle (degrees) [unused for 2 blades]

0.0 AzimB1Up - Azimuth value to use for I/O when blade 1 points up (degrees)

---------- MASS AND INERTIA ----------

0.0 YawBrMass - Yaw bearing mass (kg)

240.00E3 NacMass - Nacelle mass (kg)

56.78E3 HubMass - Hub mass (kg)

0.0 TipMass(1) - Tip-brake mass, blade 1 (kg)

0.0 TipMass(2) - Tip-brake mass, blade 2 (kg)

0.0 TipMass(3) - Tip-brake mass, blade 3 (kg) [unused for 2 blades]

2607.89E3 NacYIner - Nacelle inertia about yaw axis (kg m^2)

534.116 GenIner - Generator inertia about HSS (kg m^2)

115.926E3 HubIner - Hub inertia about rotor axis [3 blades] or teeter axis [2 blades] (kg m^2)

---------- DRIVETRAIN ----------

100.0 GBoxEff - Gearbox efficiency (%)

94.4 GenEff - Generator efficiency [ignored by the Thevenin and user-defined generator models] (%)

```
  97.0      GBRatio     - Gearbox ratio (-)
False       GBRevers    - Gearbox reversal {T: if rotor and generator rotate in opposite directions} (flag)
  28.1162E3 HSSBrTqF    - Fully deployed HSS-brake torque (N-m)
   0.6    HSSBrDT     - Time for HSS-brake to reach full deployment once initiated (sec) [used only when HSSBrMode=1]
          DynBrkFi    - File containing a mech-gen-torque vs HSS-speed curve for a dynamic brake [CURRENTLY IGNORED] (quoted string)
 867.637E6  DTTorSpr    - Drivetrain torsional spring (N-m/rad)
   6.215E6  DTTorDmp    - Drivetrain torsional damper (N-m/(rad/s))
---------------------- SIMPLE INDUCTION GENERATOR ----------------------------
9999.9      SIG_SlPc    - Rated generator slip percentage (%) [used only when VSContrl=0 and GenModel=1]
9999.9      SIG_SySp    - Synchronous (zero-torque) generator speed (rpm) [used only when VSContrl=0 and GenModel=1]
9999.9      SIG_RtTq    - Rated torque (N-m) [used only when VSContrl=0 and GenModel=1]
9999.9      SIG_PORt    - Pull-out ratio (Tpullout/Trated) (-) [used only when VSContrl=0 and GenModel=1]
---------------------- THEVENIN-EQUIVALENT INDUCTION GENERATOR ----------------
9999.9      TEC_Freq    - Line frequency [50 or 60] (Hz) [used only when VSContrl=0 and GenModel=2]
9998        TEC_NPol    - Number of poles [even integer > 0] (-) [used only when VSContrl=0 and GenModel=2]
9999.9      TEC_SRes    - Stator resistance (ohms) [used only when VSContrl=0 and GenModel=2]
```

```
9999.9      TEC_RRes    - Rotor resistance (ohms) [used only when VSContrl=0 and GenModel=2]
9999.9      TEC_VLL     - Line-to-line RMS voltage (volts) [used only when VSContrl=0 and GenModel=2]
9999.9      TEC_SLR     - Stator leakage reactance (ohms) [used only when VSContrl=0 and GenModel=2]
9999.9      TEC_RLR     - Rotor leakage reactance (ohms) [used only when VSContrl=0 and GenModel=2]
9999.9      TEC_MR      - Magnetizing reactance (ohms) [used only when VSContrl=0 and GenModel=2]
---------------------- PLATFORM -----------------------------------------------
   3        PtfmModel   - Platform model {0: none, 1: onshore, 2: fixed bottom offshore, 3: floating offshore} (switch)
"NRELOffshrBsline5MW_Platform_TLP.dat"          PtfmFile    - Name of file containing platform properties (quoted string) [unused when PtfmModel=0]
---------------------- TOWER --------------------------------------------------
  20        TwrNodes    - Number of tower nodes used for analysis (-)
"NRELOffshrBsline5MW_Tower_TLP.dat"             TwrFile     - Name of file containing tower properties (quoted string)
---------------------- NACELLE-YAW --------------------------------------------
9028.32E6   YawSpr      - Nacelle-yaw spring constant (N-m/rad)
  19.16E6   YawDamp     - Nacelle-yaw damping constant (N-m/(rad/s))
   0.0          YawNeut     - Neutral yaw position--yaw spring force is zero at this yaw (degrees)
---------------------- FURLING ------------------------------------------------
```

False Furling - Read in additional model properties for furling turbine (flag)

FurlFile - Name of file containing furling properties (quoted string) [unused when Furling=False]

---------- ROTOR-TEETER ----------

0 TeetMod - Rotor-teeter spring/damper model {0: none, 1: standard, 2: user-defined from routine UserTeet} (switch) [unused for 3 blades]

0.0 TeetDmpP - Rotor-teeter damper position (degrees) [used only for 2 blades and when TeetMod=1]

0.0 TeetDmp - Rotor-teeter damping constant (N-m/(rad/s)) [used only for 2 blades and when TeetMod=1]

0.0 TeetCDmp - Rotor-teeter rate-independent Coulomb-damping moment (N-m) [used only for 2 blades and when TeetMod=1]

0.0 TeetSStP - Rotor-teeter soft-stop position (degrees) [used only for 2 blades and when TeetMod=1]

0.0 TeetHStP - Rotor-teeter hard-stop position (degrees) [used only for 2 blades and when TeetMod=1]

0.0 TeetSSSp - Rotor-teeter soft-stop linear-spring constant (N-m/rad) [used only for 2 blades and when TeetMod=1]

0.0 TeetHSSp - Rotor-teeter hard-stop linear-spring constant (N-m/rad) [used only for 2 blades and when TeetMod=1]

---------- TIP-BRAKE ----------

0.0 TBDrConN - Tip-brake drag constant during normal operation, Cd*Area (m^2)

0.0 TBDrConD - Tip-brake drag constant during fully-deployed operation, Cd*Area (m^2)

0.0 TpBrDT - Time for tip-brake to reach full deployment once released (sec)

---------- BLADE ----------

"NRELOffshrBsline5MW_Blade.dat" BldFile(1) - Name of file containing properties for blade 1 (quoted string)

"NRELOffshrBsline5MW_Blade.dat" BldFile(2) - Name of file containing properties for blade 2 (quoted string)

"NRELOffshrBsline5MW_Blade.dat" BldFile(3) - Name of file containing properties for blade 3 (quoted string) [unused for 2 blades] ----------

------- AERODYN ----------

"NRELOffshrBsline5MW_AeroDyn.ipt" ADFile - Name of file containing AeroDyn input parameters (quoted string) ----------

NOISE ----------

NoiseFile - Name of file containing aerodynamic noise input parameters (quoted string) [used only when CompNoise=True] ----------

ADAMS ----------

"NRELOffshrBsline5MW_ADAMSSpecific.dat" ADAMSFile - Name of file containing ADAMS-specific input parameters (quoted string) [unused when ADAMSPrep=1]

---------- LINEARIZATION CONTROL ----------

"NRELOffshrBsline5MW_Linear.dat" LinFile - Name of file containing FAST linearization parameters (quoted string) [unused when AnalMode=1]

---------- OUTPUT ---------- True

SumPrint - Print summary data to "<RootName>.fsm" (flag)

True TabDelim - Generate a tab-delimited tabular output file. (flag)

"ES10.3E2" OutFmt - Format used for tabular output except time. Resulting field should be 10 characters. (quoted string) [not checked for validity!]

0.0 TStart - Time to begin tabular output (s)

```
  20          DecFact     - Decimation factor for tabular output {1: output every time step} (-)
  1.0         SttsTime    - Amount of time between screen status messages (sec)
 -3.09528     NcIMUxn     - Downwind distance from the tower-top to the nacelle IMU (meters)
  0.0         NcIMUyn     - Lateral  distance from the tower-top to the nacelle IMU (meters)
  2.23336     NcIMUzn     - Vertical distance from the tower-top to the nacelle IMU (meters)
  1.912       ShftGagL    - Distance from rotor apex [3 blades] or teeter pin [2 blades] to shaft strain gages [positive for upwind rotors] (meters)
  1           NTwGages    - Number of tower nodes that have strain gages for output [0 to 9] (-)
  10          TwrGagNd    - List of tower nodes that have strain gages [1 to TwrNodes] (-) [unused if NTwGages=0]
  1           NBlGages    - Number of blade nodes that have strain gages for output [0 to 9] (-)
  9           BldGagNd    - List of blade nodes that have strain gages [1 to BldNodes] (-) [unused if NBlGages=0]
              OutList     - The next line(s) contains a list of output parameters.  See OutList.txt for a listing of available output channels, (-)
"WindVxi  , WindVyi  , WindVzi"           - Longitudinal, lateral, and vertical wind speeds
"WaveElev"                                - Wave elevation at the platform reference point
"Wave1Vxi , Wave1Vyi , Wave1Vzi"                    - Longitudinal, lateral, and vertical wave particle velocities at platform node 1 (approx. platform reference point)
"Wave1Axi , Wave1Ayi , Wave1Azi"                    - Longitudinal, lateral, and vertical wave particle accelerations at platform node 1 (approx. platform reference point)
```

"GenPwr , GenTq" - Electrical generator power and torque

"HSSBrTq" - High-speed shaft brake torque

"BldPitch1, BldPitch2, BldPitch3" - Pitch angles for blades 1, 2, and 3

"Azimuth" - Blade 1 azimuth angle

"RotSpeed , GenSpeed" - Low-speed shaft and high-speed shaft speeds

"NacYaw , NacYawErr" - Nacelle yaw angle and nacelle yaw error estimate

"OoPDefl1 , IPDefl1 , TwstDefl1" - Blade 1 out-of-plane and in-plane deflections and tip twist

"OoPDefl2 , IPDefl2 , TwstDefl2" - Blade 2 out-of-plane and in-plane deflections and tip twist

"OoPDefl3 , IPDefl3 , TwstDefl3" - Blade 3 out-of-plane and in-plane deflections and tip twist

"TwrClrnc1, TwrClrnc2, TwrClrnc3" - Tip-to-tower clearance estimate for blades 1, 2, and 3

"NcIMUTAxs, NcIMUTAys, NcIMUTAzs" - Nacelle IMU translational accelerations (absolute) in the nonrotating, shaft coordinate system

"TTDspFA , TTDspSS , TTDspTwst" - Tower fore-aft and side-to-side displacements and top twist

"PtfmSurge, PtfmSway , PtfmHeave" - Platform translational surge, sway, and heave displacements

"PtfmRoll , PtfmPitch, PtfmYaw" - Platform rotational roll, pitch and yaw displacements

"PtfmTAxt , PtfmTAyt , PtfmTAzt" - Platform translation accelerations (absolute) in the tower-base coordinate system

"RootFxc1 , RootFyc1 , RootFzc1" - Out-of-plane shear, in-plane shear, and axial forces at the root of blade 1

"RootMxc1 , RootMyc1 , RootMzc1" - In-plane bending, out-of-plane bending, and pitching moments at the root of blade 1

"RootFxc2 , RootFyc2 , RootFzc2" - Out-of-plane shear, in-plane shear, and axial forces at the root of blade 2

"RootMxc2 , RootMyc2 , RootMzc2" - In-plane bending, out-of-plane bending, and pitching moments at the root of blade 2

"RootFxc3 , RootFyc3 , RootFzc3" - Out-of-plane shear, in-plane shear, and axial forces at the root of blade 3

"RootMxc3 , RootMyc3 , RootMzc3" - In-plane bending, out-of-plane bending, and pitching moments at the root of blade 3

"Spn1MLxb1, Spn1MLyb1, Spn1MLzb1" - Blade 1 local edgewise bending, flapwise bending, and pitching moments at span station 1 (approx. 50% span)

"Spn1MLxb2, Spn1MLyb2, Spn1MLzb2" - Blade 2 local edgewise bending, flapwise bending, and pitching moments at span station 1 (approx. 50% span)

"Spn1MLxb3, Spn1MLyb3, Spn1MLzb3" - Blade 3 local edgewise bending, flapwise bending, and pitching moments at span station 1 (approx. 50% span)

"RotThrust, LSSGagFya, LSSGagFza" - Rotor thrust and low-speed shaft 0- and 90-rotating shear forces at the main bearing

"RotTorq , LSSGagMya, LSSGagMza" - Rotor torque and low-speed shaft 0- and 90-rotating bending moments at the main bearing

"YawBrFxp , YawBrFyp , YawBrFzp" - Fore-aft shear, side-to-side shear, and vertical forces at the top of the tower (not rotating with nacelle yaw)

"YawBrMxp , YawBrMyp , YawBrMzp" - Side-to-side bending, fore-aft bending, and yaw moments at the top of the tower (not rotating with nacelle yaw)

"TwrBsFxt , TwrBsFyt , TwrBsFzt" - Fore-aft shear, side-to-side shear, and vertical forces at the base of the tower (platform)

"TwrBsMxt , TwrBsMyt , TwrBsMzt" - Side-to-side bending, fore-aft bending, and yaw moments at the base of the tower (platform)

"TwHt1MLxt, TwHt1MLyt, TwHt1MLzt" - Local side-to-side bending, fore-aft bending, and yaw moments at tower gage 1 (approx. 50% elevation)

"Fair1Ten , Fair1Ang , Anch1Ten , Anch1Ang" - Line 1 fairlead and anchor effective tensions and vertical angles

"Fair2Ten , Fair2Ang , Anch2Ten , Anch2Ang" - Line 2 fairlead and anchor effective tensions and vertical angles

"Fair3Ten , Fair3Ang , Anch3Ten , Anch3Ang" - Line 3 fairlead and anchor effective tensions and vertical angles

"Fair4Ten , Fair4Ang , Anch4Ten , Anch4Ang" - Line 4 fairlead and anchor effective tensions and vertical angles

"Fair5Ten , Fair5Ang , Anch5Ten , Anch5Ang" - Line 5 fairlead and anchor effective tensions and vertical angles

"Fair6Ten , Fair6Ang , Anch6Ten , Anch6Ang" - Line 6 fairlead and anchor effective tensions and vertical angles

"Fair7Ten , Fair7Ang , Anch7Ten , Anch7Ang" - Line 7 fairlead and anchor effective tensions and vertical angles

"Fair8Ten , Fair8Ang , Anch8Ten , Anch8Ang" - Line 8 fairlead and anchor effective tensions and vertical angles

"TipSpdRat, RotCp , RotCt , RotCq" - Rotor tip speed ratio and power, thrust, and torque coefficients END of FAST input file (the word "END" must appear in the first 3 columns of this last line).

B.5 FAST Files for Test in Irregular Wave (Turbulent wind condition) – Platform File

FAST PLATFORM FILE ----------

NREL 5.0 MW offshore baseline floating platform input properties for the TLP.

---------- FEATURE FLAGS (CONT) ----------

True PtfmSgDOF - Platform horizontal surge translation DOF (flag)

True PtfmSwDOF - Platform horizontal sway translation DOF (flag)

True PtfmHvDOF - Platform vertical heave translation DOF (flag)

True PtfmRDOF - Platform roll tilt rotation DOF (flag)

True PtfmPDOF - Platform pitch tilt rotation DOF (flag)

True PtfmYDOF - Platform yaw rotation DOF (flag)

---------- INITIAL CONDITIONS (CONT) ----------

0.0 PtfmSurge - Initial or fixed horizontal surge translational displacement of platform (meters)

0.0 PtfmSway - Initial or fixed horizontal sway translational displacement of platform (meters)

0.0 PtfmHeave - Initial or fixed vertical heave translational displacement of platform (meters)

0.0 PtfmRoll - Initial or fixed roll tilt rotational displacement of platform (degrees)

0.0 PtfmPitch - Initial or fixed pitch tilt rotational displacement of platform (degrees)

0.0 PtfmYaw - Initial or fixed yaw rotational displacement of platform (degrees)

---------- TURBINE CONFIGURATION (CONT) ----------

-16.50 TwrDraft - Downward distance from the ground level [onshore] or MSL [offshore] to the tower base platform connection (meters)

30.625 PtfmCM - Downward distance from the ground level [onshore] or MSL [offshore] to the platform CM (meters)

0.0 PtfmRef - Downward distance from the ground level [onshore] or MSL [offshore] to the platform reference point (meters)

---------- MASS AND INERTIA (CONT) ----------

XXX PtfmMass - Platform mass (kg)

XXX PtfmRIner - Platform inertia for roll tilt rotation about the platform CM (kg m^2)

XXX PtfmPIner - Platform inertia for pitch tilt rotation about the platform CM (kg m^2)

XXX PtfmYIner - Platfrom inertia for yaw rotation about the platform CM (kg m^2)

---------- PLATFORM (CONT) ----------

FltngPtfmLd PtfmLdMod - Platform loading model {0: none, 1: user-defined from routine UserPtfmLd} (switch)

"HydroData\tlpmit" WAMITFile - Root name of WAMIT output files containing the linear, nondimensionalized, hydrostatic restoring matrix (.hst extension), frequency-dependent hydrodynamic added mass matrix and damping matrix (.1 extension), and frequency- and directiondependent wave excitation force vector per unit wave amplitude (.3 extension) (quoted string) [MAKE SURE THE FREQUENCIES INHERENT IN THESE WAMIT FILES SPAN THE PHYSICALLY-SIGNIFICANT RANGE OF FREQUENCIES FOR THE GIVEN PLATFORM; THEY MUST CONTAIN THE ZERO- AND INFINITE-FREQUENCY LIMITS!]

XXX PtfmVol0 - Displaced volume of water when the platform is in its undisplaced position (m^3) [USE THE SAME VALUE COMPUTED BY WAMIT AS OUTPUT IN THE .OUT FILE!]

100 PtfmNodes - Number of platform nodes used in calculation of viscous drag term from Morison's equation (-)

35.50 PtfmDraft - Effective platform draft in calculation of viscous drag term from Morison's equation (meters)

5.59 PtfmDiam - Effective platform diameter in calculation of viscous drag term from Morison's equation (meters) NOTE: THIS WAS CHOSEN TO GIVE THE SAME CROSS-SECTIONAL AREA AS THE SQUARE BARGE!

0.6 PtfmCD - Effective platform normalized hydrodynamic viscous drag coefficient in calculation of viscous drag term from Morison's equation (-)

60.0 RdtnTMax - Analysis time for wave radiation kernel calculations (sec) [determines RdtnDOmega=Pi/RdtnTMax in the cosine transform] [MAKE SURE THIS IS LONG ENOUGH FOR THE RADIATION IMPULSE RESPONSE FUNCTIONS TO DECAY TO NEARZERO FOR THE GIVEN PLATFORM!]

0.025 RdtnDT - Time step for wave radiation kernel calculations (sec) [DT<=RdtnDT<=0.1 recommended] [determines RdtnOmegaMax=Pi/RdtnDT in the cosine transform]

---------- MOORING LINES ----------

8 NumLines - Number of mooring lines (-)

1 LineMod - Mooring line model {1: standard quasi-static, 2: user-defined from routine UserLine} (switch) [used only when NumLines>0]

LRadAnch LAngAnch LDpthAnch LRadFair LAngFair LDrftFair LUnstrLen LDiam LMassDen LEAStff LSeabedCD LTenTol [used only when NumLines>0 and LineMod=1]

(m) (deg) (m) (m) (deg) (m) (m) (m) (kg/m) (N) (-) (-) [used only when NumLines>0 and LineMod=1]

27.50	0.0	70.0	27.5	0.0	35.50	34.50	0.09	43.1	XXX	-1.0	0.00001
27.50	90.0	70.0	27.5	90.0	35.50	34.50	0.09	43.1	XXX	-1.0	0.00001
27.50	180.0	70.0	27.5	180.0	35.50	34.50	0.09	43.1	XXX	-1.0	0.00001
27.50	270.0	70.0	27.5	270.0	35.50	34.50	0.09	43.1	XXX	-1.0	0.00001
27.50	0.0	70.0	27.5	0.0	35.50	34.50	0.09	43.1	XXX	-1.0	0.00001
27.50	90.0	70.0	27.5	90.0	35.50	34.50	0.09	43.1	XXX	-1.0	0.00001
27.50	180.0	70.0	27.5	180.0	35.50	34.50	0.09	43.1	XXX	-1.0	0.00001
27.50	270.0	70.0	27.5	270.0	35.50	34.50	0.09	43.1	XXX	-1.0	0.00001

---------- WAVES ----------

1025.0 WtrDens - Water density (kg/m^3)

70.0 WtrDpth - Water depth (meters) [USE THE SAME VALUE SPECIFIED IN THE WAMIT .POT FILE!]

2 WaveMod - Incident wave kinematics model {0: none=still water, 1: plane progressive (regular), 2: JONSWAP/Pierson-Moskowitz spectrum (irregular), 3: user-defind spectrum from routine UserWaveSpctrm (irregular)} (switch)

9999.999WaveTMax - Analysis time for incident wave calculations (sec) [unused when WaveMod=0] [determines WaveDOmega=2Pi/WaveTMax in the IFFT]

0.25 WaveDT - Time step for incident wave calculations (sec) [unused when WaveMod=0] [0.1<=WaveDT<=1.0 recommended] [determines WaveOmegaMax=Pi/WaveDT in the IFFT]

8.46 WaveHs - Significant wave height of incident waves (meters) [used only when WaveMod=1 or 2]

```
  10.13         WaveTp          - Peak spectral period of incident waves (sec) [used only when WaveMod=1 or 2]
DEFAULT  WavePkShp  - Peak shape parameter of incident wave spectrum (-) or DEFAULT (unquoted string) [used only when WaveMod=2] [use
1.0 for Pierson-Moskowitz]
   0.0          WaveDir         - Incident wave propagation heading direction (degrees) [unused when WaveMod=0]
123456789  WaveSeed(1) - First  random seed of incident waves [-2147483648 to 2147483647] (-) [unused when WaveMod=0]
1011121314 WaveSeed(2) - Second random seed of incident waves [-2147483648 to 2147483647] (-) [unused when WaveMod=0]
---------------------- CURRENT ------------------------------------------------
0       CurrMod     - Current profile model {0: none=no current, 1: standard, 2: user-defined from routine UserCurrent} (switch)
   0.0     CurrSSV0   - Sub-surface current velocity at still water level (m/s) [used only when CurrMod=1]
DEFAULT  CurrSSDir   - Sub-surface current heading direction (degrees) or DEFAULT (unquoted string) [used only when CurrMod=1]
  20.0     CurrNSRef   - Near-surface current reference depth (meters) [used only when CurrMod=1]
   0.0      CurrNSV0    - Near-surface current velocity at still water level (m/s) [used only when CurrMod=1]
   0.0      CurrNSDir   - Near-surface current heading direction (degrees) [used only when CurrMod=1]
   0.0      CurrDIV       - Depth-independent current velocity (m/s) [used only when CurrMod=1]
   0.0      CurrDIDir    - Depth-independent current heading direction (degrees) [used only when CurrMod=1]
---------------------- OUTPUT (CONT) ------------------------------------------
1       NWaveKin    - Number of points where the incident wave kinematics can be output [0 to 9] (-)
```

100 WaveKinNd - List of platform nodes that have wave kinematics sensors [1 to PtfmNodes] (-) [unused if NWaveKin=0]

B.6 FAST Files for Test in Irregular Wave (Turbulent wind condition) – *.fst* File

FAST INPUT FILE ---------- NREL

5.0 MW Baseline Wind Turbine for Use in Offshore Analysis.

Properties from Dutch Offshore Wind Energy Converter (DOWEC) 6MW Pre-Design (10046_009.pdf) and REpower 5M 5MW (5m_uk.pdf); Compatible with FAST v6.0.

---------- SIMULATION CONTROL ----------

False Echo - Echo input data to "echo.out" (flag)

3 ADAMSPrep - ADAMS preprocessor mode {1: Run FAST, 2: use FAST as a preprocessor to create an ADAMS model, 3: do both} (switch)

1 AnalMode - Analysis mode {1: Run a time-marching simulation, 2: create a periodic linearized model} (switch)

3 NumBl - Number of blades (-)

9999.999 TMax - Total run time (s)

0.01 DT - Integration time step (s)

---------- TURBINE CONTROL ----------

0 YCMode - Yaw control mode {0: none, 1: user-defined from routine UserYawCont, 2: user-defined from Simulink} (switch)

9999.9 TYCOn - Time to enable active yaw control (s) [unused when YCMode=0]

1 PCMode - Pitch control mode {0: none, 1: user-defined from routine PitchCntrl, 2: user-defined from Simulink} (switch)

0.0 TPCOn - Time to enable active pitch control (s) [unused when PCMode=0]

2 VSContrl - Variable-speed control mode {0: none, 1: simple VS, 2: user-defined from routine UserVSCont, 3: user-defined from Simulink} (switch)

9999.9 VS_RtGnSp - Rated generator speed for simple variable-speed generator control (HSS side) (rpm) [used only when VSContrl=1]

9999.9 VS_RtTq - Rated generator torque/constant generator torque in Region 3 for simple variable-speed generator control (HSS side) (Nm) [used only when VSContrl=1]

9999.9 VS_Rgn2K - Generator torque constant in Region 2 for simple variable-speed generator control (HSS side) (N-m/rpm^2) [used only when VSContrl=1]

9999.9 VS_SlPc - Rated generator slip percentage in Region 2 1/2 for simple variable-speed generator control (%) [used only when VSContrl=1]

2 GenModel - Generator model {1: simple, 2: Thevenin, 3: user-defined from routine UserGen} (switch) [used only when VSContrl=0]

True GenTiStr - Method to start the generator {T: timed using TimGenOn, F: generator speed using SpdGenOn} (flag)

True GenTiStp - Method to stop the generator {T: timed using TimGenOf, F: when generator power = 0} (flag)

9999.9 SpdGenOn - Generator speed to turn on the generator for a startup (HSS speed) (rpm) [used only when GenTiStr=False]

0.0 TimGenOn - Time to turn on the generator for a startup (s) [used only when GenTiStr=True]

9999.9 TimGenOf - Time to turn off the generator (s) [used only when GenTiStp=True]

1 HSSBrMode - HSS brake model {1: simple, 2: user-defined from routine UserHSSBr} (switch)

9999.9 THSSBrDp - Time to initiate deployment of the HSS brake (s)

9999.9 TiDynBrk - Time to initiate deployment of the dynamic generator brake [CURRENTLY IGNORED] (s)

9999.9 TTpBrDp(1) - Time to initiate deployment of tip brake 1 (s)

9999.9 TTpBrDp(2) - Time to initiate deployment of tip brake 2 (s)

9999.9 TTpBrDp(3) - Time to initiate deployment of tip brake 3 (s) [unused for 2 blades]

9999.9 TBDepISp(1) - Deployment-initiation speed for the tip brake on blade 1 (rpm)

9999.9 TBDepISp(2) - Deployment-initiation speed for the tip brake on blade 2 (rpm)

9999.9 TBDepISp(3) - Deployment-initiation speed for the tip brake on blade 3 (rpm) [unused for 2 blades]

9999.9 TYawManS - Time to start override yaw maneuver and end standard yaw control (s)

9999.9 TYawManE - Time at which override yaw maneuver reaches final yaw angle (s)

0.0 NacYawF - Final yaw angle for yaw maneuvers (degrees)

9999.9 TPitManS(1) - Time to start override pitch maneuver for blade 1 and end standard pitch control (s)

9999.9 TPitManS(2) - Time to start override pitch maneuver for blade 2 and end standard pitch control (s)

9999.9 TPitManS(3) - Time to start override pitch maneuver for blade 3 and end standard pitch control (s) [unused for 2 blades]

9999.9 TPitManE(1) - Time at which override pitch maneuver for blade 1 reaches final pitch (s)

9999.9 TPitManE(2) - Time at which override pitch maneuver for blade 2 reaches final pitch (s)

9999.9 TPitManE(3) - Time at which override pitch maneuver for blade 3 reaches final pitch (s) [unused for 2 blades]

20.0 BlPitch(1) - Blade 1 initial pitch (degrees)

20.0 BlPitch(2) - Blade 2 initial pitch (degrees)

20.0 BlPitch(3) - Blade 3 initial pitch (degrees) [unused for 2 blades]

90.0 B1PitchF(1) - Blade 1 final pitch for pitch maneuvers (degrees)

90.0 B1PitchF(2) - Blade 2 final pitch for pitch maneuvers (degrees)

90.0 B1PitchF(3) - Blade 3 final pitch for pitch maneuvers (degrees) [unused for 2 blades]

---------- ENVIRONMENTAL CONDITIONS ----------

9.80665 Gravity - Gravitational acceleration (m/s^2)

---------- FEATURE FLAGS ----------

False FlapDOF1 - First flapwise blade mode DOF (flag)

False FlapDOF2 - Second flapwise blade mode DOF (flag)

False EdgeDOF - First edgewise blade mode DOF (flag)

False TeetDOF - Rotor-teeter DOF (flag) [unused for 3 blades]

False DrTrDOF - Drivetrain rotational-flexibility DOF (flag)

True GenDOF - Generator DOF (flag)

```
True        YawDOF      Yaw DOF (flag)
False       TwFADOF1    - First fore-aft tower bending-mode DOF (flag)
False       TwFADOF2    - Second fore-aft tower bending-mode DOF (flag)
False       TwSSDOF1    - First side-to-side tower bending-mode DOF (flag)
False       TwSSDOF2    - Second side-to-side tower bending-mode DOF (flag)
True        CompAero    - Compute aerodynamic forces (flag)
False       CompNoise   - Compute aerodynamic noise (flag)
---------------------- INITIAL CONDITIONS ---------------------------------
  0.0      OoPDefl     - Initial out-of-plane blade-tip displacement (meters)
  0.0      IPDefl      - Initial in-plane blade-tip deflection (meters)
  0.0      TeetDefl    - Initial or fixed teeter angle (degrees) [unused for 3 blades]
  0.0      Azimuth     - Initial azimuth angle for blade 1 (degrees)
 12.1      RotSpeed    - Initial or fixed rotor speed (rpm)
  0.0      NacYaw      - Initial or fixed nacelle-yaw angle (degrees)
  0.0      TTDspFA     - Initial fore-aft tower-top displacement (meters)
  0.0      TTDspSS     - Initial side-to-side tower-top displacement (meters) ---------------------- TURBINE CONFIGURATION ----------------------
-------------
```

-

63.0 TipRad - The distance from the rotor apex to the blade tip (meters)

1.5 HubRad - The distance from the rotor apex to the blade root (meters)

1 PSpnElN - Number of the innermost blade element which is still part of the pitchable portion of the blade for partial-span pitch control [1 to BldNodes] [CURRENTLY IGNORED] (-)

0.0 UndSling - Undersling length [distance from teeter pin to the rotor apex] (meters) [unused for 3 blades]

0.0 HubCM - Distance from rotor apex to hub mass [positive downwind] (meters)

-5.01910 OverHang - Distance from yaw axis to rotor apex [3 blades] or teeter pin [2 blades] (meters)

1.9 NacCMxn - Downwind distance from the tower-top to the nacelle CM (meters)

0.0 NacCMyn - Lateral distance from the tower-top to the nacelle CM (meters)

1.75 NacCMzn - Vertical distance from the tower-top to the nacelle CM (meters)

87.6 TowerHt - Height of tower above ground level [onshore] or MSL [offshore] (meters)

1.96256 Twr2Shft - Vertical distance from the tower-top to the rotor shaft (meters)

16.50 TwrRBHt - Tower rigid base height (meters)

-5.0 ShftTilt - Rotor shaft tilt angle (degrees)

0.0 Delta3 - Delta-3 angle for teetering rotors (degrees) [unused for 3 blades]

-2.5 PreCone(1) - Blade 1 cone angle (degrees)

-2.5 PreCone(2) Blade 2 cone angle (degrees)

-2.5 PreCone(3) - Blade 3 cone angle (degrees) [unused for 2 blades]

0.0 AzimB1Up - Azimuth value to use for I/O when blade 1 points up (degrees)

---------- MASS AND INERTIA ----------

0.0 YawBrMass - Yaw bearing mass (kg)

240.00E3 NacMass - Nacelle mass (kg)

56.78E3 HubMass - Hub mass (kg)

0.0 TipMass(1) - Tip-brake mass, blade 1 (kg)

0.0 TipMass(2) - Tip-brake mass, blade 2 (kg)

0.0 TipMass(3) - Tip-brake mass, blade 3 (kg) [unused for 2 blades]

2607.89E3 NacYIner - Nacelle inertia about yaw axis (kg m^2)

534.116 GenIner - Generator inertia about HSS (kg m^2)

115.926E3 HubIner - Hub inertia about rotor axis [3 blades] or teeter axis [2 blades] (kg m^2)

---------- DRIVETRAIN ----------

100.0 GBoxEff - Gearbox efficiency (%)

94.4 GenEff - Generator efficiency [ignored by the Thevenin and user-defined generator models] (%)

97.0 GBRatio - Gearbox ratio (-)

-

False GBRevers - Gearbox reversal {T: if rotor and generator rotate in opposite directions} (flag)

28.1162E3 HSSBrTqF - Fully deployed HSS-brake torque (N-m)

0.6 HSSBrDT - Time for HSS-brake to reach full deployment once initiated (sec) [used only when HSSBrMode=1]

DynBrkFi - File containing a mech-gen-torque vs HSS-speed curve for a dynamic brake [CURRENTLY IGNORED] (quoted string)

867.637E6 DTTorSpr - Drivetrain torsional spring (N-m/rad)

6.215E6 DTTorDmp - Drivetrain torsional damper (N-m/(rad/s))

---------- SIMPLE INDUCTION GENERATOR ----------

9999.9 SIG_SlPc - Rated generator slip percentage (%) [used only when VSContrl=0 and GenModel=1]

9999.9 SIG_SySp - Synchronous (zero-torque) generator speed (rpm) [used only when VSContrl=0 and GenModel=1]

9999.9 SIG_RtTq - Rated torque (N-m) [used only when VSContrl=0 and GenModel=1]

9999.9 SIG_PORt - Pull-out ratio (Tpullout/Trated) (-) [used only when VSContrl=0 and GenModel=1]

---------- THEVENIN-EQUIVALENT INDUCTION GENERATOR ----------

9999.9 TEC_Freq - Line frequency [50 or 60] (Hz) [used only when VSContrl=0 and GenModel=2]

9998 TEC_NPol - Number of poles [even integer > 0] (-) [used only when VSContrl=0 and GenModel=2]

9999.9 TEC_SRes - Stator resistance (ohms) [used only when VSContrl=0 and GenModel=2]

9999.9 TEC_RRes Rotor resistance (ohms) [used only when VSContrl=0 and GenModel=2]

9999.9 TEC_VLL - Line-to-line RMS voltage (volts) [used only when VSContrl=0 and GenModel=2]

9999.9 TEC_SLR - Stator leakage reactance (ohms) [used only when VSContrl=0 and GenModel=2]

9999.9 TEC_RLR - Rotor leakage reactance (ohms) [used only when VSContrl=0 and GenModel=2]

9999.9 TEC_MR - Magnetizing reactance (ohms) [used only when VSContrl=0 and GenModel=2]

---------- PLATFORM ----------

3 PtfmModel - Platform model {0: none, 1: onshore, 2: fixed bottom offshore, 3: floating offshore} (switch)

"NRELOffshrBsline5MW_Platform_TLP.dat" PtfmFile - Name of file containing platform properties (quoted string) [unused when PtfmModel=0]

---------- TOWER ----------

20 TwrNodes - Number of tower nodes used for analysis (-)

"NRELOffshrBsline5MW_Tower_TLP.dat" TwrFile - Name of file containing tower properties (quoted string)

---------- NACELLE-YAW ----------

9028.32E6 YawSpr - Nacelle-yaw spring constant (N-m/rad)

19.16E6 YawDamp - Nacelle-yaw damping constant (N-m/(rad/s))

0.0 YawNeut - Neutral yaw position--yaw spring force is zero at this yaw (degrees)

---------- FURLING ----------

False Furling - Read in additional model properties for furling turbine (flag)

-

FurlFile - Name of file containing furling properties (quoted string) [unused when Furling=False]

---------- ROTOR-TEETER ----------

0 TeetMod - Rotor-teeter spring/damper model {0: none, 1: standard, 2: user-defined from routine UserTeet} (switch) [unused for 3 blades]

0.0 TeetDmpP - Rotor-teeter damper position (degrees) [used only for 2 blades and when TeetMod=1]

0.0 TeetDmp - Rotor-teeter damping constant (N-m/(rad/s)) [used only for 2 blades and when TeetMod=1]

0.0 TeetCDmp - Rotor-teeter rate-independent Coulomb-damping moment (N-m) [used only for 2 blades and when TeetMod=1]

0.0 TeetSStP - Rotor-teeter soft-stop position (degrees) [used only for 2 blades and when TeetMod=1]

0.0 TeetHStP - Rotor-teeter hard-stop position (degrees) [used only for 2 blades and when TeetMod=1]

0.0 TeetSSSp - Rotor-teeter soft-stop linear-spring constant (N-m/rad) [used only for 2 blades and when TeetMod=1]

0.0 TeetHSSp - Rotor-teeter hard-stop linear-spring constant (N-m/rad) [used only for 2 blades and when TeetMod=1]

---------- TIP-BRAKE ----------

0.0 TBDrConN - Tip-brake drag constant during normal operation, Cd*Area (m^2)

0.0 TBDrConD - Tip-brake drag constant during fully-deployed operation, Cd*Area (m^2)

0.0 TpBrDT - Time for tip-brake to reach full deployment once released (sec)

---------- BLADE ----------

"NRELOffshrBsline5MW_Blade.dat" BldFile(1) - Name of file containing properties for blade 1 (quoted string)

"NRELOffshrBsline5MW_Blade.dat" BldFile(2) - Name of file containing properties for blade 2 (quoted string)

"NRELOffshrBsline5MW_Blade.dat" BldFile(3) - Name of file containing properties for blade 3 (quoted string) [unused for 2 blades]

---------------------- AERODYN --

"NRELOffshrBsline5MW_AeroDyn.ipt" ADFile - Name of file containing AeroDyn input parameters (quoted string) ----------

----- NOISE --

NoiseFile - Name of file containing aerodynamic noise input parameters (quoted string) [used only when CompNoise=True] ----------

--------- ADAMS --

"NRELOffshrBsline5MW_ADAMSSpecific.dat" ADAMSFile - Name of file containing ADAMS-specific input parameters (quoted string) [unused when ADAMSPrep=1]

---------------------- LINEARIZATION CONTROL ----------------------------------

"NRELOffshrBsline5MW_Linear.dat" LinFile - Name of file containing FAST linearization parameters (quoted string) [unused when AnalMode=1]

---------------------- OUTPUT -- True

SumPrint - Print summary data to "<RootName>.fsm" (flag)

True TabDelim - Generate a tab-delimited tabular output file. (flag)

"ES10.3E2" OutFmt - Format used for tabular output except time. Resulting field should be 10 characters. (quoted string) [not checked for validity!]

0.0 TStart - Time to begin tabular output (s)

20 DecFact - Decimation factor for tabular output {1: output every time step} (-)

1.0 SttsTime - Amount of time between screen status messages (sec)

-3.09528 NcIMUxn - Downwind distance from the tower-top to the nacelle IMU (meters)

0.0 NcIMUyn - Lateral distance from the tower-top to the nacelle IMU (meters)

2.23336 NcIMUzn - Vertical distance from the tower-top to the nacelle IMU (meters)

1.912 ShftGagL - Distance from rotor apex [3 blades] or teeter pin [2 blades] to shaft strain gages [positive for upwind rotors] (meters)

1 NTwGages - Number of tower nodes that have strain gages for output [0 to 9] (-)

10 TwrGagNd - List of tower nodes that have strain gages [1 to TwrNodes] (-) [unused if NTwGages=0]

1 NBlGages - Number of blade nodes that have strain gages for output [0 to 9] (-)

9 BldGagNd - List of blade nodes that have strain gages [1 to BldNodes] (-) [unused if NBlGages=0]

OutList - The next line(s) contains a list of output parameters. See OutList.txt for a listing of available output channels, (-)

"WindVxi , WindVyi , WindVzi" - Longitudinal, lateral, and vertical wind speeds

"WaveElev" - Wave elevation at the platform reference point

"Wave1Vxi , Wave1Vyi , Wave1Vzi" - Longitudinal, lateral, and vertical wave particle velocities at platform node 1 (approx. platform reference point)

"Wave1Axi , Wave1Ayi , Wave1Azi" - Longitudinal, lateral, and vertical wave particle accelerations at platform node 1 (approx. platform reference point)

"GenPwr , GenTq" - Electrical generator power and torque

"HSSBrTq" - High-speed shaft brake torque

"BldPitch1, BldPitch2, BldPitch3" - Pitch angles for blades 1, 2, and 3

"Azimuth" - Blade 1 azimuth angle

"RotSpeed , GenSpeed" - Low-speed shaft and high-speed shaft speeds

"NacYaw , NacYawErr" - Nacelle yaw angle and nacelle yaw error estimate

"OoPDefl1 , IPDefl1 , TwstDefl1" - Blade 1 out-of-plane and in-plane deflections and tip twist

"OoPDefl2 , IPDefl2 , TwstDefl2" - Blade 2 out-of-plane and in-plane deflections and tip twist

"OoPDefl3 , IPDefl3 , TwstDefl3" - Blade 3 out-of-plane and in-plane deflections and tip twist

"TwrClrnc1, TwrClrnc2, TwrClrnc3" - Tip-to-tower clearance estimate for blades 1, 2, and 3

"NcIMUTAxs, NcIMUTAys, NcIMUTAzs" - Nacelle IMU translational accelerations (absolute) in the nonrotating, shaft coordinate system

"TTDspFA , TTDspSS , TTDspTwst" - Tower fore-aft and side-to-side displacements and top twist

"PtfmSurge, PtfmSway , PtfmHeave" - Platform translational surge, sway, and heave displacements

"PtfmRoll , PtfmPitch, PtfmYaw" - Platform rotational roll, pitch and yaw displacements

"PtfmTAxt , PtfmTAyt , PtfmTAzt" - Platform translation accelerations (absolute) in the tower-base coordinate system

"RootFxc1 , RootFyc1 , RootFzc1" - Out-of-plane shear, in-plane shear, and axial forces at the root of blade 1

"RootMxc1 , RootMyc1 , RootMzc1" - In-plane bending, out-of-plane bending, and pitching moments at the root of blade 1

"RootFxc2 , RootFyc2 , RootFzc2" - Out-of-plane shear, in-plane shear, and axial forces at the root of blade 2

"RootMxc2 , RootMyc2 , RootMzc2" - In-plane bending, out-of-plane bending, and pitching moments at the root of blade 2

"RootFxc3 , RootFyc3 , RootFzc3" - Out-of-plane shear, in-plane shear, and axial forces at the root of blade 3

"RootMxc3 , RootMyc3 , RootMzc3" - In-plane bending, out-of-plane bending, and pitching moments at the root of blade 3

"Spn1MLxb1, Spn1MLyb1, Spn1MLzb1" - Blade 1 local edgewise bending, flapwise bending, and pitching moments at span station 1 (approx. 50% span)

"Spn1MLxb2, Spn1MLyb2, Spn1MLzb2" - Blade 2 local edgewise bending, flapwise bending, and pitching moments at span station 1 (approx. 50% span)

"Spn1MLxb3, Spn1MLyb3, Spn1MLzb3" - Blade 3 local edgewise bending, flapwise bending, and pitching moments at span station 1 (approx. 50% span)

"RotThrust, LSSGagFya, LSSGagFza" - Rotor thrust and low-speed shaft 0- and 90-rotating shear forces at the main bearing

"RotTorq , LSSGagMya, LSSGagMza" - Rotor torque and low-speed shaft 0- and 90-rotating bending moments at the main bearing

"YawBrFxp , YawBrFyp , YawBrFzp" - Fore-aft shear, side-to-side shear, and vertical forces at the top of the tower (not rotating with nacelle yaw)

"YawBrMxp , YawBrMyp , YawBrMzp" - Side-to-side bending, fore-aft bending, and yaw moments at the top of the tower (not rotating with nacelle yaw)

"TwrBsFxt , TwrBsFyt , TwrBsFzt" - Fore-aft shear, side-to-side shear, and vertical forces at the base of the tower (platform)

"TwrBsMxt , TwrBsMyt , TwrBsMzt" - Side-to-side bending, fore-aft bending, and yaw moments at the base of the tower (platform)

"TwHt1MLxt, TwHt1MLyt, TwHt1MLzt" - Local side-to-side bending, fore-aft bending, and yaw moments at tower gage 1 (approx. 50% elevation)

"Fair1Ten , Fair1Ang , Anch1Ten , Anch1Ang" - Line 1 fairlead and anchor effective tensions and vertical angles

"Fair2Ten , Fair2Ang , Anch2Ten , Anch2Ang" - Line 2 fairlead and anchor effective tensions and vertical angles

"Fair3Ten , Fair3Ang , Anch3Ten , Anch3Ang" - Line 3 fairlead and anchor effective tensions and vertical angles

"Fair4Ten , Fair4Ang , Anch4Ten , Anch4Ang" - Line 4 fairlead and anchor effective tensions and vertical angles

"Fair5Ten , Fair5Ang , Anch5Ten , Anch5Ang" - Line 5 fairlead and anchor effective tensions and vertical angles

"Fair6Ten , Fair6Ang , Anch6Ten , Anch6Ang" - Line 6 fairlead and anchor effective tensions and vertical angles

"Fair7Ten , Fair7Ang , Anch7Ten , Anch7Ang" - Line 7 fairlead and anchor effective tensions and vertical angles

"Fair8Ten , Fair8Ang , Anch8Ten , Anch8Ang" - Line 8 fairlead and anchor effective tensions and vertical angles

"TipSpdRat, RotCp , RotCt , RotCq" - Rotor tip speed ratio and power, thrust, and torque coefficients END of FAST input file (the word "END" must appear in the first 3 columns of this last line).